Electrochemical and IR spectroelectrochemical studies of ligand binding to the metal centres of nitrogenase

Pathinan Paengnakorn

Jesus College

Trinity Term 2014

A Thesis submitted to the Board of the Faculty of Physical Sciences, for the degree of

Doctor of Philosophy, University of Oxford

Abstract

Electrochemical and IR spectroelectrochemical studies of ligand binding to the metal centres of nitrogenase

Pathinan Paengnakorn

Jesus College, University of Oxford

A Thesis submitted for the degree of Doctor of Philosophy, Trinity Term 2014

Nitrogenase is a metalloenzyme that plays a key role in biological nitrogen fixation by catalysing the reduction of dinitrogen to ammonia. Study of nitrogenase is particularly challenging because of its unique electron transfer and catalytic components. This Thesis describes the development of a mediated electron transfer system for the MoFe protein of nitrogenase, in order to overcome the complexity of electron transfer by the native reductant Fe protein coupled to hydrolysis of ATP. A series of redox mediators was employed including $Eu^{III/II}$-polyaminocarboxylate complexes, which have reduction potentials in a very negative range. In the presence of the redox mediators, the wild type MoFe protein exhibits a catalytic current due to protein-catalysed proton reduction. With this mediated electron transfer method, the potential of proton reduction by nitrogenase was determined for the first time.

The redox mediator system was also applied in an infrared (IR) spectroelectrochemical study of CO binding to the wild type and β-98^{His} variant MoFe protein. The first IR evidence was provided for ATP-independent CO binding to the active site of the MoFe protein, in both the wild type and the variant. The peak wavenumbers and time-dependent changes in intensity found in this study are consistent with the result of previous CO coordination with nitrogenase obtained by electron transfer from the Fe protein driven by ATP. This strongly suggests that this mediated electron transfer approach can deliver low potential electrons into the MoFe protein and reduce the active site FeMoco to the substrate binding level. Moreover, this technique allows electrocatalytic activity of the protein to be monitored and the change in redox activity can be correlated directly to the potential. With the same technique, a study of cyanide binding was performed on different variant MoFe proteins of nitrogenase.

The redox properties of the isolated cofactor of Mo- and V-dependent nitrogenase were investigated in parallel to the study of the protein-bound cofactors. It was found that FeVco, the active site from V-nitrogenase, exhibited different redox properties compared to that of Mo-nitrogenase. This might account for the unexpected activity in CO reduction that was reported previously for V-nitrogenase.

Acknowledgements

First of all, I would like to give my deepest thank to Prof Kylie Vincent, my supervisor who first gives me this opportunity to be here. I am really grateful for her supervision in this work and everything; I vividly remembered from the first day she picked me up from Heathrow airport until the day we discussed a result while the baby was kicking her inside. I was so touched by her great kindness. Without her constantly support and encourage, this work would have never been done.

I would like to express my gratitude for Dr Philip Ash, who designed the special glove box and instrument used for this work. I really appreciate your willing to help with all technical problems including that disastrous 'pre-submission' day at ICL. I thank Prof Lance Seefedlt for providing the precious MoFe protein samples and our fruitful discussion across the Atlantic. Also thank Prof Marcus Ribbe for sending the isolated cofactor for this work.

My special thanks go to the Vincent group members; Juan and Zul, the first DPhil generation who taught me fundamental DPhil life, Adam for his expertise in SEC cell setup and tuck shop foundation, Holly for her great organising skill especially word formatting, Ian for his anti-leakage specialty and proofreading skill, Min-Wen for her expertise in cyanide and bubble tea, Ricardo for cell design and magic, Gary for running the tuck shop, Henry and Charlie who are the masters of Europium and myoglobin. Thank to all past and present members who make KAV group most enjoyable place to work.

I would like to thank Thai taxpayers for this invaluable scholarship. I thank also Jesus college for great financial support and the kindness of all staffs.

I am thankful for great support from my family in the hardest time. Finally, thanks to all my friends who shared great memories of wonderful four years here with me.

Abbreviations

A	amperes
Å	Angstrom (10^{-10} m)
ADP	adenosine diphosphate
ATP	adenosine triphosphate
ATR	attenuated total reflectance
°C	degrees Centigrade
Da	Dalton
E	electrode potential
E_m	midpoint potential
E°	standard reduction potential
EPR	electron paramagnetic resonance
ENDOR	electron nuclear double resonance
IR	infrared
I	current
K	Kelvin
NMR	nuclear magnetic resonance
ppm	parts per million
s	second(s)
SCE	saturated calomel electrode
SEC	spectroelectrochemistry
SHE	standard hydrogen electrode
t	time
T	temperature
UV-vis	ultraviolet-visible
V	volts

Table of contents

Abstract ..... **i**

Acknowledgements ..... **ii**

Abbreviations ..... **iii**

Table of contents ..... **iv**

CHAPTER 1

Introduction **1**

1.1 Nitrogen cycle and dinitrogen fixation 2

1.1.1 Overview 2
1.1.2 Redox enzymes in the nitrogen cycle 4
1.1.3 Nitrogen fixation 5

1.2 Nitrogenase enzymes 10

1.2.1 Mo-nitrogenase 10
1.2.2 Alternative nitrogenase 16

1.3 Nitrogenase mechanism 16

1.3.1 Electron transfer in nitrogenase 16
1.3.2 Catalytic Mechanism 17
1.3.3 Reaction pathway 19

1.4 Substrates and inhibitors 20

1.4.1 Dinitrogen 21
1.4.2 Carbon monoxide 23
1.4.3 Cyanide 24

1.5 Methods for studying nitrogenase 26

1.5.1 X-ray crystallography 26
1.5.2 X-ray spectroscopy 26
1.5.3 EPR spectroscopy 27
1.5.4 Electrochemistry 28
1.5.5 IR spectroscopy 29
1.5.6 IR spectroelectrochemistry 30

1.6 Aims and Scope of this Thesis 32

1.6.1 Development and application of mediated electrochemical control 32
1.6.2 Study of ligand binding to the redox sites 33

CHAPTER 2

Theory and Methodology 34

2.1 Electrochemistry 34

2.1.1 Redox reaction 34
2.1.2 The Nernst equation 36
2.1.3 Faradaic and non-faradaic processes 37
2.1.4 Electron mediation 39

2.2 Electrochemical techniques 40

2.2.1 Three electrode system 40
2.2.2 Cyclic voltammetry 41
2.2.3 Chronoamperometry 43

2.3 Infrared Spectroscopy 44

2.3.1 Vibrational energy 44
2.3.2 Electronic effect 47

2.4 ATR-IR spectroelectrochemistry 51

2.4.1 ATR-IR technique 51
2.4.2 ATR-IR spectroelectrochemical cell 52
2.4.3 Preparation of the ATR-IR SEC cell 54
2.4.4 ATR accessory and IR spectrometer 55

2.5 Experimental 56

2.5.1 Anaerobic handling of nitrogenase 56
2.5.2 Buffer solution 57
2.5.3 Flow system and mass flow controller 57
2.5.4 Reagents 57

CHAPTER 3

Development of a mediated electron transfer system for studying nitrogenase 59

3.1 Electrode modifications 59

3.1.1 Working electrode 60
3.1.2 Counter electrode 62
3.1.3 Reference electrode 62

3.2 Redox mediators 64

3.2.1 Europium polyaminocarboxylate complexes 65
3.2.2 Organic mediators 73
3.2.3 Mediator cocktail 75

3.3 Model systems for spectroelectrochemical study 81

3.3.1 Potassium ferricyanide 81

3.3.1 Carboxymyoglobin....85

CHAPTER 4

Electrochemical study of electron transfer in the MoFe protein....98

4.1 Introduction....98

4.1.1 Mediated electron transfer techniques....99
4.1.2 Proton reduction by nitrogenase....100

4.2 Electrochemical study of the wild type MoFe proteins....101

4.2.1 Experimental....101
4.2.2 Proton reduction by the MoFe protein....104
4.2.3 Acetylene inhibition....108
4.2.4 Discussion: Proton reduction by the MoFe protein....111

4.3 Electrochemical study of the β-98^{His} variant....115

4.3.1 Proton reduction by β-98^{His} variant MoFe protein....115
4.3.2 Discussion....118

4.4 Study of the CO interaction with wild type MoFe protein....120

4.4.1 Effect of CO on proton reduction by the MoFe protein....120
4.4.2 Electrochemistry of MoFe protein in the presence of CO....123
4.4.3 Discussion: CO inhibition....125

CHAPTER 5

IR spectroelectrochemical studies of CO binding to MoFe protein....127

5.1 Introduction....127

5.1.1 CO inhibition....128
5.1.2 IR spectra of the CO-bound nitrogenase....129
5.1.3 Reduction of CO....135

5.2 Experimental....136

5.2.1 Compatibility with protein....137

5.3 Study of CO binding to the MoFe protein....139

5.3.1 CO binding to the β-98^{His} variant MoFe protein....139
5.3.2 CO binding to the wild type MoFe protein....147

5.4 Discussion....154

5.4.1 CO inhibition of wild type and β-98^{His} variant MoFe protein....154
5.4.2 CO bound peaks....155
5.4.3 Time course of CO binding....158
5.4.4 Potential-dependence of CO binding....159
5.4.5 CO binding mechanism....161

CHAPTER 6

Study of cyanide binding to the metal centres of nitrogenase 164

6.1 Introduction 164

6.1.1 Reduction of cyanide by nitrogenase 165
6.1.2 Cyanide binding to isolated FeMoco 167
6.1.3 Previous spectroelectrochemical studies of FeMoco-CN 168

6.2 Cyanide binding to variant MoFe protein 170

6.3 Experimental.....172

6.3.1 Sample preparation.....172
6.3.2 Preparation of the ATR-IR SEC cell.....172
6.3.3 Cyanide in solution 173

6.4 IR spectroelectrochemical studies on cyanide binding to the MoFe proteins 175

6.4.1 Cyanide interactions at the resting state.....175
6.4.2 Potential-dependent cyanide binding to MoFe proteins.....178
6.4.3 Isotopically-labelled ^{13}CN.....182
6.4.4 Discussion 184

6.5 Alternative approaches 189

6.5.1 EDTA treatment.....189
6.5.2 Solution displacement 191
6.5.3 Dialysis membrane.....192

6.6 Discussion.....193

CHAPTER 7

Electrochemical study of isolated cofactors.....196

7.1 Experimental.....196

7.1.1 Isolated cofactor samples 196
7.1.2 Electrochemical cell setup.....197

7.2 Electrochemistry of FeMoco and FeVco.....198

7.2.1 Isolated FeMoco.....198
7.2.2 The effect of thiophenol 199
7.2.3 Isolated FeVco 201

7.3 CO-binding to isolated cofactors.....203

7.4 Isocyanide binding to FeMoco 204

7.4.1 Preparation of methyl isocyanide.....204
7.4.2 Titration of FeMoco with methyl isocyanide.....205
7.4.3 Conclusion.....208

CHAPTER 8

Conclusion 209

Bibliography 215

Chapter 1

Introduction

Nitrogen is one of the most essential elements for all living organisms on Earth. A growth of world population was once limited by the availability of nitrogen fertilizer in agricultural fields until the synthetic fixation of nitrogen was invented by Fritz Haber and Carl Bosch in the 1910s. Since then, the population has increased dramatically and demand for synthetic nitrogen products has been rising continuously. In the search for more efficient and energy-saving methods for the industrial nitrogen fixation, a study of nitrogenase, the key enzyme in nitrogen fixation in nature, has been of interest for scientists. As the enzyme-catalysed reduction of dinitrogen takes place at room temperature and relatively mild conditions, the elucidation of this mechanism will be beneficial for the development of novel catalysts for synthetic nitrogen fixation. While the invention of the ‘Haber-Bosch process’ was acclaimed as one of the greatest technologies to have changed the world a century ago, the understanding of biological nitrogen fixation remains a great challenge to the present day.

One important question in the nitrogenase mechanism is how substrates and inhibitors bind to the enzyme. This Thesis is focused on a study of ligand binding to the active site of nitrogenase using electrochemical techniques coupled with infrared (IR) spectroscopy. This combination of characterisation techniques, together with specially mutated enzymes produced by collaborators, should give new insight into the mechanism of the enzyme.

1.1 Nitrogen cycle and dinitrogen fixation

Nitrogen is a mandatory element required in the formation of many biological molecules. It is a major component of fundamental units such as amino acids and nucleotides, which build up important macromolecules in the cell including proteins, DNAs and RNAs. It is also a component in chlorophyll, a key biomolecule in photosynthesis by plants and other photosynthetic organisms. Thus, growth of plants is dependent upon the availability of nitrogen and the nitrogen cycle is related to all organisms in ecosystems. Interestingly, most reactions in the nitrogen cycle occur in the cells of microorganisms and involve a variety of enzymes.

1.1.1 Overview

Nitrogen can be found in various chemical forms in nature, from a free element to organic compounds. The global nitrogen cycle comprises several processes of transformation between different forms of nitrogen as shown in Figure 1-1.

The largest reservoir of nitrogen is dinitrogen gas (N_2), the elemental form of nitrogen, which makes up 78% by volume of the Earth's atmosphere. At the beginning of the cycle, this atmospheric dinitrogen is converted into reduced forms, ammonia (NH_3) or ammonium ions (NH_4^+), in a process called 'nitrogen fixation'. This process mostly occurs biologically by

nitrogen-fixing bacteria and artificially in large scale chemical processes. A relatively small amount of dinitrogen in the air is fixed by lighting.

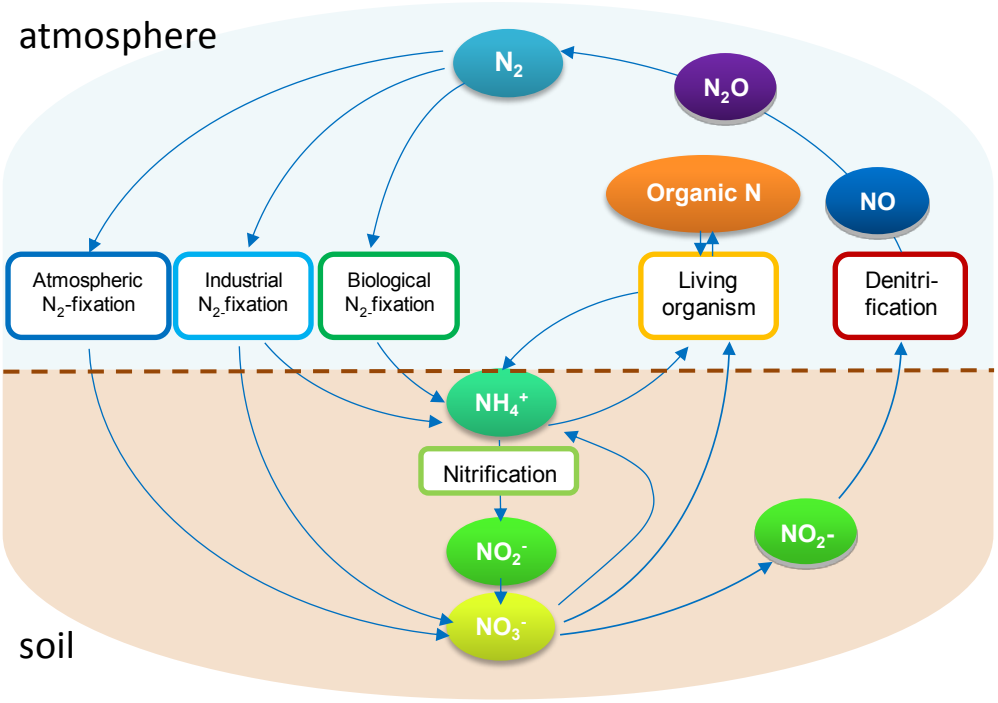

Figure 1-1: The global nitrogen cycle involves various forms of nitrogen in the environment including dinitrogen (N_2), nitrite (NO_2^-), nitrate (NO_3^-) and ammonium (NH_4^+). [1, 2]

In aerobic soil, ammonium ions are processed to nitrite (NO_2^-) and then nitrate (NO_3^-) by nitrifying microorganisms *via* a nitrification process. Then, plants assimilate these inorganic nitrogen compounds, either ammonium or nitrate, and convert them into organic compounds like amino acids before they are consumed by animals and organic nitrogen is passed through food chains. All animals and other organisms that cannot directly absorb inorganic nitrogen need to gain nitrogen-containing nutrients entirely from their food. The nitrogen-containing waste from protein metabolism is expelled mostly in the form of ammonia and urea. When plants and animals die, the organic nitrogen is converted back to ammonium ion by decomposers *i.e.* bacteria and fungi *via* an ammonification process.

To complete the cycle, nitrate is reduced back to nitrogen gas *via* a denitrification process. In the marine system, it was found that nitrite and ammonium can be directly converted into dinitrogen gas in the anaerobic ammonia oxidation (anammox) process.[3]

1.1.2 Redox enzymes in the nitrogen cycle

A broad range of redox enzymes play key roles in driving the biological nitrogen cycle by catalysing specific reactions at each step. These enzymes catalyse reactions involving electron transfer and change the oxidation state of nitrogen as shown in Figure 1-2.[4-6] These biological catalysts contain one or more transition metals in their active sites coordinated with amino acids from the surrounding protein. In general, the metal active site obtains its electron supply from an external electron source *via* a long-range electron transfer process; meanwhile a supply of substrate to the active site is provided through a substrate channel inside the protein structure. Each enzyme system has unique means of assembly and fabrication resulting in specific catalytic properties of the enzyme.

Nitrogen fixation, the process by which dinitrogen gas is reduced to ammonium ions, is catalysed by nitrogenase. This enzyme is found in a specific group of bacteria living in the soil or root nodules of legume plants. The active site of nitrogenase is found to contain an Fe and Mo cluster.

The following process, nitrification, is carried out by two groups of nitrifying bacteria. First, ammonium is oxidised into nitrite *via* the intermediate hydroxylamine. Later, nitrite is oxidised to nitrate. The key enzymes in the nitrification process are ammonia monooxygenase (AMO), hydroxylamine oxidoreductase (HAO) and nitrite oxidoreductase (NXR).

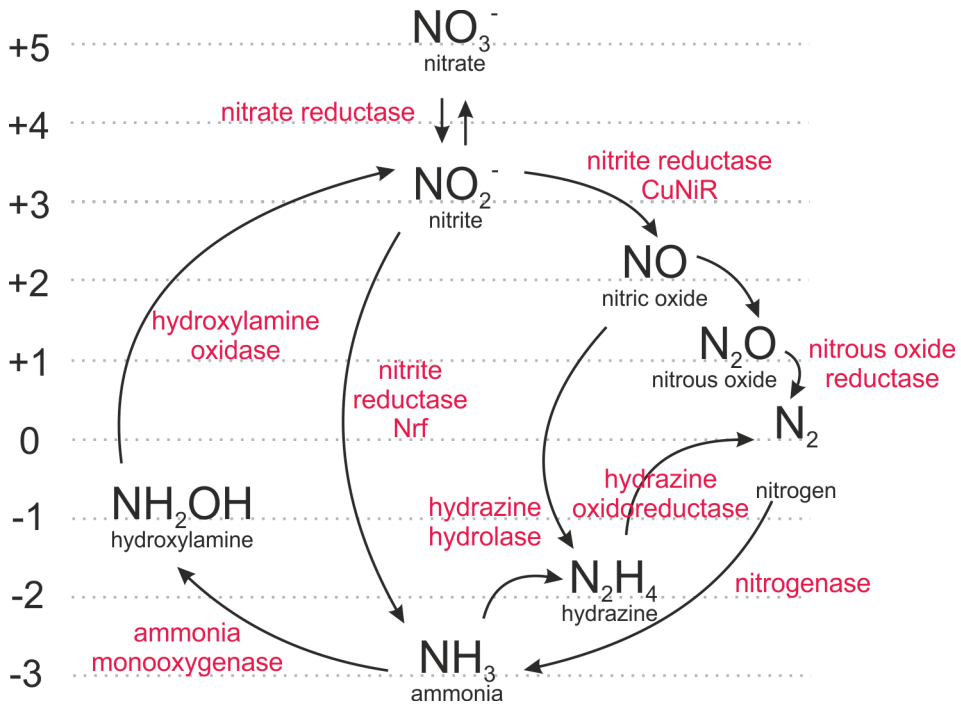

Figure 1-2: A diagram showing the relationship between various enzymes in the nitrogen cycle. The oxidation number of nitrogen in their substrate and products are indicated on the left.

In the reverse process, denitrification, nitrate is converted back to nitrite through a two–electron reduction by molybdenum-containing nitrate reductase. Then, an intermediate nitrite is reduced to nitric oxide (NO) by copper-containing nitrite reductase (CuNiR), followed subsequently by a series of reduction processes from nitric oxide to nitrous oxide and dinitrogen as a final product.

In an alternative pathway, nitrate is converted to ammonia in a process called dissimilatory nitrate reduction to ammonia (DNRA). After a two–electron reduction of nitrate, nitrite undergoes through a six-electron reduction into ammonia directly. This reaction is catalysed by cytochrome c nitrite reductase (Nrf), a deca-haem homodimeric enzyme.

1.1.3 Nitrogen fixation

Nitrogen fixation is the most important part of the overall nitrogen cycle. The availability of nitrogen in the bio-accessible forms, ammonium or nitrate, is a crucial factor for plant growth.

A lack of nitrogen nutrients will decrease the productivity of any agricultural land. Nowadays, nearly half of global nitrogen fixation is carried out by nitrogen-fixing microorganisms and the other half is processed by the chemical industry. Only a small amount of dinitrogen in the atmosphere is fixed under extreme conditions during lightening, by which dinitrogen combines with dioxygen to yield nitrogen oxides which successively react with water and precipitates down to Earth as nitric acid in the rain.

1.1.3.1 Biological nitrogen fixation

Although dinitrogen gas makes up more than three quarters of the lower atmosphere, it cannot be utilised directly by most living organisms due to its inertness. In the biosphere, only a special group of microorganisms called diazotroph is responsible for conversion of dinitrogen into biologically accessible ammonia. These bacteria contain the NIF gene encoding the enzyme nitrogenase, which can catalyse the nitrogen reduction reaction under ambient conditions. These are two types of diazotroph; free-living bacteria in soil (e.g. *Azotobacter*) and symbiotic bacteria living in the root nodules of specific plants (e.g. *Rhizobia* associated with legume plants and *Frankia* associated with alder trees). Under nitrogen-deficient conditions, the host plant will form a symbiotic relationship with nitrogen-fixing bacteria by developing the root nodules. Within the root nodules, anaerobic conditions are provided for the oxygen-sensitive nitrogen fixing enzymes. The microbes obtain energy from photosynthesis product of plants while plants will gain nitrogen nutrients back. Therefore, legume plants are usually included in rotation crop for replenishment of nitrogen in the soil.

1.1.3.2 The Haber-Bosch process

At the beginning of the twentieth century, the invention of the synthetic nitrogen fixation process called the ‘Haber-Bosch process’ allowed unrestricted access to nitrogen-containing fertilizers, which led to the development of modern agriculture and the growth of the world

population. Fritz Haber and Carl Bosch developed the synthesis of ammonia from dinitrogen and hydrogen gas using an iron-based catalyst at high temperatures and pressures (about 400 °C and 200 bars), which earned them two Nobel prizes (Haber in 1918 and Bosch in 1931). Since then, modern agriculture has relied upon the production of ammonia fertilizers.

In the Haber-Bosch process, dinitrogen and dihydrogen molecules adsorb on the metal catalyst surface, then the intramolecular bonds are split and the two different species recombine to form the product ammonia. The rate determining step of this reaction is the cleavage of the dinitrogen triple bond.[7] The high temperature is required to overcome this kinetic barrier, while the high pressure is applied in order to shift the thermodynamic equilibrium of the reaction towards the formation of ammonia molecules. The key steps in the reaction mechanism are shown below.[8]

$$N_{2(g)} \rightarrow N_{2ad} \rightarrow 2N_{ad}$$

$$H_{2(g)} \rightarrow H_{2ad} \rightarrow 2H_{ad}$$

$$N_{ad} + H_{ad} \rightarrow NH_{ad} \xrightarrow{+H_{ad}} NH_{2\,ad} \xrightarrow{+H_{ad}} NH_{3\,ad} \rightarrow NH_{3\,(g)}$$

1.1.3.3 Future tends

In recent years, human activities have contributed approximately 45% to global nitrogen fixation through the production of nitrogen fertilizers.[5, 9] As the global population increased dramatically after the industrial revolution, the fertilizer demand for increasing crop yields and food production rose rapidly. In 2012, the Haber-Bosch process produced over 400 million tonnes of nitrogen fertilizer.[10]

On the other hand, this procedure consumes a large amount of energy (1.2% of global primary energy consumption)[11] and uses natural gas as a major hydrogen source. Thus, many scientists have been interested in ways to enhance the efficiency of nitrogen fixation.

First, it has long been sought to improve some parts of the Haber-Bosch process by adding promoting agents such as potassium, alumina and cobalt to the Fe catalyst to increase the activity, or by replacing the Fe-based catalyst with a more active ruthenium-based one to lower operating pressure. Nonetheless, it is predicted that the main part of this conventional process will remain unchanged for the next 15 years as the new technology takes time to scale up into an industrial one.

The second effort is to use genetic engineering to modify nitrogen-fixing bacteria to be compatible with other host species or to directly insert a nitrogen-fixing gene into a plant, especially cultivated plants.[12] In theory, these self-nitrogen fixing crops will reduce the demand of conventional fertilizers. However, the additional process of nitrogen fixation might consume more energy than that plant could produce by photosynthesis process and might lower total crop yields. A balance of energy consumption between ammonia production and carbohydrate synthesis has to be carefully considered.

Alternatively, a range of biologically-inspired organometallic catalyst has been designed aimed at reduction of dinitrogen under mild condition by mimicking the active site of the enzyme nitrogenase. For example, a Mo-containing catalyst with a triamidoamine ligand ($HIPTN_3N$) can catalyse reduction of dinitrogen to ammonia under ambient conditions (Figure 1-3A).[13-15] A synthetic Fe-based catalyst with a tris(phosphine)borane ligand has been reported to bind dinitrogen and reduce it to ammonia, with 7.0 NH_3 equivalents per Fe equivalent under mild conditions (Figure 1-3B).[16] A hemilabile role of the boron centre in this complex was suggested to be similar to that of the carbon atom of the FeMoco cluster.

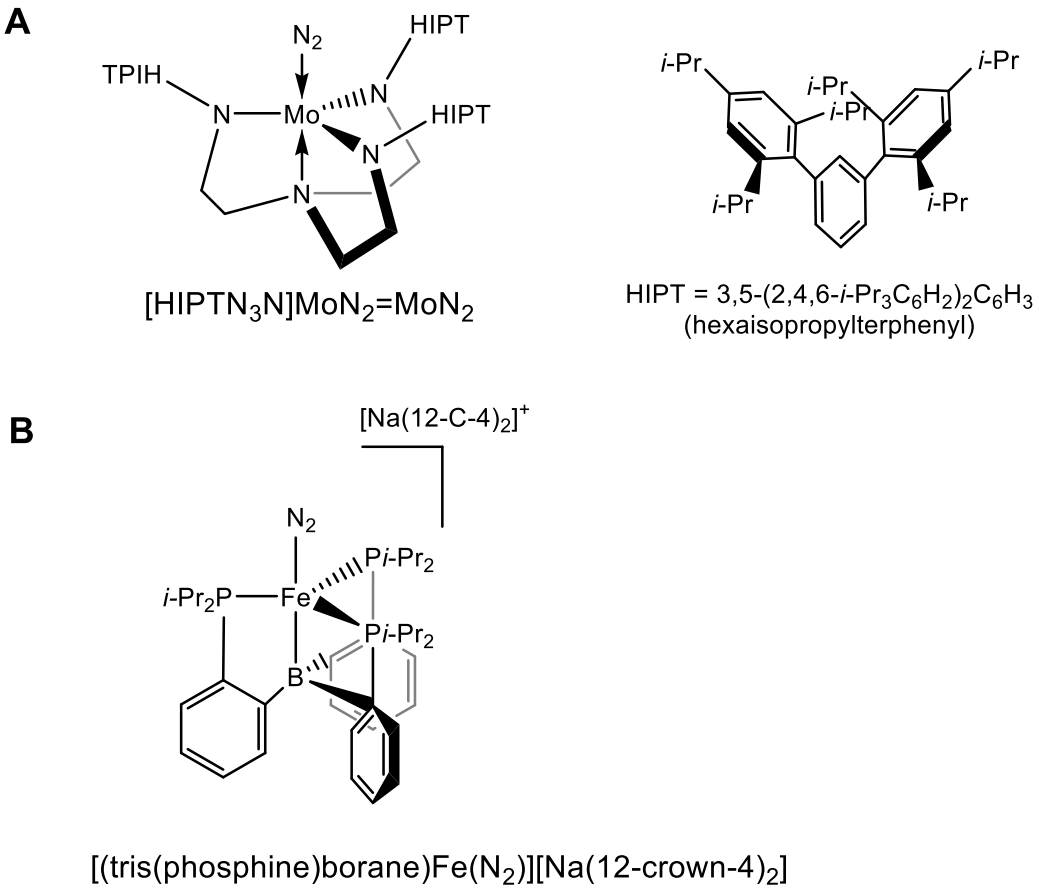

Figure 1-3: Structures showing a dinitrogen binding site on mononuclear catalysts for reduction of dinitrogen (A) $[HIPTN_3N]MoN_2{=}MoN_2$ complex (HIPT; hexaisopropylterphenyl)[13] and (B) $[(tris(phosphine)borane)Fe(N_2)][Na(12\text{-}crown\text{-}4)_2]$ complex. [16]

1.2 Nitrogenase enzymes

Nitrogenase is the enzyme found in nitrogen fixing bacteria living in the soil and in the roots of certain plants. It plays a key role in biological nitrogen fixation by catalysing the reduction of N_2 into biologically accessible ammonium ions. This enzyme-catalysed nitrogen fixation by bacteria occurs under ambient conditions of temperature and pressure. However, nitrogenase is very sensitive to oxygen and only functions under anaerobic condition.

Four classes of nitrogenase have been established so far: Molybdenum (Mo), Vanadium (V), Iron (Fe) and superoxide-dependant nitrogenase.[17-20] In the former three classes, the nitrogen reduction mechanisms are similar, although with different stoichiometries as shown in Equations 1 to 3, according to the difference in metal atoms in the active site.[21] The fourth class is different in structure and uses superoxide anion radicals (O_2^-) as the electron donor.[22]

Mo-nitrogenase : $N_2 + 8H^+ + 8e^- + 16MgATP \rightarrow 2NH_3 + H_2 + 16MgADP + 16P_i$ 1-1

V-nitrogenase : $N_2 + 12H^+ + 12e^- + 24MgATP \rightarrow 2NH_3 + 3H_2 + 24MgADP + 24P_i$ 1-2

Fe-nitrogenase : $N_2 + 24H^+ + 24e^- + 48MgATP \rightarrow 2NH_3 + 9H_2 + 48MgADP + 48P_i$ 1-3

1.2.1 Mo-nitrogenase

The most studied nitrogenase is the Molybdenum-dependent one. The Mo-nitrogenase from free-living bacteria, such as *Azotobacter vinelandii* and *Klebsiella pneumonia*, has been extensively studied for decades.[23-25] The specific *nif* genes encoding nitrogenase are highly conserved and it is believed that they were evolved very early in biological evolution.[26] Mo-nitrogenase is a binary enzyme system comprising two component proteins: the Fe protein and the MoFe protein, as shown in Figure 1-4.

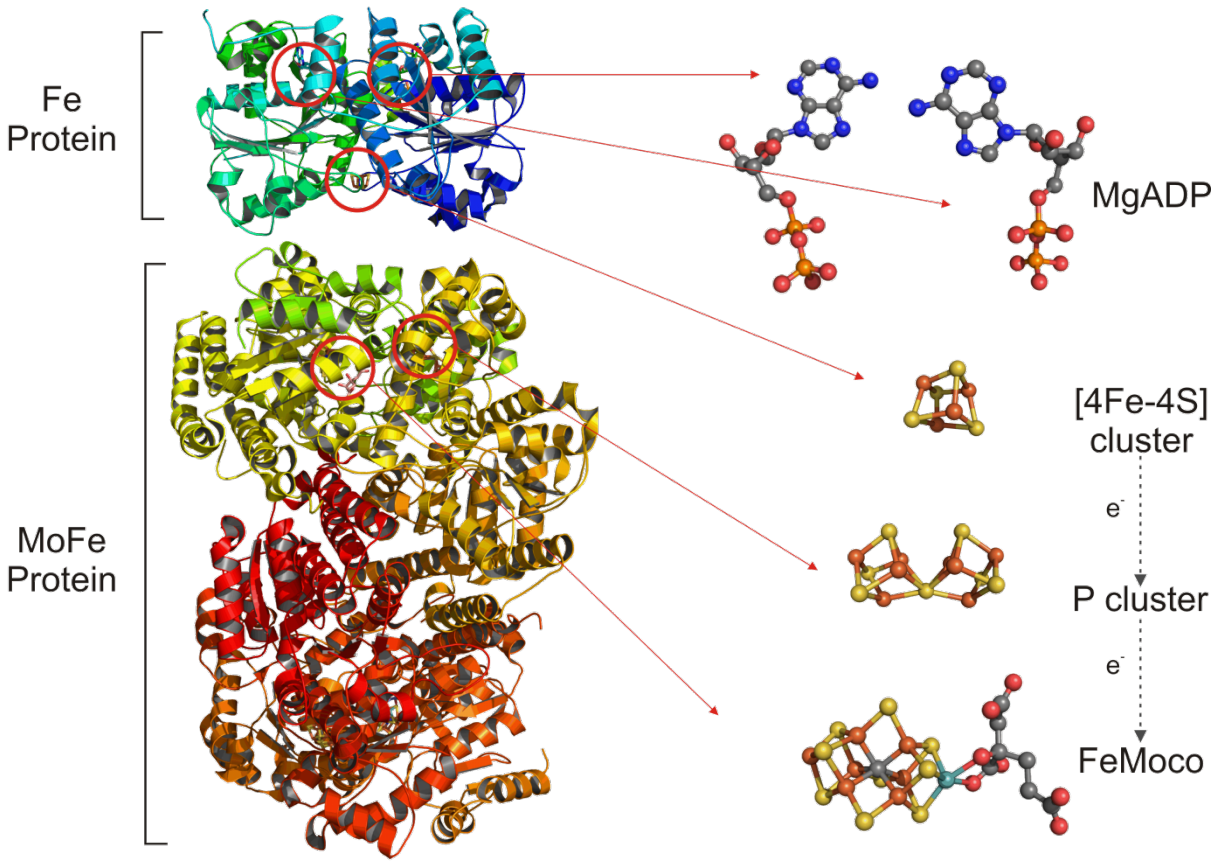

Figure 1-4: Structures of the Fe protein and MoFe protein of nitrogenase from *Azotobacter vinelandii* (1FP6 and 3U7Q from RCSB PDB, respectively) showing locations of its prosthetic groups. All cofactors shown in stick-and-ball format with Fe, S, N, P, O, C and Mo atoms represented as brown, yellow, blue, orange, red, grey and cyan spheres, respectively.

1.2.1.1 Fe protein

The Fe protein is a α_2-homodimer ($M_r \approx 64{,}000$ kDa) containing one ATP binding site in each subunit and a [4Fe-4S] cluster bridge in between. The [4Fe-4S] cluster is coordinated by four thiol groups from cysteine amino acid residues as shown in Figure 1-5. It is encoded by *nifH* and also called nitrogenase reductase or component II, due to the fact that it serves as an electron transmitter to the MoFe protein during enzyme turnover. The Fe protein requires hydrolysis of a pair of ATP to complete each electron transfer from [4Fe-4S] cluster. This Fe protein component is the only known reductant which can activate the MoFe protein to reduce dinitrogen to ammonia successfully. Apart from shuttling electrons during catalysis, the Fe

protein also participates in the biosynthesis of the MoFe protein as well. The Fe protein plays a key role by inserting the Mo atom and an *R*-homocitrate molecule into a precursor cluster to complete the maturation of FeMoco.[27]

The [4Fe-4S] cluster has two oxidation states involved in the electron transfer to the MoFe protein: $[4Fe\text{-}4S]^{+}$ and $[4Fe\text{-}4S]^{2+}$.[19] However, it was found that the all-ferrous state $[4Fe\text{-}4S]^{0}$ could be achieved using low potential reductants like Ti^{III}-citrate, Cr^{II}-EDTA, Eu^{II}-EGTA or Eu^{II}-DTPA.[28-30]

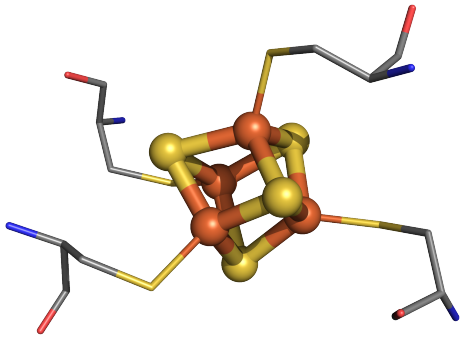

Figure 1-5: A [4Fe-4S] cluster of the Fe protein ligated by four cysteine amino acids, two from each of protein subunits (generated from 1FP6 PDB file). Fe, S, N, P, O, and C atoms are represented in colour brown, yellow, blue, red, and grey, respectively.

1.2.1.2 MoFe protein

The MoFe protein (also called dinitrogenase or component I, M_r ≈250,000 kDa) is a $\alpha_2\beta_2$-heterotetramer, encoded by *nifDK*. Each αβ-dimer contains one [8Fe-7S] cluster called the P-cluster, and one iron-molybdenum cofactor called FeMoco.

Iron-molybdenum cofactor

The active site of nitrogenase, the FeMo cluster or FeMoco, is a [Mo-7Fe-9S-C-homocitrate] complex, which can be considered as [4Fe-3S] and [Mo-3Fe-3S] clusters jointed together with three bridging sulphides (S^{2-}) and one carbide (C^{4-}) in the centre as shown in Figure 1-6. This unusual cluster resides in each α subunit and is bound to the surrounding protein *via* only

two amino acid residues, one is α-275^{Cys} *via* a thiol group to the terminal Fe atom and the other is α-442^{His} *via* an imidazole group to the terminal Mo atom, which is also coordinated to an *R*-homocitrate ligand.

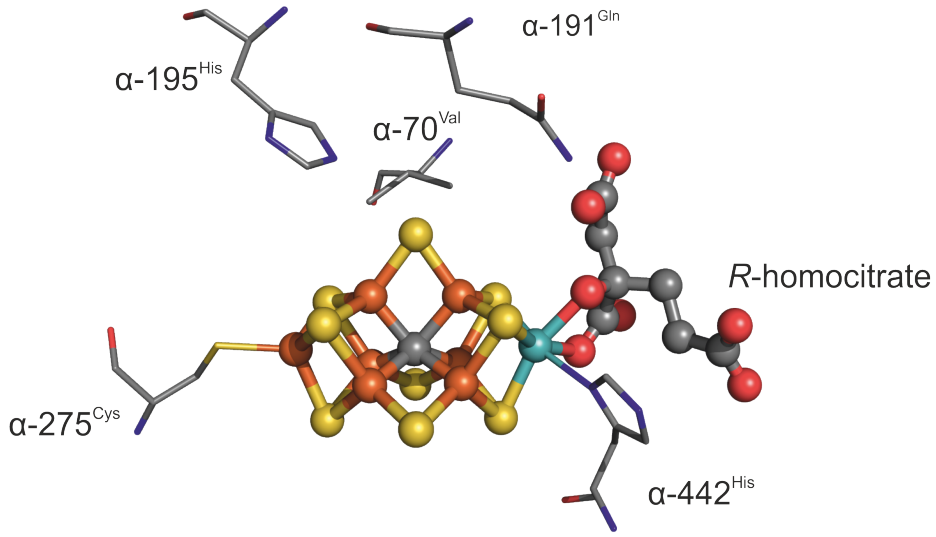

Figure 1-6: The FeMoco of nitrogenase shows as ball-and-stick format (generated from 3U7Q PDB file). The coordinated amino acids and some nearby residues were located as in the MoFe protein. Fe, S, N, O, C and Mo atoms are represented in colour brown, yellow, blue, red, grey and cyan, respectively.

Interestingly, this interstitial atom inside FeMoco cluster was discovered by Einsle *et al.* using a high-resolution crystallographic analysis (at 1.16 Å) and was thought to be either C, N or O atom due to its electron density.[31] This atom had been referred to as X until it was identified as a carbon atom simultaneously by Spatzal *et al.* [32] and Lancaster *et al.* [33] Further study of nitrogenase assembly indicated that the source of this carbon atom is a methyl group of *S*-adenosyl methionine (SAM), which is inserted into the protein during the coupling between a pair of [4Fe-4S] cluster precursors to form the FeMoco.[34] A recent study showed that this central carbide was unable to be exchanged or incorporated into the product during turnover. The role of this central carbon in catalysis is still unknown.[35]

FeMoco has one *R*-homocitrate molecule ligated to the Mo atom *via* 2-hydroxy and 2-carboxy groups. Previous studies showed that substitution of the homocitrate with other homocitrate analogues, likes citrate and isocitrate, resulted in malfunctioning nitrogenase.[36] The presence of the homocitrate ligand not only contributes an overall negative charge to FeMoco, but is also able to assist in the assembly of FeMoco into the MoFe protein during the final step of biosynthesis.[37, 38] The FeMoco cluster including *R*-homocitrate can be extracted intact into the organic solvent *N*-methylformamide (NMF), where it is thought that the amide group helps to stabilise the cofactor.[39, 40] Reconstitution of the extracted cofactor into the protein enabled the enzyme to completely regain its catalytic activity.[39]

Although it has been established that the FeMoco is the active site of the enzyme, at which the substrate was bound and reduced, there is controversy about the position of substrate binding site on the cofactor. Current opinion is divided between the Fe and Mo atoms being the catalytic centre.[41-43]

P-cluster

The P-cluster of nitrogenase is a [8Fe-7S] cluster located at the interface between the α and β subunits. It is coordinated with six cysteine residues, three from each subunit. The P-cluster serves as a mediating centre in the electron transfer pathway, from the [4Fe-4S] of the Fe protein to the FeMoco of the MoFe protein accompanied by ATP hydrolysis. In addition, the biosynthesis of the P-cluster also requires the presence of both the Fe protein and ATP.[44]

The P-cluster exists in the all ferrous oxidation state in the resting state (P^N) and can be oxidised to various oxidation states although only the first two or three states are likely to be involved in the electron transfer process: P^+, P^{2+} and P^{3+}.[45] It was found that the oxidation of P^N to P^{2+} resulted in conformational changes, in which P^{2+} forms two additional bonds to the β-188^{Ser} residue and an amine group of α-88^{Cys} residue as shown in Figure 1-7.[46]

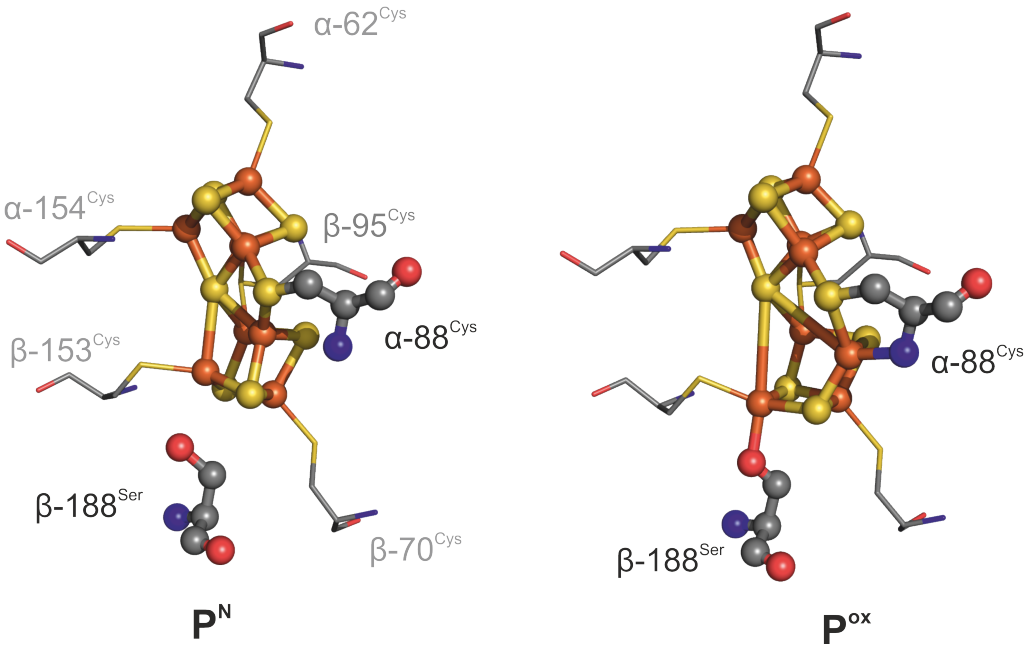

Figure 1-7: The P-cluster of nitrogenase in different redox states shows as ball-and-stick format (P^N and P^{Ox} generated from 3MIN and 2MIN PDB files, respectively).

In addition to the two metal clusters, a recent study revealed that the MoFe protein also contains an extra Fe^{II} atom 21 Å away from the FeMoco centre, located at the interface of two β subunits.[47] This ferrous centre is coordinated with six ligands in an octahedral geometry as shown in Figure 1-8.

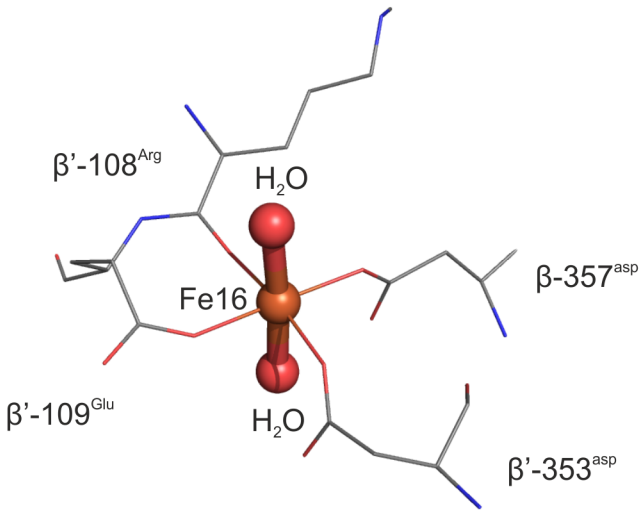

Figure 1-8: A sixteenth Fe atom of the MoFe protein coordinated with four carboxyl groups from nearby amino acid residues and two water molecules (generated from 4TKU PDB files).

1.2.2 Alternative nitrogenase

Another class of nitrogenase is vanadium-dependent nitrogenase, which is expressed in cells under molybdenum-deficient conditions. Although the Mo- and V-nitrogenase structures resemble one another, the V-dependent nitrogenase has unique components and properties. Although no crystal structure exists for the V-nitrogenase yet, recent studies have indicated that V-nitrogenase comprises protein and cofactor that are different from those in the Mo-nitrogenase in both structure, topology and electronic properties. For instance, the VFe protein of V-nitrogenase from *Azotobacter vinelandii* consists of four subunits in each dimer ($\alpha\beta\delta_2$), as compared to the MoFe ($\alpha\beta$).[48] However, the isolated FeVco from V-nitrogenase can activate cofactor-deficient Mo-nitrogenase and *vice versa*, suggesting that the difference in properties of the enzymes result from the protein and cofactor environment.[49]

1.3 Nitrogenase mechanism

One important question in studying the mechanism of nitrogenase is how a substrate is bound to the active site. Although the whole structure of nitrogenase and its cofactors has been elucidated completely, no one has successfully captured the substrate-bound state of the enzyme under turnover conditions yet. Therefore, the exact mechanism of nitrogen reduction by nitrogenase is still unknown. The major challenges lie on a complex electron transfer and uncontrollable side reaction.

1.3.1 Electron transfer in nitrogenase

Nitrogenase has a very unique electron transfer pathway: the MoFe protein can only be reduced by the Fe protein partner coupled with ATP hydrolysis. During catalysis, it needs the Fe protein to transport an electron from the electron donor to the P-cluster inside the MoFe protein. Recently, Seefeldt and co-workers proposed the ‘deficit-spending’ mechanism, as

shown in Figure 1-9.[50] It was found that at the beginning Fe protein with a reduced $[4Fe\text{-}4S]^{+}$ cluster binds to the MoFe protein and triggers conformational change within the MoFe protein. This allows a fast initial electron transfer from the P-cluster to FeMoco to take place, followed by an electron transfer from the $[4Fe\text{-}4S]^{+}$ cluster to the P-cluster coupled with hydrolysis of two MgATP molecules. Subsequently, the Fe protein with an oxidised $[4Fe\text{-}4S]^{2+}$ is dissociated.[51]

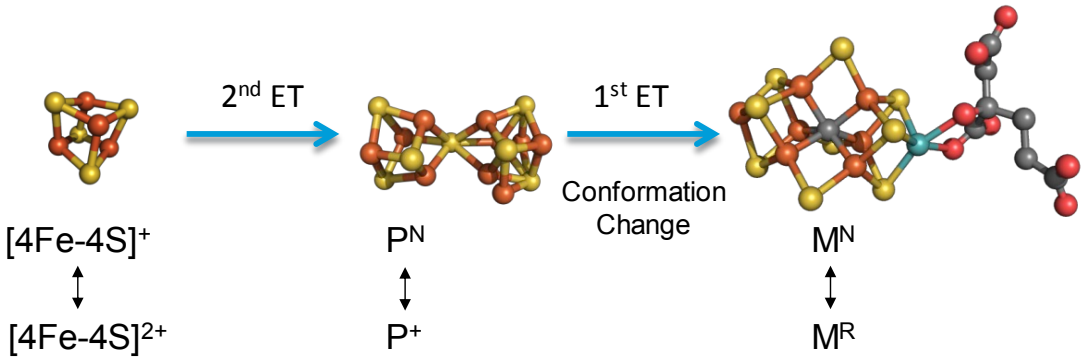

Figure 1-9: A schematic representation of electron transfer (ET) process from the [4Fe-4S] cluster of the Fe protein to the MoFe protein as proposed by Seefeldt and co-workers. (M presents the protein-bound FeMoco, N is the resting state and R is reduced state.)[50, 51]

1.3.2 Catalytic Mechanism

In dinitrogen reduction, the Mo-nitrogenase requires 8 electrons to reduce dinitrogen to ammonia and dihydrogen (H_2) as shown in Equation 1. During the catalytic cycle, FeMoco is successively reduced *via* several Fe protein cycles and undergoes several intermediate steps before products are released as shown in Figure 1-10. In the absence of substrate, nitrogenase is able to catalyse proton reduction and consume ATP.

Due to the multiple electron transfer steps, the nitrogenase catalytic reaction cannot easily be controlled and it is difficult to trap particular intermediate states during catalysis. A previous study indicated that dinitrogen can bind to the active site only at the three- or four-electron

reduced state (E_3 or E_4) and no substrate can bind to it at the resting state (E_0). Recently, it was suggested that these electrons are accumulated in metal-hydride bonds formed at FeMoco during proton-coupled reduction steps.[52, 53] This may be related to the observation that some H_2 is always produced as a by-product of N_2 fixation.

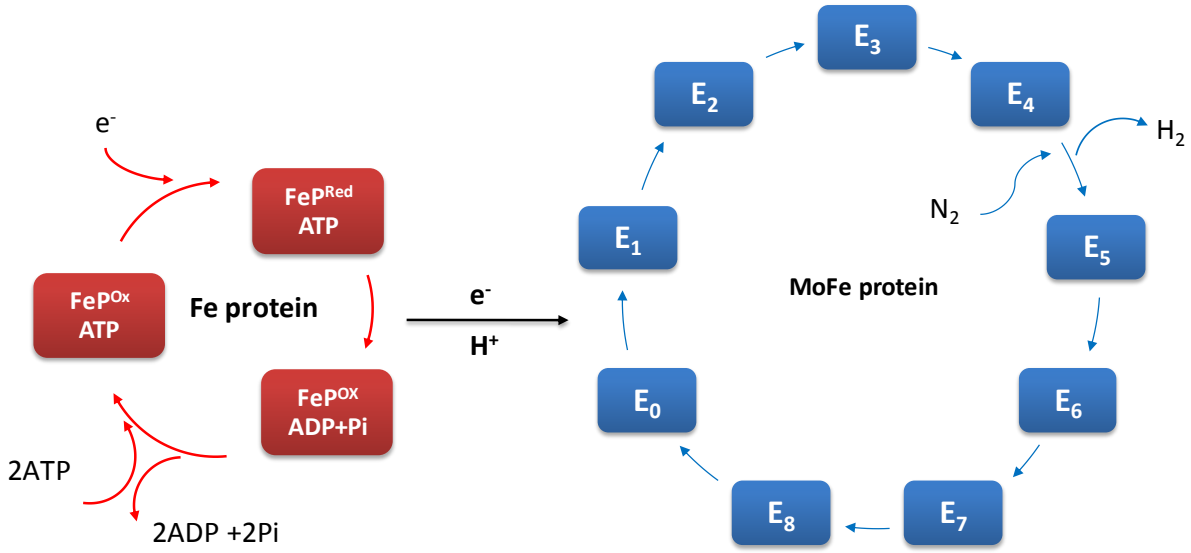

Figure 1-10: Schematic representation of nitrogenase turnover cycle adapted from the mechanism proposed by Thorneley and Lowe.[54]

This complicated mechanism makes control of electron transfer to the MoFe protein in the presence of Fe protein unfeasible. However, a genetic approach was recently demonstrated to overcome this obstruction. With genetically-modified MoFe protein, driving enzyme catalysis by a chemical reducing agent or a photoelectrochemical process is possible. Danyal *et al.* demonstrated that the variant MoFe protein (β-98$^{Tyr\rightarrow His}$) can catalytically reduce hydrazine using a Eu-polyaminocarboxylate complex as a low potential reductant.[55] Roth *et al.* showed the photocatalytic reduction of acetylene and protons by a variant MoFe protein with a Ru-photosensitizer attached.[56]

1.3.3 Reaction pathway

It is the key to the elucidation of the dinitrogen reduction pathway that the intermediate(s) are trapped during turnover by the protein. It has proven difficult to achieve this in practice as the catalytic reaction could not be synchronised. So far, two different reaction mechanisms have been proposed: distal and alternating. The former mechanism involves hydrogenation of the distal N atom and release of the first NH_3 product before reduction of another N atom. This scheme is paralleled with mechanism of dinitrogen reduction catalysed by mononuclear Mo complexes.[57, 58] The other proposed mechanism is known as the alternating pathway, in which N_2 is bound and protonated at either one or more binding sites. In the alternating scheme, the N–N bond is cleaved and two NH_3 are released near the end of the cycle. This scheme is mainly supported by the observation that nitrogenase is able to reduce hydrazine, one of the potential intermediates proposed in the pathway.[59-61]

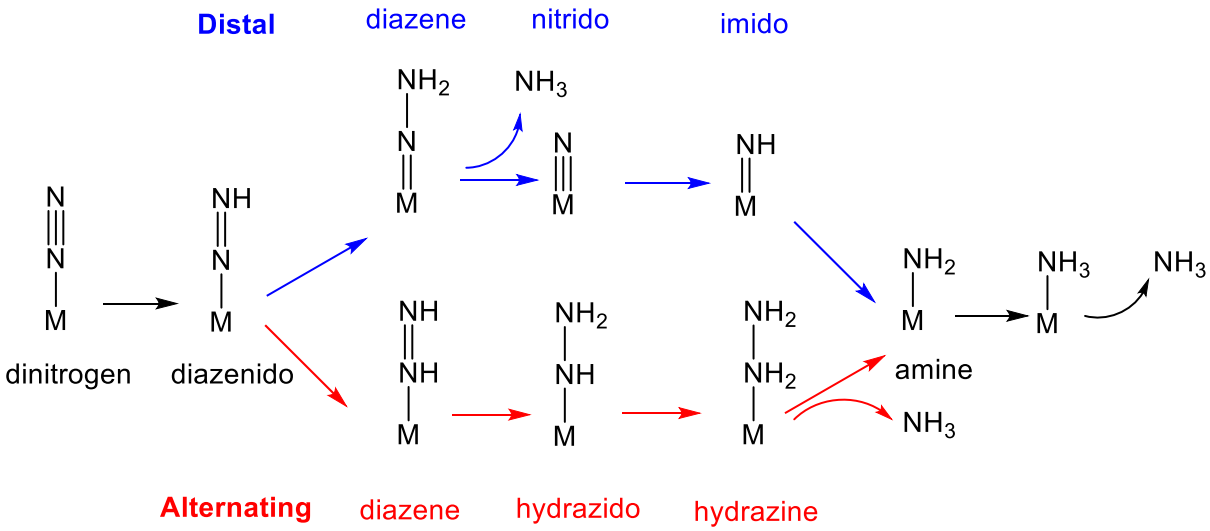

Figure 1-11: Two proposed reaction pathways for the reduction of dinitrogen by nitrogenase (M represents the binding site on the FeMoco cluster).

1.4 Substrates and inhibitors

Apart from physiological substrates, dinitrogen and proton, Mo-nitrogenase is also capable of catalysing the reduction of other small multiply-bonded substrates such as ethene, ethyne (acetylene) and propyne.[62] It is still unclear whether these reactions may be involved in the physiological function of the enzyme or be a part of an ancient metabolic pathway. On the other hand, some small molecules act as inhibitors of nitrogenase, *e.g.* CN^-, CO and NO.[63, 64] A difference effect of inhibitors has been observed on various substrate reductions as shown in Table 1-1.

Table 1-1: Nature of inhibition in the Mo-nitrogenase (adapted from work of Hwang *et al.*).[63]

substrate	Inhibitor						
	N_2	N_3^-	acetylene	CN^-	CH_3NC	H_2	CO
N_2		-	non-competitive	non-competitive	–	competitive	non-competitive
N_3^-	–		non-competitive	competitive	competitive	no inhibition	non-competitive
Acetylene	–	non-competitive		–	–	no inhibition	non-competitive
ATP hydrolysis	enhanced	enhanced	inhibited	enhanced* (<3 mM)	enhanced* (<10 mM)	no inhibition	no inhibition
Proton reduction	inhibited	inhibited	inhibited	inhibited	inhibited	no inhibition	no inhibition

* enhanced at low concentration only

Non-competitive inhibition is generally a result of an inhibitor binding to an enzyme at a different site from the substrate. However, as in a redox enzyme, it is possible that non-competitive inhibition is caused by an inhibitor binding to the same site of an enzyme as the substrate but in a different oxidation state. Thus, a study of inhibitors like CO and cyanide coordinated to nitrogenase can be used as the model for binding of the substrate to the enzyme.

1.4.1 Dinitrogen

Dinitrogen is the main physiological substrate of nitrogenase for the production of ammonia. Although dinitrogen is abundant in the atmosphere, it is unreactive with most reducing agents under mild conditions. There are many factors that contribute to the inertness of dinitrogen molecule. The triple bond between the two N atoms is one of the strongest bonds among molecules (bond dissociation enthalpy 946 kJ mol^{-1}), which requires a large amount of energy to cleave it. The dinitrogen molecule has 10 valence electrons with the electron configuration $1\sigma_g^2 1\sigma_u^2 1\pi_u^4 2\sigma_g^2$, as in Figure 1-12. A large energy gap between the highest occupied molecular orbital (HOMO) and the lowest unoccupied molecular orbital (LUMO) makes it difficult to accept electrons from a mild reducing reagent. Also, the low polarisabilty of the dinitrogen molecule makes it unreactive for formation of coordination complexes. However, in some case, dinitrogen can coordinate to a metal centre, *e.g.* $[Ru(NH_3)_5(N_2)]^{2+}$, with an end-on binding mode.[7, 57, 58] As a ligand, dinitrogen can participate in π-backbonding with strongly reducing metals, in which electron density from the metal is transferred into the $1\pi_g$ orbitals of nitrogen.

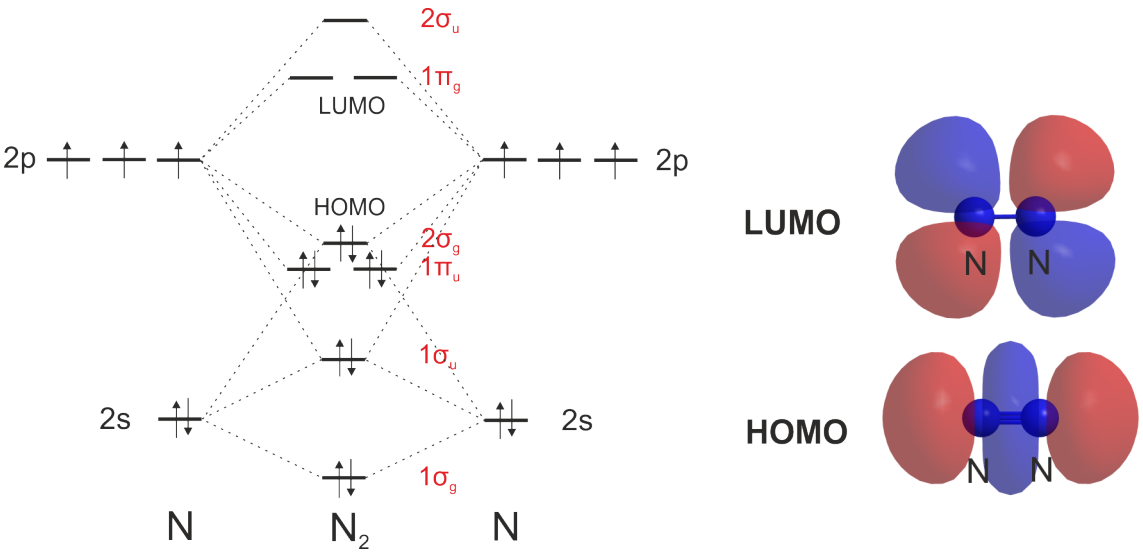

Figure 1-12: A diagram of molecular orbital energy level of dinitrogen molecule (left). Only valance electrons are shown here. The HOMO and LUMO of dinitrogen are shown as Hückel molecular orbitals (right) (calculated by extended Hückel method, ChemBio 3D).

For the reduction of nitrogen, the overall reaction is exergonic and exothermic so the reaction is thermodynamically feasible but the major obstacle is the large kinetic activation energy. The large amount of energy is required to break bonds and form intermediate complexes in the reaction as illustrated in Figure 1-13.[65] For this reaction to proceed, nitrogen-fixing organisms have to use 16 ATP molecules, which is a high metabolic cost. The mechanism for this reaction is still unclear as no enzyme-bound intermediate has been trapped to confirm it.

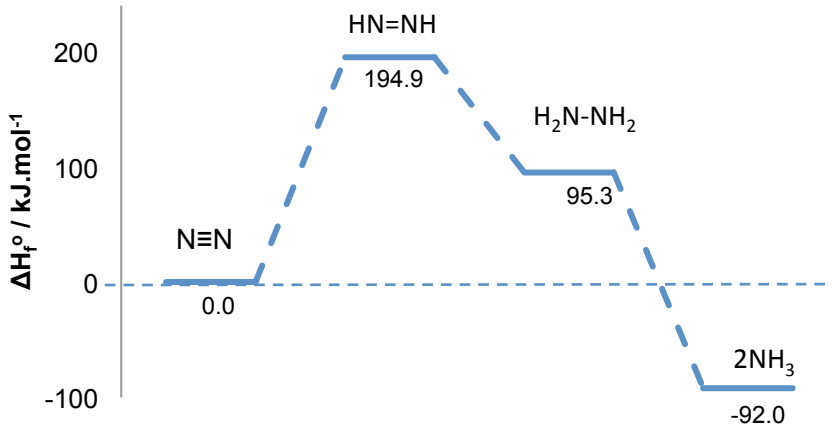

Figure 1-13: Potential energy diagram for the reduction of dinitrogen *via* the proposed mechanism with intermediate diazene and hydrazine.[65] Standard enthalpies of formation (ΔH_f^o) from ref. [66].

1.4.2 Carbon monoxide

Carbon monoxide (CO) is a diatomic gas which is isoelectronic with dinitrogen. It has a triple bond with a bond length similar to that dinitrogen (112.8 pm) but a larger bond dissociation energy (1072 kJ.mol^{-1}). It has the electron configuration $1\sigma^2 2\sigma^2 1\pi^4 3\sigma^2$ as shown in Figure 1-14. The HOMO (3σ) has non-bonding character and is localised on the carbon atom, while the LUMO (2π) is antibonding.

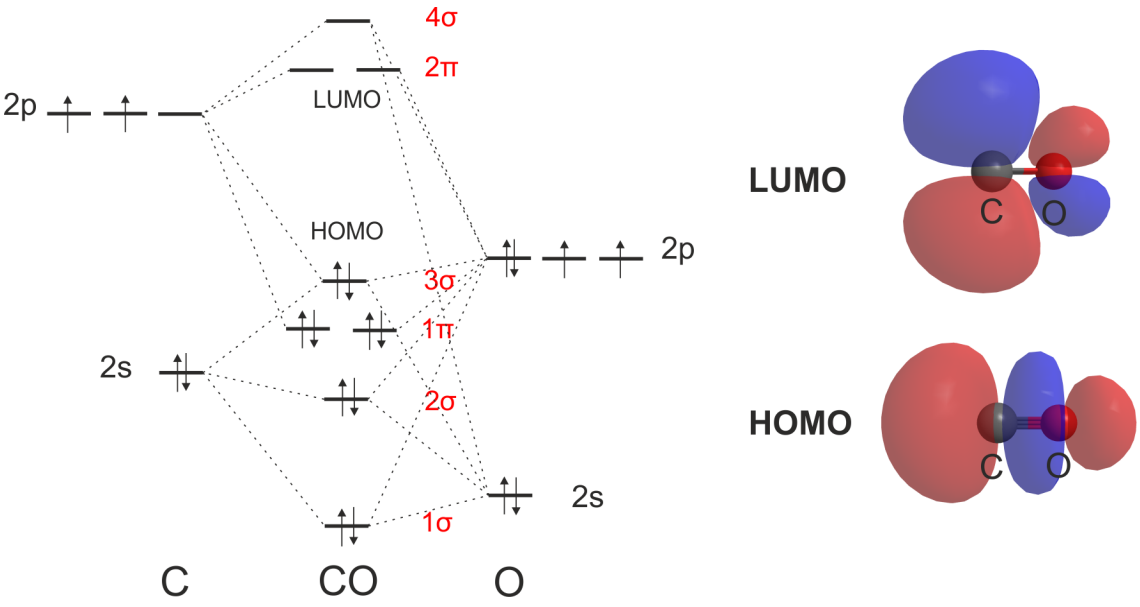

Figure 1-14: The diagram of molecular orbital energy level of CO (left). The HOMO and LUMO of CO are shown as Hückel molecular orbitals (right) (extended Hückel method, ChemBio 3D). The HOMO of CO is largely nonbonding and localised on C atom.

CO is a strong-field ligand with poor σ-donor but good π-acceptor characteristics. It can form a coordination complex with low oxidation metal centres *via* π backbonding. The HOMO of CO donates its 'lone pair' of electrons to the metal d-orbitals to form a σ bond, while the π* LUMO of CO accepts electrons from the d orbitals of the metal to form a π bond. This π-back donation strengthens the bond between the metal and CO (M–CO) but weakens the triple bond of CO (C–O) since the antibonding π* orbital is occupied.

Previous studies have established that CO acts as a non-competitive inhibitor for nitrogenase.[63, 67, 68] However, Ribbe and co-workers recently reported that V-nitrogenase from *Azotobacter vinelandii* is able to catalyse the reduction of CO to C_2H_4, C_2H_6 and C_3H_8 under conditions of 100% CO.[69] They investigated further and found that the source of hydrogen in the hydrocarbons is protons from the solution.[70] A study by Seefeldt and coworkers showed that modified MoFe protein, $\alpha\text{-}70^{Val\rightarrow Ala/Gly}$, is also able to catalyse reduction of CO to hydrocarbons.[71] Ribbe and co-workers demonstrated slow CO reduction by wild type Mo-nitrogenase from *Azotobacter vinelandii,* resulting in the formation of small hydrocarbon chains.[72] They reported further that the isolated cofactor from both Mo- and V-nitrogenase can reduce CO and CN^- using low potential Eu^{II}-polyaminocarboxylate complexes as a reductant.[73]

1.4.3 Cyanide

Cyanide (CN^-) is isoelectric with CO and N_2 and has similar yet different molecular orbitals as shown in Figure 1-15; the 3σ HOMO is slightly antibonding and the 2π LUMO is antibonding which leads to some difference in its coordination chemistry. As a ligand, CN^- has stronger σ-donor but poorer π-acceptor character than CO. It is capable of coordinating to both low and high oxidation state metals due to its σ-donor property. The higher oxidation state of the metal atom the stronger the σ bond of the cyano-metal complex.

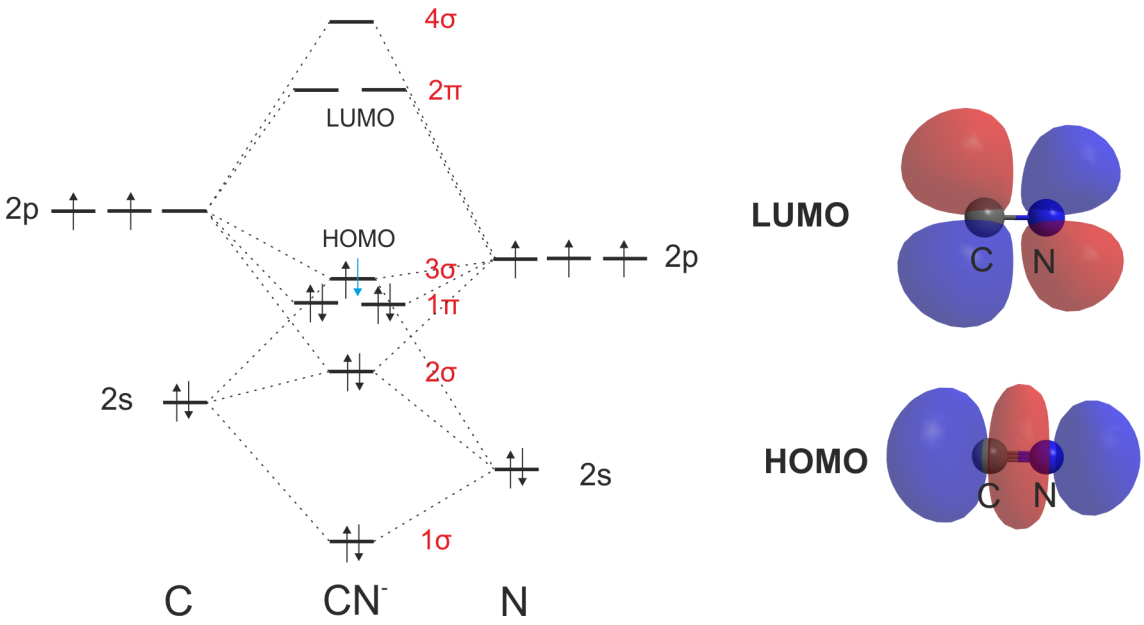

Figure 1-15: The diagram of molecular orbital energy level of CN^- ion (left). Nitrogen atomic orbital has lower energy than the carbon one because nitrogen is more electronegative than carbon. An additional electron is from the ion charge (blue arrow). The HOMO and LUMO of CN^- are shown as Hückel molecular orbitals (right) (extended Hückel method, ChemBio 3D).

For nitrogenase, Burgess and coworkers reported that CN^- is a reversible inhibitor but HCN is a substrate for the enzyme, which it reduces to methylamine or methane and ammonia as shown in the equations below.[74]

$$HCN + 4H^+ + 4e^- \rightarrow CH_3NH_2 \qquad 1\text{-}4$$

$$HCN + 6H^+ + 6e^- \rightarrow CH_4 + NH_3 \qquad 1\text{-}5$$

Later, it was proposed that HCN and CN^- bind to the same site, possibly by replacing a ligand at the active site, and they bind to nitrogenase in a more oxidised state than N_2 and protons.[75]

Later, Seefeldt and coworkers used a genetic approach to demonstrate that cyanide and acetylene can react with specific amino acid-substituted MoFe proteins, α-96^{Gln}, α-96^{Leu}, α-96^{His} and α-96^{Ala}, in the resting state (EPR signal S = 3/2 level).[76] Also, Roth *et al.* showed that Ru-photosensitiser-modified MoFe protein is capable of photoreduction of HCN.[77]

1.5 Methods for studying nitrogenase

Nitrogenase has been of great interest since biological nitrogen fixation was discovered in 1880, with the enzyme first extracted in 1960. Many advanced physical techniques have been employed to study nitrogenase. A large amount of data on structure and mechanism has been gathered to solve the puzzle of this enzyme but some pieces of information are still missing from the whole picture.

1.5.1 X-ray crystallography

Protein X-ray crystallography is the essential technique used to determine the structure of proteins. A diffraction pattern is obtained from scattering of X-rays by a crystal of protein and gives structural information about the protein including electron density, atom dimension and bond length.

The crystallographic structure of nitrogenase protein components were first reported by Rees and co-workers in 1992, showing the structure of the active site as a [Mo-7Fe-8S] cluster ligated with *R*-homocitrate.[78-80] The existence of the internal atom in the active site was discovered later in the high resolution (1.16 Å) crystal structure reported by Einsle *et al*.[31] They later identified this central atom as carbon using data from the higher resolution (1.0 Å) structure.[32] The crystallographic method has been used in conjunction with different genetically-modified nitrogenase variant to obtain more data on the role of each cofactor and protein residue. For example, the crystal structure of α-$70^{Val\rightarrow Ile}$ MoFe protein was used to study the role of the α-70 residue in controlling substrate access to the binding site.[81]

1.5.2 X-ray spectroscopy

X-ray absorption spectroscopy (XAS) is one of X-ray based techniques that have been used to study nitrogenase. The energy of incident X-rays can be absorbed by the protein where it

excites electrons in the constituent atoms, giving useful information on the oxidation state and chemical environment of each element of the complexes. For nitrogenase, XAS was used to determine electronic structure of the metal clusters. The structures of MoFe and VFe protein, including their isolated cofactors, were investigated in the extended X-ray absorption fine structure (EXAFS) region. It showed that both species have similar electronic structures.[82-84] Additionally, it found that the FeVco cluster had a distorted octahedral symmetry.[49] This XAS result is useful since no crystal structure is available for the V-nitrogenase yet.

X-ray emission spectroscopy (XES) is another technique that gives useful information on electronic structure of each element in the complexes. Recently, XES spectra were used to help assign the central atom in the FeMoco as carbon.[33]

1.5.3 EPR spectroscopy

Electron paramagnetic resonance (EPR) spectroscopy is widely used to study Fe in the redox site of metalloproteins. This technique is restricted to paramagnetic species as it relies on resonant absorption of microwave radiation by unpaired electrons in a magnetic field. An EPR spectrum of the MoFe protein of nitrogenase in the resting state showed that the FeMoco exhibits an S=3/2 rhombic signal but the P-cluster is EPR silent (S=0), presumably as all Fe are in 2+ oxidation state. Under turnover conditions, the S=3/2 EPR signal from the FeMoco disappeared.[85] In addition, the isolated FeMoco in NMF exhibited the S=3/2 EPR signal in the dithionite-reduced state and is EPR silent in the oxidised state,[40] similar to that of the enzyme-bound FeMoco. For the Fe protein, the dithionite-reduced $[4Fe\text{-}4S]^{+}$ cluster exhibits both S=1/2 and S=3/2 EPR signals, which disappears when the cluster is oxidised to $[4Fe\text{-}4S]^{2+}$.[85] Moreover, the interaction between inhibitor can be monitored by a change in EPR signals. For instance, when CO binds to the cofactor during turnover, it exhibits three different sets of EPR signals depending on the concentration of CO and other conditions.[86-88]

1.5.4 Electrochemistry

Electrochemical techniques are useful for studying a dynamic system like a redox enzyme. In the case of nitrogenase, due to the restriction on direct electrochemical control of the enzyme, a mediated electrochemical approach is often applied to study the redox properties of the enzyme. The midpoint potentials of cofactors have been determined by potentiometric titration with redox mediators in conjunction with EPR spectroscopy. It was reported that the [4Fe-4S] cluster in the free Fe protein had a midpoint potential of the first redox couple $[4Fe\text{-}4S]^{2+/+}$ at *ca* –300 mV *vs* SHE and shifted to –420 and –460 mV upon MgATP and MgADP binding, respectively.[89, 90] The P-cluster was found to have the same midpoint potential for the first two redox couples, $P^{+/N}$ and $P^{2+/+}$, at –307 mV while the third couple $P^{3+/2+}$ had a higher midpoint potential at +90 mV.[24] The protein-bound FeMoco has a midpoint potential for the first oxidised couple ($M^{ox/N}$) at –42 mV,[24] but it was found that further reduction of FeMoco required much lower potential redox mediators. Interestingly, it was reported that the binding between the Fe protein to the MoFe protein shifted the midpoint potential of the cofactors to more negative values; the potential shifted to –620 mV for the $[4Fe\text{-}4S]^{2+/+}$ couple and to –390 mV for the $P^{2+/N}$ couple, as shown in Figure 1-16.[91] This indicates that the interaction between the two protein components has a great effect on the redox properties of the enzyme.

The redox property of the isolated FeMoco has also been investigated using electrochemical measurements. A cyclic voltammogram of the extracted FeMoco in NMF show at least three redox processes, leading to assignment of the redox states: oxidised, semi-reduced, reduced and super-reduced, as shown in Figure 1-16.[40, 92] The addition of ligands, like thiophenol, CO and CN^-, changed the reduction potentials of this isolated cofactor, indicating different ligand binding has an impact on the redox properties of the cofactor.[92-94]

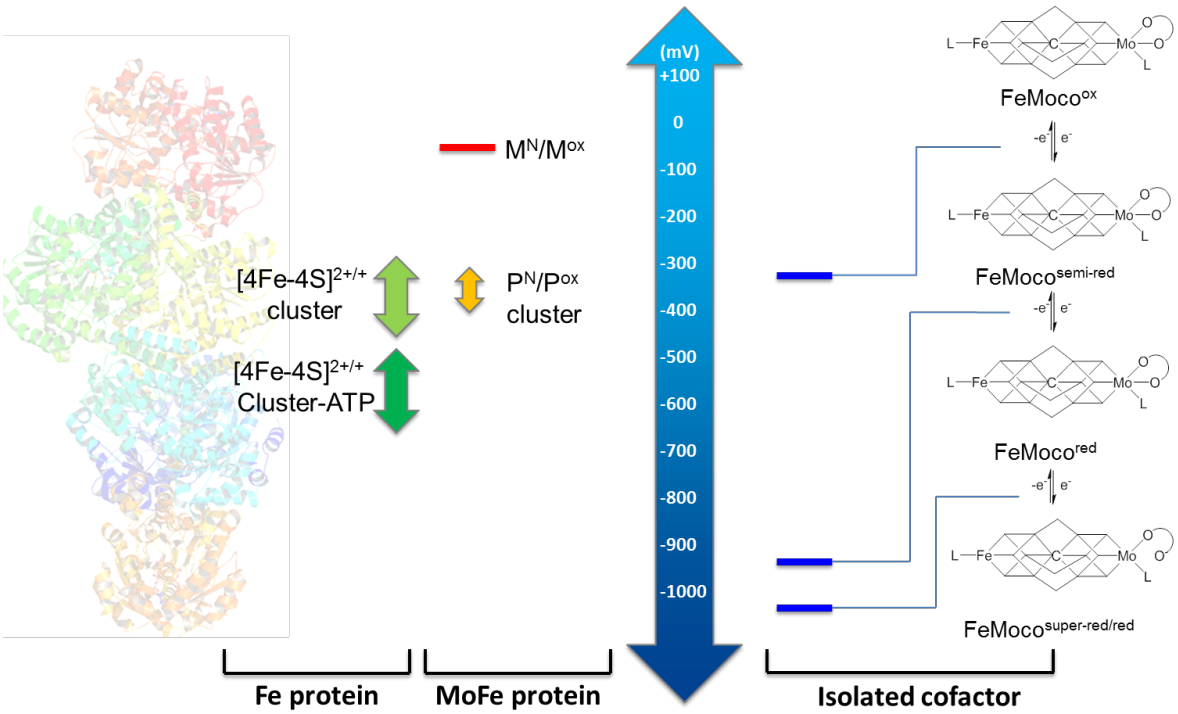

Figure 1-16: The midpoint potentials of the enzyme-bound cofactors (left) and the isolated FeMoco (right).

1.5.5 IR spectroscopy

Infrared spectroscopy is based on absorption of mid-infrared light in range 400-4000 cm^{-1} by a molecule. An IR spectrum shows transitions in the vibrational energy levels of molecules and gives information on the chemical bonds present and thus the molecular structure. It can be applied to study biological molecules containing an IR chromophore such as hydrogenase, which contain CO and CN^- ligands at the active site;[95, 96] but it can also be used to characterise exogenous ligand binding to metal centres inside proteins. Many small π-acid ligands, such as CO, CN and isocyanide (RNC), have strong absorption bands in a part of the IR region which is clear of other protein vibrational features. These small molecules can be used as a probe to study metal centre of metalloproteins, as seen in studies of CO binding to the haem proteins myoglobin and cytochrome *c*.[97-99]

For nitrogenase, the study of π-acid ligands bound to the active site have been of interest for many years; particularly CO, as it is isoelectronic with N_2. The studies of CO binding to

nitrogenase from *K. pneumoniae* and *A. vinelandii* have been carried out using a stopped-flow IR spectroscopy (SF-IR) approach.[68, 100] In the SF-IR setup shown in Figure 1-17, a solution of CO-saturated ATP and a mixture of Fe protein and MoFe protein were mixed in the IR cuvette in the optical path. The results showed that CO-bound nitrogenase exhibited two different sets of peaks for CO stretching, ν(CO), under different conditions: a ν(CO) peak at 1904 cm^{-1} at a low CO concentration (~60 µM CO) and ν(CO) peaks at 1880, 1906, 1936 and 1960 cm^{-1} at a high CO concentration (~0.5 mM). The former was assigned to bridging CO binding and the latter were assigned as terminal CO species. This indicated that the ligand concentration affected the number and mode of CO species bound. The SF-IR technique was also used to continuously monitor the reduction of azide, CO inhibition and ATP hydrolysis by nitrogenase.[59] It showed that azide reduction was inhibited in the presence of CO. However, these interactions required the presence of Fe protein and ATP to supply electrons to the MoFe protein continuously, resulting in a mixture of states. Thus, the redox states at which CO bound to the cluster are undetermined.

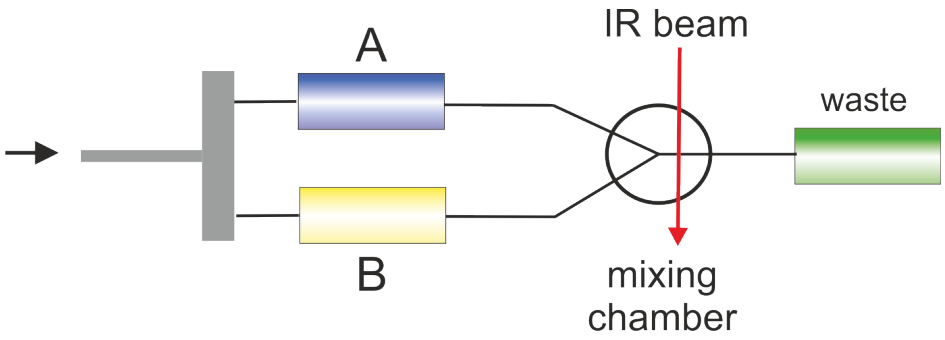

Figure 1-17: A schematic diagram of the stopped-flow and IR cuvette system. (Adapted from ref. [101])

1.5.6 IR spectroelectrochemistry

The concept of spectroelectrochemistry (SEC) is to spectroscopically investigate electrochemically-generated species in the sample. With infrared spectroelectrochemistry (IR-SEC), it is possible to monitor a ligand with an IR-active vibration bound to a redox site under

electrochemical control. For example, IR-SEC can be used to monitor a change in coordination chemistry of a metal ion inside a protein environment following reduction. Thus IR-SEC can give insight into mechanistic pathways by monitoring inhibitors or intermediates generated during turnover of an enzyme. This technique can be usefully applied to study ligand binding to many metalloproteins (e.g. myoglobin, ferredoxin, and cytochrome c) and redox enzymes like hydrogenase and carbon monoxide dehydrogenase.[102-106]

Previously, the IR-SEC technique has been used to investigate the ligand binding to the isolated FeMoco. It showed that CO could be coordinated with FeMoco upon reduction to the reduced state.[92] Upon reduction, a ν(CO) peak shift to lower wavenumber was observed, indicating increased π backbonding in the reduced cluster. In addition, an increase in CO pressure led to conversion of bridging CO to terminal CO and additional CO binding, similar to the observation of the CO bound to the FeMoco inside the MoFe protein. Meanwhile, CN^- could bind at oxidised state of the isolated FeMoco.[94] This is due to the fact that CN^- is a stronger σ-donor and weaker π-acceptor than CO, thus π backbonding has less effect on cyanide and it can bind to high oxidation state metals. Moreover, it was demonstrated that CO and CN^- could synergically bind to the isolated FeMoco at the oxidised state as seen by the shifted wavenumbers of both ligands.[94] This indicated that ligand binding to the cluster is redox-dependent and the wavenumbers of bound ligands are sensitive to the change in the electron density on the cluster.

Thus, the IR SEC technique should provide a suitable platform to study the redox-dependence of ligand binding to the active site inside the protein structure. This approach could be feasible to apply to nitrogenase MoFe protein, providing suitable mediators are available.

1.6 Aims and Scope of this Thesis

The main focus of this Thesis is to study ligand binding to the active site of nitrogenase using the IR spectroelectrochemical technique. This Thesis investigates whether it is possible to electrochemically control the nitrogenase MoFe protein and its variants during spectroscopic study *via* a series of redox mediators. Spectroelectrochemical study of ligand binding should give new insight into redox chemistry of nitrogenase.

The contents of each result chapter in this Thesis are linked together but can be divided into two major parts focusing on results from electrochemical and IR spectroelectrochemical methods, respectively.

1.6.1 Development and application of mediated electrochemical control

In order to avoid the complexity of mixed redox states generated during conventional electron transfer by the Fe protein and ATP, electrochemical control on the MoFe protein is needed. Transfer of a low potential electron is required to achieve the substrate-binding oxidation level of the protein. Therefore, Chapter 3 will describe the development of a mediated electron transfer system using Eu-ligand complexes as low potential mediators, together with the model tests for other conditions required for study MoFe protein by IR spectroelectrochemical technique.

Chapter 4 will present electrochemical results from the application of mediated electrochemical control on the wild type and variant MoFe proteins. The first electrochemically-driven proton reduction by the MoFe protein, including interaction with inhibitors, will be presented and discussed.

1.6.2 Study of ligand binding to the redox sites

To combine electrochemistry and IR spectroscopy, the attenuated total reflectance (ATR) technique was employed to examine sample molecules under mediated electrochemical control. Chapter 5 describes the *in situ* spectroscopic investigation into the interaction between CO and the reduced active site of the MoFe protein, following up the observation of CO inhibition of proton reduction presented in Chapter 3. The first spectra of ATP-independent CO binding to MoFe protein will be presented and discussed.

Chapter 6 presents the IR spectroelectrochemical results of cyanide binding to the MoFe protein. A specific variant of the protein is used to study ligand binding to different redox states. The interaction between cyanide and the metal cluster will be discussed.

In Chapter 7, the redox properties of isolated FeMoco and FeVco have been studied. The results of electrochemical studies of small ligand binding to the isolated cofactors will be presented and discussed.

The overall results of electrochemical and spectroelectrochemical studies will be highlighted and concluded in Chapter 8.

Chapter 2

Theory and Methodology

Electrochemical and spectroscopic methods are the fundamental techniques used throughout this Thesis. In electrochemical studies, redox properties of the MoFe protein and the isolated cofactors were studied under either direct or mediated electrochemical control. In IR spectroelectrochemical part, the attenuated total reflectance (ATR) technique was employed to examine sample molecules under electrochemical control. This chapter will describe the theory of each approach and the experimental methods used for studying nitrogenase in this Thesis.

2.1 Electrochemistry

2.1.1 Redox reaction

In general, redox reactions involve the transfer of electrons from one species to another, a reducing agent (reductant) loses electron *via* an oxidation process while an oxidising agent (oxidant) gains electrons *via* a reduction process. Redox reactions are fundamental processes in biological systems, with a large part of the total energy requirement of many organisms coming from energy released in the oxidation or reduction of biological molecules; these

biological redox reactions are often catalysed by specific enzymes. Therefore, a range of redox enzymes have been subjected to electrochemical study.

In an electrochemical cell, a redox reaction takes place at the interface between an electrode and an electrolyte solution. In order to drive the reduction or oxidation reaction at the electrode, a certain potential is applied to the electrode, i.e. the energy of the electrons within the electrode are adjusted by means of an applied voltage as shown in Figure 2-1. In theory, reduction reactions can take place when the energy of an electron in the electrode is increased, the electrode has an applied negative potential, high enough to make the transfer into the empty LUMO of the species present in solution favourable. The electron flow (the current) measured from this process is a reduction current and is given a negative value. In contrast, if a positive potential is applied to the electrode, which lowers the energy level of the electrons in the electrode, an electron in the HOMO of a species in solution can be transferred into the electrode. An oxidation current (with a positive value) is generated in this case.

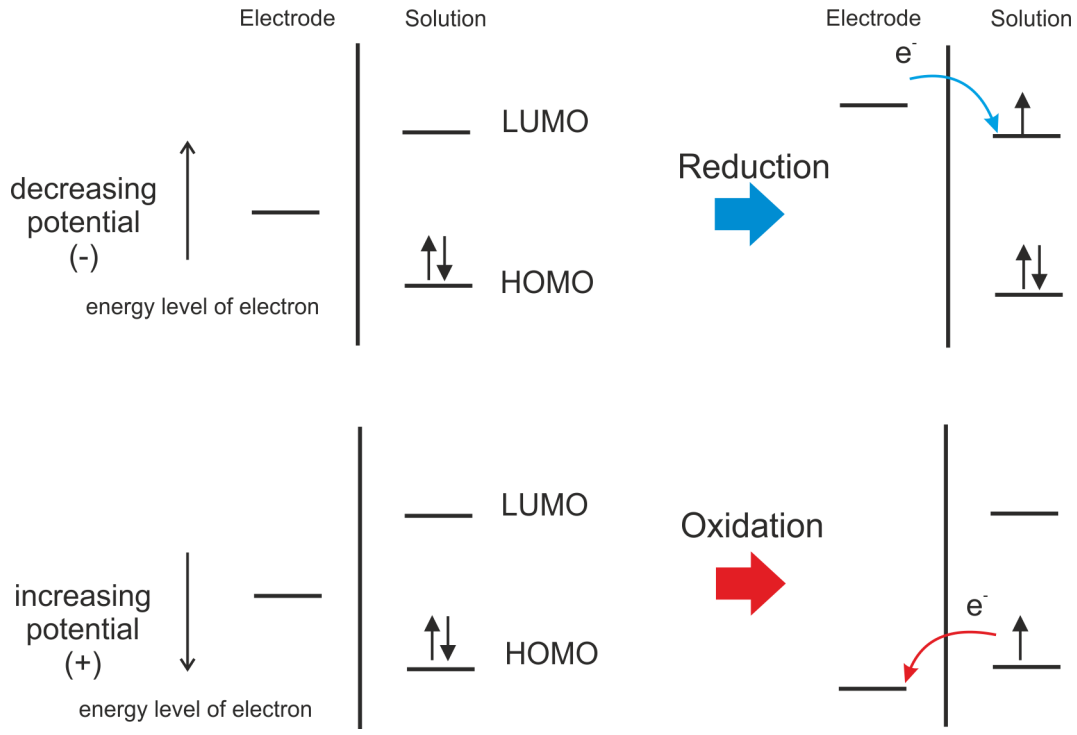

Figure 2-1: Schematic representations of reduction and oxidation processes of a species in solution occurred on the electrode surface.

2.1.2 The Nernst equation

A redox reaction consists of two half reactions: an oxidation and a reduction. Each half reaction links the reduced and oxidised form of each species in what is called a redox couple. For an overall reaction shown as:

$$A_{ox} + B_{red} \leftrightarrow A_{red} + B_{ox}$$

each half reaction with *n* electron can be written as:

$$A_{ox} + ne^- \leftrightarrow A_{red}$$

$$B_{red} \leftrightarrow B_{ox} + ne^-$$

The relationship between the equilibrium potential and the concentrations of each species present can be expressed in terms of the Nernst equation:

$$E_A = E_A^0 + \frac{RT}{nF} \ln \frac{[A_{ox}]}{[A_{red}]} \quad 2\text{-}1$$

$$E_B = E_B^0 + \frac{RT}{nF} \ln \frac{[B_{ox}]}{[B_{red}]} \quad 2\text{-}2$$

where E is electrode potential, E^0 is standard reduction potential of the redox couple, R is the gas constant, T is the absolute temperature and F is the Faraday constant.

The voltage available from the overall reaction is the difference of the potentials of two redox couples.

$$E = E_A - E_B \quad 2\text{-}3$$

Thus,

$$E = E_A^0 - E_B^0 + \frac{RT}{nF} \ln \frac{[A_{ox}][B_{red}]}{[A_{red}][B_{ox}]} \quad 2\text{-}4$$

At equilibrium, the potential difference is zero. The Gibbs free energy of reaction, $\Delta_r G^0$ is related to the potentials as shown:

$$\Delta_r G^0 = -RT \ln K \quad 2\text{-}5$$

$$K_{eq} = \frac{[A_{ox}][B_{red}]}{[A_{red}][B_{ox}]} = exp\left(-\frac{nF}{RT}(E_A^0 - E_B^0)\right) = exp\frac{\Delta_r G^0}{RT} \quad 2\text{-}6$$

$$\Delta_r G^0 = -nF(E_A^0 - E_B^0) \quad 2\text{-}7$$

In term of thermodynamics, the reaction is spontaneous if the equilibrium constant, *K*, is greater than one and the potential difference is greater than zero.

The half reaction $2H^+ + 2\ e^- \rightarrow H_2$, with protons as unit activity under 1 bar hydrogen, has been assigned the standard reduction potential of 0 at all temperatures. Therefore, the reduction potential of other redox couples can be measured and reported against the H^+/H_2 couple.

2.1.3 Faradaic and non-faradaic processes

When a voltage is applied to the working electrode, a current is observed as a result of two different processes that occur at the interface of the electrode and solution. First is the faradaic current arising from electrons transferred across the interface *via* reduction or oxidation processes. This process is described by Faraday's law, in which the number of charges transferred is proportional to the amount of chemical reactions that have taken place. As

current, I is the rate of electron flow, the number of moles, N of generated product from the reaction can be calculated using this relation:

$$I = nF\frac{dN}{dt} \qquad 2\text{-}8$$

The other current observed is capacitive current, caused by different processes that do not involve electron transfer across electrode surface, so called non-faradaic processes. A non-faradaic current could arise from different incidents such as adsorption/desorption, movement of ions in solution and structural changes at the interface.

Double-layer charging on the electrode surface is commonly responsible for the non-faradaic current observed in voltammetric measurements. Several layers of solution can be formed on the electrode surface and this electrode-solution interface can act as capacitor. When a potential is applied across the interface, different charges will accumulate on the electrode and solution sides, called the electrical double layer as shown in Figure 2-2.

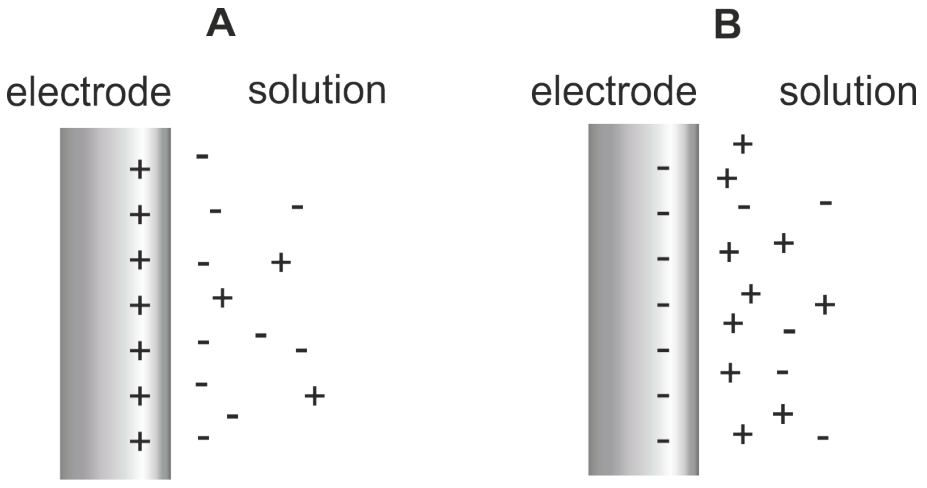

Figure 2-2: A diagram representative of double layer on the electrode-solution interface; (A) positive charge reflect deficiency of electron on electrode and (B) negative charge arising from excess electron on the electrode.

2.1.4 Electron mediation

A study of the electrochemical properties of nitrogenase is challenging as direct electron transfer from a working electrode to the active site of the protein is unfeasible. According to Marcus theory, the rate constant for the outer sphere electron transfer, $k_{ET,}$ depend on the activation free energy ΔG* as shown: [107]

$$k_{ET} = KAexp(-\Delta G^*/RT) \quad 2\text{-}9$$

where *K* is electronic transmission coefficient and *A* is the collision frequency.

The relationship between activation free energy ΔG* and standard Gibb free energy ΔG^0 can be expressed as;

$$\Delta G^* = \frac{(\Delta G^0 + \lambda)^2}{4\lambda} \quad 2\text{-}10$$

$$\Delta G^0 \approx nF\eta$$

where λ is the reorganisation energy for electron transfer and η is the overpotential.

k_{ET} is also related to the distance of electron transfer, *d*;

$$k_{ET} = k_0 exp(-\beta(d - d_0)) \quad 2\text{-}11$$

where k_0 is the rate constant of the electron transfer at the distance of the closest contact d_0 and β is between 8.5 – 11.5 nm^{-1}.

As k_{ET} decreases exponentially with the distance of electron transfer, a mediated electron transfer is typically required to study large proteins or those with redox sites buried far away from the protein surface. In order to minimise both *d* and λ, a small redox active molecule is

employed as a redox mediator to deliver electrons from the electrode to the redox site of the protein instead. A good redox mediator is considered to possess some of these properties:[107]

- Reversible redox properties with stable reduce and oxidised forms
- Fast electron exchange with the redox enzyme
- No auto-oxidation
- Proper solubility in aqueous solution
- A pH –independent potential

2.2 Electrochemical techniques

2.2.1 Three electrode system

In potentiostatic electrochemical techniques, the potential of the working electrode is controlled with a value chosen to acquire a current response from the chemical reaction of interest. The applied potential is determined with respect to a reference electrode, which has a constant and well-defined electrode potential. However, for a precise potential measurement, it is not ideal to have significant current passed by the reference electrode. Therefore, a counter or auxiliary electrode is required to create a closed circuit with working electrode and allow current to pass during the measurement.

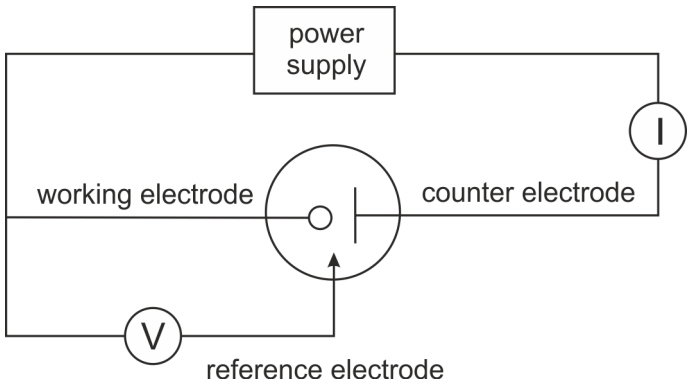

Figure 2-3: A schematic circuit diagram of a three electrode system.

In a three-electrode system as shown in Figure 2-3, a potential at the working electrode is imposed with respect to the reference electrode, with the counter electrode is adjusted to equalise the reaction on the working electrode.

2.2.2 Cyclic voltammetry

Cyclic voltammetry is an electrochemical technique whereby the current is measured while the potential applied to the working electrode is cycled between two potential values, as shown in Figure 2-4A. A cyclic voltammogram is a plot of current response as a function of potential, showing a reduction peak on the reductive sweep and an oxidation peak on an oxidative sweep. An example of a cyclic voltammogram of the $Eu^{3+/2+}$ couple is shown in Figure 2-4B. It can be seen that the reduction current increases in magnitude as the oxidised species of the redox couple in solution are reduced as the potential approaches the reduction peak potential (E_{pc}). At the reduction peak, the rate of the reduction is maximised and the current measured at this point is i_{pc}. After E_{pc}, the reduction current decreases due to effects of diffusion control. At this point the concentration of the analyte near the electrode has decreased to zero and the rate of diffusion to the electrode is slower than the rate of electron transfer. Further current flow requires diffusion of species from further and further away, at a correspondingly slower and slower rate, leading to a fall-off in the current. When the applied potential ramp is switched back, the process is reversed. Reduced species are oxidised and an oxidation current is measured. A midpoint potential can be determined in between E_{pc} and E_{pa}, which corresponds to the standard reduction potential.

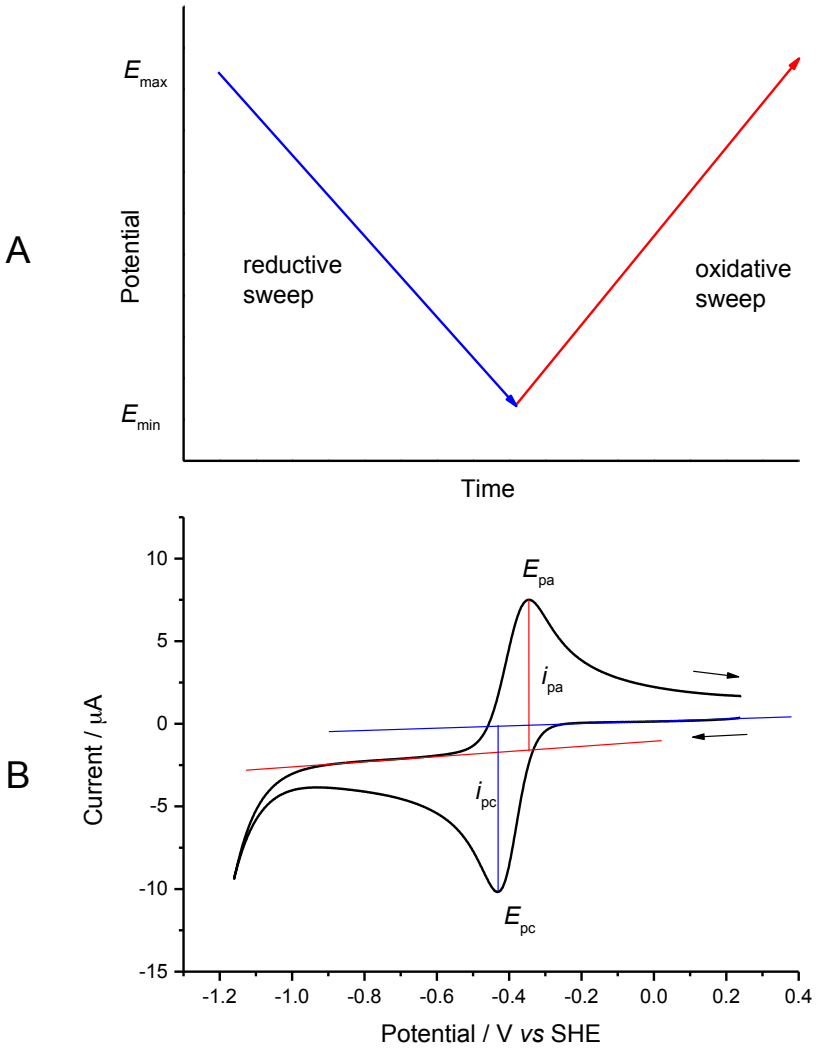

Figure 2-4: (A) A potential applied as functions of time during cyclic voltammetry. (B) A cyclic voltammogram of 2 mM $Eu^{3+/2+}$ in Tris-HCl buffer solution pH 7.4 on a glassy carbon working electrode recorded at a rate of 50 $mV.s^{-1}$.

Cyclic voltammetry can therefore give information on the reduction potential and redox nature of the analyte. In a reversible system, the ratio of current from reduction and oxidation is nearly unity (i_{pa}/i_{pc} ~1) and the different between E_{pc} and E_{pa} depends on the number of electron passed in the process, n as shown;[108]

$$\left|E_{pc} - E_{pa}\right| = 2.218\frac{RT}{nF} \quad \text{or} \quad \frac{57}{n}\ \text{mV at 298 K} \qquad 2\text{-}12$$

2.2.3 Chronoamperometry

Chronoamperometry is an electrochemical technique, in which one constant voltage is applied to the working electrode at the time and the current response is measured as a function of time. A series of potential steps can be applied to monitor a redox change at each potential. Also, it can be applied to study inhibition of a redox enzyme by introducing an inhibitor to the solution during a current measurement at a certain potential.

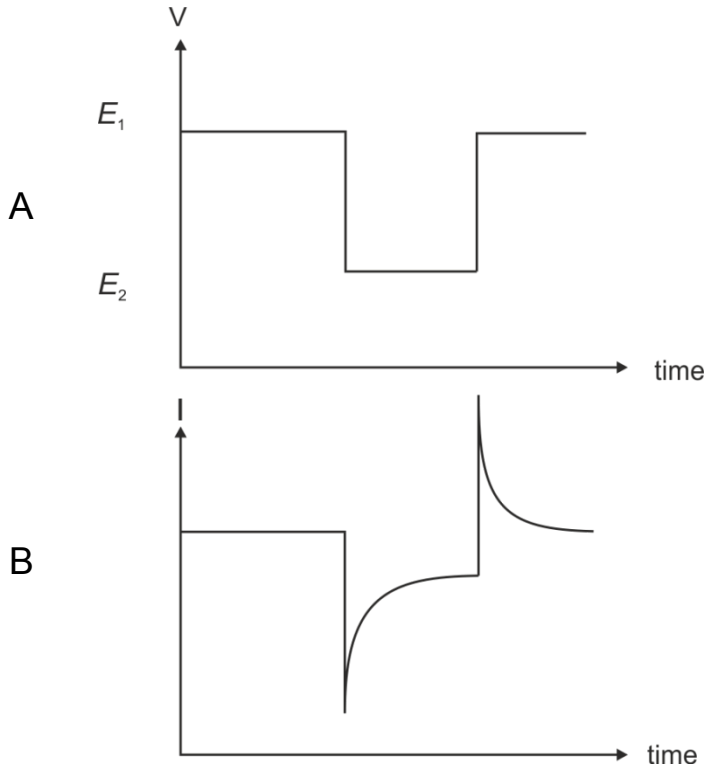

Figure 2-5: A plot of applied potential (A) and current response (B) as a function of time.

For the chronoamperogram in Figure 2-5, when the applied potential is stepped to a more negative potential, the reduction current from the faradaic process is overwhelmed by a large negative current arising from the charging process occurring in the double layer on the working electrode lasting about 10 s. A similar process takes place when a more positive potential step is applied, with a positive charging current observed. After that, current from the reduction process decreases exponentially with time as the concentration of the redox

active species near the electrode decreased. The decay of the measured current, I, as a function of time, t, for a planar electrode is given by the Cottrell equation as shown below,

$$I = nFAJ = \frac{nFAc^0\sqrt{D}}{\sqrt{\pi t}} \qquad 2\text{-}13$$

where A is surface area of the planar electrode (in cm^2), J is the flux of redox analyte, c^0 is initial concentration of the analyte ($mol.cm^{-3}$) and D is the diffusion coefficient of the analyte.

2.3 Infrared Spectroscopy

2.3.1 Vibrational energy

The energy of a molecule can be considered as a combination of three components: electronic energy (E_{ele}), vibrational energy (E_{vib}) and rotational energy (E_{rot}).

$$E_{total} = E_{ele} + E_{vib} + E_{rot}$$

The molecule can absorb a quantum of energy if it matches the transition energy between the ground and excited level of a molecule as shown in Figure 2-6.

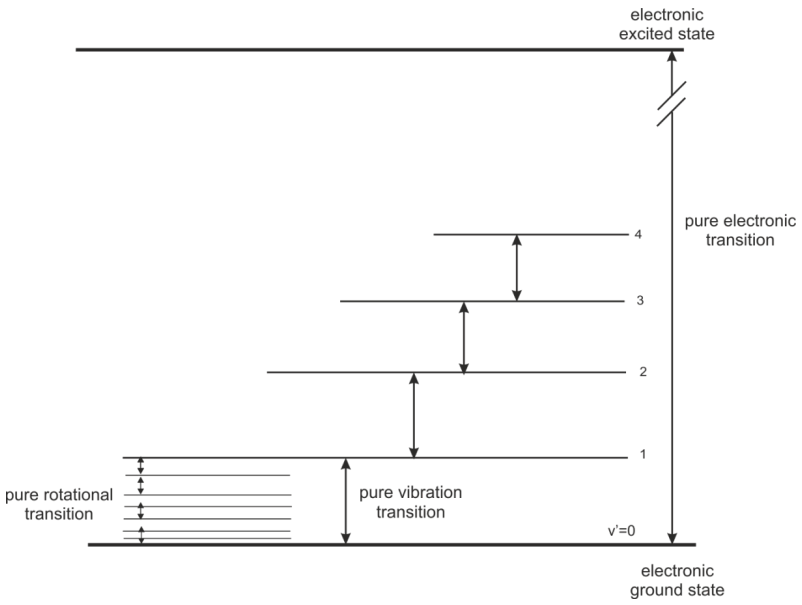

Figure 2-6: A diagram showing simplified energy level of diatomic molecule (not to scale).

From the relation between frequency (v) and wavenumber ($\tilde{v}$);

$$v = \frac{c}{\lambda} \quad \text{2-14}$$

$$\tilde{v} = \frac{1}{\lambda} \quad \text{2-15}$$

Thus, the energy difference between two quantised states that the molecule can absorb or emit can be written as:

$$\Delta E = hv = hc\tilde{v} \quad \text{2-16}$$

Infrared (IR) radiation is electromagnetic radiation with a wavelength between *ca* 1 – 1000 μm or wavenumber between 10 – 10,000 cm^{-1}. The IR region can be divided into three parts, the near-IR (1 – 2.5 μm or 4,000 – 10,000 cm^{-1}), mid-IR (2.5 – 25 μm or 400 – 4,000 cm^{-1}) and far-IR (25 – 1,000 μm or 10 – 400 cm^{-1}). The vibration transitions of molecules appear in the wavenumber range 100 – 10,000 cm^{-1}. Therefore, mid-IR spectroscopy is the most commonly used range to study the fundamental vibrations of molecules.

According to the harmonic oscillator selection rule, the transition is allowed if $\Delta v = \pm 1$. However, only the fundamentals from the translation from $v = 0$ to $v = 1$ in the ground state can be observed generally, as the vast majority of molecule are in the ground state. The number of vibrational modes of a molecule containing N atoms can be determined as $3N–5$ modes for a linear molecule and $3N–6$ modes for a non-linear molecule. The vibrational mode is infrared-active if it results in a net change in the electric dipole moment of a molecule. Therefore, the number of active modes depends on the symmetry of the molecule.

In the simple harmonic model, the molecule is modelled as point masses joined together with springs. According to Hooke's law, the restoring force, F, is proportional to the displacement, x. The potential energy, V, of such a harmonic oscillator at position x is determined as:

$$F = -kx \tag{2-17}$$

$$V = -\frac{1}{2}kx^2 \tag{2-18}$$

The wavenumber of molecular vibrations can be calculated as;

$$\tilde{\nu} = \frac{1}{2\pi c}\sqrt{\frac{k}{\mu}} \tag{2-19}$$

where k is the bond force constant (indicative of the bond strength) and μ is the reduced mass of the two masses m_1 and m_2,

$$\mu = \frac{m_1 m_2}{m_1 + m_2} \tag{2-20}$$

Therefore, the wavenumber of an IR absorption can provide primary information on the bond strength and functional group of a compound, as shown in Figure 2-7.

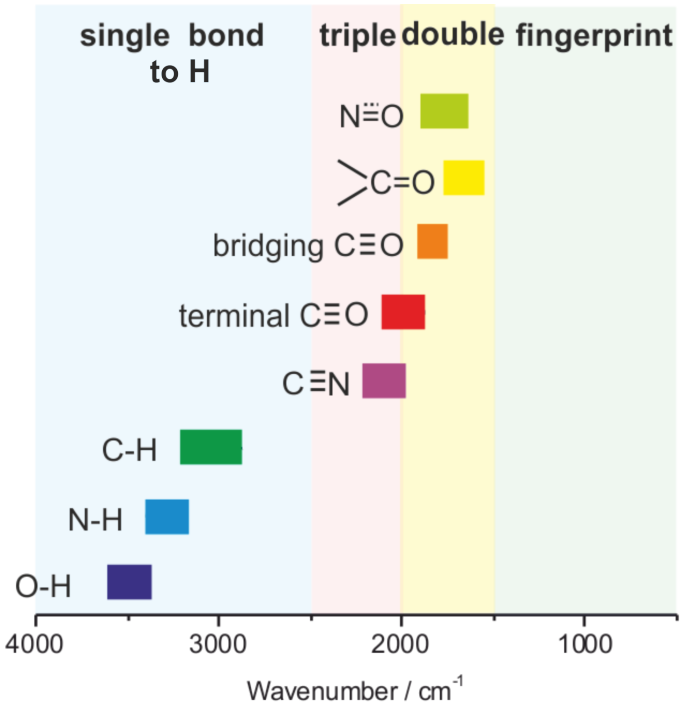

Figure 2-7: The fundamental stretching wavenumber of some common molecular species.

2.3.2 Electronic effect

IR spectroscopy can be applied to study the coordination chemistry between the metal and ligand in organometallic complexes. When coordinated with a transition metal, π-acid ligands act as σ-donors and π-acceptors. The position of the absorption peak in an IR spectrum can indicate the influence of the metal on the ligand's electron density and bond strength. In this Thesis, two ligands, CO and CN^-, were used as probes to study the active site of nitrogenase.

Carbonyl complexes

In the case of CO, as a poor σ-donor but a strong π-acceptor, π back-donation plays an important part in complex formation between CO and low oxidation state metal atoms. When CO is coordinated to a *d*-metal centre, electrons from the relatively non-bonding HOMO on the C atom of CO is transferred to empty orbitals of the metal atom forming a weak σ bond, while electrons from filled *d* orbitals are transferred to the empty π* LUMO of CO forming a

strong π bond as shown in Figure 2-8. This bonding is synergistic and can occur only when the metal atom has *d* orbitals with suitable π symmetry.

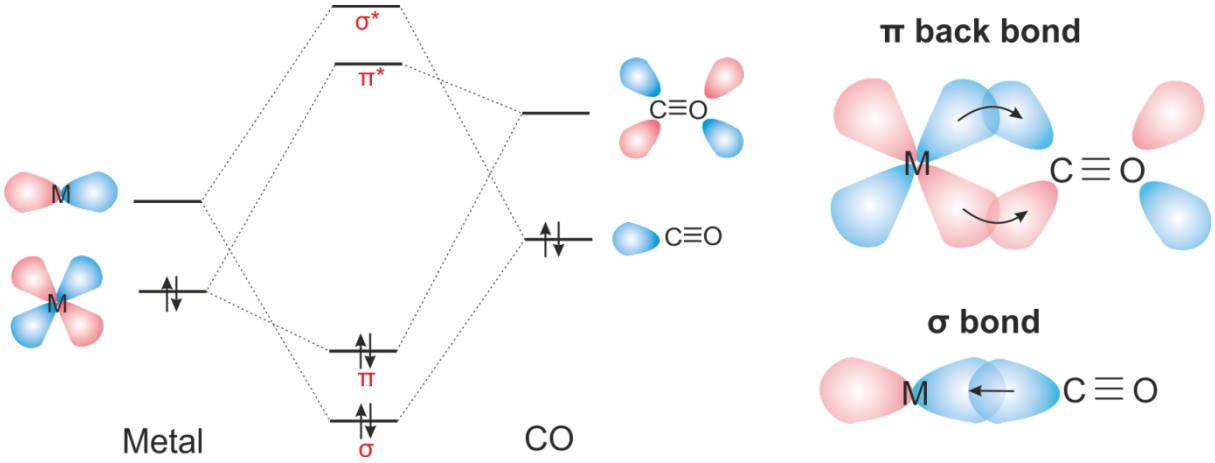

Figure 2-8: A molecular orbital diagram of metal-carbonyl coordination (left). Schematic representation of molecular orbitals in σ-bonding and π-bonding (right).

As the π orbital on the CO ligand is anti-bonding, π back-donation significantly strengthens the metal–CO bond but weakens the C-O triple bond which results in a decrease in the vibrational wavenumber for the CO stretching mode *ν*(CO). The *ν*(CO) wavenumber is sensitive to electron density on the metal centre; an increase in negative charge on the central atom lowers the *ν*(CO) wavenumber in the complex. For example,[109]

	***ν*(CO) / cm^{-1}**
free CO	2143
$Ni(CO)_4$	2094
$[Co(CO)_4]^-$	1946
$[Fe(CO)_4]^{2-}$	1788

In addition, the CO ligand can be coordinated to more than one metal atom by forming a bridging bond. In general, bridging CO has a lower wavenumber than terminal CO because of

an increase in electron density on the π anti-bonding orbital from more π back-donation. The typical wavenumber ranges for terminal CO and bridging CO species are 1900 – 2100 and 1600 – 1900 cm^{-1}, respectively.

In biological systems, CO is one of the most important signalling molecules. One example of CO binding to metalloproteins is carboxymyoglobin (MbCO), which is the protein myoglobin with a CO molecule bound to the Fe^{II} atom of its haem centre, in an end-on linear geometry.[110] In this geometry, the π-back donation from *d* orbitals of the Fe to π* orbitals of CO is dominant over the σ-bonding from σ orbitals of CO to the empty orbitals of Fe as shown in Figure 2-9. As a result of π-backbonding, the C-O bond in MbCO is weakened so it exhibits ν(CO) absorption around 1940 – 1960 cm^{-1}. As the *ν*(CO) wavenumber is sensitive to a change in the nearby protein environment, CO can be used as a probe to study the role of each amino residue inside the protein pocket.

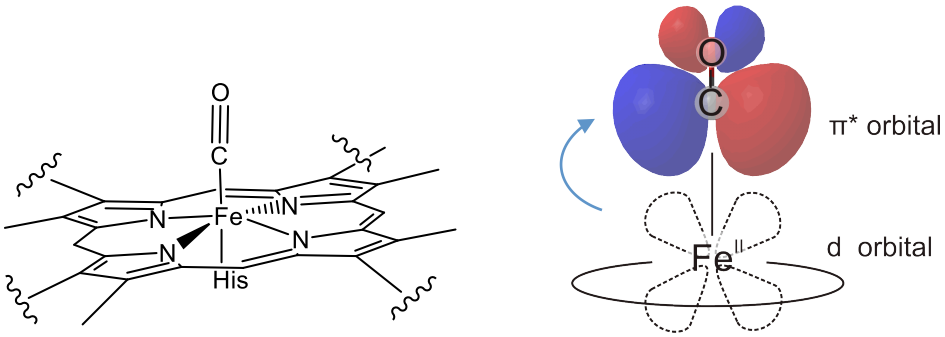

Figure 2-9: A schematic molecular orbital diagram showing π-back donation from the Fe atom to CO. The Fe-C-O angle is close to 180° and helps maximise the backbonding effect in the carboxymyoglobin complex.

Cyano complexes

Cyanide is a stronger σ-donor and weaker π-acceptor than CO, thus π back-bonding has less effect on cyanide and it can form a complex with high valent metals. When cyanide binds to metals in a higher oxidation state, a strong σ bond to the metal centre is formed *via* charge

transfer from the slightly anti-bonding HOMO of CN^- to the metal orbital. This σ bonding stabilises the C–N bond leading to an increase in wavenumber for the CN stretching mode *ν*(CN). On the other hand, when the central metal atom is reduced, CN^- can act as π acceptor to accept charge donation from reduce metal atom into π anti-bonding LUMO, resulting in a *ν*(CN) peak shift to lower wavenumber. The major factors that increase *ν*(CN) wavenumber are electronegativity and oxidation number. In contrast, increase in coordination number will decrease the *ν*(CN) of the complex.

For example, in ferricyanide $[Fe(CN)_6]^{3-}$ and ferrocyanide $[Fe(CN)_6]^{4-}$ complexes, the Fe atom is coordinated with six cyanide ligands in an octahedral geometry. Both complexes have the O_h point group that can generate an infrared-active stretching mode with the T_{1u} geometry as illustrated in **Figure 2-10**.

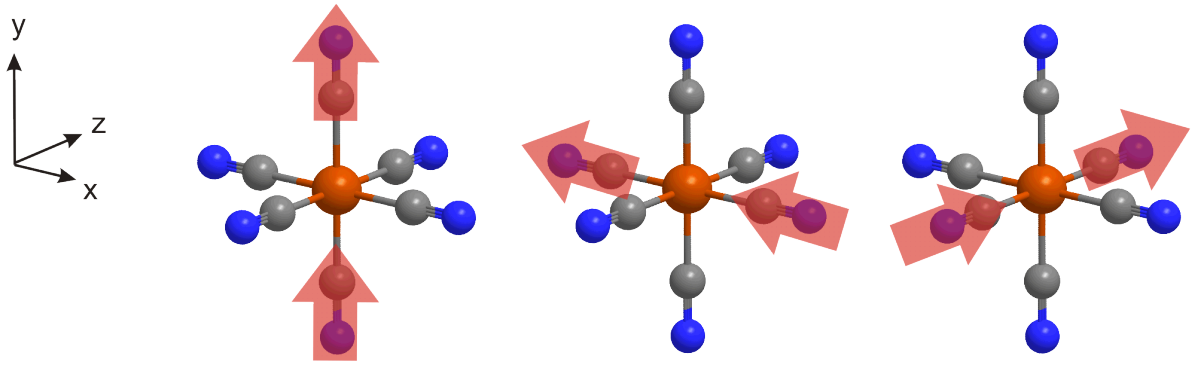

Figure 2-10: The triply degenerate IR-active stretching mode with T_{1u} symmetry in an octahedral complex.

These asymmetric stretching modes of the C–N bond (*ν*(CN)) cause a change in dipole moment of the molecules and give distinctive IR vibrational features in the mid-IR region; the ferricyanide ion ($[Fe(CN)_6]^{3-}$) shows a vibrational peak of *ν*(CN) at 2116 cm^{-1}, while the ferrocyanide ion ($[Fe(CN)_6]^{4-}$) has a *ν*(CN) peak at lower wavenumber 2036 cm^{-1}. This shift in *ν*(CN) wavenumber reflects increased back-donation as the C–N bond is more weakened by π-bonding from the metal centre with lower oxidation number.

2.4 ATR-IR spectroelectrochemistry

This study investigates whether it is possible to electrochemically control the nitrogenase MoFe protein during IR spectroscopic study. In order to combine electrochemistry and IR spectroscopy, the attenuated total reflectance (ATR) technique was employed to examine sample molecules efficiently under electrochemical control.

In the Vincent group, an ATR-IR spectroelectrochemical (SEC) technique has been developed for studying biological redox systems, for example, hydrogenase and ferredoxin.[102, 103]

2.4.1 ATR-IR technique

In the ATR method, an IR beam enters the ATR prism at an angle exceeding the critical angle, causing the internal IR beam to be totally reflected at the prism surface. This will generate an evanescent IR wave that samples protein molecules near the surface of prism as shown in Figure 2-11A. The penetration depth of the evanescent wave depends on the refractive index of the prism and sample, and varies with wavelength of the IR beam. This ATR-IR technique gives us the benefit of multiple reflections into the thin layer of sample as shown in Figure 2-11B. The number of reflections for horizontal ATR is determined by Equation 2-21; where N is number of reflections, l is the prism length, t is the prism thickness and θ is the incidence angle.

$$N = \frac{l}{2t.\tan\theta} \qquad 2\text{-}21$$

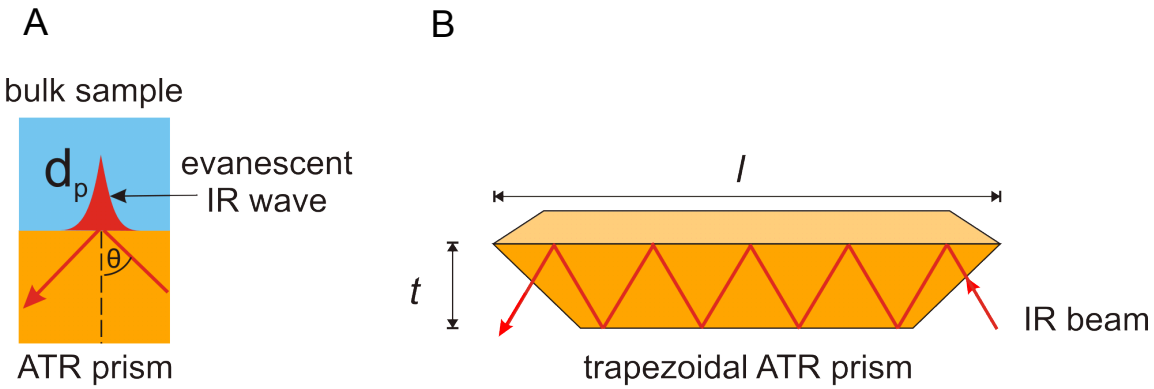

Figure 2-11: (A) Graphical representation of internal reflection at the surface of an ATR prism. (B) Specifications for the ATR prism.

2.4.2 ATR-IR spectroelectrochemical cell

The ATR SEC cell used in this work was designed by R. Hidalgo Gonzalez (DPhil. student, Oxford) and constructed by the PTCL workshop, Department of Chemistry. Figure 2-13 shows the SEC cell design fitted with a trapezoidal prism. The whole cell body and base plate were made of polyether ether ketone (PEEK). The set up was designed to be able to introduce gas or solution either directly into solution in the back of the cell or *via* the flow system while a constant potential was applied on the protein film. The ATR element used in this study is Si (8.39x5x1 mm^3 with an incidence angle of 39°, Crystal GmbH), with calculated penetration depth in aqueous solution of *ca* 0.50 µm

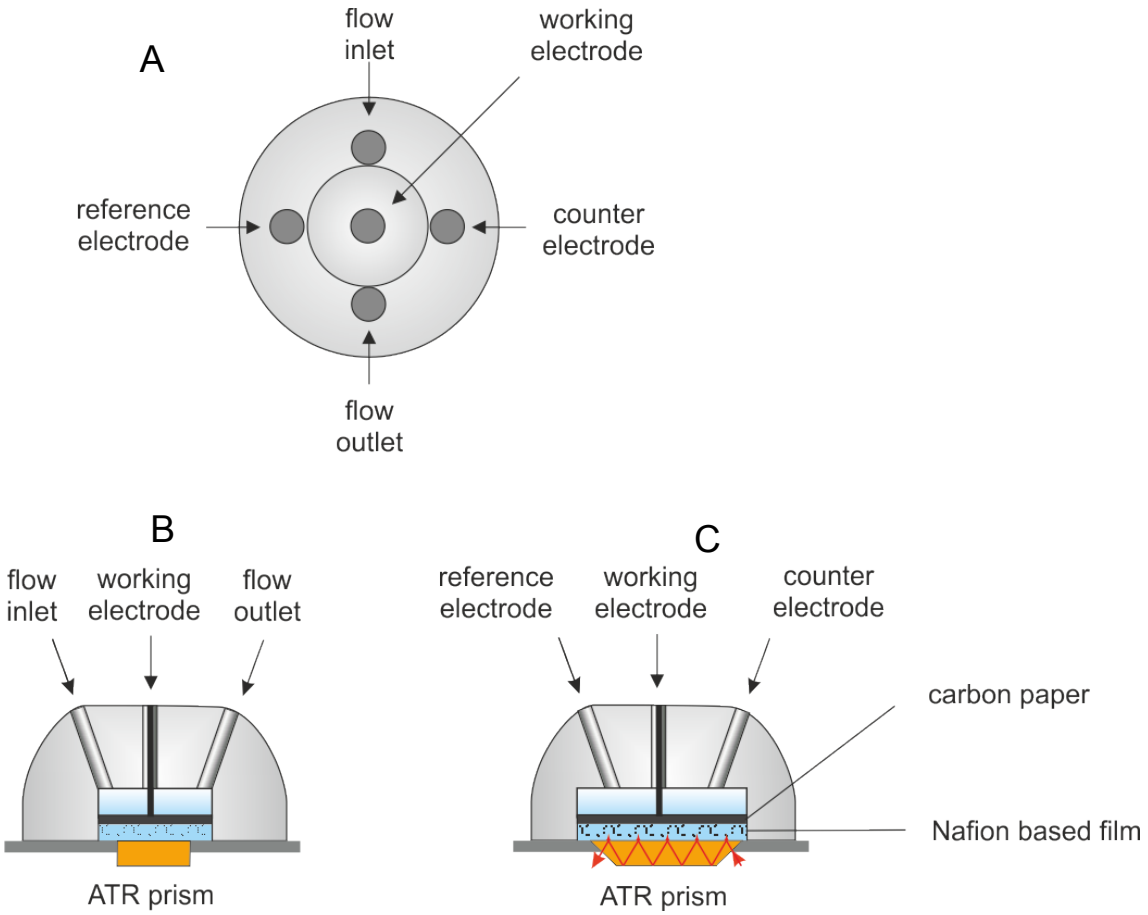

Figure 2-12: A graphic illustration of ATR-IR SEC cell with a prism, three electrodes and flow system from top view (A), cross-section front view (B) and side view (C). A cavity inside the cell showing a Nafion-protein layer on ATR prism in contact with a carbon paper working electrode and electrode connector.

In order to trap the protein sample near the ATR prism surface, Nafion® perfluorinated ion-exchange resin was utilised to create a layer of conductive polymer network in this SEC set up. Nafion is commonly used as an ionic conductor in fuel cells; however it was found that Nafion can be titrated to neutral pH and can be applied to use with the biological molecules.[111, 112]

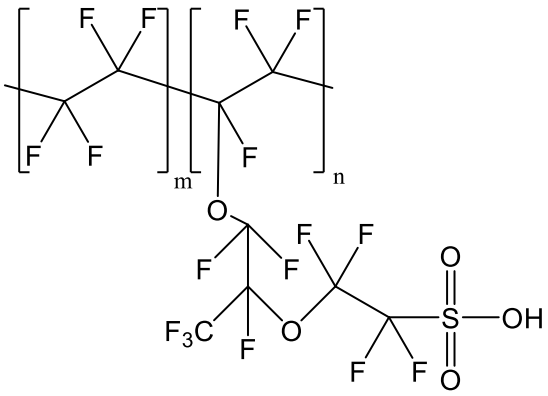

In the KAV group, Nafion was adapted for use in combination with carbon nanoparticles to create a high surface area working electrode to study the electrocatalytic properties of enzymes. It was shown that the Nafion-based working electrode allows IR spectroelectrochemical study of redox enzymes like hydrogenase under direct electrochemical control.[102, 103, 113] However, this study of nitrogenase was mainly performed at very low potentials, therefore the nanoparticles were omitted to minimise competing proton reduction by the working electrode.

2.4.3 Preparation of the ATR-IR SEC cell

A layer of Nafion polymer containing protein sample was prepared by mixing a solution of protein sample with aqueous Nafion in Tris-HCl buffer titrated to pH 7.4 with NaOH. The mixture was deposited onto the ATR prism and was concentrated by partial evaporation. The working electrode and cell body were assembled on top of the film as shown in Figure 2-13. The cell was then filled with buffer solution (about $200-250$ μL) and the counter and reference electrodes were screwed in at the back to seal the cell. This ATR-IR SEC cell preparation was carried out inside an anaerobic glove box.

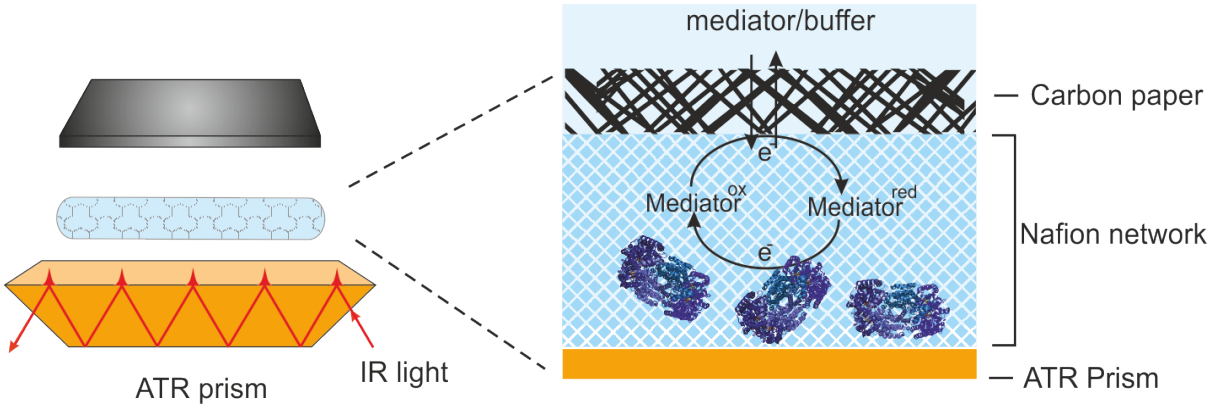

Figure 2-13: Cartoon showing protein molecules trapped in the Nafion network layer between the electrode and the prism surface.

The SEC cell containing the protein sample was then transferred to an adjoining anhydrous, anaerobic glove box, where the IR spectroelectrochemical experiment takes place. All the electrochemistry was controlled by a potentiostat (Autolab PGSTAT 128N). All potentials are shown quoted versus the standard hydrogen electrode (SHE) ($E_{SHE} = E_{SCE} + 0.241$ V at 298 K).

To work in the ATR-IR SEC cell, electrodes had to be modified for suitable electrochemical control of the protein. The details of the electrode modification will be described in the Chapter 3.

2.4.4 ATR accessory and IR spectrometer

In this Thesis, IR spectra are recorded and presented as absorbance, A (optical density, O.D.), which is related to the intensities of the incident (I_0) and reflected (I) radiation as shown:

$$A = -\log\frac{I}{I_0} \qquad 2\text{-}22$$

An 'absolute' spectrum, i.e. the $I(v)$ spectrum, is recorded and processed against a pre-recorded background spectrum (the $I_0(v)$ spectrum) of an empty cell on the ATR prism. In

general the peaks arising from single ligand bonds at the active site are small in comparison to the absorption of the amino acids in the protein and the aqueous electrolyte. In order to examine these vibrations in more detail, , two absolute spectra obtained before and after a change (e.g. introduction of an inhibitor, change in potential) are processed by subtracting one form another to produce a 'difference' spectrum.

For the SEC set up, all spectra were recorded inside the modified anaerobic glove box (Glove Box Technology) using a Varian 680-IR spectrometer equipped with a GladiATR™ accessory (PIKE technology, custom modified). The glovebox was filled with a N_2 atmosphere and was maintained at a dew point of *ca* 75 – 85 °C to minimise contributions of water vapour to the infrared spectrum.

2.5 Experimental

2.5.1 Anaerobic handling of nitrogenase

In this work, both wild type and amino acid substituted MoFe proteins from *A. vinelandii* (β-98^{His}, α-96^{Gln} and apo-MoFe protein) were provided by collaborator, Lance Seefeldt, Utah State University. Cell growth and protein isolation procedures are described elsewhere.[114-116] All proteins were carefully handled inside an anaerobic glove box (Glove Box Technology) under a N_2 atmosphere (< 1 ppm O_2). A reducing agent, sodium dithionite ($Na_2S_2O_4$) was added to protein samples to keep them in a reduced state during transportation. Before commencing a spectroscopic experiment, methyl viologen test paper was used to test for the presence of dithionite in the sample. For some SEC experiments, $Na_2S_2O_4$ had to be washed out of the sample using a centrifugal filter with a 100 kDa cut off membrane (Centricon) beforehand, in order to avoid competing redox chemistry from dithionite.

2.5.2 Buffer solution

A solution of MoFe protein samples were prepared in 100 mM Tris-HCl buffer (Sigma-Aldrich) pH 7.4 with 100 mM NaCl (Fisher) unless stated otherwise. Ultra-high purity water (MilliQ Millipore, 18 MΩ cm^{-1}) was used throughout. All solutions were flushed with N_2 before being taken into the glovebox.

2.5.3 Flow system and mass flow controller

A flow system consists of a peristaltic pump (Whatman) and tubing equipped with fitting (diameter 0.1 mm, kinetic technologies).

A flow rate of gas was regulated by a mass flow control (controlled by Brooks Smart Interface). A gas was flown through an oxygen scrubbing filter (Restek Super Clean gas filter, <1 ppm O_2) before go into the anaerobic glovebox.

Gasses used in this study were from commercial cylinders with high purity; CO (BOC); N_2 (BOC), Ar (BOC). Acetylene was generated from CaC_2 (Sigma Aldrich) reacts with water.

2.5.4 Reagents

Cyanide solution was prepared from a stock solution of 1.0 M KCN (Fisher) and adjusted to neutral pH by adding 3 M HCl.

Potassium ferricyanide, $K_3Fe(CN)_6$ (Sigma-Aldrich) was dissolved in water or buffer as appropriate. The solid was stored in the dark to minimise the effects of degradation by light.

Eu^{III}-ligand complexes were prepared mixing Eu^{3+} and ligand solution in 1:1 molar equivalent ratio. Eu^{3+} was obtained by dissolve Eu_2O_3 (Alfa Aesar) in 0.5 M HCl. Each ligand (DTPA,

EGTA, BAPTA and HDTA; purchased from Sigma Aldrich) solution was prepared in 0.25 M NaOH.

The redox mediators phenazine methosulfate, methylene blue, indigo-tetrasulfonate, 2-hydroxy-1,4-naphthoquione, anthraquinone-2-sulfonate, benzyl viologen, and methyl viologen were purchased from Sigma Aldrich and dissolved in water or buffer as appropriate.

Chapter 3

Development of a mediated electron transfer system for studying nitrogenase

The IR spectroelectrochemical technique gives us the possibility to monitor *in situ* a redox-dependent change in conformation and structure of the sample under electrochemical control. However, there are some factors that must be carefully considered when it is applied to enzyme studies as these biomolecules can be extremely sensitive to changes in their environment. This chapter describes the establishment of a specific electron transfer system for mediated IR spectroelectrochemical study of nitrogenase.

3.1 Electrode modifications

In each ATR-IR SEC setup for different enzyme systems, custom modifications were applied to the electrodes in order to achieve suitable electrochemical control for each protein. For the study of ligand binding to nitrogenase, all electrodes in the system have to be compatible with the protein and ligands used. The three electrodes used in the SEC cell for the nitrogenase system are described here.

3.1.1 Working electrode

In the case of nitrogenase, carbon materials were chosen for the working electrode for two main reasons. First, a carbon electrode provides a wider potential range than a gold electrode, without proton reduction. This will able us to study electrochemistry of the enzyme at very low potentials (down to –1000 mV *vs* SHE). A study of β-98^{His} nitrogenase MoFe protein showed that the reduction of hydrazine to ammonia is possible by using Eu^{II}-EGTA and -DTPA complexes as reductants, which have reduction potentials of –880 mV and –1140 mV respectively,[55] implying that the potential for the redox state of nitrogenase relevant for substrate binding should be in this range. Second, a carbon electrode is relatively inert and does not react with exogenous ligands of interest. For example, a gold electrode can interact with cyanide ions and form a complex $Au(CN)_2^-$ in aqueous solution, which has an absorption peak of ν(CN) at 2147 cm^{-1} in the IR spectrum.[117]

In this SEC setup, it is important to shorten the distance between the working electrode and the ATR prism surface as much as possible. Also, the surface area of the working electrode has to be large enough to get efficient electrochemical control over the enzyme in the IR sampling area. Therefore, the working electrode used in the SEC cell consists of two parts; a piece of high surface area carbon paper and a small carbon electrode connector.

Carbon paper is made of carbon fibres woven together and acts like a conductive mesh, which is permeable to gases and solvents, as shown in the SEM (Figure 3-1). When assembling the SEC cell, a piece of carbon paper (AvCarb P50 Gas Diffusion Layer, Ballard) with *ca* size of ATR prism was put on top of a semi-dried Nafion-based protein film and gently pressed down to assure a good contact between the two layers. This carbon paper backing helps support the Nafion film and increases the electrode surface area.

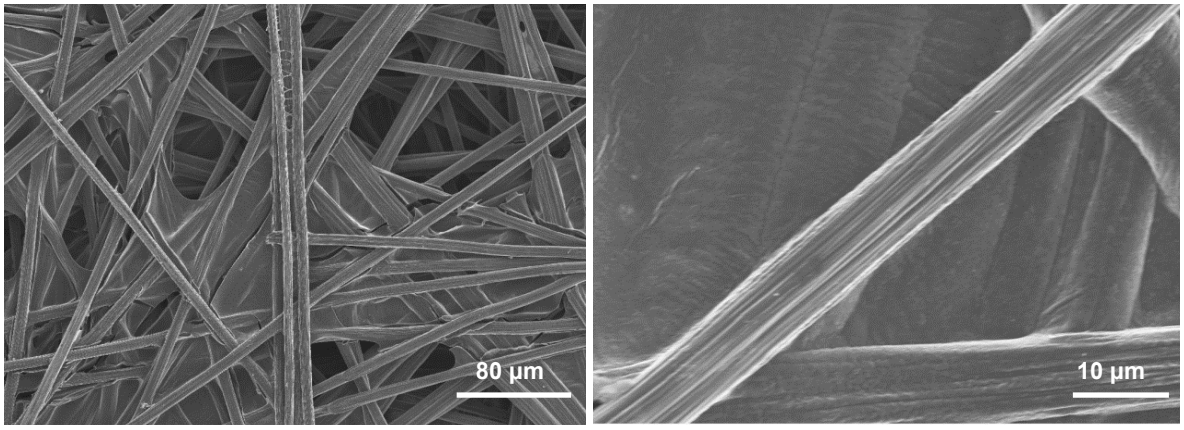

Figure 3-1: SEM images of carbon paper at two magnifications, showing the carbon fibre network. The diameter of each carbon fibre is approximately 10 µm. (Recorded by J. Quinson, Oxford.)

In order to have a rigid connection to the carbon paper, a small carbon electrode connector was constructed from a piece of glassy carbon rod (Alfa Aesar, diameter 1.0 mm) joined with a piece of silver wire inside a Teflon tube. The end of the electrode was sealed with epoxy resin, allowing only the carbon part to be in the solution. This carbon electrode, together with the cell body, was then placed in contact with the piece of carbon paper on prism surface. A silver wire was then connected with a cable from the controlling potentiostat hardware as illustrated in Figure 3-2.

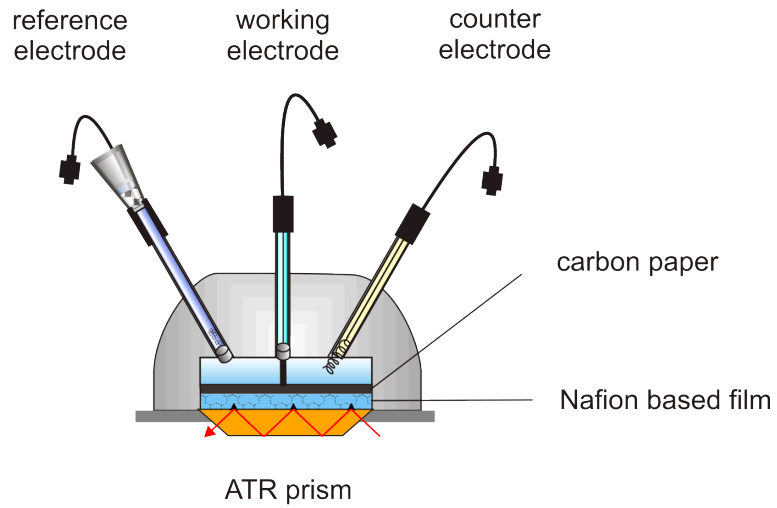

Figure 3-2: A schematic diagram of the assembly of three electrodes in the spectroelectrochemical cell. The position and size are not to scale.

3.1.2 Counter electrode

In order to have a high surface working electrode, it is necessary for the counter electrode to have a sufficient surface area immersed in the bulk solution to ensure that the current can pass through it fast enough so the reaction at the working electrode can occur smoothly and to control the potential of the working electrode accurately. The counter electrode or auxiliary electrode used in this SEC study is a Pt wire. In the SEC setup, a coiled Pt wire (immerged length *ca* 5 mm, diameter 0.2 mm) was put inside a short Teflon tube and pierced through a small rubber septum at the external end. The Pt counter electrode then was connected directly to a cable from the potentiostat.

3.1.3 Reference electrode

Previous studies in the Vincent group mainly used an Ag/AgCl reference electrode in the SEC setup but this electrode is incompatible with the Tris-HCl buffer used with nitrogenase, so a saturated calomel reference electrode (SCE) was employed in this work. A SCE consists of mercury (Hg) and mercury chloride (calomel, Hg_2Cl_2) immersed in a saturated potassium chloride (KCl) solution. The electrode potential is based on the following reaction:

$$Hg_2Cl_{2\,(s)} + 2e^- \leftrightarrow 2Hg_{(l)} + 2Cl^-$$

The potential of the SCE is –0.241 V *vs* SHE at 25 °C.[118] The potential of the electrode depends on the concentration of chloride ions, thus it is necessary to keep the KCl solution saturated all the time. An advantage of the SCE is that its potential can remain constant for a long time.

A small SCE was designed to be able to fit into the ATR-IR SCE cell as illustrated in Figure 3-3. The top part of the SCE comprises Hg and Hg_2Cl_2 (Fisher) in a micro-point pipette tip

with epoxy resin securing a Pt wire on top. The bottom part contains a saturated KCl solution in a piece of polyolefin heat-shrink tubing (*ca* 5 cm length, 2.0 mm diameter) sealed with an aluminosilicate molecular sieve (Sigma Aldrich, 1.6 mm diameter) as a salt bridge. The electrode was stored in a pot of saturated KCl solution to maintain a constant concentration of chloride ions and to prevent the molecular sieve from drying out. The potential of the mini electrode was regularly tested against a commercial SCE electrode before use. It was found that this custom-made SCE has a potential error less than 5.0 mV.

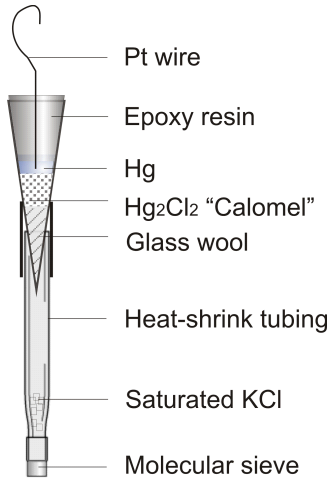

Figure 3-3: Design of a mini saturated calomel reference electrode for the ATR-IR spectroelectrochemical cell.

3.2 Redox mediators

One of the major challenges of controlling electron transfer with proteins is the size of the protein molecule causing slow diffusion rates. In a study of small metalloproteins like myoglobin (18 kDa) or an enzyme like hydrogenase (80 – 90 kDa), the proteins can diffuse to and exchange electrons with a working electrode at a rate that allows a reasonable equilibration time (less than 500 s).[102] In the case of the larger enzymes like nitrogenase (250 kDa), it is unlikely to be able to diffuse to the electrode and arrange itself in the right orientation within a useful timescale for spectroscopic measurement. Another difficulty is that some enzymes have its redox sites buried deep inside the protein unit, so cannot exchange electron with the electrode directly.

In order to study electrochemistry property of particular redox enzyme, a redox mediator is required to transfer electrons to redox centres of the enzyme. Due to smaller size of mediator molecules, it usually has faster diffusion rate than the target biomolecule. Thus, addition of a redox mediator to the biological system will speed up redox process in bulk electrolyte and help the system to reach equilibrium faster. In some cases, a redox mediator will facilitate electron transfer from the electrode to the redox site of the protein in the first place. As a redox couple itself, these redox mediators can help electron transfer from electrode to protein redox sites most efficiently when the solution potential (E_h) is close to the mediator midpoint potential (E_m). A mixture of different redox mediators with E_m covering the potential range of interest is commonly used. Thus, appropriate choice of redox mediators is a key issue in establishing a system suitable for studying the redox processes of interest.

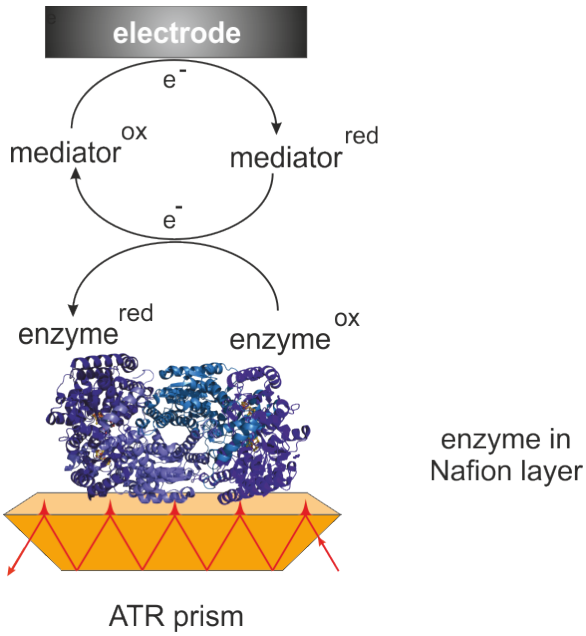

Figure 3-4: A schematic representation of a mediated electron transfer system inside the ATR-IR SEC cell. Redox mediators can be reduced at the working electrode when an appropriate potential is applied. The reduced mediators then diffuse through the Nafion layer and reduce the active site of enzyme. Later the oxidised mediators return to the working electrode and are reduced again.

The concept of the mediated electron transfer system in the SEC setup is to have small redox mediators act as an electron shuttle between a working electrode and the redox site of an enzyme trapped near the ATR prism surface as shown in Figure 3-4. In the following section, a cocktail of redox mediators will be built up in order to facilitate electron transfer to the redox centres of nitrogenase.

3.2.1 Europium polyaminocarboxylate complexes

The electrochemical control of the nitrogenase MoFe protein is particularly challenging due to the fact that wild type nitrogenase has been found to only accept electrons from the Fe protein, the redox partner of the MoFe protein *in vivo*. In the presence of the Fe protein, a sequence of electron transfer from the reduced Fe protein to the MoFe protein will be continued until all the redox centres in the MoFe protein achieve reduced states relevant to the binding of substrates for turnover. For each one electron transfer by the Fe protein, a

hydrolysis of two ATP molecules is required. Thus, ATP has to be continuously supplied during turnover conditions. However, in the presence of Fe protein and ATP, the MoFe protein can also reduce protons and return to its oxidised state spontaneously, resulting in the formation of mixed redox states of the protein. The complexity of electron transfer *via* the Fe protein has so far made it impractical to control nitrogenase electrochemically.

Nevertheless, recent studies have shown that some variants of the MoFe proteins can catalyse two- and four-electron reduction processes by using a Eu^{II}-polyaminocarboxylate complex as a low potential reducing agent.[55, 119, 120] For instance, Seefeldt and co-workers demonstrated that a β-$98^{Tyr\rightarrow His}$ variant of the MoFe protein is able to catalyse two-electron reduction of hydrazine to ammonia without Fe protein coupling.[55] This variant appears to be locked in an electron-transfer ready confirmation. Ribbe and co-workers reported a europium complex-driven reduction of CO and cyanide by the isolated FeMoco active site of nitrogenase.[119] Later, they also showed that a variant of the MoFe protein containing a P-cluster precursor is capable of reducing CO, CO_2 and cyanide into hydrocarbons by using a Eu^{II}-polyaminocarboxylate complex.[120]

To date there have been no reports of a successful cycle for complete reduction of dinitrogen by native nitrogenase in the absence of the associated Fe protein. However, the studies using Eu^{II}-ligand systems as electron donors suggest that electrochemical control of the MoFe protein for two- to four-electron substrate reductions may be possible *via* low potential electron mediators.

3.2.1.1 Electrochemistry of europium complexes

Europium (Eu) is an element with atomic number 63 (atomic configuration; $[Xe].4f^7.6s^2$). It is in the lanthanide series, in the f-block of period six in the periodic table. Lanthanide elements commonly exhibit the oxidation state +3 and can form complexes with ligands up to

coordination number 9.[7, 121] However, unlike most of lanthanides, europium can form either Eu^{II} or Eu^{III} complexes in solution. The stability of Eu^{II} complexes is owing to its half-filled electron subshell ($4f^7$). The Eu^{2+} ion has been thought to form a stable aqua complex as $[Eu(H_2O)_8]^{2+}$ under anaerobic conditions.[122] Another noteworthy property of lanthanide complexes is that f-electrons are largely contracted by the nucleus as a result of poor shielding of f-orbitals. Their ligand field stabilization energies are minimized due to weak metal-ligand orbital interaction. It accounts for the rapid ligand exchange reactions of lanthanide complexes in solution, which can reach equilibrium within seconds.[121]

Due to the fact that Eu^{II} is isoelectronic with Gd^{III}, many Eu^{II}-polydentate ligand complexes have been previously studied as redox-responsive contrast agents for *magnetic resonance imaging* applications.[123-125] It was found that exceptionally tight binding of polyaminocarboxylate ligands such as diethylenetriamine-*N,N,N′N″,N″*-pentaacetate (DTPA) shift the reduction potential of the $Eu^{III/II}$ couple in the negative direction. The X-ray structure of Eu^{II}-DTPA revealed that Eu^{II} ion is chelated by the octadentate DTPA ligand and one water molecule as shown in Figure 3-5A.[123]

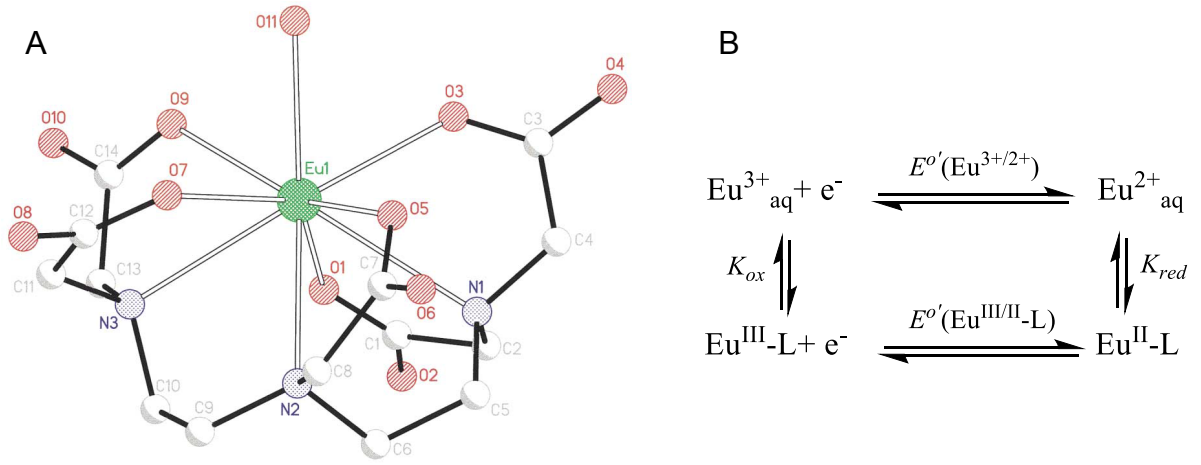

Figure 3-5: (A) X-ray crystal structure of $[C(NH_2)_3]_3[Eu^{II}(DTPA)(H_2O)].8H_2O$ (Reproduced with permission from ref. [123]) Copyright (c) 2000 Wiley-VCH Verlag GmbH & Co. KGaA, Weinheim. (B) Schematic representation of *in situ* formation of Eu-ligand (L) complex as a low potential reductant. K_{red} and K_{ox} are the formation constants for complexes with Eu^{2+} and Eu^{3+}, respectively.

However, Eu^{II}-DTPA complexes can be rapidly oxidized by water and oxygen as shown in equations below, respectively;[124]

$$\left[Eu^{II}(DTPA)(H_2O)\right]^{3-} + H_2O \rightarrow \left[Eu^{III}(DTPA)(H_2O)\right]^{2-} + \frac{1}{2}H_2 + OH^-$$

$$\left[Eu^{II}(DTPA)(H_2O)\right]^{3-} + O_2 + H_3O^+ \rightarrow \left[Eu^{III}(DTPA)(H_2O)\right]^{2-} + \frac{1}{2}H_2O_2$$

A study by Vincent *et al.* demonstrated that the Eu^{II} form can be generated *in situ* and that Eu^{II} -polyaminocarboxylate complexes form instantaneously in aqueous solution as a low potential reductant (Figure 3-5B). It was found that some Eu^{III}-polyaminocarboxylate complexes, including Eu^{II}-DTPA complexes, have lower reduction potentials than common reducing agents likes sodium dithionite (*ca* –660 mV) and deazaflavin (*ca* –650 mV), and these Eu^{II} complexes are able to reduce nitrogenase Fe protein to its super-reduced state $[4Fe\text{-}4S]^0$ (*ca* –800 mV).[30]

In addition to a very low reduction potential, there are several other advantages of using Eu-polyaminocarboxylate complexes as redox mediators;

- The Eu^{2+} ion can easily be prepared electrochemically by reducing the Eu^{3+} ion under anaerobic conditions at a relatively mild potential (approximately –400 V) in an electrolysis cell.[30]

- A range of $Eu^{III/II}$-ligand couples exhibit reversible redox processes in aqueous solution.[123]

- The reduction potential of the $Eu^{III/II}$-DTPA couple is resistant to a change in pH at pH values above 4.[124]

- Eu^{II} and Eu^{III} complexes have weak absorption peaks in the UV-visible region at 260 and 330 nm, respectively. These do not interfere with monitoring of changes at metal clusters within enzymes in the UV-visible spectral range below 300 nm.[30, 124]

- Eu^{III} complexes exhibit no significant EPR signal while Eu^{II} complexes have a distinctive feature at $g = 2$ which can be distinguish from EPR signals from the sample.[125]

In this study, Eu-polyaminocarboxylate complexes were tested as low potential electron transmitters for the MoFe protein without the presence of the Fe protein and ATP.

In work by H. Waite (Part II Thesis, 2011) carried out under my supervision, redox properties of Eu-polyaminocarboxylate complexes were examined under the conditions relevant for nitrogenase experiments. The following ligands (Figure 3-6) were chosen based on the reduction potential when they complex with the Eu^{III} ion: *N*′-(2-hydroxyethyl) ethylenediamine-*N,N,N*′-triacetate (HDTA), 1,2-*bis*(*o*-aminophenoxy)ethane-*N,N,N*′,*N*′-tetraacetic acid (BAPTA), ethylene glycol-*bis*(2-aminoethylether)-*N*,*N*,*N*′,*N*′-tetraacetic (EGTA) and DTPA.

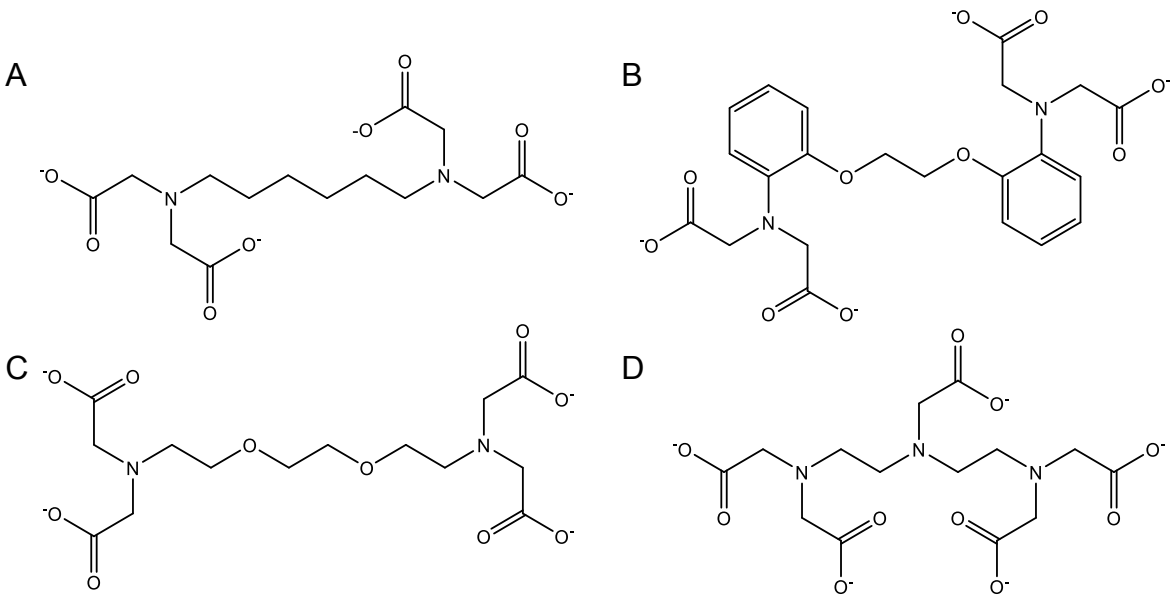

Figure 3-6: Structures of chelating ligands used in Eu-ligand system: (A) HDTA, (B) BAPTA, (C) EGTA and (D) DTPA.

Cyclic voltammetry was employed to study electrochemical properties of the chosen Eu-ligand complexes. Samples were prepared as described in Chapter 2. All Eu^{III}-ligand complexes were formed by adding each ligand to Eu^{3+} solution at a molar ratio of 1:1. Experiments were performed under anaerobic conditions and a three-electrode electrochemical system was used comprising glassy carbon working electrode, Pt wire counter electrode and SCE reference electrode.

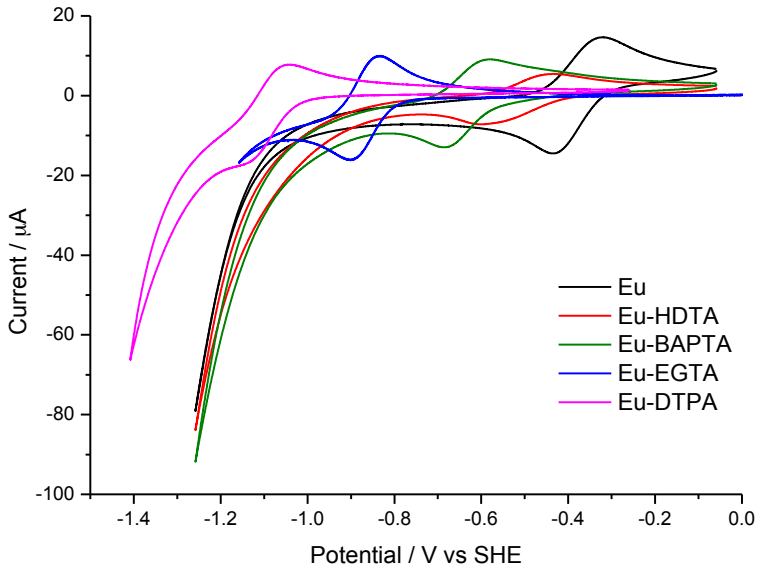

Figure 3-7: Cyclic voltammograms of individual $Eu^{3+}_{(aq.)}$ and Eu^{III}-ligand complexes (Eu-HDTA, Eu-BAPTA, Eu-EGTA, and Eu-DTPA) 2.0 mM in Tris-HCl buffer pH 8.0. All voltammograms were recorded at 20 mVs^{-1}.

Table 3-1: The observed reduction potential of Eu-ligand complexes in aqueous solution at pH 8.0

Redox complexes	Potential *vs* SHE (mV)				Current (μA)		
	E_{pc}	E_{pa}	ΔE_p	$E^{0\prime}$	i_{pc}	i_{pa}	i_{pa}/i_{pc}
$Eu^{3+/2+}_{aq}$	–432	–325	108	**–379**	15.0	13.2	**0.88**
$Eu^{III/II}$-HDTA	–597	–437	159	**–517**	6.4	4.0	**0.63**
$Eu^{III/II}$-BAPTA	–683	–584	98	**–634**	8.5	7.6	**0.90**
$Eu^{III/II}$-EGTA	–900	–835	64	**–868**	12.0	10.8	**0.90**
$Eu^{III/II}$-DTPA	–1136	–1045	91	**–1090**	16.0	4.8	**0.30**

Figure 3-8 shows cyclic voltammograms of $Eu^{3+}_{(aq)}$ and four Eu^{III}-ligand complexes in Tris-HCl buffer, a buffer system relevant for work on nitrogenase. At pH 8.0, the $Eu^{3+/2+}$ couple exhibited a reversible wave with a mid-point potential of –379 mV. The reversibility of the $Eu^{3+/2+}$ couple was determined by the ratio of the cathodic current (i_{pc}) from reduction and the anodic current (i_{pa}) from re-oxidation. As shown in Table 3-1, the result 0.88 is slightly less

than unity suggesting the reaction was only quasi-reversible. Also, the observed difference in potential between the reduction peak (E_{pc}) and re-oxidation peak (E_{pa}), the peak-to-peak potential separation (ΔE_p), was larger than that theoretically predicted for a reversible one-electron reaction (≈57 mV at 298 K).[108] It is possible that this could stem from slow electron transfer kinetics at the working electrode.

As expected, it was observed that chelating Eu^{3+} ions with each ligand significantly shifted the reduction potential of the $Eu^{3+/2+}$ couple to more negative values. The midpoint potentials of Eu-EGTA at –870 mV and Eu-DTPA at –1090 mV at neutral pH, are in agreement with previous studies.[30] Eu-BAPTA gives slightly less negative reduction potentials compared to Eu-EGTA and Eu-DTPA, indicating slightly weaker complexes with Eu^{III} ion, thus the central Eu atom is easier to be reduced. Eu-HDTA has a smallest reduction potential shift from Eu^{3+} among Eu-ligand complexes. It is thought to be a result of the difference in coordination number as HDTA is a hexadentate ligand while others are octadentate.

All $Eu^{III/II}$-ligand couples exhibited quasi-reversible redox processes. $Eu^{III/II}$-EGTA and $Eu^{III/II}$-BAPTA have ratios of redox current similar to $Eu^{3+/2+}$, suggesting similar redox reversibility. It was noted that current measurement of $Eu^{III/II}$-DTPA could not be used to determine its reversibility partly because its reduction peak overlapped with proton reduction by the working electrode, and also some Eu^{II}-DTPA molecules reduced protons in the solution so less Eu^{II}-DTPA were re-oxidised at the electrode resulting in less re-oxidation current. In the case of Eu-HDTA, both redox currents was relatively small as it was found to partly precipitate at neutral pH values.

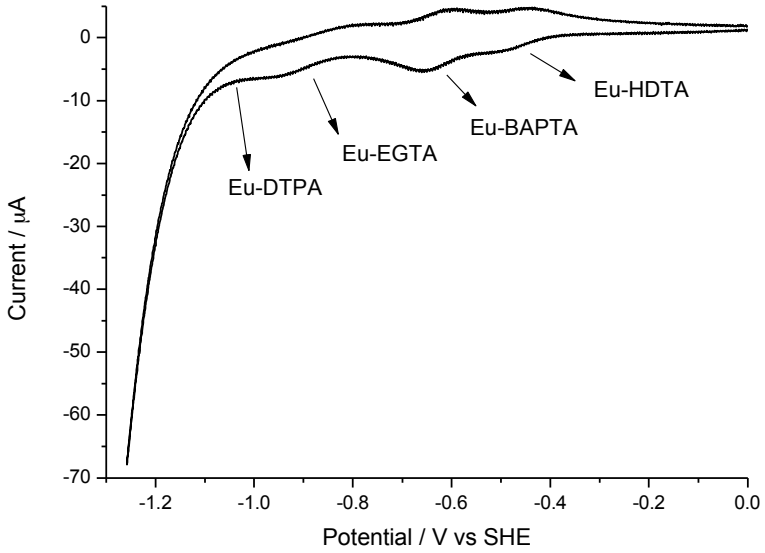

Figure 3-8: A cyclic voltammogram of a mixture of four Eu-ligand complexes in equal amounts in Tris-HCl buffer pH 7.4; Eu-HDTA, Eu-BAPTA, Eu-EGTA, and Eu-DTPA at 0.5 mM each). A voltammogram was recorded at 20 mVs^{-1}.

In Figure 3-8, a cyclic voltammogram of all Eu-ligand complexes together in solution was recorded at pH 7.4. The redox features of each Eu-ligand couple are retained when the complexes are combined stoichiometrically. It implies that a mixture of mediators could provide electron transfer over a continued potential range covering the region of interest where redox changes relevant to catalysis in the MoFe protein could occur.

3.2.2 Organic mediators

A number of water-soluble organic compounds have been employed as redox mediators or electron donors/acceptors in many studies of biological systems. In previous studies, some organic mediators were used to transfer electrons in potentiometric titrations with nitrogenase or other iron-sulphur cluster-containing enzymes as listed in Table 3-2. Theses organic molecules were found to be compatible with the proteins and have midpoint potentials (E_m) between 0 and –400 mV *vs* SHE.

Table 3-2: mid-point potentials of organic mediators used in previous redox studies of nitrogenase and other metalloenzymes

Redox mediator	Molecular formula (Molecular weight g/mol)	Molecular structure	E_m (mV)	Ref.
phenazine methosulfate	$C_{13}H_{11}N_2 \cdot CH_3SO_4$ (306.34)	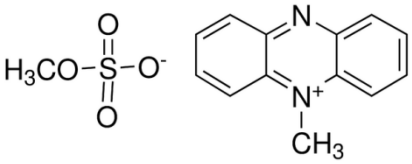	+80	126
methylene blue	$C_{16}H_{18}ClN_3S \cdot 3H_2O$ (373.90)	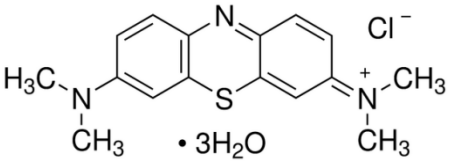	+11	24, 91, 105, 126
indigo-tetra sulfonate	$C_{16}H_6K_4N_2O_{14}S_4$ (734.88)	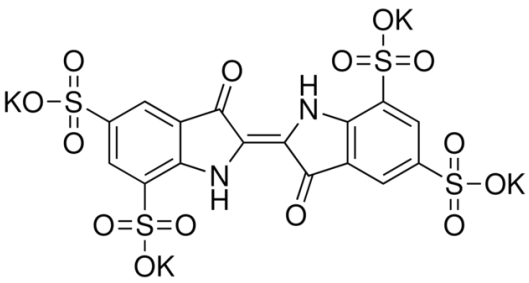	–46	105
indigo-disulfonate	$C_{16}H_8N_2Na_2O_8S_2$ (466.35)	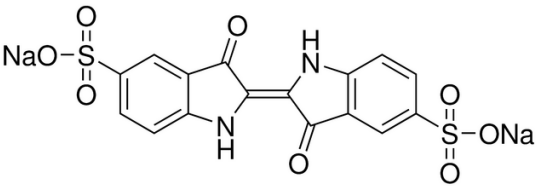	–125	24, 91, 127
2-hydroxy-1,4-naphthoquinone	$C_{10}H_6O_3$ (174.15)	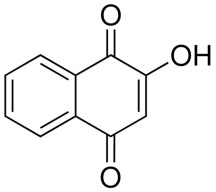	–139	24, 105
anthraquinone-2-sulfonate	$C_{14}H_7NaO_5S$ (310.26)	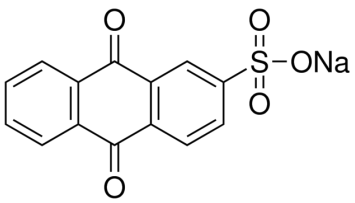	–225	24, 105, 126

Redox mediator	Molecular formula (Molecular weight g/mol)	Molecular structure	E_m (mV)	Ref.
benzyl viologen	$C_{24}H_{22}Cl_2N_2$ (409.35)	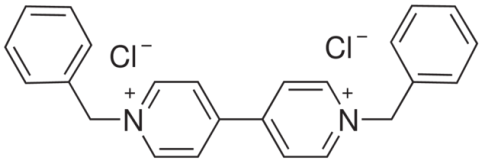	–361	24, 91, 105, 126-128
methyl viologen	$C_{12}H_{14}Cl_2N_2 \cdot xH_2O$ (257.16)	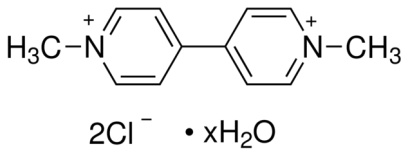	–440	24, 91, 105, 126-128

The following mediators were chosen due to their reversible redox properties, good stability and solubility in the Tris-HCl buffer system and other conditions used in this study: methylene blue; 2-hydroxy-1,4-naphthoquione; benzyl viologen and methyl viologen. In our SEC studies, a mixture of mild-potential organic compounds was added into the electrolyte in a Nafion-protein layer on an ATR prism and the bulk solution in the cell, in order to help transfer electrons into metal clusters inside the MoFe protein in the mid potential range.

3.2.3 Mediator cocktail

In this chapter, a cocktail of redox mediators was developed in order to provide mediated electron transfer to nitrogenase continuously in a wide potential window. A series of redox mediators with different reduction potentials from 0 mV to –1000 mV was chosen to cover a potential range of interest in which ligand binding to metal clusters of nitrogenase could occur, as shown in Figure 3-9; methylene blue (+11 mV); 2-hydroxy-1,4-naphthoquione (–139 mV); benzyl viologen (–361 mV); methyl viologen (–440 mV); Eu-BAPTA (–633

mV); Eu-EGTA (–868 mV) and Eu-DTPA (–1094 mV). This mixture is referred to subsequently as the 'nitrogenase redox mediator cocktail'.

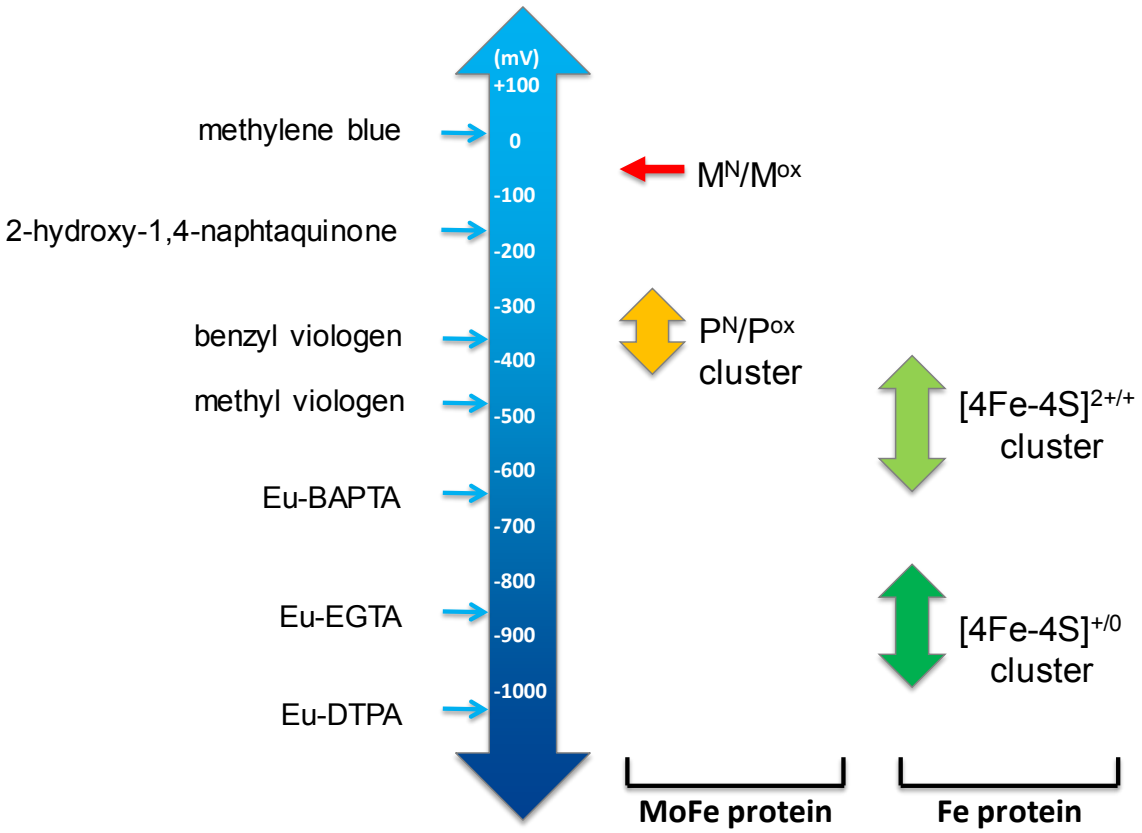

Figure 3-9: Potential range covered by electron transfer from the chosen redox mediators (left); midpoint potentials of some relevant redox couples in nitrogenase (right).[24, 30, 91, 129] The FeMoco active centre inside the MoFe protein is designated 'M'.

3.2.3.1 Compatibility test

A set of experiments was designed to test compatibility of the nitrogenase redox mediator cocktail and the IR-SEC cell. All stock solutions of redox mediators were prepared freshly inside an anaerobic glovebox and mixed together in Tris-HCl buffer to give a final concentration of 0.25 mM each. A SEC cell was set up with a Nafion layer containing a mixture of the chosen redox mediators. The Nafion layer was prepared by mixing 2.0 µL of 7% aqueous Nafion suspension in pH 7.4 Tris-HCl with 2.0 µL of mediator solution before coating on a Si prism. A piece of carbon paper was placed on top of the semi-dried Nafion

layer and connected with a glassy carbon working electrode connector. A cell body equipped with a Pt counter electrode and a saturated calomel reference electrode was attached to the prism base and then the cell was filled with the 0.25 mM redox mediator cocktail in pH 7.4 Tris-HCl buffer.

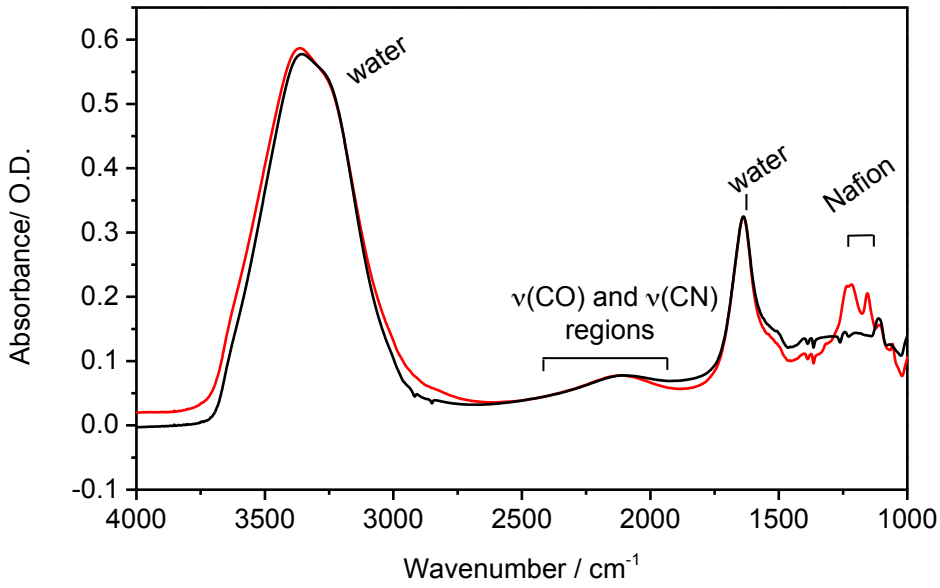

Figure 3-10: An IR spectrum of a Nafion film containing 0.25 mM of redox mediator cocktail (black) compared with a spectrum of the cell filled with Tris-HCl buffer pH 7.4 only (red). The spectra were processed against a spectrum of an unmodified Si ATR prism (500 scans co-added, 4 cm^{-1} resolution).

Without potential applied, an IR absorbance spectrum was recorded against the unmodified Si prism background. Figure 3-10 shows a spectrum of the Nafion-mediator film revealing vibrational bands of water (stretching mode around 3000 – 3500 cm^{-1} and bending mode at 1640 cm^{-1}) and Nafion features (1100 – 1250 cm^{-1}). No interfering peaks are observed in the region between 1800 and 2200 cm^{-1} where peaks from CO and CN ligands interacting with metal cluster are expected to appear, with the exception of a broad water feature.

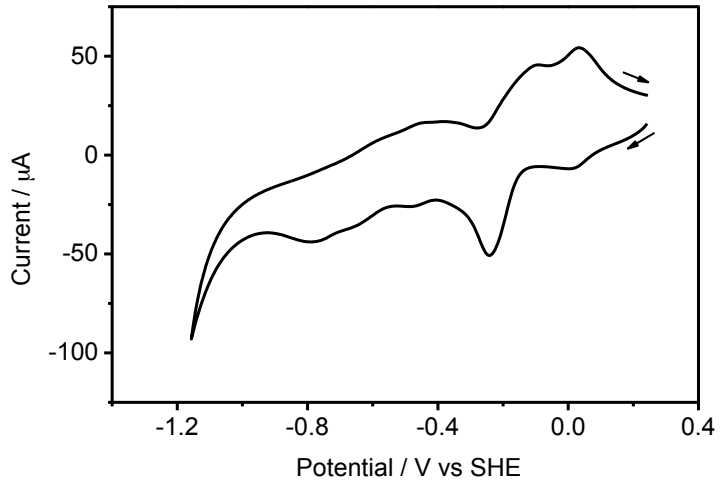

Figure 3-11: A cyclic voltammogram of the nitrogenase redox mediator cocktail 0.25 mM in a Nafion film and bulk solution recorded in the SEC cell at scan rate 50 mVs^{-1}.

Figure 3-11 shows a series of redox processes corresponding to all components of the nitrogenase mediator cocktail in the SEC cell. As the potential at the working electrode was swept down to negative values, reduction peaks of each redox mediator were observed. Some mediators might interact more strongly with the electrode, which could lead to differences in the observed intensities for different mediators. A strong reduction peak at –250 mV could be a result of overlapping of two reduction peaks; 2-hydroxy-1,4-naphthoquione at –150 mV and benzyl viologen at –300 mV. It was noted above that reduction of Eu^{III}-DTPA is masked by proton reduction at the electrode surface at potentials below –1000 mV. The voltammogram suggests that the redox mediators are compatible with each other and Nafion film. Thus, their reductions should provide continuous control in the potential range of interest for studying nitrogenase.

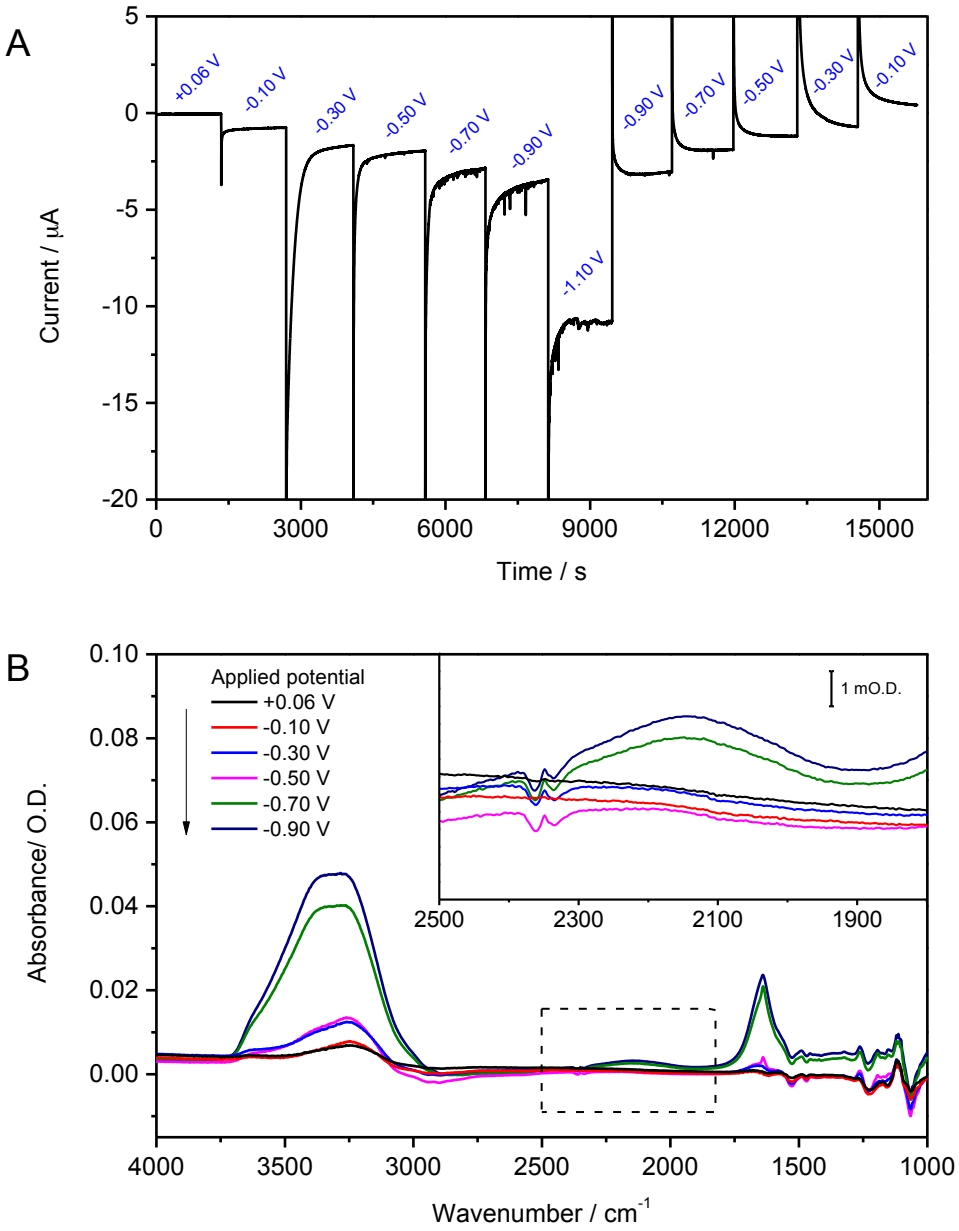

Figure 3-12: (A) Chronoamperogram showing potential steps applied to a Nafion film. The cell was filled with the nitrogenase redox mediator cocktail. (B) IR spectra recorded following potential steps to negative potentials, processed against a background spectrum recorded before potential was applied (500 scans co-added, 4 cm^{-1} resolution). Inset showing a zoom in of a region of interest between 2300 – 1800 cm^{-1}.

In Figure 3-12A, when a set of potential steps was applied to the Nafion film with redox mediators present two current contributions were observed at each potential, due to the charging current at the electrode surface and Faradaic processes. The charging current decays relatively quickly and the Faradaic current decays more slowly at each potential down to –900 mV, reaching a plateau at a small residual current. At potentials more negative than –900 mV,

the residual negative current increased significantly and the measurement was disrupted by proton reduction as shown in Figure 3-11, arising directly from the carbon electrode and also catalytically from the Eu-ligand complexes. Figure 3-12B shows IR spectra recorded following each of the potential steps shown in Figure 3-12A. The inset in Figure 3-9B shows that there were no interfering peaks in the ν(CO) and ν(CN) region (1800 – 2300 cm^{-1}), where peaks from ligands bound to metal centres of the enzyme should appear. This indicates that the redox mediator mixture is compatible with the Nafion film and provides a good background for IR study of metalloenzymes. However, changes in the water bands in the spectra were observed at potentials below –700 mV. It might stem from a potential-dependent structural change within Nafion film leading to more hydration in the Nafion layer. This should not affect the ability to observe ligand binding to nitrogenase since any bands expected from CO and CN^- interaction would be much sharper and distinguishable from broad changes in spectral baseline.

In summary, a specific spectroelectrochemical method for controlling and studying nitrogenase over a wide potential range has been developed. The mediated electron transfer system demonstrated an indirect electrochemical control covering a wide potential window (between 0 mV to –1000 mV). Electron transfer at very negative potentials can be achieved by using Eu-ligand complexes as redox mediators in combination with organic mediators for milder potentials. This system gives an IR spectrum free of interfering features in ν(CO) and ν(CN) regions which are suitable for monitoring ligand binding to nitrogenase.

3.3 Model systems for spectroelectrochemical study

In order to achieve both an efficient electrochemical control and a good spectroscopic result, many factors need to be considered while using the ATR-IR SEC cell. At the beginning, a series of experiments on simple model systems were performed to test the SEC cell setup. These tests allowed us to practise preparing the SEC cell before starting to use it to study nitrogenase. More importantly, they helped to optimise conditions for spectroelectrochemical studies whilst minimising the amount of precious protein samples used.

3.3.1 Potassium ferricyanide

A preliminary test for spectroelectrochemistry in the SEC cell was carried out using potassium ferricyanide complexes as a model system. The main aim of this test was to examine electrochemical control within the IR sampling volume. Also, diffusion rates of redox molecules in the SEC cell were monitored.

Potassium ferricyanide (potassium hexacyanoferrate, $K_3[Fe(CN)_6]$) is commonly used as a redox mediator in organic chemistry and biochemistry according to the redox potential of the ferricyanide anion ($[Fe(CN)_6]^{3-}$).[130, 131] A low spin Fe^{III} central atom can be easily reduced to Fe^{II} without breaking any coordinate bond between Fe and CN^- ligand, resulting in the ferrocyanide anion ($[Fe(CN)_6]^{4-}$). This redox reaction is reversible and its potential is shown in Equation 3-1.[132]

$$[Fe(CN)_6]^{3-} + e^- \Leftrightarrow [Fe(CN)_6]^{4-} \qquad E^o = 0.36\ V \qquad \text{3-1}$$

Both ferricyanide and ferrocyanide have distinctive vibrational features in the mid-IR with relatively high molar absorptivity coefficients; the ferricyanide ion ($[Fe(CN)_6]^{3-}$) has a vibrational peak of ν(CN) at 2115 cm^{-1}, while ferrocyanide ($[Fe(CN)_6]^{4-}$) has a ν(CN) peak at

lower wavenumber, 2040 cm^{-1}, in aqueous solution.[133-135] This shift in ν(CN) reflects increased back-bonding from the more electron-rich Fe(II), as the C–N bond is weakened by π back-donation from the metal centre in the lower oxidation state.

Thus, the ferri/ferrocyanide couple ($[Fe(CN)_6]^{3-/4-}$), as a redox-dependent IR-active complex, is suitable to be used as a proof-of-concept model system for testing spectroelectrochemistry inside the ATR-IR SEC cell.

3.3.1.1 Spectroelectrochemistry test

In this test, the ATR-IR SEC cell was set up with a Nafion-based film on the ATR prism containing 10 nmol of $[Fe(CN)_6]^{3-}$ from a 10 mM $K_3[Fe(CN)_6]$ stock solution. A piece of carbon paper used as a working electrode was placed on top of the Nafion film, then the SEC cell was assembled and filled with Tris-HCl buffer solution (pH 7.4). A piece of platinum wire as a counter electrode and custom-made SCE reference were used as described in the previous section.

The redox potential of 10 mM potassium ferricyanide solution in a 0.1 M Tris buffer solution at pH 8.0 with the ionic strength *ca* 0.1 M NaCl was previously reported as 431±0.3 mV at 25 °C.[136] At the beginning, the potential was held at 440 mV for a few minutes to oxidise the majority of complexes into $[Fe(CN)_6]^{3-}$, then an IR spectrum was recorded to be used as a background for the rest of the experiment. A potential-dependent change in IR spectra of the $[Fe(CN)_6]^{3-/4-}$ couple was monitored assuming this system to be diffusion controlled.

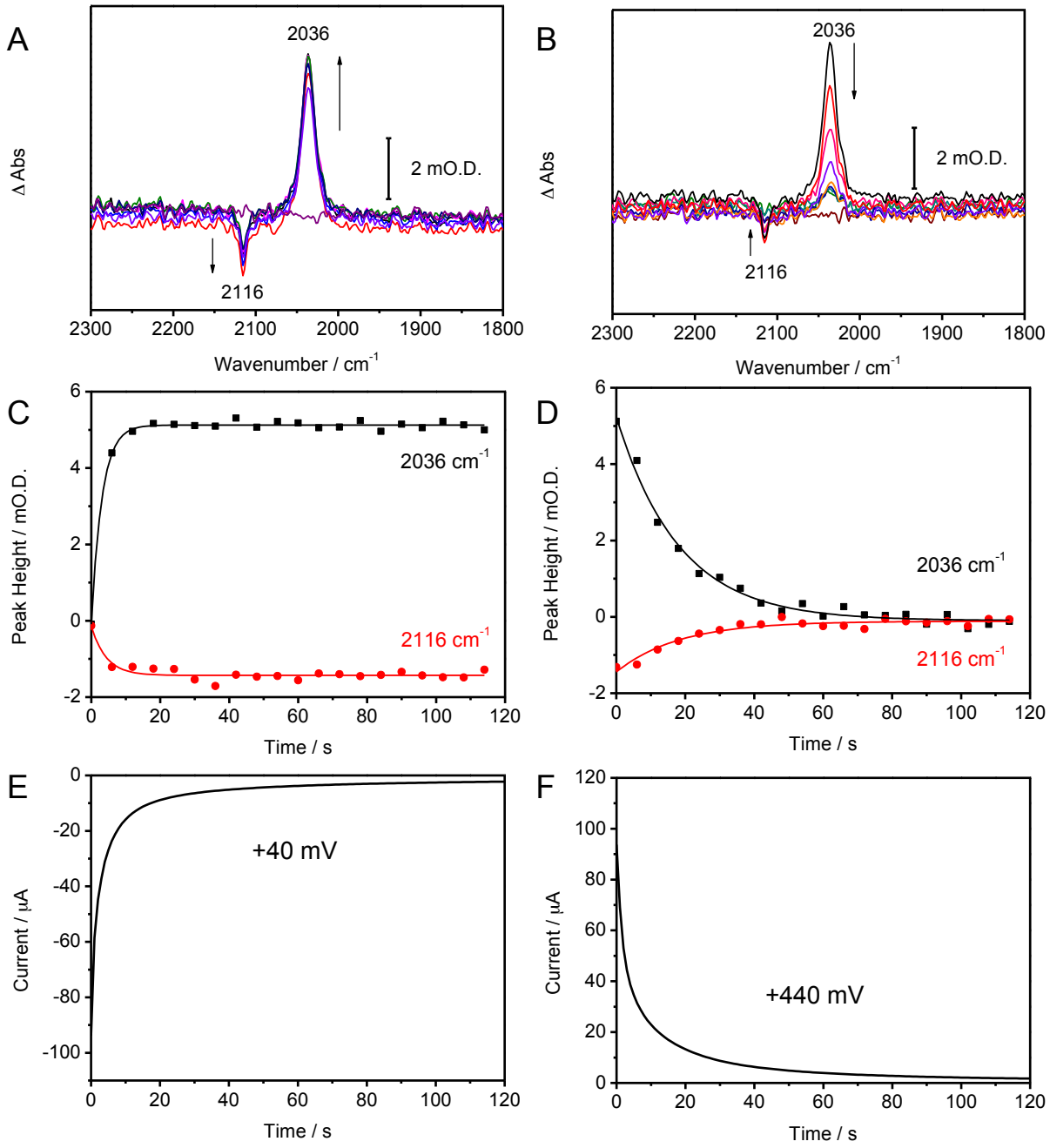

Figure 3-13: (Panel A and B) Time-series sets of difference spectra against a background recorded at +440 mV (10 scans co-added, 4 cm^{-1} resolution) after applying a potential of 40 mV (A), then stepping to 440mV again (B). (Panel C and D) Plots of peak height ($\Delta A = A_t - A_{background}$) *vs* time (interval time 6 s) during the reduction (C) and re-oxidation (D), showing a *ν*(CN) peak height of $[Fe(CN)_6]^{4-}$ at 2036 cm^{-1} (black) and $[Fe(CN)_6]^{3-}$ at 2116 cm^{-1} (red). (Panel E and F) Plots of current *vs* time (interval time 1 s) during the reduction (E) and re-oxidation (F).

Figure 3-13A shows loss of the *ν*(CN) peak of $[Fe(CN)_6]^{3-}$ at 2116 cm^{-1} and growth of the *ν*(CN) of $[Fe(CN)_6]^{4-}$ at 2036 cm^{-1} as the $[Fe(CN)_6]^{3-}$ ion was reduced to $[Fe(CN)_6]^{4-}$ when a

potential of +40 mV was applied at the working electrode. In the reverse process, shown in Figure 3-13B, when a potential of +440 mV was applied, a loss of both the positive ν(CN) peak of $[Fe(CN)_6]^{4-}$ at 2036 cm^{-1} and the negative peak ν(CN) of $[Fe(CN)_6]^{3-}$ at 2116 cm^{-1} was observed. This indicated a fully reversible interconversion of $[Fe(CN)_6]^{4-}$ and $[Fe(CN)_6]^{3-}$ within the IR sampling area.

In Figure 3-13C and D, plots of peak height with time showed that each reaction reached the equilibrium within 40 s, consistent with the current passed in the chronoamperograms as shown in Figure 3-13E and F. This confirms efficient electrochemical control between the Nafion-modified working electrode and the IR sampling area on the ATR prism. The kinetic behaviour of the $[Fe(CN)_6]^{3-/4-}$ couple in the cell gives an indication of how other redox mediators are likely to behave inside the Nafion film.

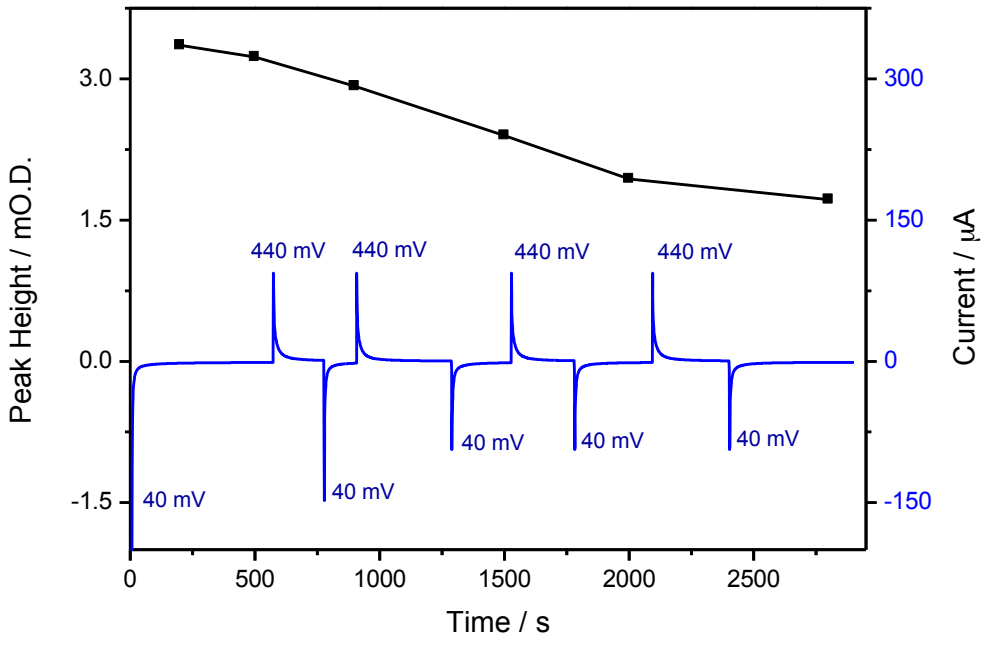

Figure 3-14: A plot of peak heights (black) and current (blue) against time over the experiment course. Each peak height was measured from a ν(CN) peak of $[Fe(CN)_6]^{4-}$ at 2036 cm^{-1} in a spectrum recorded during each reduction of $[Fe(CN)_6]^{3-}$ (40 mV applied) processed against a background of $[Fe(CN)_6]^{3-}$ at 0 s (10 scans co-added, 4 cm^{-1} resolution).

However, Figure 3-14 shows that the peak height of both species gradually decreased to almost 50% after several reduction (40 mV) and re-oxidation (440 mV) steps over a 30 minute period, indicating the loss of $[Fe(CN)_6]^{3-/4-}$ from the Nafion layer over time into the bulk solution above the working electrode film. To prevent small molecules diffusing away from the film, the same concentration of mediator solutions are therefore needed in the bulk electrolyte.

3.3.1 Carboxymyoglobin

In the next step, it was essential to test the SEC setup with a biological system as a large macromolecule could behave differently from a simple coordination complex used in the preliminary test. Studying proteins is challenging since many critical conditions are required, *eg.* pH value, ionic strength and temperature etc. Myoglobin was chosen as a biological model system for spectroelectrochemical study in the SEC cell due to the fact that it is well characterised and commercially available. It was used to demonstrate potential-dependent CO binding to a protein redox centre.[99, 137, 138] This model system was also used to optimise conditions for working with proteins in the SEC cell.

Myoglobin (Mb) is an oxygen-binding protein found in muscle tissues of vertebrates and almost all mammals. It is a single-chain globular protein ($M_r \approx 18$ kDa) with one haem centre which consists of a Fe atom coordinated equatorially with four nitrogen atoms of a porphyrin ring and linked axially to an imidazole group of a proximal histidine residue (His^{93}). An oxidation state change of this central Fe atom is a key feature in the oxygen storage and release in muscle cells. When Fe atom is reduced into Fe^{II}, myoglobin can reversibly bind a dioxygen molecule (O_2) to form oxymyoglobin. If the Fe atom is in the oxidised Fe^{III} state, called metmyoglobin, it cannot bind O_2 anymore. This haem active site is not only able to

bind a dioxygen, but also other small molecules such as CO and NO. It is known that reduced myoglobin can bind CO more strongly than O_2.[99, 137, 138]

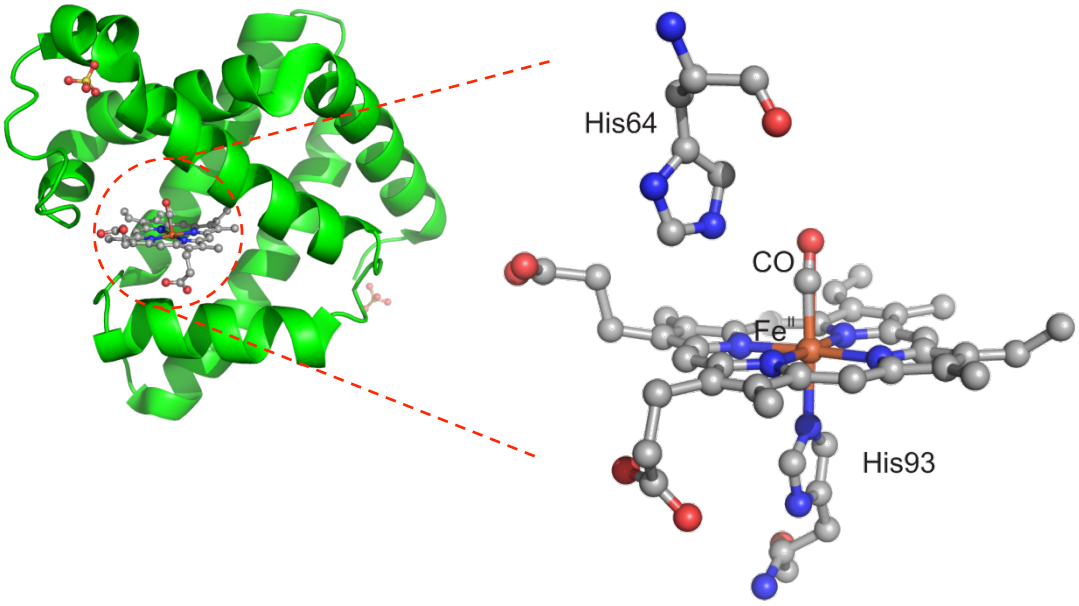

Figure 3-15: Structure of wild type myoglobin (from horse heart) complexed with CO (1DWR from RCSB PDB). Fe, N, O, and C atoms are represented as brown, blue, red, and grey spheres, respectively.

Carboxymyoglobin (MbCO) is myoglobin with the Fe^{II} centre bound to a CO molecule in a nearly end-on linear geometry (see Figure 3-15).[110] It has been employed as an IR spectroscopic probe as it exhibits a strong absorption band of ν(CO) when CO is bound to the Fe^{II} atom.[139, 140] The ν(CO) position of the CO adduct is shifted from ν(CO) of free CO (2155 cm^{-1})[109] to about 1940 – 1960 cm^{-1}, due to the π back-donation effect on the CO bond. The ν(CO) band position of MbCO is strongly influenced by the electrostatic environment inside a haem cavity, particularly the conformation of the distal histidine residue (His64) located above the Fe atom.[141, 142] So far, three major IR vibrational bands of ν(CO) have been reported; ~1965 cm^{-1} (A_0), ~1944 cm^{-1} (A_1) and ~1930 cm^{-1} (A_3). A change in the intensity of those bands largely depends on experimental conditions such as temperature, pH and pressure.[143-148]

A preliminary spectroelectrochemical study of CO binding to myoglobin was previously designed and performed by A. J. Healy (DPhil Thesis, 2013) in order to demonstrate the efficiency of the ATR-IR SEC approach. In this study, similar sets of carboxymyoglobin experiments were carried out to test various conditions necessary for nitrogenase study including gas access, stability of proteins in Nafion and the use of a flow system. The series of myoglobin work presented here was done with the assistance of C. McKenna (Part II student, 2010).

3.3.1.1 Gas access

A test for gas access into a Nafion-protein film in the SEC cell was done by monitoring CO binding to myoglobin *in situ* when it is converted into the reduced state in the presence of CO saturated solution.

In the gas-tight ATR-IR SEC cell, a Nafion-particle film containing 10 nmol of oxidised myoglobin (metmyoglobin from equine skeletal muscle, Sigma Aldrich) was prepared. A 2.0 μL aliquot of 5% Nafion mixture in 50 mM phosphate buffer, pH 6.0, was added to oxidised myoglobin solution mixed with 1.5 μL of carbon black particle suspension (10 mg/mL). The mixture was gently stirred before being applied on the ATR prism. The film was partly-dried, a piece of carbon paper (size *ca* 4 mm × 7 mm) was put on top and the cell body was assembled. Then, CO-saturated phosphate buffer pH 6.0 was introduced into the cell *via* a flow system. A Pt counter electrode and a mini Ag/AgCl reference electrode were used. No redox mediators were added in this setup since it was assumed that myoglobin is small enough to diffuse to and exchange electrons with the working electrode directly. Instead, the carbon black particles were used to form a 3D high-surface working electrode. The preparation of these particle-network working electrodes has been described elsewhere.[103]

After being left to equilibrate for 30 minutes, a background IR spectrum of oxidised myoglobin was recorded.

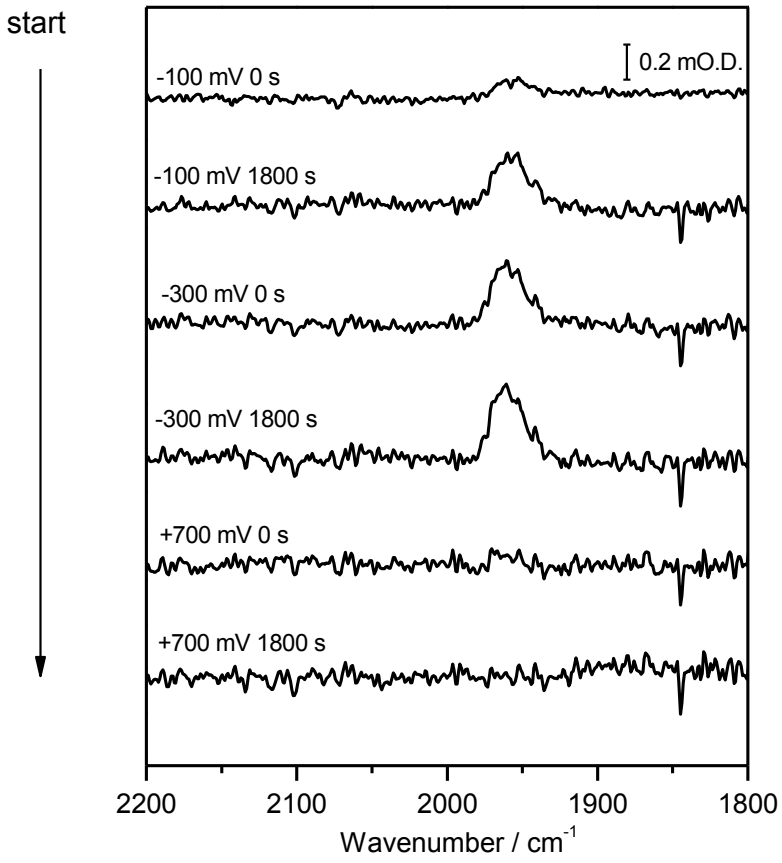

Figure 3-16: Difference spectra showing CO binding to reduced Fe(II) in myoglobin, followed by releasing of CO from oxidised Fe(III) in the particle film. All spectra were processed against the same background of oxidised myoglobin (500 scans co-added, 2 cm^{-1} resolution) and recorded at each potential step and time stated on the figure. Spectra are offset in chronological order and the spectral baseline corrections are applied.

In Figure 3-18, when a potential at –100 mV was applied, a *v*(CO) peak of carboxymyoglobin appeared at 1960 cm^{-1} indicating that Fe^{III} inside myoglobin was reduced to Fe^{II} and bound a CO molecule from the surrounding solution. A further reduction to –300 mV showed an increase in the peak intensity implying that a greater number of carboxymyoglobin molecules were formed at this potential.

Later, when the potential was stepped up to 700 mV, the Fe^{II} was re-oxidised to Fe^{III} and the bound CO molecules were released, resulting in total loss of the ν(CO) peak at 1960 cm^{-1}.

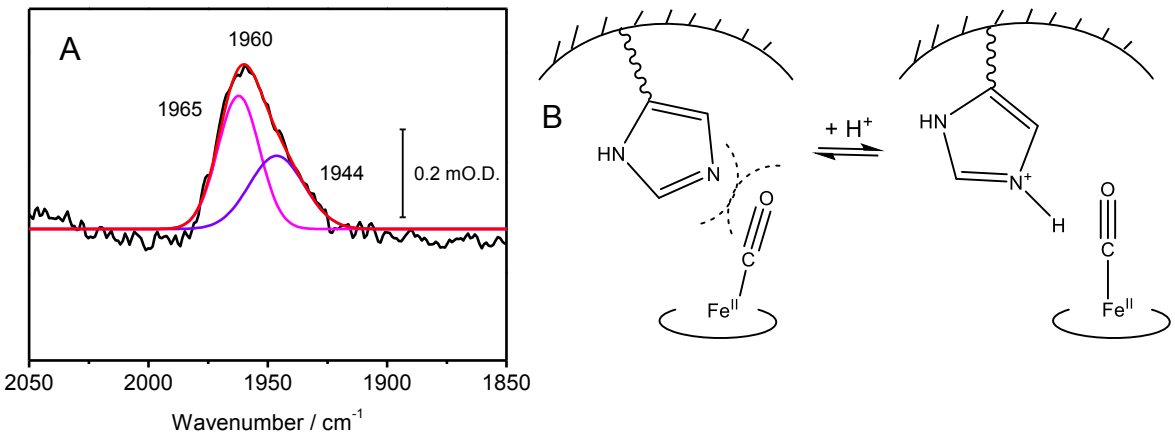

Figure 3-17: (Panel A) A fitting of a peak at 1944 cm^{-1} (purple) and 1965 cm^{-1} (pink) to a ν(CO) peak centered around 1960 cm^{-1} (red). The peak fitting was calculated using the Voigt profile (OriginPro 8.1). (Panel B) the proposed conformation change with the haem pocket of myoglobin upon protonation of His64 residue located above the active site.

In Figure 3-16, the asymmetric shape of the ν(CO) peak centred around 1960 cm^{-1} is likely to be the result of overlapping of two ν(CO) peaks; 1944 (A_1) and 1965 (A_0) cm^{-1} (see Figure 3-17A). In previous studies of myoglobin from various organisms, the peak at lower wavenumber has been found to be dominant at neutral pH, whilst the one at higher wavenumber has been found to arise from carboxymyoglobin at more acidic pH.[143, 144] It has been suggested that a conformational change at the distal histidine residue (His^{64}), as illustrated in Figure 3-17B, accounts for this shift in ν(CO) wavenumber.[109, 149] At neutral pH, the N atom of the imidazole side chain can interact with the Fe-CO bond resulting in a tilting of CO relative to the porphyrin plane. Consequently, a tilted bond causes overlapping between a π orbital of pyrrole in the porphyrin plane and a π* orbital of CO which lowers the vibrational wavenumber of CO. When the pyrrole group is protonated under acidic conditions, the tilting effect is diminished. Thus, the position of ν(CO) in the IR spectra of Figure 3-16 suggests that carboxymyoglobin molecules are partially protonated at pH 6.0.

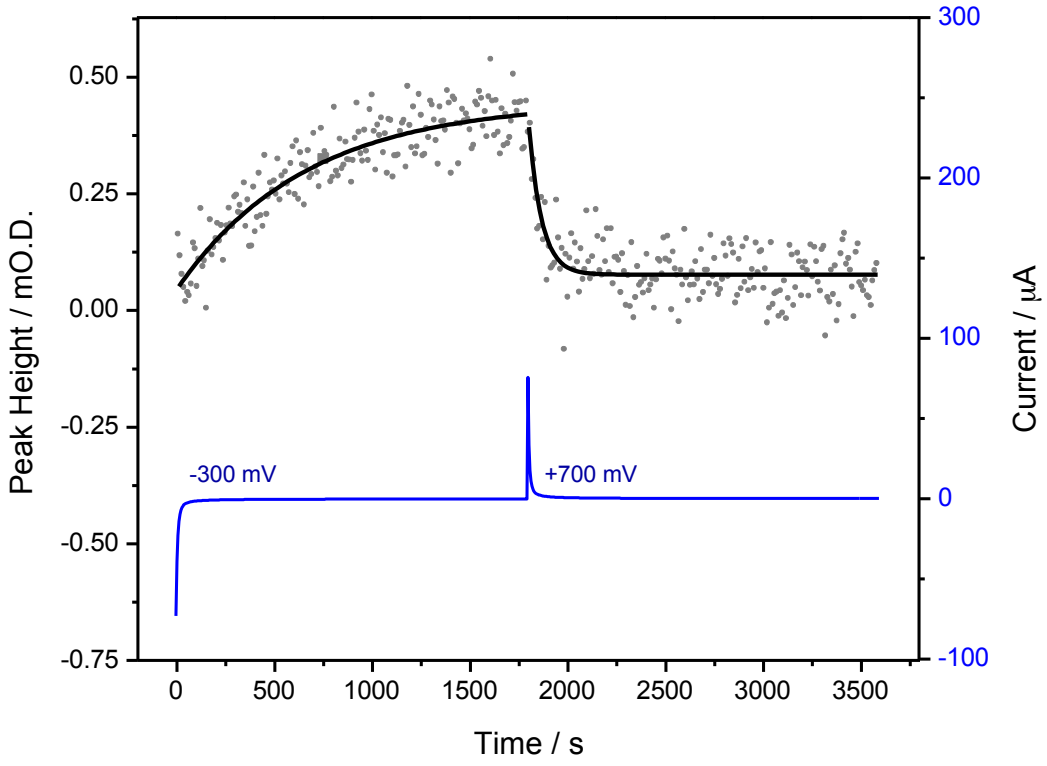

Figure 3-18 : A kinetic plot of *ν*(CO) peak height at 1960 cm^{-1} (grey points, experimental data; fitting curve solid black line) against time during the reduction (–300 mV) and re-oxidation (+700 mV) of 10 nmol of myoglobin in CO-saturated phosphate buffer at pH 6.0 (18 scans co-added, 2 cm^{-1} resolution). A chronoamperogram of applied voltages is shown in blue. Data reproduced from the D.Phil Thesis of A. Healy.[150]

According to a kinetic study of CO binding inside the SEC cell by A. Healy (DPhil Thesis, 2013) shown in Figure 3-18, when a reducing potential was applied, a rapid growth of a *ν*(CO) peak at 1960 cm^{-1} indicated that CO molecules in the Nafion-particle film on the prism surface were spontaneously bound to the reduced myoglobin. This presumably causes a depletion of CO concentration in the film, necessitating more CO from solution at the back of the SEC cell to diffuse into the film and bind to other reduced myoglobin. This resulted in a steady increase of a peak at 1960 cm^{-1} until it reached equilibrium when all reduced myoglobin molecules were bound to CO molecules. This implied that Nafion-particle network allowed CO molecules in the CO-saturated solution (*ca* 1.0 mM CO) to diffuse into it within a reasonable time frame.

In addition, a dramatic decrease of the same peak when the working electrode was switched to high potential implies that majority of myoglobin molecules became oxidised and released bound CO molecules at once. This is indicative of effective electrochemical control inside the Nafion network layer of the SEC cell.

3.3.1.2 Effect of buffer and pH on Nafion

It is important that experimental conditions inside the IR-SEC cell are compatible with biological molecules. The stability and reactivity of a given protein largely depends on the kind of buffer solution and pH value used. Despite the fact that a phosphate buffer proves to be compatible with myoglobin, other buffer systems are commonly used in a nitrogenase assay such as Tris-HCl buffer and HEPES buffer in the pH range 7-8.[63, 67, 68, 76, 151]

In our SEC set up, a Nafion mixture is the key component that traps protein molecules at the prism surface. It is important to verify that a Nafion mixture still has its binder property after mixing with different buffer solutions at specific pH values. Thus, several sets of myoglobin-CO SEC experiments were performed using mixtures of Nafion with various buffer solutions and pH values as listed in Table 3-3.

.

Table 3-3: Conditions of Nafion mixture in various buffer solutions

No.	protein sample layer	wt %	bulk solution	conc. (mM)	pH
1	No Nafion	–	KPB	50	6.0
2	Nafion – KPB	5.0	KPB	50	6.0
3	Nafion – HEPES	5.0	HEPES buffer	50	7.4
4	Nafion – HEPES	6.7	HEPES buffer	50	7.4
5	Nafion – Tris-HCl	5.0	Tris-HCl buffer	50	7.4
6	Nafion – Tris-HCl	6.7	Tris-HCl buffer	50	7.4

* Nafion – KPB at pH 7.4 was omitted as it is too viscous to be handled.

In each experiment, a Nafion solution was prepared by titration of 10 wt % Nafion resin as an aqueous suspension (pH 1-2, Sigma-Aldrich) with conc. NaOH until it reached neutral pH value, and then it was mixed with desired buffer solution at either 1:1 or 2:1 ratio to give a mixture of 5.0 – 6.7 % Nafion in 50 mM of buffer. The pH value of the mixture was adjusted with either NaOH or HCl to achieve a determined value. At this stage, the texture of a Nafion solution is viscous but can still be dispensed using a pipette. The mixture then was left open inside an anaerobic glove box overnight to get rid of all air trapped inside.

A set up of the SEC cell with 10 nmol of oxidised myoglobin in a Nafion layer and CO-saturated buffer solution in the back of the cell was done in the same way as described in the gas access test (section 3.3.1.1). A spectrum of oxidised myoglobin was recorded and later used as the background for the rest of the spectra.

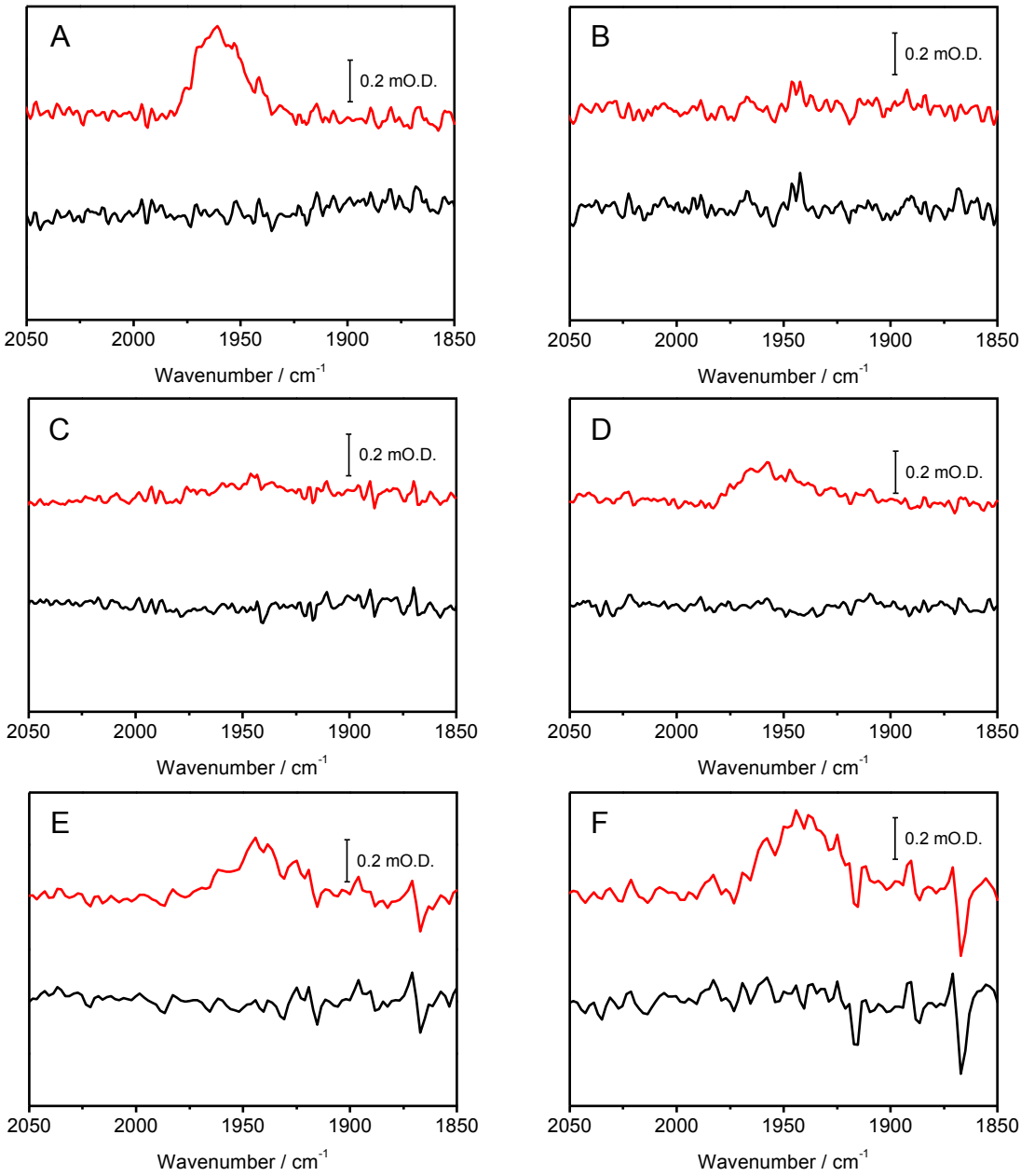

Figure 3-19: Difference spectra of carboxymyoglobin in various Nafion–buffer conditions; (A) Nafion-KPB 5.0% pH 6.0, (B) KPB pH 6.0 no Nafion, (C) Nafion-HEPES 5.0% pH 7.4, (D) Nafion-HEPES 6.7% pH 7.4, (E) Nafion-Tris 5.0% pH 7.4 and (F) Nafion-Tris 6.7% pH 7.4. Each panel shows CO binding at the reduced level (–300 mV, red line) and the following CO release from the oxidised state (+700 mV, black line). All spectra were processed against the oxidised myoglobin background recorded before applying potential (500 scans co-added, 2 cm^{-1} resolution) and the baseline corrections were applied.

Figure 3-19 shows that after applying a potential of –300 mV for 30 minutes, myoglobin was reduced and carboxymyoglobin was formed in most of the Nafion-based films, while no

v(CO) peak was detected in the case of non-Nafion film (Panel B). Following the re-oxidation step, carboxymyoglobin in all of Nafion-based films responded in a similar way by releasing CO molecules, resulting in complete loss of *v*(CO) peaks. This is evidence that the Nafion polymer is able to trap the protein molecules onto the prism surface and prevent the protein diffusing away into the bulk solution during the experimental time frame.

At pH 7.4, it was shown that the peak intensity of *v*(CO) in Nafion with Tris-HCl buffer was significantly higher than the one with HEPES buffer. This suggests that Nafion network in Tris-HCl is more suitable for trapping myoglobin molecules within it compared to the Nafion in HEPES at the same pH. The *v*(CO) peaks observed in both buffer systems at pH 7.4 have lower wavenumbers positions than the one in phosphate buffer at pH 6.0 showing the pH effect on the conformational change inside the haem pocket as discussed previously.

An effect of the ratio between the Nafion and buffer solution was also tested using the carboxymyoglobin system. It was found that increasing a percentage of Nafion in solution from 5.0 to 6.7 gave a more viscous mixture, resulting in enhancement in a *v*(CO) peak intensity in both Tris-HCl and HEPES buffer systems. This may imply that using more concentrated Nafion polymer helps accommodate a larger number of protein molecules within its layer. However, a percentage of Nafion in buffer beyond 6.7% gave mixtures that were too viscous to be handled properly.

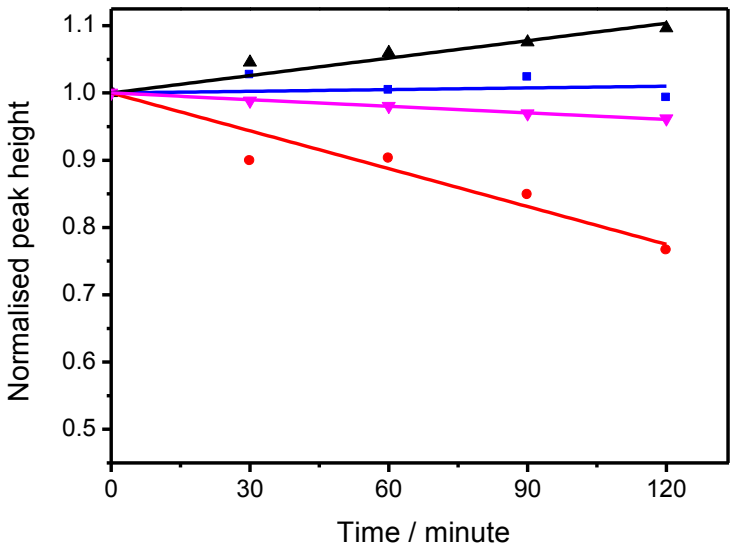

Figure 3-20: Plots of normalised peak height of the amide II band at 1545 cm^{-1} under various experimental conditions as a function of time; Nafion-KPB 5.0% pH 6.0 (black), Nafion-Tris 6.7% pH 7.4 (blue), Nafion-HEPES 6.7% pH 7.4 (pink) and KBP pH 6.0 non-Nafion (red). Peak heights were taken from spectra of the myoglobin film in the SEC cell recorded every 30 minutes and processed against a background of the unmodified Si prism (500 scans co-added, 2 cm^{-1} resolution).

In Figure 3-20, the stability of trapped myoglobin on the prism surface under various conditions was compared by monitoring changes in the amide II band (~1545 cm^{-1}) from spectra recorded over a period of 120 minutes. As expected, it was found that peak heights of the amide II band in the Nafion-based protein films remain more constant compared to the one without the Nafion component. A lack of Nafion network results in a loss of approximately 25% of the protein population at the prism surface over 2 hours, whereas the Nafion layers retain at least 95% of original myoglobin population over the same time course. In the Nafion-phosphate, the intensity of the amide II feature slightly increased over time. This may be a result of dehydration in the Nafion film causing an increase in protein concentration close to the prism surface. In conclusion, a mixture of Nafion 6.7% in Tris-HCl buffer pH 7.4 seems to be the most suitable condition to use with nitrogenase in the SEC cell setup. Although myoglobin cannot entirely represent all metalloproteins, this optimised condition will be the starting point for studying nitrogenase.

3.3.1.3 Flow system

A study of potential-dependent ligand binding to the redox site of an enzyme requires introduction of substrate or inhibitor while the protein sample is under electrochemical control. In this way, a change in the vibrational frequency of a ligand can be monitored *in situ* as it binds to the active site at certain redox states. This will provide useful information about the potential dependence of ligand binding.

In this experiment, the SEC cell with 10 nmol of oxidised myoglobin was set up similar to the previous myoglobin-CO experiment, except that CO-saturated buffer was omitted. A potential of –300 mV was applied at the working electrode for 20 minute before a background spectrum of myoglobin in the reduced state was recorded. Then, CO-saturated buffer was introduced to the SEC cell *via* a peristaltic pump at flow rate 0.40 mL per minute, while the potential was still held at –300 mV. The CO-saturated solution was circulated for approximately 5 minutes before the flow was stopped and the system was left to equilibrate. Then, a set of spectra were recorded against a background of reduced myoglobin in the absence of CO.

After the flow was stopped, the spectra showed a growth of the ν(CO) peak of carboxymyoglobin completing within 20 minutes similar to the previous experiment. It indicated that CO molecules were transferred into bulk solution in the SEC cell by the flow system, and diffused into the particle network film. When the potential was stepped to 700 mV to generate the oxidised state of myoglobin, loss of the ν(CO) peak was observed immediately. This also suggested that the particle film was stable and undisturbed under the solution flow.

This experiment demonstrated that an enzyme substrate or inhibitor can be introduced to the Nafion film while it is under stable electrochemical control. For longer duration experiments

this flow system could be modified by maintaining constant flow of gas-saturated buffer into the SEC cell, providing that the whole setup is in the glove box and there is a gas out channel into a flume hood.

In summary, this carboxymyoglobin test system shows that study of potential-dependent ligand binding to a redox site inside a protein using the ATR-IR SEC approach is feasible. It suggests that this system could be suitable to apply to nitrogenase MoFe protein.

Chapter 4

Electrochemical study of electron transfer in the MoFe protein

In this chapter, electrochemical techniques were utilised to study the nitrogenase MoFe protein. Electron transfer to the nitrogenase MoFe protein was demonstrated using the electron-mediated system described in Chapter 3. The first nitrogenase-catalysed substrate reduction under electrochemical control is presented. Electrocatalytic activity and inhibition of different variants are investigated and discussed in the following section.

4.1 Introduction

A study of ligand binding to the MoFe protein of nitrogenase has proved demanding due to the difficulty in controlling electron transfer, and the occurrence of coupled proton reduction. In order to explore the properties of nitrogenase, electrochemical control over electron transfer in the protein would be beneficial.

4.1.1 Mediated electron transfer techniques

Determination of substrate-binding potential in nitrogenase is essential to elucidating substrate reduction catalytic mechanism of this redox metalloenzyme. However, a major challenge lies in electrochemical control over nitrogenase. Under turnover condition, the MoFe protein of nitrogenase requires electron transfer from the Fe protein counterpart coupled with ATP hydrolysis. This complicates control of the electron transfer process, and hinders direct electrochemical control of nitrogenase.

Therefore, in this work, an electron-mediated method is developed to overcome this electron transfer hurdle. Previously, structure and redox properties of nitrogenase metal clusters have been studied using potential titration with redox mediators, coupled with other characterisation techniques such as EPR spectroscopy and X-ray absorption spectroscopy.[24, 84, 91, 152] However, most commonly used organic compounds mediators have midpoint potentials in a mildly-reducing range of 0 to –600 mV, and are unable to achieve the reduction potential required for turnover of the enzyme.

More recently, some novel approaches have been developed to provide ATP-independent turnover conditions for nitrogenase catalysis. The use of Eu-polycarboxylate complexes as powerful reductants has been shown to support two- and four-electron substrate reduction by nitrogenase MoFe protein variants as described in Chapter 3. Another approach was developed by Roth and co-workers, by attaching a photosensitising Ru compound on the protein surface near the redox sites. It was shown that the modified MoFe protein was capable of photocatalysis of the reduction of protons, acetylene and hydrogen cyanide.[56, 153] Despite that, the dinitrogen reducing level remains unreachable by other mediated electron transfer than Fe protein and ATP. It has been suggested that reduction of dinitrogen might require Fe protein interaction not only to obtain electrons but also to induce conformational change that

allows dinitrogen binding and cleavage of its triple bond.[55, 85] This Fe protein-induced change could be the limitation of mediated-electron transfer technique and needs to be investigated further.

4.1.2 Proton reduction by nitrogenase

In nitrogenase, catalysis of proton reduction to dihydrogen, also referred to as hydrogen evolution, spontaneously occurs when the MoFe protein is under the turnover condition in the absence of other substrates. This reaction requires two electrons transferred by the Fe protein, each electron transfer coupling with hydrolysis of two ATP molecules. Interestingly, a study by Eady and co-workers revealed that *Klebsiella pneumoniae* nitrogenase in the presence of MgADP and AlF_4^- showed small activity of proton reduction, so they suggested that ATP was not the only molecule that can transfer energy to this process.[154] It was reported that proton reduction reactivity strongly depends on pH value and an optimum pH for proton reduction under Ar of *A. vinelandii* nitrogenase was found to be at pH 7.5 with catalytic activity *ca* 500 nmol H_2 per minute per mg total protein. It was shown that the rate decreased by 50% at pH lower than 6.3 and higher than 9.0.[67] Reduction of protons is also competitive with reduction of dinitrogen under the turnover condition of nitrogenase.[19, 155] It was found that dinitrogen can only partly suppress this proton reduction and the limiting ratio between these two reactions depends on the type of nitrogenase and experimental conditions. For instance, the limiting stoichiometry of reduced N_2 to produced H_2 in the cases of Mo-nitrogenase and V-nitrogenase are 1:1 and 1:3.5, respectively.[85, 156] On the other hand, many early studies showed that acetylene and cyanide were able to fully inhibit proton reduction.[63, 157]

A complete mechanism of the proton reduction and the importance of this reaction to the main dinitrogen fixation process are still unknown. Both experimental and computational studies have indicated that binding of protons and release of dihydrogen happen at the early

oxidation states of the enzyme, either two- or four-electron reducing state.[155, 158-160] It has been suggested that proton binding to the active site involves formation of a metal hydride, with production of dihydrogen *via* a reductive elimination pathway.[53, 161]

The catalytic capability of hydrogen production in nitrogenase has been compared to those of Mo-containing heterogeneous catalysts such as molybdenum disulphide (MoS_2). This inorganic Mo compound was found to be able to catalyse proton reduction with low over-potential under mild conditions[162] so it has been of interest for an alternative catalyst for industrial hydrogen production.[163-165] Therefore the Mo atom on the FeMoco might involve in the proton reduction activity of the enzyme.[53, 67]

4.2 Electrochemical study of the wild type MoFe proteins

In this section, electrochemical study was performed on wild type MoFe protein in the absence of the partner Fe protein and ATP supply. A system of low-potential redox mediators, Eu-polycarboxylate complexes, was exploited to transfer electrons from an electrode surface to the active site of the enzyme at very negative potentials.

4.2.1 Experimental

4.2.1.1 Protein samples

In this section, two MoFe proteins of nitrogenase from *Azotobacter vinelandii* were examined; wild type MoFe protein and apo-protein (FeMoco-deficient variant). These protein samples were prepared by collaborator from Lance Seefeldt and his group at Utah State University, United States. The activity assay in the presence of Nafion, the polymer used as an electrolyte and binder in the SEC setup, was performed by our collaborator and it was found that Nafion has no significant effect on catalytic activity of the MoFe protein.

The samples were stored in a liquid nitrogen dewar and handled in an anaerobic glove box. Prior to an experiment, the protein sample was first washed with Tris-HCl buffer to remove any trace of sodium dithionite, a reductant that is used for stabilising the protein during the delivery. In some cases, sample solution was concentrated in a 100 kDa cut-off microcentricon tube to get a suitable concentration for formation of the Nafion-protein film (approximately 80 $mg.mL^{-1}$).

4.2.1.2 Electrochemical cell

An electrochemical cell used in this chapter was slightly modified from the SEC cell described in the previous chapter. The entire cell body and base plate were made of polyether ether ketone (PEEK) material; the ATR-IR prism part was omitted as shown in Figure 4-1.

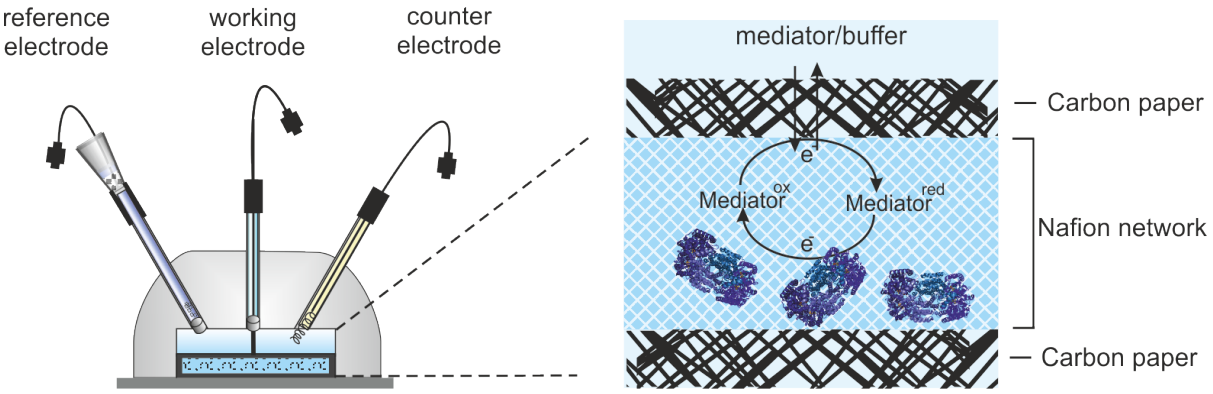

Figure 4-1: A schematic diagram of electrochemical cell with three-electrode system (left). A cartoon showing protein trapped in Nafion network in between two carbon papers served as an extended working electrode (right).

The cell body houses three electrodes on the top and electrolyte solution inside the cell cavity (*ca* 250 µL). Nafion polymer was also employed as an electrolyte and a binder, which traps protein molecules within its network. The Nafion-based protein film will allow solution to be flowed over and makes it possible to introduce solutes without losing the protein from the film. Carbon paper was used as a working electrode placed at the bottom of the cell. Its

carbon fabric mesh helps increase an electrode surface area but allows mediators to diffuse into the Nafion-protein layer.

4.2.1.3 Low potential redox mediators

As this chapter focuses on an electron transfer in the very low potential range, a system of low potential redox mediators was utilised exclusively. Three $Eu^{III/II}$-complexes were selected to use for this purpose; Eu-BAPTA (–634 mV), Eu-EGTA (–868 mV) and Eu-DTPA (–1090 mV) Electrochemical properties and compatibilities of these complexes were presented previously in Chapter 3. A mediator solution containing 0.25 mM of each of the three Eu-complexes in Tris-HCl buffer pH 7.4 was prepared as described previously.

4.2.1.4 Electrochemical cell preparation and current measurement

The electrochemical cell containing a protein sample was prepared in a similar manner to the cell for SEC study, however slight differences are described here. First, the 5.0 µL dithionite-free protein sample was mixed with 2.5 µL Nafion-Tris suspension pH 7.4. Then, the mixture was deposited directly on a piece of carbon paper (size 4 × 7 mm^2) to form a Nafion-protein film on the working electrode. The protein sample was concentrated by partial evaporation to give a total of approximately 2.0 nmol of protein in Nafion network. Another piece of carbon paper was placed on top of the film before the carbon electrode connector was contacted to it. Later, the cell body was assembled and filled with redox mediators in Tris-HCl buffer solution. A counter electrode (Pt) and a reference electrode (SCE) were screwed in last to avoid air bubbles trapped in the back of the cell.

All cell preparation and experiments were carried out inside an anaerobic glove box under a N_2 atmosphere, unless indicated otherwise. The electrochemistry was controlled and current was measured using a potentiostat (Autolab).

An analytical electrochemical technique, chronoamperometry, was employed, by which the MoFe protein was reduced indirectly *via* redox mediators at a particular electrode potential and the corresponding current was measured as a function of time. All potentials were converted and quoted against SHE ($E_{SHE} = E_{SCE} + 0.241$ V at 25 °C).[118] The observed negative current corresponds to electron transfer for an electrochemical reduction.

4.2.2 Proton reduction by the MoFe protein

In this set of experiments, a sequence of potential steps was applied on the working electrode in the cell containing protein sample and redox mediators. Each potential was held for at least 5 minutes to allow the system to equilibrate and obtain a steady current ahead of the next potential step. At first, the working electrode was held at –300 mV to keep the Eu-ligand mediators in their Eu^{III} forms. Then, potential steps were applied starting from –700 mV and becoming increasingly negative in 50 mV intervals to trigger reduction of Eu^{III}-BAPTA, Eu^{III}-EGTA and Eu^{III}-DTPA, respectively. However, it should be noted that a further step beyond -1000 mV was avoided as proton reduction at the carbon paper working electrode occurred, as described previously in Chapter 3, resulting in a massive current that masks the catalytic current of interest and leads to H_2 bubbles that disturb the Nafion-protein film.

In Figure 4-2, the chronoamperogram for a cell containing only the three Eu-ligands complexes (*i.e.* no protein) shows a slight increase in magnitude of reduction current (*ca* 2.5 μA) when the potentials was decreased to –700 mV. At more negative potentials, from –800 to –950 mV, it shows no significant increase in reduction current. Thus, the observed small reduction current was arises from reduction of the Eu^{III}-ligand complexes. From this control experiment, it confirmed that proton reduction by the carbon working electrode was not observed in this potential window.

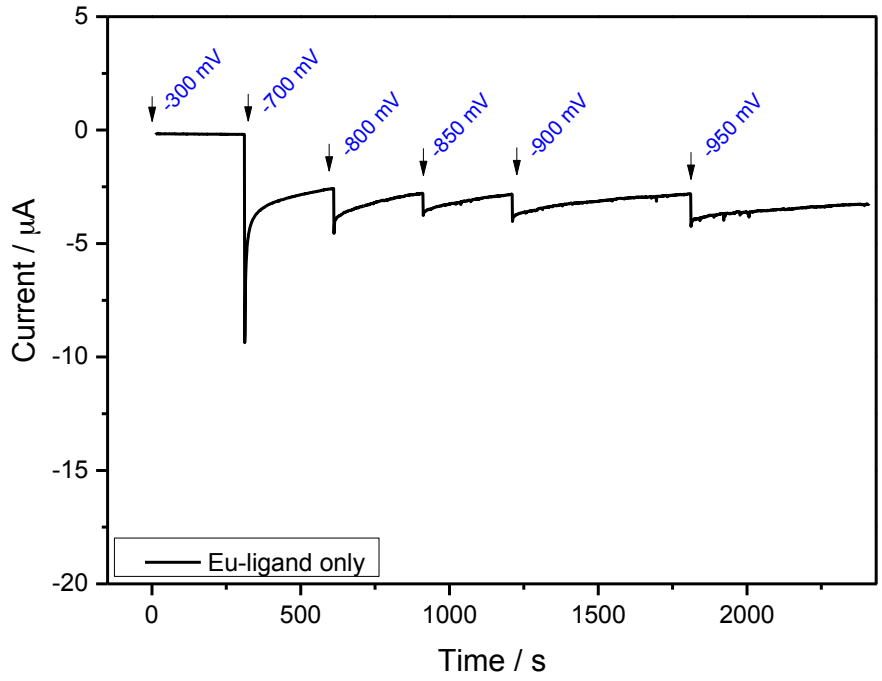

Figure 4-2: Chronoamperograms of Eu-ligand mediator solution, consisting of Eu-BAPTA, Eu-EGTA and Eu-DTPA 0.25 mM each, in the electrochemical cell. A sequence of potential steps was applied at the indicated times.

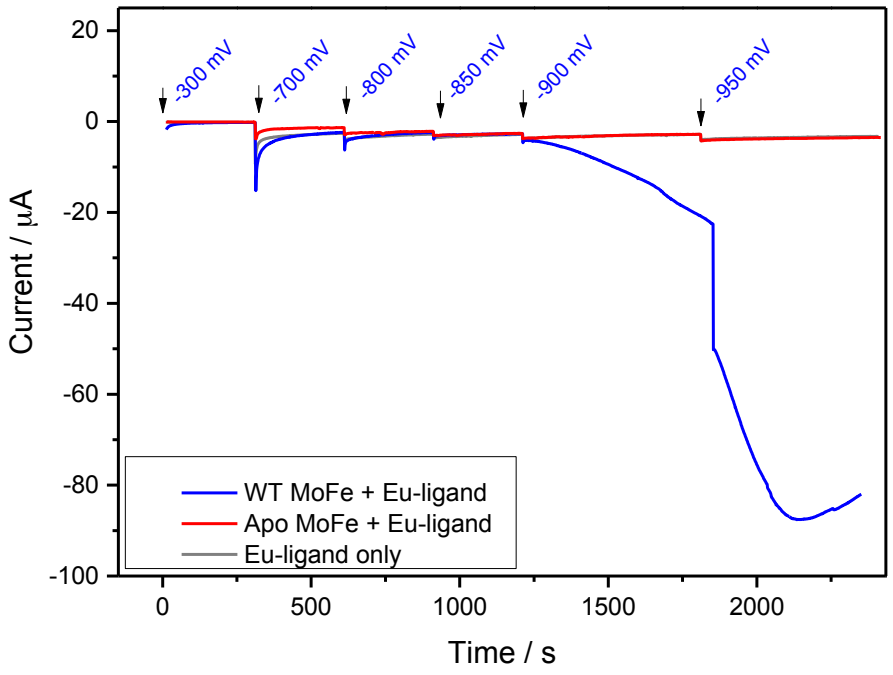

Figure 4-3: Chronoamperograms of 2.0 nmol wild type MoFe protein (blue), 2.0 nmol apo-protein (red) both in presence of Eu-ligand mediators (0.25 mM each of Eu-BAPTA, Eu-EGTA and Eu-DTPA) and control experiment with Eu-ligand mediators only (grey). The protein sample was trapped Nafion while the Eu-ligands were in the cell solution in contact with the Nafion. A sequence of potential steps was applied at the indicated times.

In Figure 4-3, the chronoamperogram of the wild type MoFe protein recorded in the presence of Eu-ligand mediators shows no significant increase in reduction current when the electrode potential was held at values from –300 mV to –850 mV. After application of a –900 mV potential, a building up of catalytic current was observed. At potential –950 mV, the catalytic current continued increasing for *ca* 500 second, reaching a maximum of –80 μA, before it started to drop. After a decline in current, some current disruptions were observed indicating interruption in electrochemical control. Later, it was found that this disruption was caused by gas bubbles as shown in Figure 4-4. Bubbles were not seen in either apo-protein or the blank experiments with Eu-ligand complexes only.

In the apo-protein case, the MoFe variant that contains only the P-cluster but no FeMoco active site, no notable catalytic current was observed throughout apart from small background current of less than 5 μA, similar to that in the experiment with the Eu-ligand complexes alone.

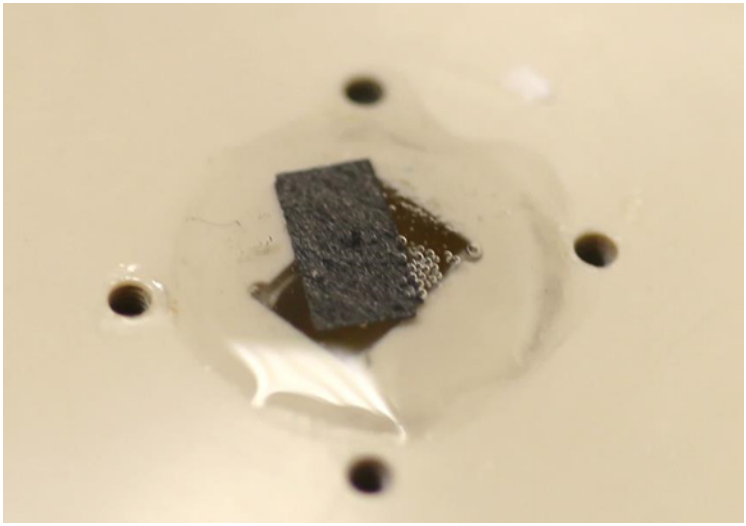

Figure 4-4: Gas bubbles were observed on the Nafion layer containing the wild type MoFe protein after application of the potential –950 mV.

In order to confirm that the catalytic current from the MoFe protein relies upon mediation by the reduced Eu-ligand complexes, a set of control experiments without the Eu-ligand complexes were conducted. In Figure 4-5, the wild type protein shows no significant catalytic current in the low potential range compared to the one in Eu-ligand mediator system. At –950 mV, a slight increase in catalytic current (*ca*1 µA) was observed over time. For the apo-protein in the absence of the Eu-ligand mediators, no significantly increasing current was observed, similar to the one from the cell containing buffer only.

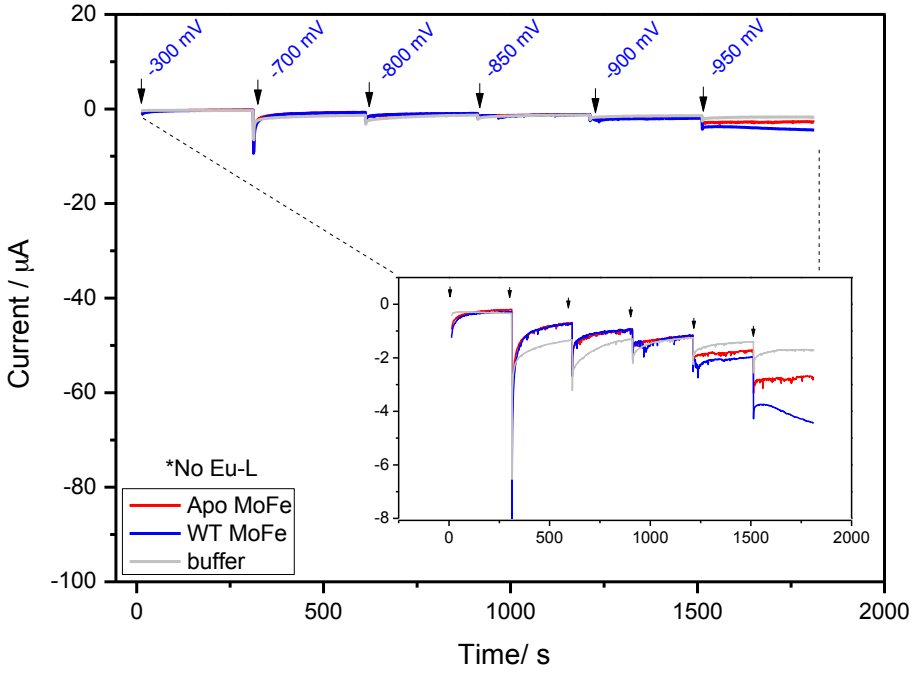

Figure 4-5: Non-mediated electron transfer experiment of 2.0 nmol wild type MoFe protein (blue) and 2.0 nmol apo-protein (red) in Tris-HCl buffer pH 7.4 compared to the buffer only 'blank' experiment (grey)

Another set of experiments (Figure 4-6) were performed under an inert Ar atmosphere to investigate the possible electrocatalytic reduction of N_2 by the MoFe protein in the previous experiment. In this set up, an electrochemical cell was filled with Ar-saturated redox mediator solution. For the experiment on the wild type MoFe protein, as potential steps were applied, a reduction current started to increase slightly at –850 mV and rose further at lower potential. After completing all steps, the bulk solution in the cell was replaced by N_2-saturated solution.

Similar reduction currents were obtained when the same potential sequence was applied on the N_2 saturated system.

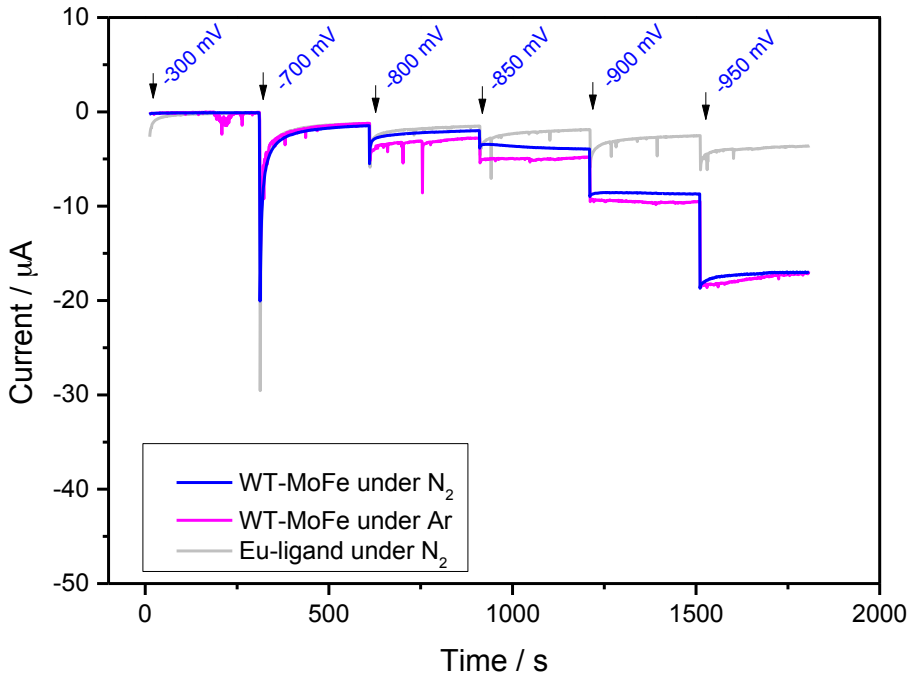

Figure 4-6: Chronoamperograms of 2.0 nmol wild type MoFe protein in presence of Eu-ligand mediators saturated with Ar (pink) and N_2 (blue) compared with control experiment with Eu-ligand mediators only (grey). A sequence of potential steps was applied at indicated times.

4.2.3 Acetylene inhibition

According to previous studies, acetylene is able to inhibit nitrogenase-catalysed reduction of dinitrogen, azide and protons. Here, acetylene inhibition was used to confirm the reduction of protons by the MoFe protein under mediated electrochemical control. Acetylene gas used in these experiments was generated by reacting calcium carbide (CaC_2) with O_2-free water in a custom-made flask inside the glove box (Figure 4-7). An acetylene production reaction is shown below.

Production of acetylene: $CaC_2 + 2\ H_2O \rightarrow C_2H_2 + Ca(OH)_2$

A small amount of dithionite was added to the water to minimise contramination of oxygen from CaC_2. During the reaction, the product gas was isolated and then blown into a vial of the Eu-ligand mediator solution which was flowed continuously into the electrochemical cell at a flow rate of 1.0 mL per minute.

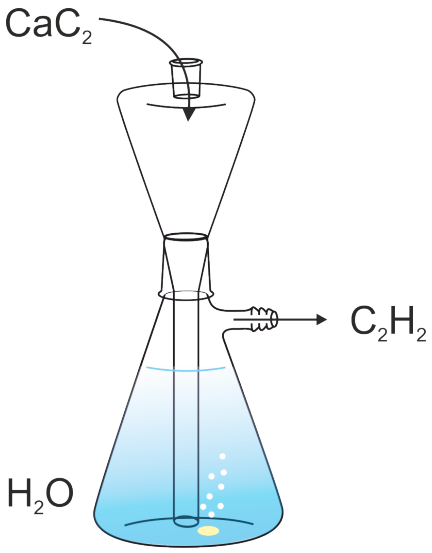

Figure 4-7: A custom-made acetylene-generating bottle. A gas product outlet is connected with the flow system and acetylene gas is flushed into the solution which is flowed through the electrochemical cell.

An experiment involving introduction of acetylene is shown in Figure 4-8. Addition of acetylene to the wild type MoFe protein at an applied potential of –900 mV caused a sudden drop of catalytic current. Then acetylene was flushed out, and the current became steady after that *ca* 5 minutes. When the potential was lowered to –950 mV, the reduction current recovered partly until another addition of acetylene was made. The decrease in current in response to acetylene was now smaller compared to the addition at –900 mV. The current again became steady after acetylene was removed.

Interestingly, in the case of apo-protein shown in Figure 4-9, a similar change in current response upon introduction of acetylene was observed but on a much smaller scale than the wild type MoFe protein. This observation will be discussed in the following section.

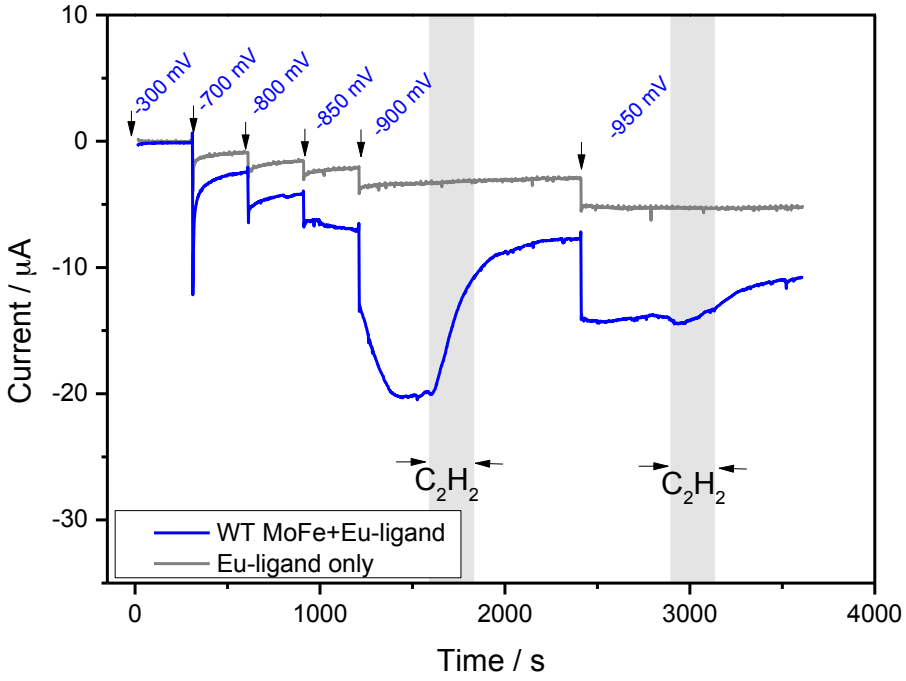

Figure 4-8: Chronoamperograms of 2.0 nmol wild type MoFe protein in presence of Eu-ligand mediators with the flow system at flow rate 1.0 mL per minute (blue). Acetylene was introduced to the flow system at the time periods indicated by a grey background. A control experiment with Eu-ligand mediators only was performed (grey line).

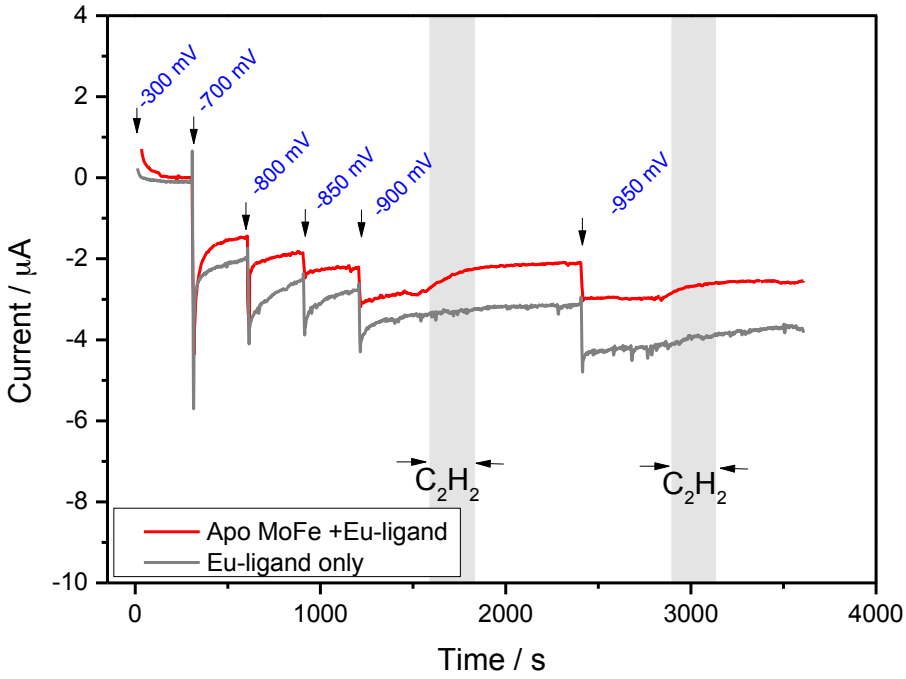

Figure 4-9: Chronoamperograms of 2.0 nmol apo-protein in presence of Eu-ligand mediators with the flow system at flow rate 1.0 mL per minute (red). Acetylene was introduced *via* the flow system at the time periods indicated by a grey background.

4.2.4 Discussion: Proton reduction by the MoFe protein

First, an increase in the magnitude of the reduction current for the wild type MoFe protein case on stepping to –900 mV is significantly higher than the reduction currents from Eu-ligand complexes alone. The potential at –900 mV is close to the reduction potential of the $Eu^{III/II}$-EGTA couple (–868 mV), and Eu^{II}-EGTA has been previously reported to be able to transfer electrons to a genetically-modified MoFe protein for reduction of hydrazine (section 3.2.1).[55] Another potential step to –950 mV seemed to encourage more electron transfer to the protein as shown in Figure 4-10. Due to the fact that this potential lies between $Eu^{III/II}$-EGTA and $Eu^{III/II}$-DTPA couples (–1090 mV), this observation is consistent with several previous reports on the use of Eu^{II}-DTPA as an effective reducing agent for some substrate reductions by MoFe protein variants.[55, 119, 120] Thus, it is highly possible that the observed increased current arises from electron transfer from Eu^{II}-EGTA and Eu^{II}-DTPA mediators to the MoFe protein. It was noted that with the wild type MoFe protein in the flow cell, a small catalytic current was observed at –850 mV, which was unable to be detected without solution flow. This implied that electron transfer by Eu-ligand complexes to the MoFe protein is under diffusion control. A control experiment with the wild type MoFe protein in the absence of Eu-ligand complexes showed no significant reduction current at either –900 mV or –950 mV, confirming that the redox mediators were required to support electron transfer in the system.

Subsequently, a MoFe protein-catalysed substrate reduction was considered and the plausible substrates for the MoFe protein present in the system were dinitrogen and protons. Both of them have never been reported to be reduced electrocatalytically by nitrogenase before. A reduction of dinitrogen was ruled out by the control experiment under Ar gas, in which a catalytic current response was still observed at low potential. Therefore, proton reduction catalysed by the MoFe protein is likely as shown in Scheme 4-1.

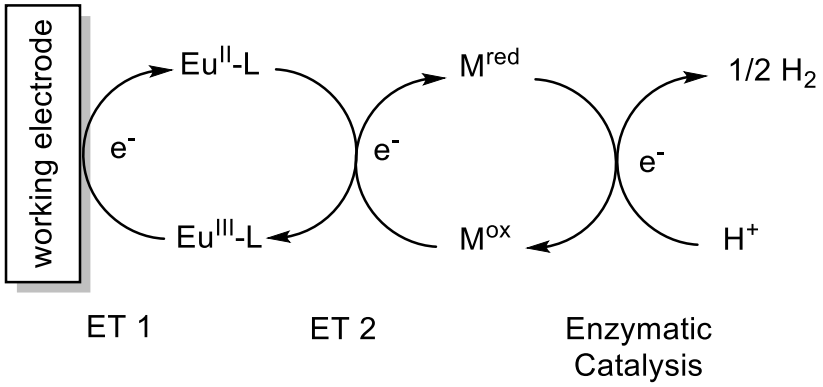

Scheme 4-1: The proposed electrochemically-driven electron transfer steps to support proton reduction by MoFe protein. M represents the enzyme-bound redox sites. The first electron transfer (ET) occurs on the electrode surface and the second in solution inside the Nafion layer.

Although previous studies found that Eu^{II}-EGTA and Eu^{II}-DTPA are able to reduce protons and acetylene, no notable change in current was observed when adding acetylene to the control experiment containing only Eu-ligand complexes in solution, probably due to the low concentration of Eu-ligand used. Thus, the observed catalytic current in the case of the protein sample has to arise from mediated electron transfer from Eu^{II}-ligand to the MoFe protein.

The presence of acetylene appeared to partially suppress the MoFe protein-dependent reduction current at –900 mV and below. This is consistent with previous studies that established acetylene as an inhibitor for catalysis of proton reduction by nitrogenase.[63, 157] After acetylene removal, the current slowly became steady but catalytic current was not recovered. When the potential was decreased to more a negative value, a small catalytic current was again observed. This current could be stemmed from some remaining active protein molecules which did not react with acetylene at previous potential step. The fact that no activity recovered after removal of the inhibitor could suggest that the recovery process is slow and possibly required redox reactivation at a more negative potential or that inhibition is irreversible under the experimental condition. The reduction of acetylene itself was not observed in these experiments, although it is possible that an increase in current magnitude

from acetylene reduction could be masked by the decreasing current from acetylene inhibition of proton reduction. Alternatively, this might indicate that acetylene is able to block proton reduction by the MoFe protein at this redox level, presumably acetylene must bind if it inhibits, but is unable to bind and be reduced by the protein under these experimental conditions.

Interestingly, acetylene also caused a drop in the small catalytic current observed in the apo-protein. Although there has been no direct evidence reported that the apo-protein can catalyse proton reduction, a recent study showed that the apo-protein (Δ*nifB*) is able to catalyse reduction of CO and cyanide using Eu^{II}-DTPA as a reducing agent, although with a very low rate.[120] This suggests that electron transfer to the apo-protein by Eu^{II}-ligand complexes is possible. The observation of acetylene inhibition from this experiment implies that the apo-protein might also be able to catalyse a trace of proton reduction.

In this present study, the electrochemical data points out that the observed catalytic current arises from proton reduction catalysed by the wild type MoFe protein under electrochemical control *via* the Eu-ligand mediators. An electron transfer to the protein at low potential can be achieved using a system of Eu-ligand mediators.

Figure 4-10 shows a rate of electrons passed from the electrode at each potential step. The number of moles of product generated can be calculated from Faraday's law, assuming that 100% of the electrons passed were used in the electrocatalysis reaction;

$$N = \frac{It}{nF}$$

Where N is number of generated products (mol), I is rate electron flow or current (A), t is total time passed (s), n is number of electrons involved in the reaction and F is Faraday's constant (9.6485×10^4 A.s.mol^{-1}).

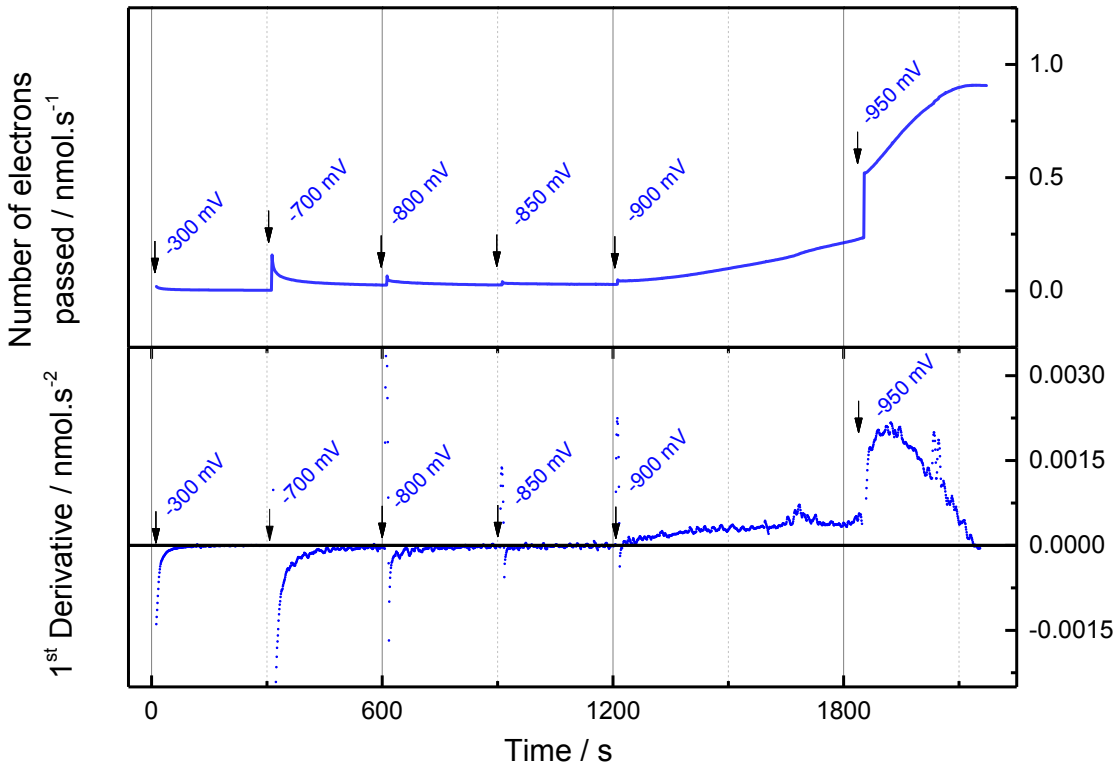

Figure 4-10: The plots of a number of electrons passed from the electrode against time from the experiment of the wild type MoFe protein in presence of Eu-ligands (above) showing the rate of electron transfer and its first derivative against time (bottom) showing the change in a rate of electron upon changing potentials.

At the most negative potential applied at –950 mV, it was found that the number of electrons passed is 95 nmol electron per minute per mg of wild type MoFe protein as shown, or 48 nmol H_2 per minute per mg of protein, given that one electron transfer to the protein will generate half an equivalent of H_2 (for producing H_2). In contrast, the apo-protein produces dihydrogen at – 950 mV with the maximum rate *ca* 2.4 nmol H_2 per minute per mg of protein. According to assays from a previous study, nitrogenase MoFe protein from *A. vinelandii* in the presence of Fe protein and ATP at pH 7.4 shows catalytic activity of proton reduction at about 450 nmol H_2 per minute per mg of total protein.[67] This indicates that proton reduction by electrochemical-driven mediated electron transfer can only achieve approximately 10% of the efficiency in catalytic activity of the ATP-dependent electron transfer process *via* the Fe protein, but still occurs at a significant rate.

4.3 Electrochemical study of the β-98^{His} variant

According to a study by Danyal *et al.*, the genetically modified variant, β-98$^{Tyr→His}$ MoFe protein, is capable of two-electron reduction of hydrazine (N_2H_4) to ammonia using two Eu-polyaminocarboxylate complexes, Eu^{II}-EGTA or Eu^{II}-DTPA, as low potential reductants.[55] Study of this variant should provide more insight into the substrate-catalytic pathway and the role of specific amino acid residues in controlling electron transfer as shown in Figure 4-11.

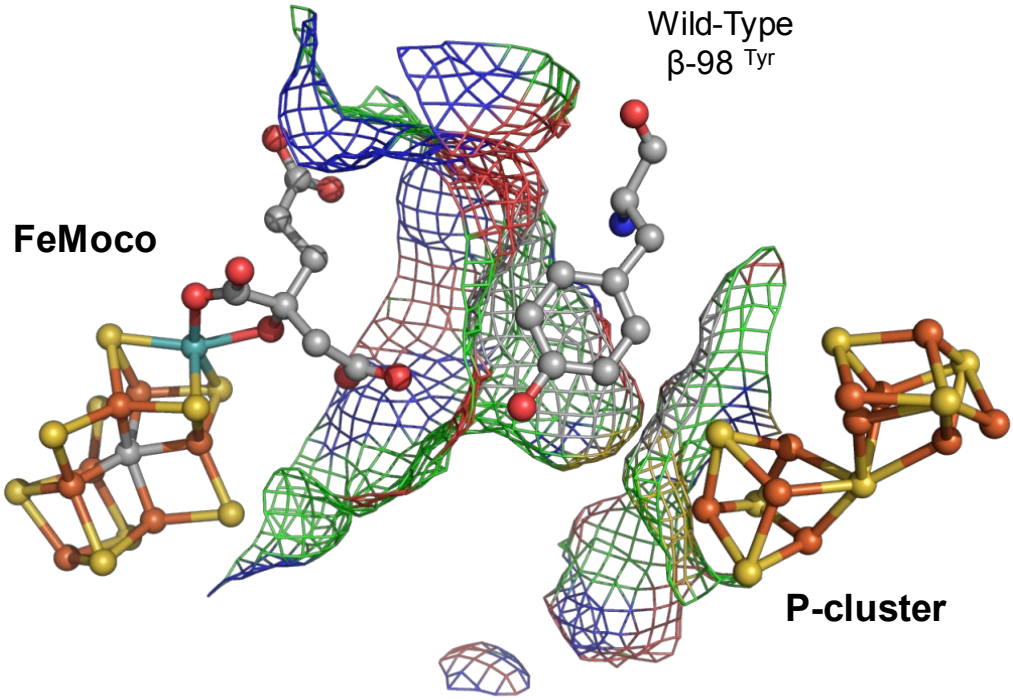

Figure 4-11: Positions of two metal clusters and β-98^{Tyr} amino acid residues as in the MoFe protein shown with surface mesh of the metalloclusters. (Generated from 3U7Q from RCSB PDB.)

4.3.1 Proton reduction by β-98^{His} variant MoFe protein

In order to investigate the effect of changing an amino residue that is likely to be involved in the electron transfer pathway of nitrogenase, the proton reduction and acetylene inhibition of this 'electron transfer' variant were explored under electrochemical control using the low potential mediator system as described in the previous section.

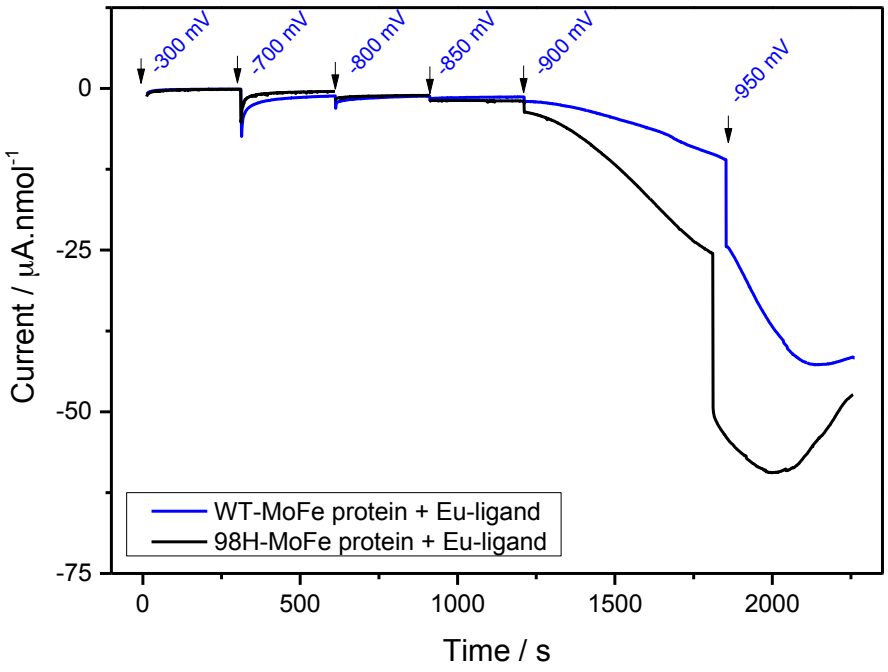

Figure 4-12: Chronoamperograms of β-98^{His} variant (black) and wild type MoFe protein (blue), both in the presence of Eu-ligand mediators (0.25 mM each of Eu-BAPTA, Eu-EGTA and Eu-DTPA). A sequence of potential steps was applied at indicated times. The currents are presented in units of µA per nmol of protein sample used for comparison.

In this experiment, an electrochemical cell containing β-98^{His} variant was prepared and the same sequence of potential steps as in experiments in the previous section was applied. Figure 4-12 shows that the β-98^{His} variant exhibited a catalytic current at the potential –900 mV which continued rising as the potential was decreased to –950 mV. This is similar to the catalytic current from proton reduction observed in the wild type MoFe protein case. Interestingly, the current per protein unit from β-98^{His} variant was significantly higher than that of the wild type. A slow decrease in reduction current over time at –950 mV was observed for both the wild type and β-98^{His} variants; this might be due to depletion of protons and/or build-up of H_2 in the protein layer.

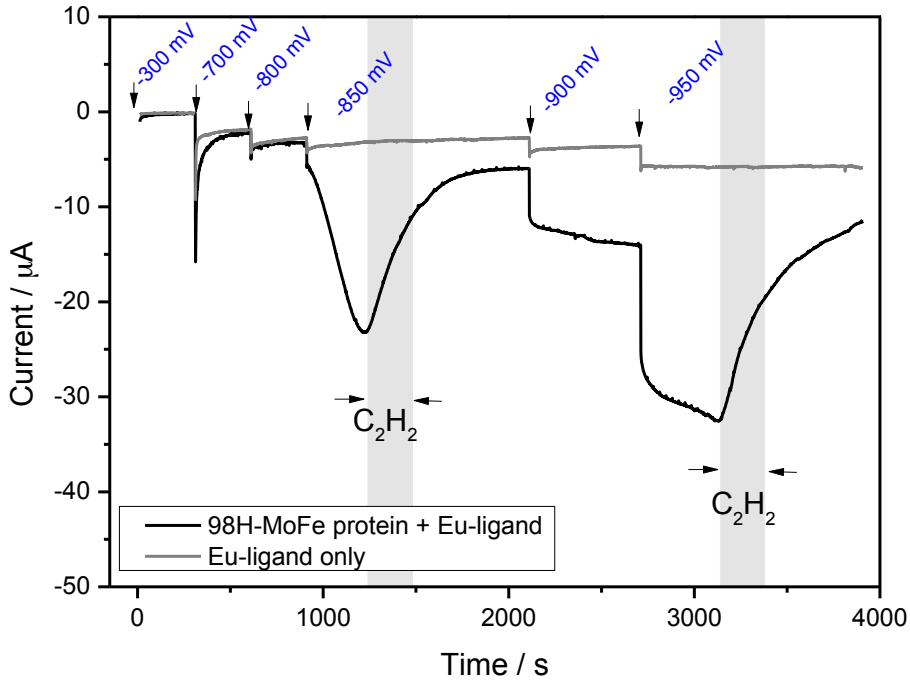

Figure 4-13: Chronoamperograms of 1.8 nmol β-98^{His} MoFe protein variant in the presence of Eu-ligand mediators with the flow system at flow rate 1.0 mL per minute (black). Acetylene was introduced to the flow system at the time periods indicated as grey area in the background.

Figure 4-13 shows that β-98^{His} variant under the flow system exhibited a significant catalytic current at a potential of -850 mV, higher than that in the stationary cell at the same potential. This might suggest that the previous experiment without the flow system was mass transport limited. A slow diffusion rate of reduced mediators from electrode into the protein film could account for the absence of electrocatalytic activity in the setup without a flow system, while with the flow system the activity was enhanced by better convection of mediators. This was also observed in the wild type case, in which the activity of proton reduction at –850 mV was slightly increased in the setup with the flow redox mediator solution.

An acetylene test was then added on the β-98^{His} variant to confirm the proton reduction. It showed that catalytic current was supressed rapidly when acetylene was added to the system at –850 mV or –950 mV. The current became steady after acetylene was flushed out, similar to the case of the wild type.

4.3.2 Discussion

In experiments with the wild type protein, it was found that the electrochemically-driven proton reduction by MoFe protein was possible. As redox mediators, Eu-ligand complexes are able to shuttle electrons to the redox sites of the protein in a very low potential range. This section focuses mainly on an electron transfer pathway in the MoFe protein and the electrochemical results of the β-98^{His} MoFe protein variant will be discussed in comparison with those of the wild type.

The β-98^{His} MoFe protein variant showed an electrochemical response different from that of wild type protein under the same conditions. In the stationary system, the β-98^{His} variant exhibited significantly larger catalytic current at –900 mV, *i.e.* with significantly faster rate of electron exchange per protein unit. At –950 mV, the β-98^{His} variant has maximum activity of proton reduction at 73 nmol H_2 per minute per mg of protein, *ca* 1.5 times greater than that of the wild type MoFe protein shown in previous section. In the flow cell, the variant showed a notable increase of catalytic current at the earlier potential –850 mV, while the wild type only showed relatively small catalytic current at this potential. This might suggest that the β-98^{His} variant was more effective to accept electrons from the Eu-ligand mediator compared to the wild type.

Additionally, an acetylene test on the β-98^{His} variant showed a rapid inhibitive effect on the catalytic current at –850 mV, implying that electron transfer at this potential supplied electrons for catalysis of proton reduction by the variant. As in the case of wild type, the current reached a plateau shortly after acetylene was removed from the system. The reduction current was partly retained when the potential was decreased to –900 mV and –950 mV. It was noted that an increase rate of the catalytic current after acetylene inhibition in the variant case was higher than that of the wild type.

According to the previous study on this 'electron-transfer' variant, they stated that amino acid residues between the P-cluster and the FeMoco played a key role in electron transfer of the MoFe protein. By the substitution of a particular amino acid, $\beta\text{-}98^{Tyr\rightarrow His}$, the protein variant processes an ability to accept electron from low potential reducing agent and use it to reduce hydrazine to ammonia with higher catalytic rate than the wild type protein.[55] They suggested that the substituted residue might mimic the structural changes inside the MoFe subunit which are normally triggered by the Fe protein upon associating with the MoFe protein, allowing it to accept electrons from other reductants. The results of the present study are consistent with this because the $\beta\text{-}98^{His}$ MoFe protein has higher catalytic activity than the wild type. In addition, the efficiency in electron transfer of the $\beta\text{-}98^{His}$ variant might help accelerate the re-activation process(es) from acetylene inhibition. However, this variant did not show the reduction of acetylene, which could imply that changing β-98 amino residue, had no effect on acetylene inhibition.

Thus, the result of this electrochemical study provides evidence to support previous reports about the importance of amino acid $\beta\text{-}98^{Tyr}$ in the electron transfer pathway of the MoFe protein.

4.4 Study of the CO interaction with wild type MoFe protein

In this section, CO binding to the nitrogenase MoFe protein in the absence of its Fe protein and ATP was investigated under electrochemical control combined with the mediated electron transfer system. The electrochemical results of the wild type MoFe protein under different CO condition will be presented and discussed here.

4.4.1 Effect of CO on proton reduction by the MoFe protein

A chronoamperometric technique was used to explore the effect of CO on the proton reduction observed in section 4.2. In this section, experiments involving introduction of CO were conducted in the SEC cell and the redox mediator cocktail described in Chapter 3 was used, in order to cover a wide potential range from 0 to –1000 mV. A sequence of potential steps was applied to the wild type MoFe protein associated with redox mediators and the current response was recorded as a function of time.

For CO experiments, the SEC cell was equipped with a flow system to circulate CO solution into the cell throughout the course of the experiment. CO gas was purified through an oxygen scrubbing filter (Restek Super Clean gas filter, <1 ppm O_2) before bubbling in redox mediator solution inside a glove box as illustrated in Figure 4-14. In the case of CO saturation, the solution was kept bubbling with CO gas for at least 30 minutes. This is to maximise the concentration of dissolved gas and to maintain a constant concentration of dissolved gas in solution throughout the experiment.

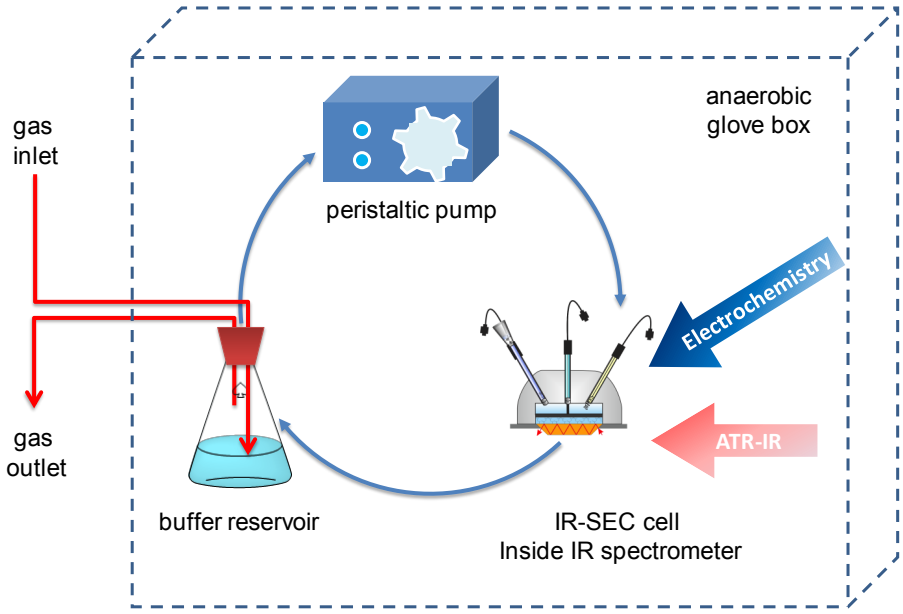

Figure 4-14: A schematic diagram of the flow system with a gas bubbler inside the anaerobic glove box.

In the chronoamperogram shown in Figure 4-15, catalytic current from proton reduction by the wild type MoFe protein was observed at –900 mV in the SEC cell set up, consistent with that in the electrochemical cell observed in previous section. It was noted that charging currents observed at the beginning of each potential steps in the SEC cell were relatively larger than in the electrochemical cell. This might be due to double layer capacitance arising from the ATR prism surfaces in contact with the working electrode in the cells.

When CO gas (100% CO, *ca* 14 kPa) was introduced to the SEC cell *via* a flow system during proton reduction, the reduction current was immediately suppressed as shown in Figure 4-15. As the CO solution continued to be circulated throughout the experiment, after a sudden drop, the current reached a plateau and no change was observed afterward.

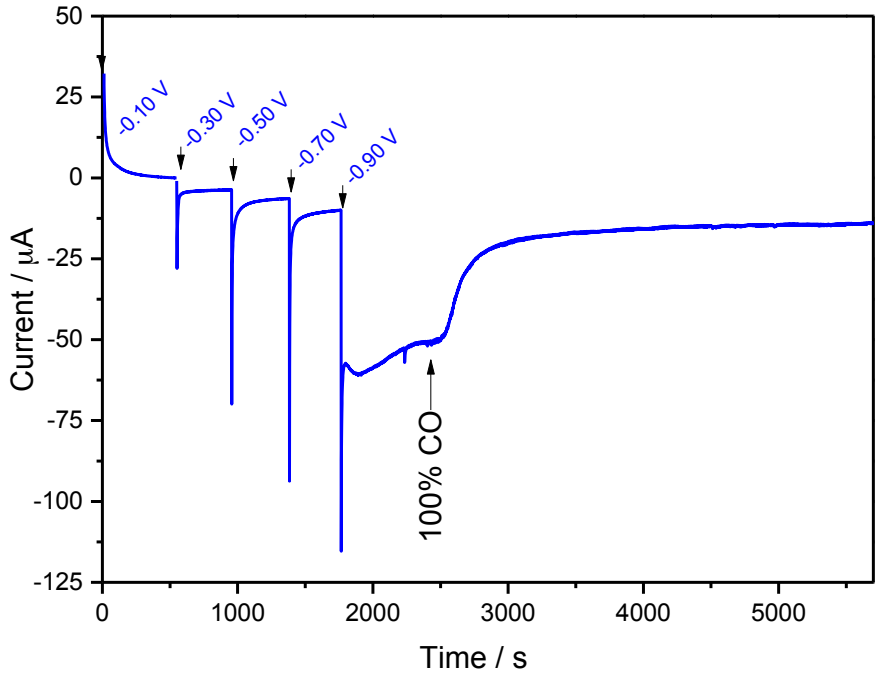

Figure 4-15: A chronoamperogram of 2.0 nmol wild type MoFe protein in a SEC cell with 0.25 mM redox mediator cocktail. A sequence of potential steps was applied and addition of CO was started as indicated in the figure.

A similar change was observed in the case of the wild type after being exposed to lower CO concentrations as shown in Figure 4-16. While the potential was held at –900 mV, a reduction current from proton reduction was observed before adding CO to the flow system. Starting from 6% CO and 94% N_2, it showed a dramatic decline in reduction current shortly after bubbling a gas mixture into the flow solution. The current decreased further after increasing the ratio of CO to 50% and then 100% of the gas mixture. The current was steadily decreasing in magnitude until reaching a plateau 3000 s after exposure to CO.

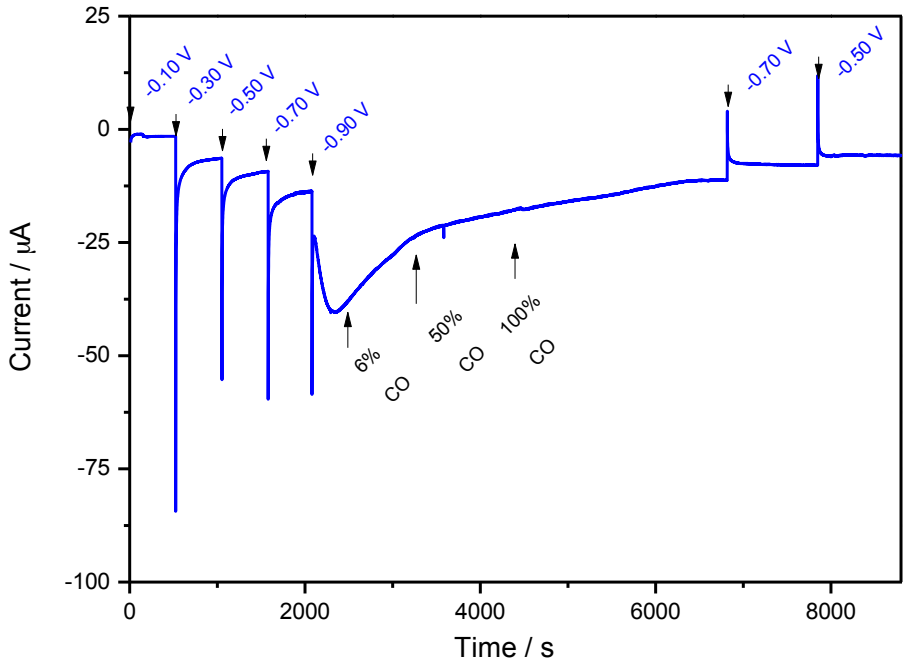

Figure 4-16: A chronoamperogram of wild type MoFe protein showing a change in current upon being exposed to CO from a low concentration at the potential –900 mV. A percentage of CO in N_2 gas mixture used was increased as indicated in the figure.

4.4.2 Electrochemistry of MoFe protein in the presence of CO

In another set of experiments, a CO saturated solution was introduced to a SEC cell containing the wild type MoFe protein from the outset when the potential was held at –100 mV, just below the midpoint potential of the enzyme-bound FeMoco$^{ox/semi\text{-}red}$ couple, –42 mV.[24] The concentration of saturated CO in aqueous solution was approximately 1 mM.[68]

Figure 4-17 shows only a small reduction current when the potential was decreased stepwise down to –900 mV, compared with the catalytic current of proton reduction observed in the case of wild type protein in the absence of CO. Also, there was no significant change in current observed at the more negative potential of –1000 mV.

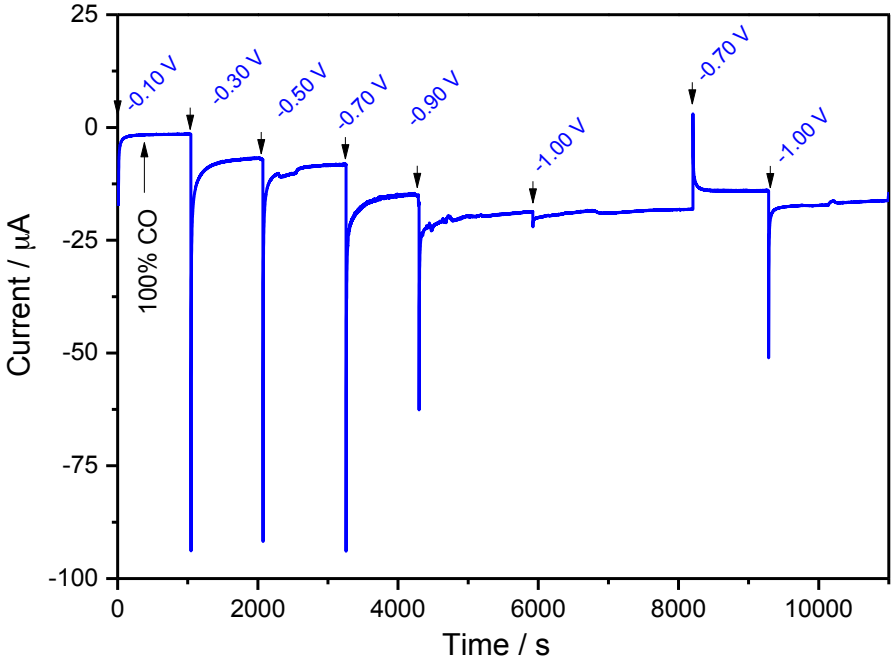

Figure 4-17: A chronoamperogram of 2.0 nmol wild type MoFe protein in the presence of CO. A sequence of potential steps was applied and a flow of CO saturated mediator solution was started as indicated in the figure. The CO gas was bubbling into the flow solution at flow rate 1.0 mL per minute throughout the experiment.

Figure 4-18 shows an experiment in which the wild type protein was exposed to a lower concentration of CO in solution. From the potential –100 mV to –900 mV, the reduction current was very small, as previously observed in the case of the wild type protein under the higher concentration of CO. As the potential was stepped to –1000 mV, a slight increase of reduction current was observed, differing from the high-CO condition. This reduction current was depleted when the potential was switched back to –900 mV again.

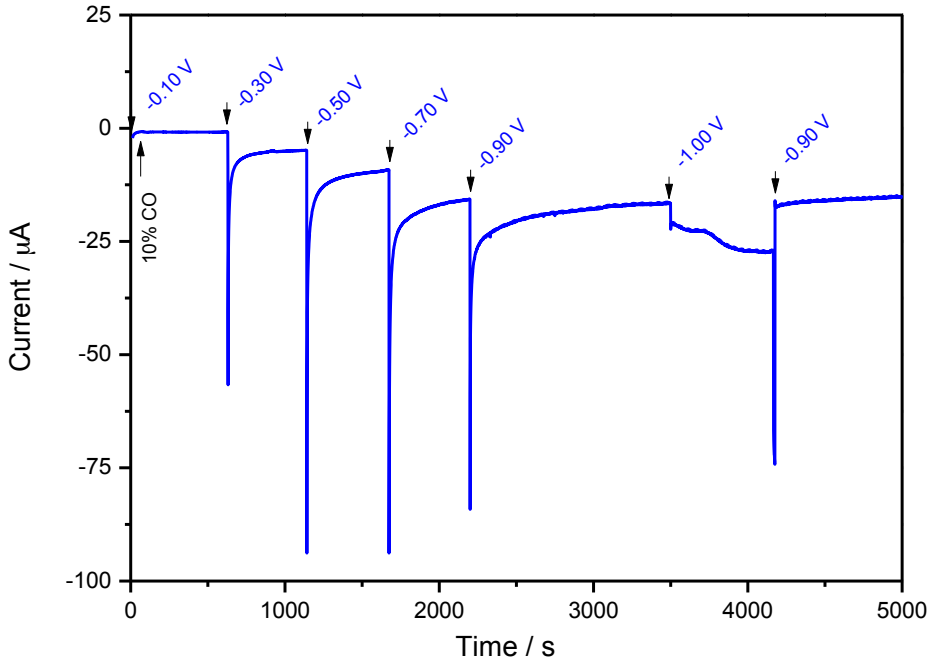

Figure 4-18: A chronoamperogram of 2.0 nmol wild type MoFe protein in the presence of low concentration of CO. A gas mixture of 10% CO in N_2 was bubbling into the flowing redox mediator solution at flow rate 1.0 mL per minute throughout the experiment.

4.4.3 Discussion: CO inhibition

From the electrochemical results, it was obvious that the reduction current from protein-catalysed proton reduction was suppressed upon exposure to CO. In the case when CO was added at the proton-reduction potential (–900 mV), the catalytic current decreased shortly after CO was introduced to the system, similar to that of the acetylene inhibition. It was noted that suppressed current took a longer time to become stable under the low-CO condition than the high-CO one. On the other hand, when adding CO at the more oxidising potentials, no significant increase in catalytic current from proton reduction was detected at proton-reduction potentials. Only in the case of low CO concentration, a small rise of reduction current was observed at –1000 mV, lower than the potential that protein-catalysed proton reduction was observed in the absence of CO. This indicated that difference in concentration of CO solution had an effect on suppression of proton reduction current, but only at very negative potential.

Therefore, the results suggest that CO could inhibit the proton reduction process by the wild type MoFe protein. Although the proton reduction by nitrogenase has been previously reported to be unaffected by CO under optimal assay condition at pH 7.4,[23, 63, 166] a study on effect of pH on CO inhibition by Pham and Burgess reported that proton reduction by native Mo-nitrogenase is inhibited by CO at high pH.[67] In the Pham and Burgess study, it was shown that the activity of proton reduction under CO was significantly lowered at pH value above 7.5 compared with that under Ar. From this observation, they suggested that CO binding to the FeMoco might cause a shift in pK_a of a nearby amino acid residue responsible for regulating proton reduction, or alternatively proton reduction might undergo a different mechanism in the presence CO.[67] Another EPR study on variant MoFe proteins by Hales and co-workers demonstrated that CO was able to inhibit proton reduction (*ca* 40%–100%) in some specific variants; α-96$^{Arg\rightarrow Lys}$, α-191 $^{Gln\rightarrow Lys}$, Δ*nifV*, α-359 $^{Arg\rightarrow Lys}$ and α-96 $^{Arg\rightarrow Lys}$/α-359 $^{Arg\rightarrow Lys}$ MoFe protein variants.[166] However, no correlation was found between EPR signals and CO inhibition of proton reduction in these variants. Thus the authors suggested that observed CO inhibition was a result of CO binding to a different site from the one that elicited the CO-bound EPR signals.[166] From these studies, it could imply that CO bound to different sites or under different condition can have an effect on proton reduction process. In this present study, a difference in electron transfer method might account for the observation of the stronger inhibition by CO than in the previous studies.

This observation of CO inhibition will lead to investigation of the interaction between CO and the redox sites in the following Chapter. The IR absorption property of CO will provide a platform for using IR spectroelectrochemical technique to monitor a redox-dependent change in IR spectra upon CO bound to the reduced metal clusters.

Chapter 5

IR spectroelectrochemical studies of CO binding to MoFe protein

Following the electrochemical results on electron transfer to the MoFe protein described in the previous chapter, this chapter focuses on CO binding to the MoFe protein. Characterisation of the interaction between CO and the metal clusters of the two MoFe proteins, wild type and β-98^{His} variant, was performed using an IR spectro-electroelectrochemical technique. Here, the first IR evidence of CO binding to the MoFe protein without requirement for the Fe protein will be presented and discussed.

5.1 Introduction

Due to the fact that CO and dinitrogen are isoelectronic with each other, CO binding to the enzyme has been used as a model study to elucidate the nature of dinitrogen coordination. As an IR-chromophore, the CO molecule is an important probe for studying redox-dependent binding using an IR spectroelectrochemical technique as demonstrated in the carboxymyoglobin case in Chapter 3.

5.1.1 CO inhibition

CO inhibition of Mo-dependent nitrogenase has been investigated extensively. In early studies, it was reported that CO is a non-competitive inhibitor for *in vitro* nitrogenase-catalysed reduction of N_2, azide (N_3^-) and acetylene.[63, 157, 167] A number of studies have indicated that CO binds to the active centre of the enzyme, FeMoco; for instance, a substitution of homocitrate ligand and some nearby amino acid residues directly affects CO inhibition.[85, 155] It was found that CO can bind to native nitrogenase only at its reduced state, not the resting state.[4]

EPR studies have shown that, when CO binds on the FeMoco inside the MoFe protein under turnover conditions, it exhibits two sets of EPR signals under different CO conditions; one set of EPR signals corresponded to FeMoco-CO complex (S=1/2) under low pressure CO condition (*ca* 0.08 bar) denoted as 'lo-CO', while the other one corresponded to FeMoco-CO (S=1/2) under high pressure CO (>0.5 bar) denoted as 'hi-CO'.[86] Following that, a result from the ENDOR technique revealed that one and two CO molecules are bound to FeMoco under 'lo-CO' and 'hi-CO', respectively.[168, 169] A ^{57}Fe ENDOR investigation suggested that the single CO in the 'lo-CO' case forms a bridging bond with two Fe atoms of the FeMoco, while each CO in the 'hi-CO' case binds to FeMoco as a terminal ligand, as illustrated in Figure 5-1.[87] Later, it was proposed that the resting state, 'lo-CO' and 'hi-CO' were at the same oxidation state [170] Another EPR study showed that turnover conditions were required to form both lo-CO and hi-CO complexes but were not necessary for interconversion of these two complexes.[88] Also, a new set of EPR signals called 'hi(5)-CO' was detected under the hi-CO condition with high electron flux (MoFe protein : Fe protein = 1:1) and assigned to the CO-bound FeMoco (S=3/2).[88] It was found that removal of CO resulted in a slow loss of both EPR

signals corresponding with the hi-CO conditions. A further study with different variant MoFe proteins suggested that the 'hi(5)-CO' signal arose from two bridging CO ligands.[166]

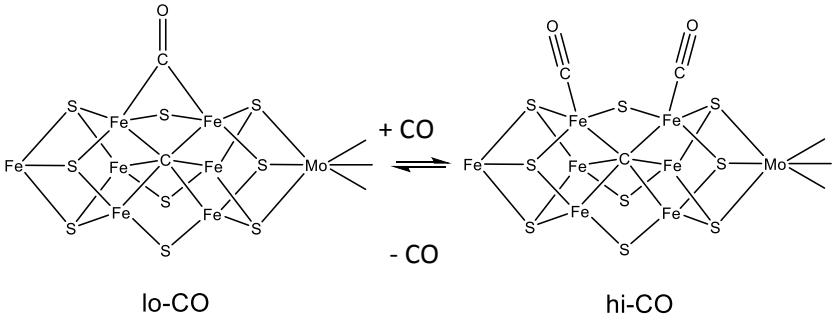

Figure 5-1: Schematic representation of the proposed CO binding to the active site FeMoco within MoFe protein under two different conditions; low concentration of CO (lo-CO) and high concentration CO (hi-CO). (Adapted from ref. [87])

5.1.2 IR spectra of the CO-bound nitrogenase

According to an IR spectroscopic study by George *et al.* using a stopped-flow IR (SF-IR) technique, evidence for CO binding to wild type Mo-nitrogenase was in agreement with EPR and ENDOR results as they exhibited two sets of ν(CO) absorption bands under corresponding conditions. Under the lo-CO condition, a transient ν(CO) peak was observed at 1904 cm^{-1} for a short time before it evolved to a ν(CO) peak at 1715 cm^{-1}. [59, 68] It was thought that the former peak arose from terminal CO binding to the intermediate complex and the latter was assigned as bridging CO bound to another Fe atom. On the other hand, under the hi-CO condition, ν(CO) peaks were observed at 1880, 1906, 1936 and 1960 cm^{-1}, all assigned as terminal CO binding.[68] It was suggested that these species were the result of CO binding to separate sites or different redox states of the metal cluster, including some EPR-silent states.

Another SF-IR study of steric effects on the FeMoco-CO complex demonstrated that changing the side chain size of α-70^{Val} amino acid residues located above the 4Fe-4S face of the FeMoco cluster resulted in an IR wavenumber shift of ν(CO) peaks under hi-CO condition, as shown in Table 5-1.[100] It was observed that MoFe protein variants substituted

with a less bulky residue, α-70$^{Val→Gly}$, show a shift of the *ν*(CO) peak of both lo-CO and hi-CO forms to higher wavenumber. Later, it was found that this α-70^{Gly} MoFe protein variant was capable of CO reduction into hydrocarbons.[71] This suggested that the shorter side chain of glycine amino acid might open up more space near the FeMoco allowing CO to bind to a different site and be reduced.

Table 5-1: the assigned *ν*(CO) bands of wild type and different variants of MoFe protein from *A. vinelandii* (adapted from ref.[100])

MoFe protein variants	lo-CO (cm^{-1})	hi-CO (cm^{-1})		
α-70^{Val} (Wild type)	1906	1936	1880	1960
α-70^{Ile}	1895	1936	1880	1957
α-70^{Ala}	1904	1936	1870	1955
α-70^{Gly}	1911	1946	1870	–

A study on CO inhibition of azide reduction using the SF-IR approach by Tolland *et al.* showed that addition of azide had no impact on formation of lo-CO and hi-CO bands, consistent with CO as a non-competitive inhibitor for azide reduction and CO having a different binding site from azide. [14]

The susceptibility of the bound CO ligands to photolysis was investigated using EPR and SF-IR spectroscopy.[171-173] In the EPR study, it was shown that the hi-CO complex converts to the lo-CO one after irradiation under visible light at 12 K and this lo-CO product was converted back to the hi-CO form by increasing the temperature to 77 K, with the calculated activation energy of the reaction being 3.9 $kJ.mol^{-1}$.[171] In contrast, it was found that the protein sample

with lo-CO and hi(5)-CO signals was photo-stable.[171] A SF-IR study on photolysis at low temperature (4 K) showed that photolysis of CO-bound wild type MoFe protein resulted in loss of new hi-CO peak at 1973 cm^{-1} and the appearance of peaks at 2135 and 2123 cm^{-1}, assigned as two free CO molecules trapped inside the protein.[172] Another study of different variants reported that changing the α-$195^{His \rightarrow Gln}$ amino acid residue resulted in a new EPR-silent CO-bound MoFe protein, assigned as two terminal CO ligands that coupled to each other with a separation of 2.7 Å.[173]

An IR SEC study of CO binding to isolated FeMoco by Pickett and co-workers showed that CO was able to bind to the reduced state of the isolated FeMoco ($FeMoco^{red}$) and new oxidation processes of CO-bound products were observed.[92, 93] In their IR spectra, it was found that reduction under low CO pressure gave rise to redox-related peaks at 1808 and 1835 cm^{-1}, likely to be bridging CO species on the Fe-S core.[92] This set of peaks was converted to a peak at 1885 cm^{-1} under higher CO pressure, indicating a transformation from bridging to terminal binding on the Fe atom. Another peak at 1920 cm^{-1} was observed independently increasing upon reduction under high CO pressure, assigned as terminal CO bound to the Mo atom.[92] From this study, they suggested two separate CO binding sites of the FeMoco that involved with two different electron transfer processes; the Fe atom on Fe-S core and the Mo atom as illustrated in Figure 5-2.

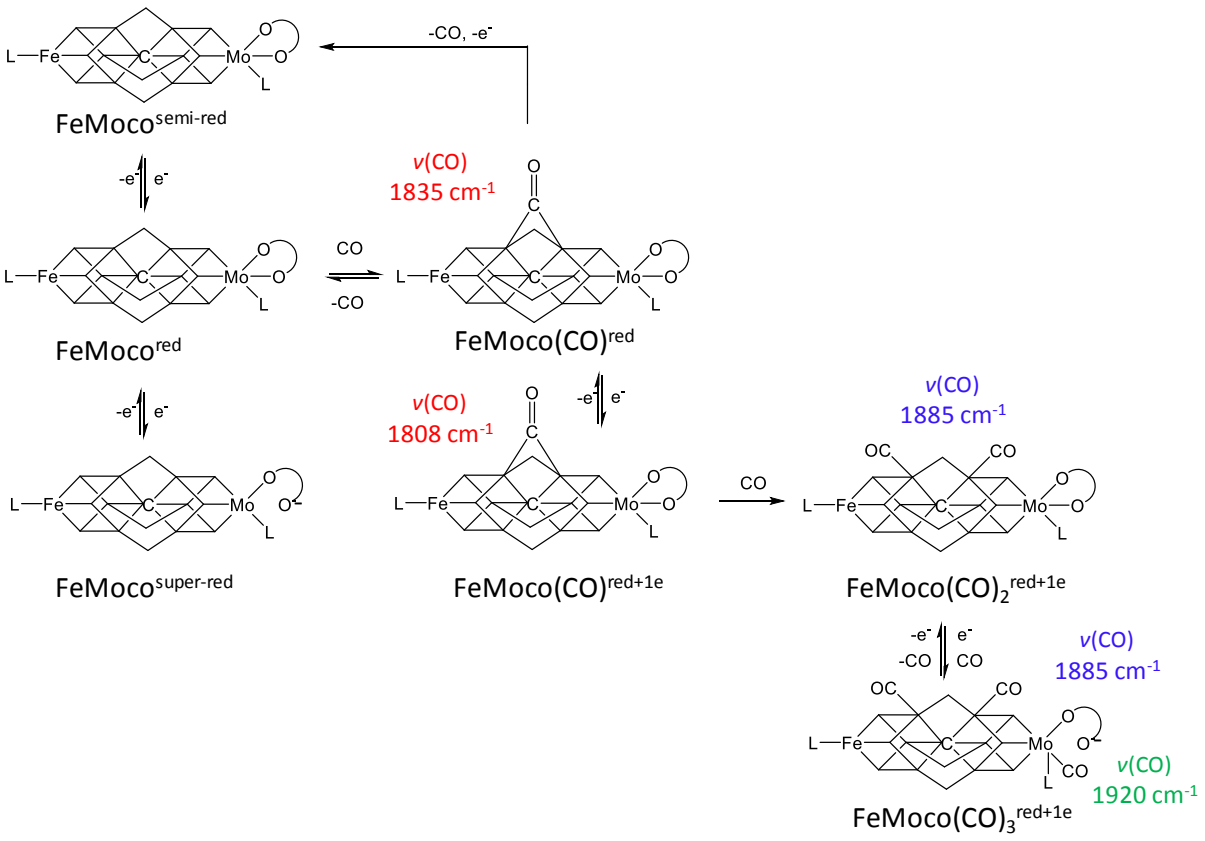

Figure 5-2: A proposed model for CO binding to the isolated FeMoco from study by Pickett *et al.*, involving formation of various CO bound species at different CO condition and redox state. The observed IR absorption wavenumber of *ν*(CO) are indicated. (Adapted from ref. [92])

In addition, a study of CO and cyanide binding to the isolated cofactor by the same group revealed that both ligands were able to synergically bind to isolated FeMoco at its oxidised and semi-reduced states.[94] A strong vibrational coupling of CO and CN^- in the IR spectrum was observed: it was shown that the wavenumber of the *ν*(CO) peak shifted from 1885 to 1937 cm^{-1}, in the presence of cyanide. Thus, it was suggested that CO and CN^- were co-aligned bound to Fe atoms on the Fe-S unit rather than to the single Fe or Mo atom.

Recently, a crystal structure of CO-bound nitrogenase was reported by Rees and co-workers.[174] In the presence of Fe protein and ATP, it showed that CO was bound to the FeMoco by replacing S atom on the central Fe-S core and forming bridging bonds between two Fe atoms on the site near the α-70^{Val} and α-195^{His} residues as shown in Figure 5-3.[174] It

was suggested that S displacement could be the result of proton donation from the α-195^{His} residues and the position of the bound CO was within H-bonding distance of the α-195^{His} residue. The bond length between CO and Fe was determined to be 1.86 Å, shorter than the bond length between Fe and the original bridging S at 2.20 Å.[174] The coordination with CO was found to also change the geometry of the FeMoco by shortening the distance between the two Fe atoms to which CO bound (2.5 Å), relative to other pairs of Fe atoms on the Fe-S core (2.6 Å). Moreover, it was reported that the MoFe protein was reactivated upon removal of CO and the S atom was reinserted into the FeMoco. These findings indicate that CO binding is reversible under the experimental conditions used.[174] Although this CO-bound structure was generated under different conditions from previous EPR and SF-IR studies, so it cannot be directly linked to any previously assigned state, it is possible that it could be related to the lo-CO complex.

The structure of Rees and co-workers provides new evidence that the CO binding site is on the Fe-S cluster near the α-70^{Val} residue. This structure gives new insight into the study of the CO inhibition and the mechanism of nitrogenase.[175] However, questions remain about the binding mechanism and which state of the active site CO binds to.

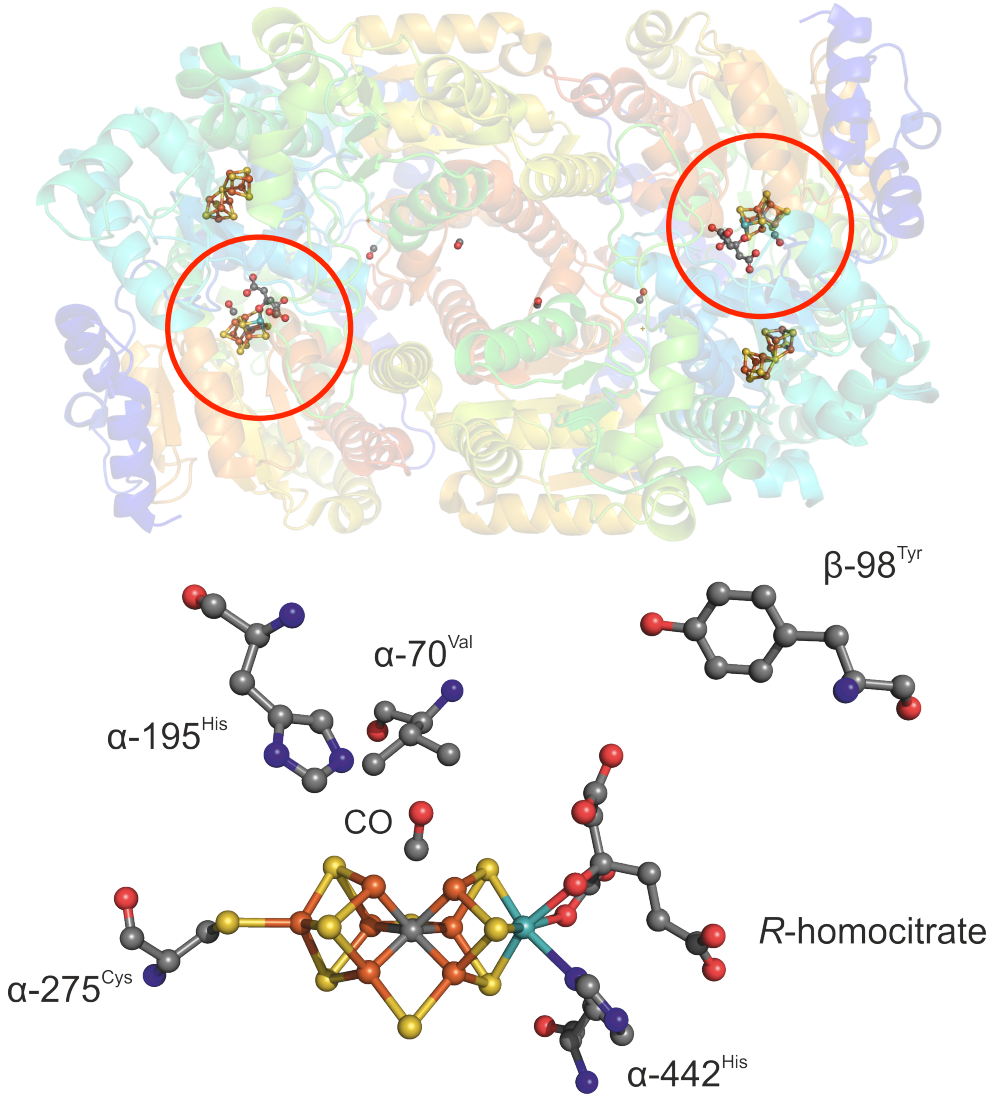

Figure 5-3: A structure of CO-bound FeMoco of the MoFe protein from *A. vinelandii.* (generated from 4TKV PDB file). The coordinated amino acids and some nearby residues were located as in the MoFe protein. Fe, S, N, O, C and Mo atoms are represented in colour brown, yellow, blue, red, grey and cyan, respectively.

The observation of redox-dependent CO binding in the isolated FeMoco suggests that an IR spectroelectrochemical approach will be useful to study CO coordination to the FeMoco active site inside the MoFe protein. Together with mediated electron transfer that allows electrochemical control of the protein, the investigation of the redox-dependence of CO binding should be possible.

5.1.3 Reduction of CO

In recent years, several studies have shown novel catalytic ability for CO reduction by Mo- and V-nitrogenase. Ribbe and co-workers reported that V-dependent nitrogenase from *A. vinelandii* is able to catalyse reduction of CO to small hydrocarbon products such as C_2H_4, C_2H_6 and C_3H_8 (*ca*150 nmol C_2H_4 per nmol protein per hour).[69] Later, they discovered that, when they scaled up a CO reduction assay, Mo-nitrogenase also catalysed this reaction, but with relatively lower rate compared to V-nitrogenase (~0.1% in H_2O and ~2% in D_2O).[72] Another study by Seefeldt and co-workers showed that α-70^{Ala}, α-70^{Gly}, α-70^{Ala}/α-96^{His} and α-70^{Ala}/α-191^{Ala} MoFe protein variants are capable of CO reduction (*ca* 6 and 7 nmol C_2H_4 per nmol protein per hour for the α-70^{Ala} and α-70^{Gly} variants, respectively). It was found that increasing the CO pressure in the reaction not only yielded more products but also made the formation of longer chain hydrocarbons a more favourable reaction. From this observation, they proposed a mechanism of nitrogenase-catalysed hydrocarbon formation, paralleling the Fischer-Tropsch reaction as shown in Figure 5-4. In this mechanism, two CO molecules bind to the FeMoco at two adjacent sites, and then the bound-CO pair is partially reduced to a -CH intermediate. This intermediate can either be fully reduced to methane or coupled together to form longer hydrocarbon chain products.[71]

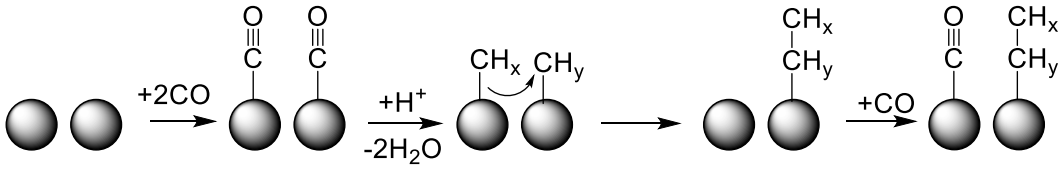

Figure 5-4: A proposed mechanism of CO reduction to hydrocarbons catalysed by nitrogenase (adapted from ref. [71])

As well as ATP-driven reaction, CO reduction was also observed in the ATP-independent systems with different nitrogenase variants. With Eu^{II}-DTPA as reductant, catalysis of CO

reduction by isolated FeMoco and FeVco has been reported (*ca*55 and 20 nmol CH_4 per μmol cofactor per hour, respectively),[119] showing that capabilities of CO reduction are not limited to the active site inside the protein. It has also been shown that nitrogenase variants with only P-cluster or P-cluster precursor are able to catalyse conversion of CO to hydrocarbons (6 and 83 nmol CH_4 per μmol protein per hour, respectively).[120]

This discovery of CO reduction activity in nitrogenase has revealed a new aspect for study of CO binding to the protein. The spectroscopic investigation of interaction between CO and the active site under electrochemical control could be the next step toward understanding the CO reduction mechanism of nitrogenase.

5.2 Experimental

In this chapter, the studies of CO binding to three variants of MoFe proteins were performed using an IR spectroelectrochemical technique, as introduced in Chapter 2. The protein samples used in these studies were the wild type, β-98^{His} and apo-MoFe protein, provided by Lance Seefeldt, Utah State University. Protein preparation and dithionite removal processes were done in the same manner as for electrochemical study in Chapter 4.

The preparation of the SEC cell was done as described in the set up for the carboxymyoglobin test in Chapter 3. In the SEC cell, a Nafion-Tris-HCl mixture containing approximately 2 nmol protein sample was directly deposited on an ATR prism. A piece of carbon paper placed in contact with the protein-Nafion film served as a working electrode. A Pt counter electrode and a SCE reference electrode were employed. The cell body was filled with 0.25 mM redox mediator cocktail in Tris-HCl buffer pH 7.4, in order to cover a wide potential range, as listed in Table 5-2

Table 5-2: Reduction potentials of redox mediators used in the ATR-IR SEC experiments as previously demonstrated in Chapter 3

Redox mediator	$E_m'^0$ *vs* SHE (mV)
methylene blue	+11
2-hydroxy-1,4-naphtaquinone	–139
benzyl viologen	–359
methyl viologen	–446
Eu-BAPTA	–633
Eu-EGTA	–868
Eu-DTPA	–1094

A CO-dissolved solution was introduced into the SEC cell *via* a flow system as previously described in section 4.4.1. A ratio of the gas mixture was controlled by a mass flow controller.

5.2.1 Compatibility with protein

At the beginning, compatibility of using the SEC cell and 'mediator cocktail' with MoFe protein was tested. A cell was prepared containing the wild type MoFe protein in Nafion and a mixture of all the mediators listed in Table 5-2

Figure 5-5 presents an IR absorbance spectrum between $1000 - 4000$ cm^{-1} recorded in the SEC cell containing MoFe protein sample, and shows two distinct bands apart from water (stretching mode at $3000 - 3500$ cm^{-1} and bending mode at 1640 cm^{-1}) and Nafion features (around 1200 cm^{-1}). Two important IR absorption features of protein observed here were the amide I band at 1650 cm^{-1} (overlapping the water bend) arising from the C=O stretching vibration, and the distinctive amide II (1545 cm^{-1}) band arising from the combination of the

NH in plane bend and the amide CN stretching vibration.[176] These bands are indicative of the presence of intact folded protein trapped in the Nafion layer. No interfering peaks are observed in the CO and CN region between 1800 and 2200 cm^{-1} where peaks of interest are expected. Thus, this system gives a clear background spectrum in the ν(CO) and ν(CN) regions which are suitable for monitoring these ligands bound to metal centres in the protein.

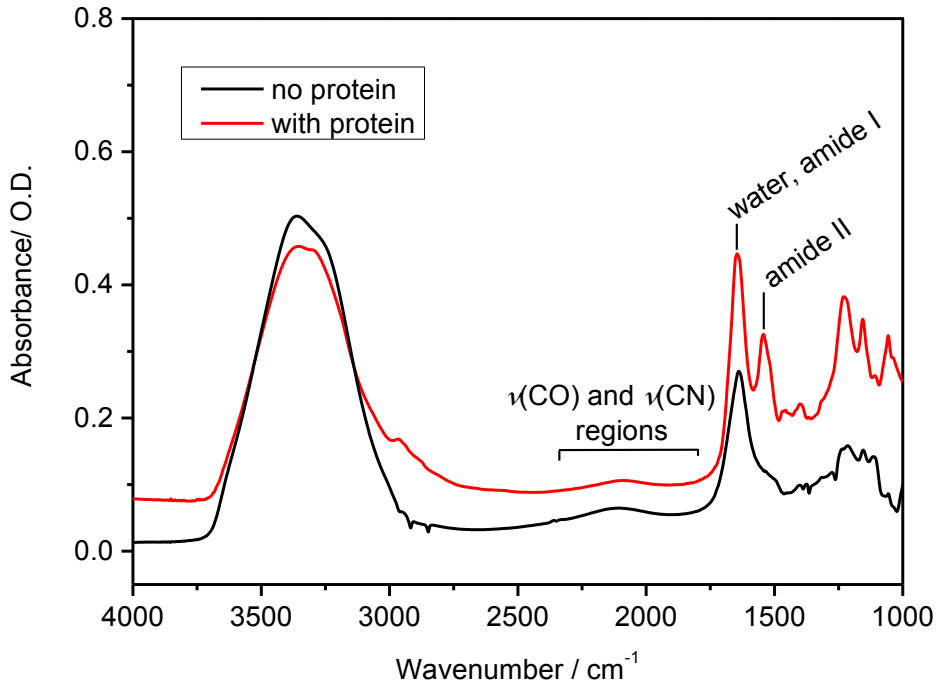

Figure 5-5: IR spectra show the comparison between the Nafion film with 2 nmol of wild type MoFe protein sample (red) and blank Nafion film (black, no protein). The ATR-IR SEC cell contained a mixture of 7 mediators at 0.25 mM each in Tris-HCl buffer pH 7.4. The cell was set up and left to equilibrate for 20 minutes before scan without applied potential. Each spectrum was processed against unmodified Si ATR prism background (500 scans co-added, 4 cm^{-1} resolution).

5.3 Study of CO binding to the MoFe protein

In order to *in situ* investigate the interaction between CO and the metal clusters that is responsible for the inhibition effect on the MoFe protein, an ATR-IR spectroelectrochemical approach was employed in this chapter. Electrochemical control on the MoFe protein was enabled *via* the mediated electron transfer system established in chapter 4, which allowed exploration of redox-dependent ligand binding. Coordination between CO and the metal sites will be monitored by IR spectroscopy.

5.3.1 CO binding to the β-98^{His} variant MoFe protein

Coordination between CO and 'electron transfer' variant MoFe protein was investigated *in situ* using IR spectroelectrochemistry. According to the electrochemical results in the chapter 4, the β-98^{His} variant MoFe protein exhibited greater reactivity toward proton reduction. This ability should enable more interaction between CO and the redox sites, which should give more information for characterisation of CO binding to the MoFe protein. As the position of β-98 amino acid substitution is in a different location from the proposed CO binding sites on the FeMoco, this modification should not interfere with the CO binding to the FeMoco as shown in Figure 5-6.

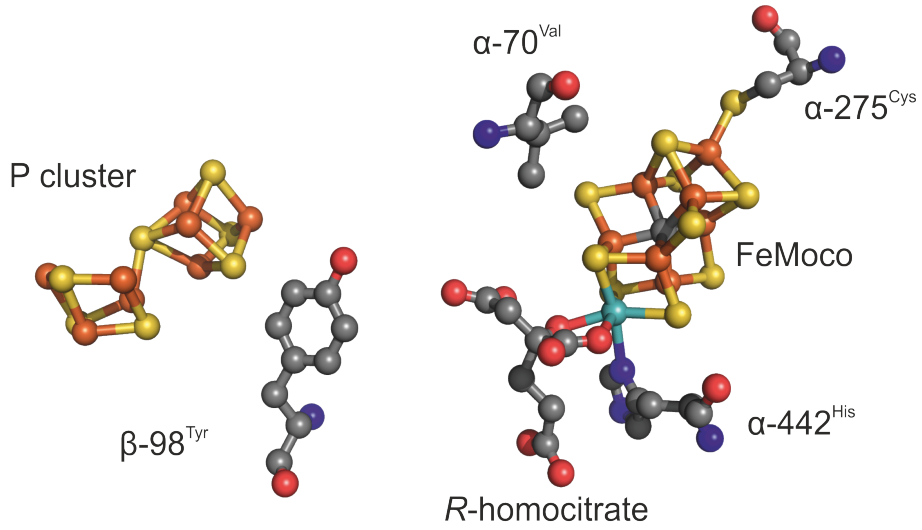

Figure 5-6: Positions of two metal clusters and some relevant amino acid residues in the MoFe protein. The site of β-98^{Tyr} residue is located in between the P-cluster and FeMoco. (1M1N from RCSB PDB)

A SEC study of CO binding on the β-98^{His} variant was performed in the presence of CO saturated redox mediator cocktail. The similar potential step used for a study of proton reduction in the applied the variant in section 4.3.1 but with starting potential extending to less negative values.

A potential of –100 mV was applied before a flow of CO-saturated redox mediators was introduced to the SEC cell. An IR spectrum recorded prior to introduction of CO was used as a background spectrum for the following potential steps. In order to monitor more resolved potential-dependent CO binding to the redox sites, a sequence of small potential steps was applied to the system as indicated on the chronoamperogram in Figure 5-7.

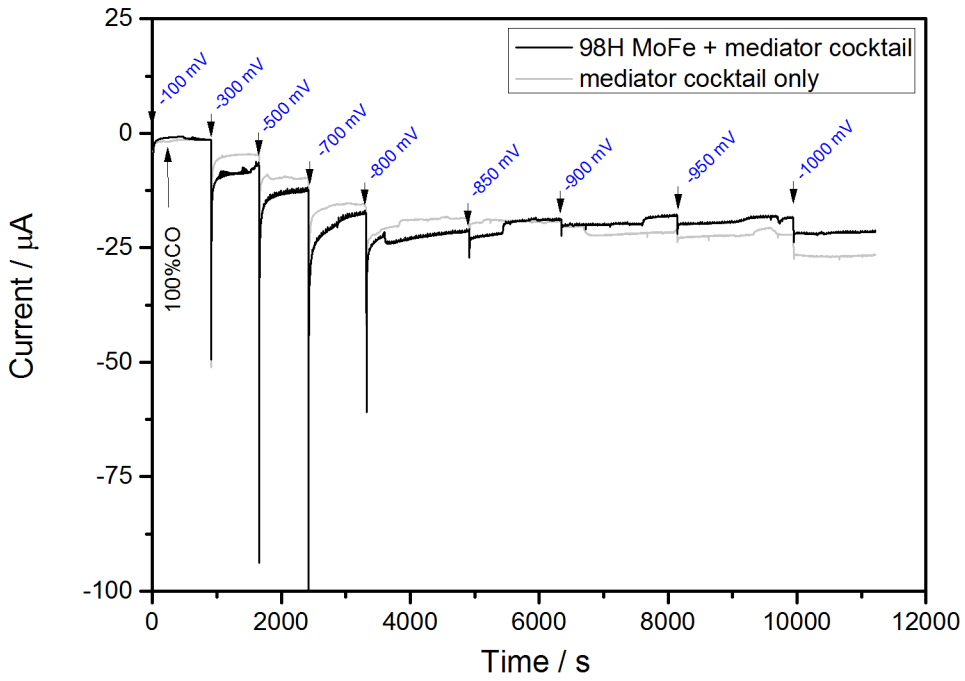

Figure 5-7: A chronoamperogram of the β-98^{His} variant MoFe protein in the SEC cell recorded in the presence of saturated CO solution (black). The SEC scell contained 1.8 nmol of protein sample in the Nafion layer and was filled with the redox mediator cocktail. A chronoamperogram of the same SEC cell containing only CO-saturated redox mediator cocktail is also presented (grey) The sequence of potential steps was applied at the indicated times.

Figure 5-7 shows no significant current from β-98^{His} MoFe protein-catalysed proton reduction arising at low potentials in the presence of CO, similar to the result from the previous electrochemical experiment on section 4.4.1 of the wild type protein in the presence of CO. This indicates that CO was able to inhibit the proton reduction by the β-98^{His} variant MoFe protein.

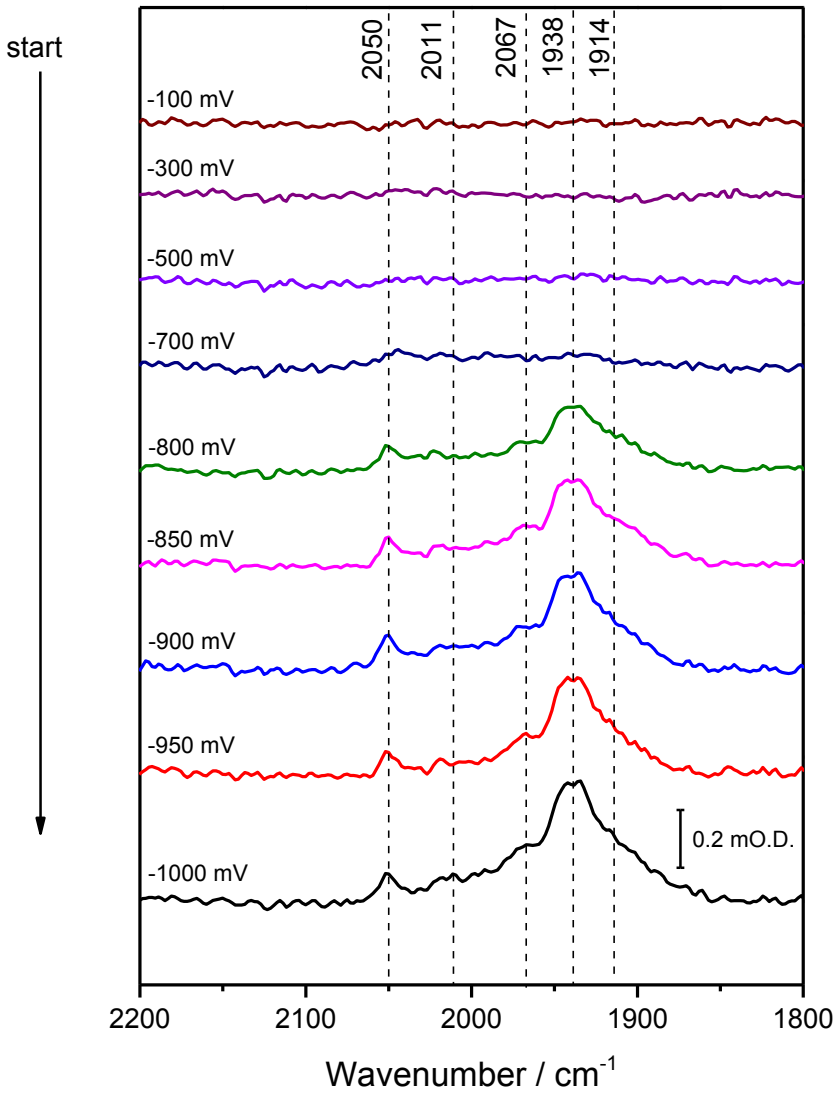

Figure 5-8: IR absorbance spectra of 1.8 nmol of β-98^{His} variant MoFe protein after introduction of CO saturated solution (*ca* 1.0 mM) followed by application of a sequence of potential steps. Each spectrum was recorded when the system was in equilibrium at each holding potential and processed against a background spectrum at –100 mV prior to addition of CO (500 scans co-added, 4 cm^{-1} resolution).

In Figure 5-8, IR spectra recorded between potentials of –100 mV and –700 mV show no significant spectral change in the ν(CO) region between 1800 to 2200 cm^{-1}. Only small and unresolved absorption bands around wavenumber 1950 – 2050 cm^{-1} were observed in the spectrum at the potential –700 mV. Upon applying a potential of –800 mV, dramatic formations of a strong and broad absorption peak at 1938 cm^{-1} and a small sharp peak at 2050 cm^{-1} were clearly observed. At the following potential step to –850 mV, there was a large increase in intensity of all the existing peaks but no new ν(CO) peaks were observed.

Following further potential steps downward to –1000 mV, the peak at 1938 cm^{-1} became more dominant while the peak at 2050 cm^{-1} increased in intensity slightly.

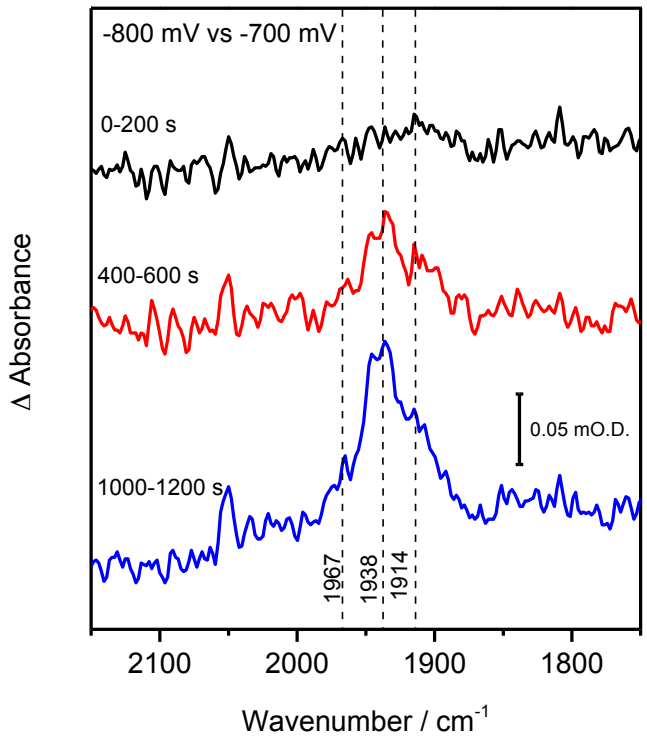

Figure 5-9: Time-resolved spectra of the β-98^{His} variant MoFe protein under saturated CO condition recorded during reduction following a potential step from –700 mV to –800 mV, processed against a spectrum recorded after equilibration at a potential of –700 mV (500 scans co-added, resolution 4 cm^{-1}) .

In Figure 5-9, a time series of difference spectra recorded following application of the potential step from –700 mV to –800 mV showed formation of the peak at 1938 cm^{-1} from the very beginning of this potential step. At 200 s after applied the potential, it shows that a small peak at 1914 cm^{-1} was formed accompanied with narrow bands at 1807 and 2048 cm^{-1}. After 600 s, a stronger peak at 1938 cm^{-1} emerged while a peak at 1914 cm^{-1} also increased. These two peaks were distinct until 600 s, when the peak at 1938 cm^{-1} became dominant and the small peak at 1914 cm^{-1} appeared as a shoulder. After 800 s, the growth of these peaks became slower as shown in a plot of peak height with time in Figure 5-10. It was also noted that increase of another shoulder peak at 1967 cm^{-1} has a similar rate to that of the peak at 1914 cm^{-1}.

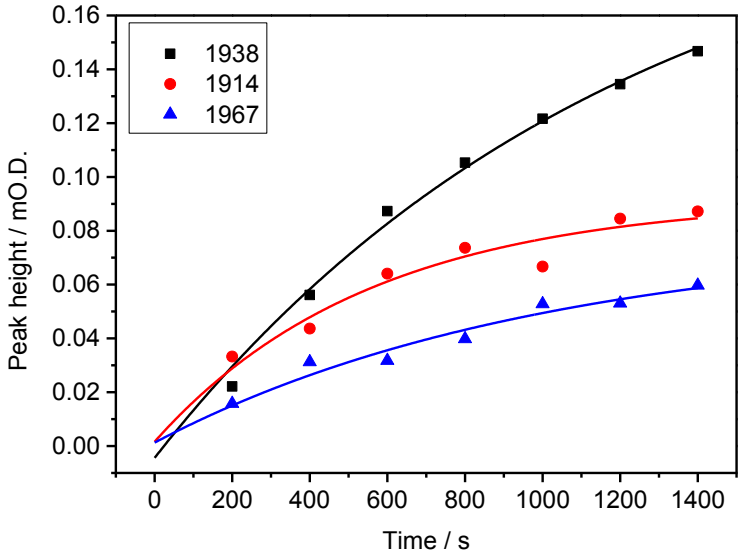

Figure 5-10: A plot showing the change in peak height of *ν*(CO) peaks at 1914 (red), 1938 (black) and 1967 (blue) cm^{-1} as a function of time following a potential step from –700 mV to –800 mV. The peak heights were obtained from a set of time-series difference spectra of the β-98^{His} variant MoFe protein in the presence of saturated CO solution recorded at the potential step –800 mV and processed against a spectrum recorded at the end of the previous potential step at –700 mV. (Raw data shown as points with fitted traces calculated by exponential growth function, Origin Programme 9.0.)

The wavenumber of these overlapped peaks were used for peak fitting in the spectra of the following potential steps. In Figure 5-11, a fitted trace to an experimental spectrum shows that the broad peak at *ca* 1938 cm^{-1} had at least four overlapping component peaks at 1914, 1938, 1967 and 2011 cm^{-1}. The unusually great width of some peaks might stem from CO binding to the less-constrained site, resulting in the slightly different CO-bound conformations as previously described in the carboxymyoglobin case in Chapter 3. This wavenumber is closely matched with that of SF-IR results of previous study on CO-bound nitrogenase in the presence of the native redox partner Fe protein coupled with ATP hydrolysis. This observation will be discussed further in the discussion section of this chapter.

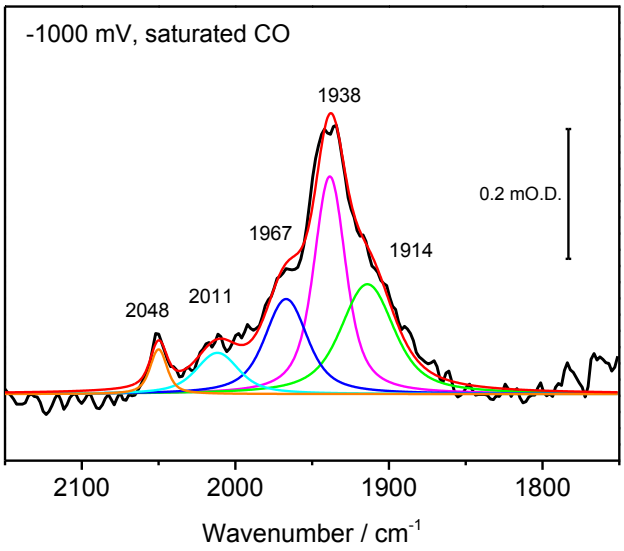

Figure 5-11: An IR spectrum of the β-98^{His} variant MoFe protein in the presence of CO recorded at final potential at –1000 mV processed against a background spectrum at –100 mV in the absence of CO (black). Overlaid fitted trace (red) was a result of combination of five individual peaks fitted to the data; 1914 (green), 1938 (magenta), 1967 (blue), 2011 (cyan) and 2048 (orange) cm^{-1}. (Peaks fitted to a Voigt function by Origin 9.0 program.)

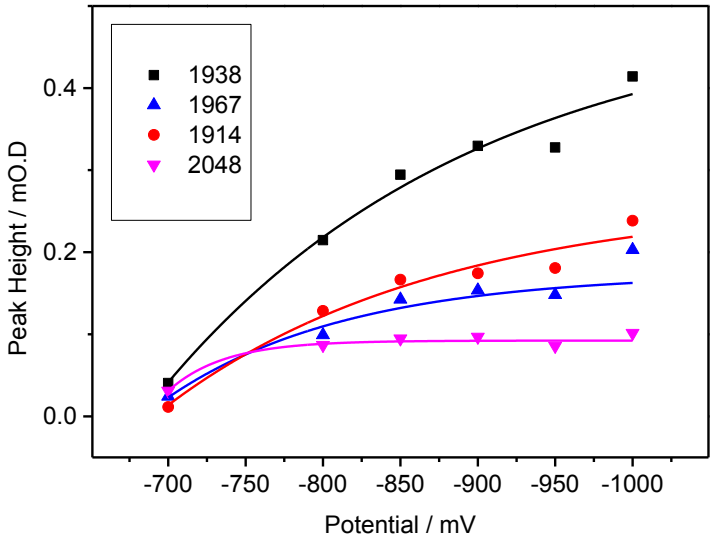

Figure 5-12: A plot showing the change in peak height as a function of potential of *ν*(CO) peaks at 1914 (red), 1938 (black), 1967 (blue) and 2048 (magenta) cm^{-1} as a function of applied potential. The peak heights were obtained from a set of spectra of the β-98^{His} variant MoFe protein in the presence of saturated CO solution recorded after equilibration at each potential step and processed against a background spectrum recorded at the potential –100 mV prior to addition of CO. (raw data shown as dots with fitted traces calculated by exponential growth function, Origin Programme 9.0)

In Figure 5-12, a plot of peak height against potential demonstrates that growth of four peaks at 1914, 1938, 1967 and 2048 cm^{-1} was predominant at the potential –800 mV. As the potential was stepped to increasingly negative potential values, the intensity of the principle peak at 1938 cm^{-1} continuously dominated, while the intensities of two shoulder peaks at 1914 and 1967 cm^{-1} increased relatively more slowly than that of the peak at 1938 cm^{-1}. In contrast, a peak at 2048 cm^{-1} arose at the potential –800 mV and remained unchanged as the potential was stepped down to more negative values.

Interestingly, upon re-oxidation to –100 mV, Figure 5-13 shows that there is small negative peak at 1914 cm^{-1} indicating a partial reversibility of the CO-bound species that corresponded to the formation of the peak at 1914 cm^{-1} observed at the very beginning of the potential step to –800 mV.

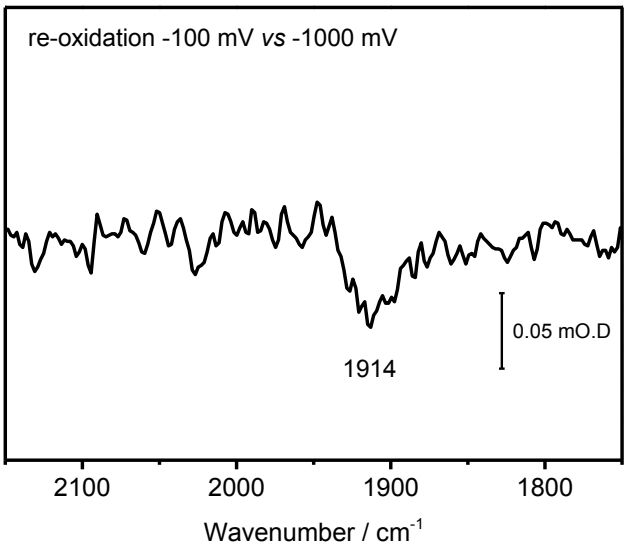

Figure 5-13: A difference spectrum of the β-98^{His} variant MoFe protein under hi-CO condition recorded during reoxidation at –100 mV processed against a spectrum recorded after equilibration at the last reduction potential step at –1000 mV (500 scans co-added, resolution 4 cm^{-1}) .

5.3.2 CO binding to the wild type MoFe protein

An IR SEC of CO binding to the wild type MoFe protein was performed in order to prove that observed CO binding to the variant is corresponding to that of the wild type as the similar CO inhibition of proton reduction was observed in both cases (section 4.4.1 and 5.3.1). The preparation for SEC experiment was done in the same manner as the β-98^{His} variant described in section 5.2.1. The same cocktail of redox mediators was used to facilitate electron transfer over a wide potential window.

In this study two SEC set ups were designed to investigate the reaction occurring with different CO concentration, high and low CO concentrations, that corresponding to the previous study of CO binding to the wild type nitrogenase by SF-IR technique under the turnover condition

5.3.2.1 High CO concentration condition

A saturated CO solution was used, *ca* 1.0 mM of CO in solution, to achieve the high CO concentration condition as described in the previous stopped-flow IR spectroscopy studies on the hi-CO complex generated under turnover conditions (0.5 – 1.0 mM CO).[68, 100] In the SEC experiment, a CO saturated flow solution was introduced to the SEC cell, while a potential of –100 mV was applied at the working electrode. In the presence of the saturated CO solution, the potential was decreased stepwise to –300 mV, –500 mV, –700 mV and –900 mV, as shown in Figure 5-14. A set of IR spectra was recorded simultaneously while these potentials were being applied.

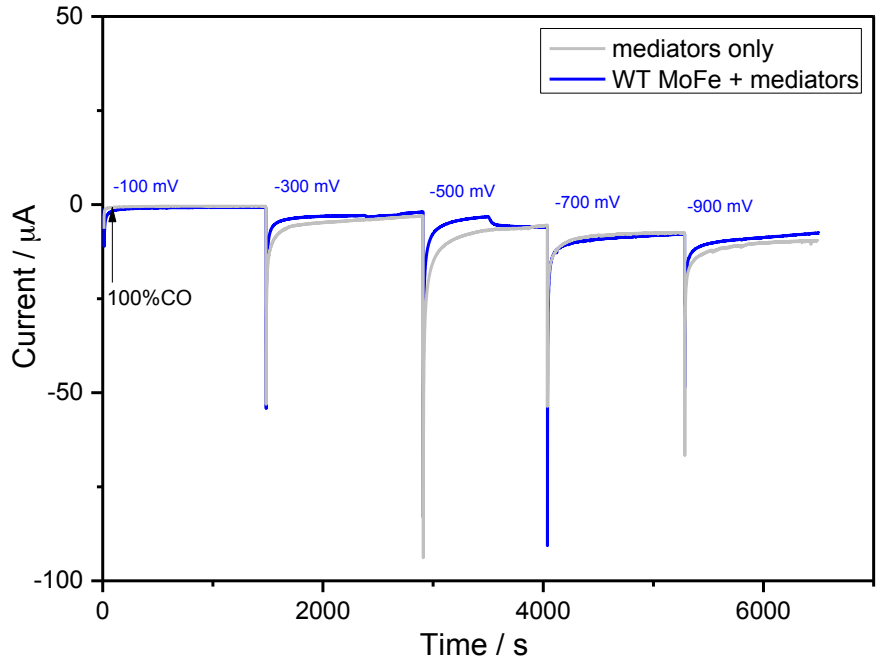

Figure 5-14: A chronoamperogram of the wild type MoFe protein in the SEC cell recorded in the presence of saturated CO solution (blue). The SEC scell contained the 2.0 nmol protein sample in the Nafion layer and was filled with the redox mediator cocktail. A chronoamperogram of the same SEC cell containing only CO-saturated redox mediator cocktail is also presented (grey) The sequence of potential steps was applied at the indicated times.

In Figure 5-14, a chronoamperogram of the wild type protein in the presence of saturated CO solution (hi-CO condition) shows no significant difference in current compared to that of redox mediators only. This is consistent with the observation in section 4.5.2 that CO could suppress proton reduction catalysed by the MoFe protein. The slight step in current for the protein film at –500 mV might be due to small bubbles that could get into the flow system and the SEC cell sometimes.

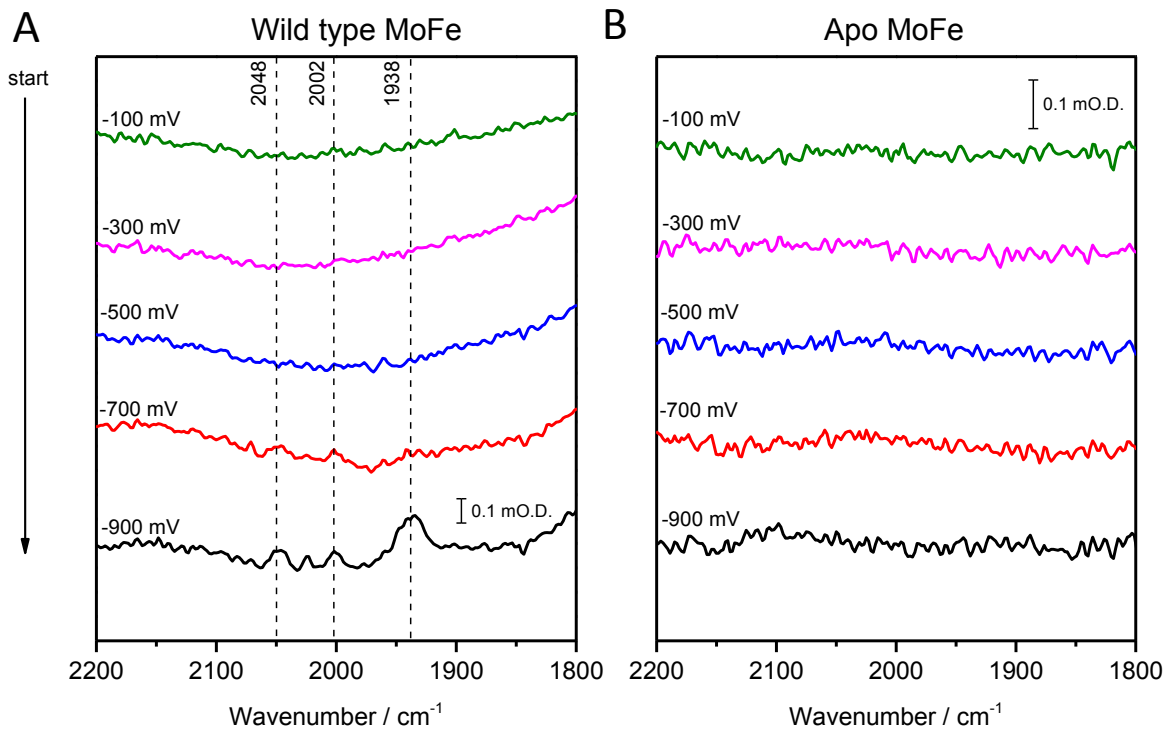

Figure 5-15: IR absorbance spectra of 2.0 nmol wild type MoFe (A) and apo-MoFe (B) after addition of CO saturated solution (*ca* 1.0 mM) followed by application of a sequence of potential steps. Each spectrum was recorded when the system was in equilibrium at each holding potential and processed against a background spectrum at –100 mV prior to addition of CO (500 scans co-added, 4 cm^{-1} resolution).

From a set of IR spectra of the wild type protein showing the *ν*(CO) region between 1800 and 2200 cm^{-1} in Figure 5-15A, no significant spectral changes were observed when the potential was applied from –100 mV down to –700 mV. As the potential was stepped down further to –900 mV, a positive peak at 1938 cm^{-1} emerged and continued growing gradually as a time increased. After 1200 s, the system was at equilibrium, and at least three positive peaks were observed at 1938, 2002, 2048 cm^{-1}. In a control experiment of apo-MoFe protein, shown in Figure 5-15B, IR spectra exhibited no significant spectral changes in the *ν*(CO) region when the same sequence of potential steps was applied in the presence of saturated CO solution.

Details of the spectral changes upon stepping the potential are clearly seen in difference spectra calculated between each potential step. Here each spectrum recorded at the end of a

potential step was used as a background spectrum for subsequent spectra. Selected difference spectra are shown in Figure 5-16. In Figure 5-16A, at –700 mV, only a small change is seen around the range of 1900 – 2050 cm^{-1} barely exceeding the noise level. Figure 5-16B shows a sharp peak at 1938 cm^{-1} that increased significantly at –900 mV with a small overlapping peak at 1900 cm^{-1}, while two smaller bands at 2002 and 2048 cm^{-1} increased slightly and became detectable.

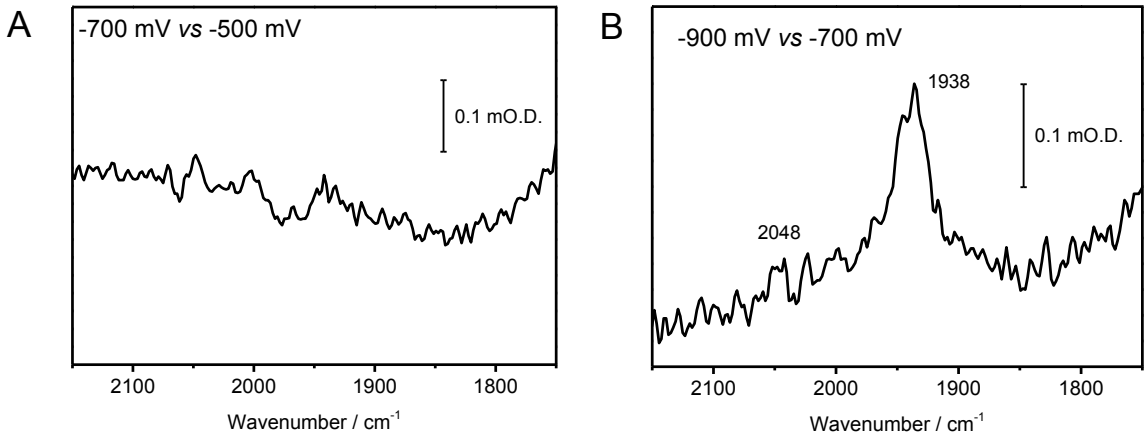

Figure 5-16: Difference spectra of the wild type MoFe protein in the presence of CO recorded after equilibration at potentials of (A) at –700 mV processed agiant –500 mV and (B) at –900 mV processed against –700 mV (500 scans co-added, resolution 4 cm^{-1}).

In order to monitor the reversibility of this process, the potential was stepped up to a more oxidised level again. Upon re-oxidation to the potential –100 mV, the difference spectrum in Figure 5-17A shows partial loss of the peak at 1938 cm^{-1} with a shoulder at 1900 cm^{-1}. Upon a further potential step to re-reduce at –900 mV, the peak at 1938 cm^{-1} was regained, although with low intensity as shown in Figure 5-17B. It was also noted that a small peak at 2048 cm^{-1} increased during the re-reduction but with no sign of corresponding peak loss during the re-oxidation process. This suggests build-up of a redox inactive form of the protein.

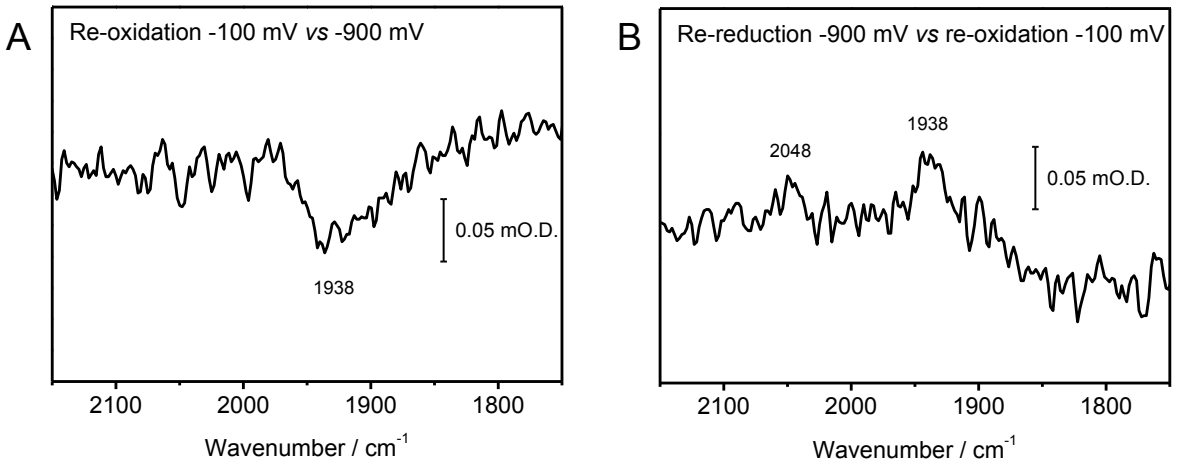

Figure 5-17: Difference spectra of the wild type MoFe protein in the presence of CO recorded during (A) re-oxidation at –100 mV processed against –900 mV and (B) re-reduction at –900 mV processed against re-oxidation at –100 mV (500 scans co-added, resolution 4 cm^{-1}).

After the experiment, the integrity of the Nafion-protein film was investigested as shown in Figure 5-18. It showed that the intensity of both amide bands decreased by 14% compared to the beginning of the experiment, indicating that the amount of the protein trapped in the Nafion layer in the IR sampling area was slightly lowered.

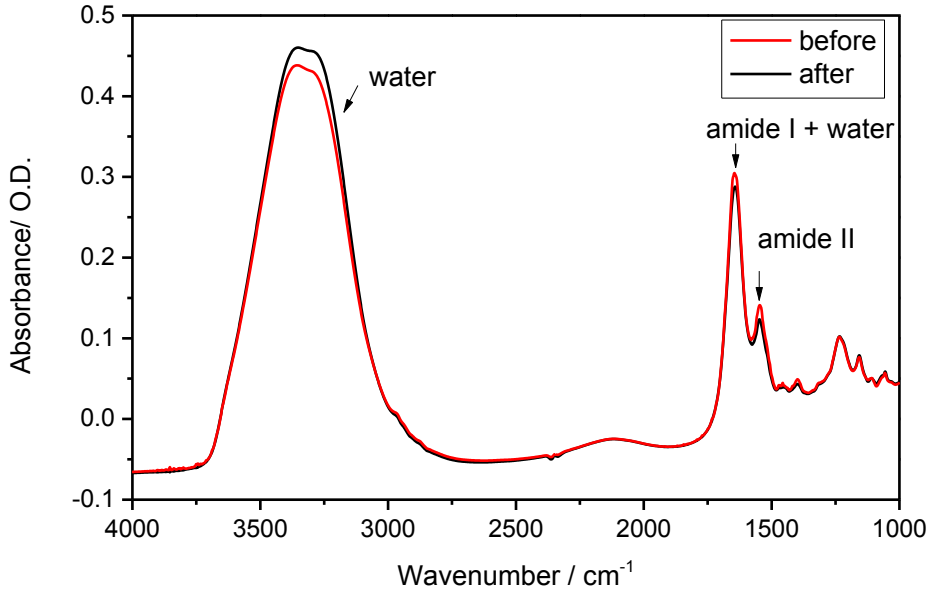

Figure 5-18: IR spectra showing the comparison between the Nafion film with 2 nmol of wild type MoFe protein sample before (red) and after (black) the experiment. A CO-saturated redox mediator solution was flowed into the SEC cell throughout the experiment. Each spectrum was processed against unmodified Si ATR prism background (500 scans co-added, 4 cm^{-1} resolution).

5.3.2.2 Low CO concentration condition

Another set of SEC experiments was performed under lower CO concentration condition, achieved by adding low CO gas mixture in to the flow solution during the proton reduction process. According to the previous report that showed *v*(CO) peak of lo-CO complexes in the presence of *ca* 60 μM CO,[68] a low CO gas mixture used in this study started at 6% CO in N_2 (*ca* 60 μM CO). The composition of the gas mixture was controlled by mass flow controllers.

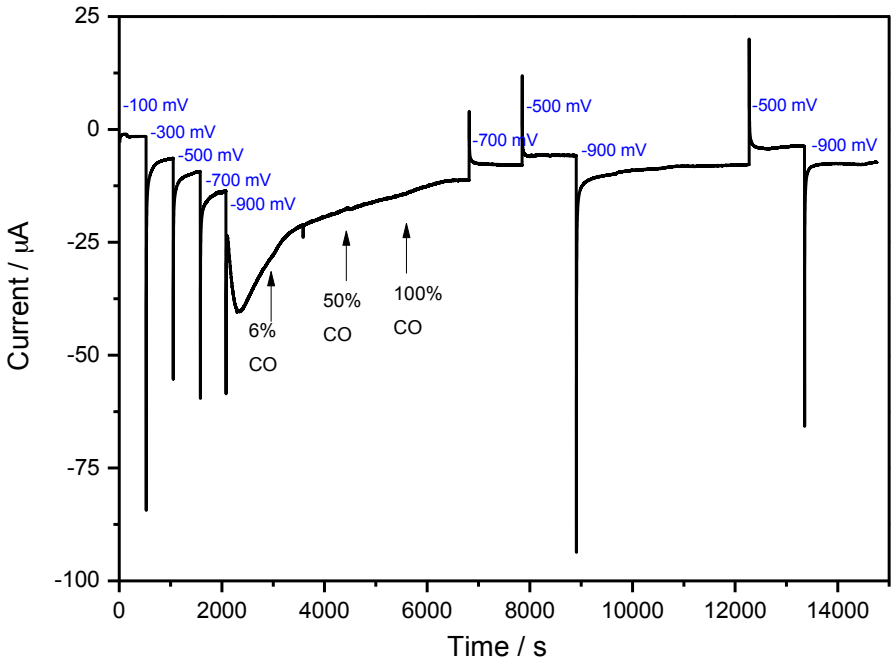

Figure 5-19: A chronoamperogram of 2.0 nmol wild type MoFe protein in the SEC cell with the redox mediator cocktail. The sequence of potential steps was applied at the indicated times. A CO/N_2 gas mixture was added at –900 mV and the ratio of CO was increased as indicated.

In Figure 5-19, as previously described in section 4.4.1, it is clear that the catalytic current from proton reduction arising at the potential –900 mV was suppressed upon addition of 6% CO.

In the IR spectra collected during this proton reduction process, it was found that the amide I and amide II bands were decreased at 1640 and 1545 cm^{-1}, respectively. This could be a result

of disruption in the Nafion layer within the IR sampling area by H_2 product generation. No spectral change in the *v*(CO) region was observed upon addition of 6% CO and beyond.

In Figure 5-20, after re-reduction to –900 mV, again in the presence of 100% CO, a difference spectrum shows an increase of a small positive *v*(CO) peak at 1938 cm^{-1}. This indicates that only a small amount of protein sample remained in the sampling area after the disruption by the evolution of dihydrogen.

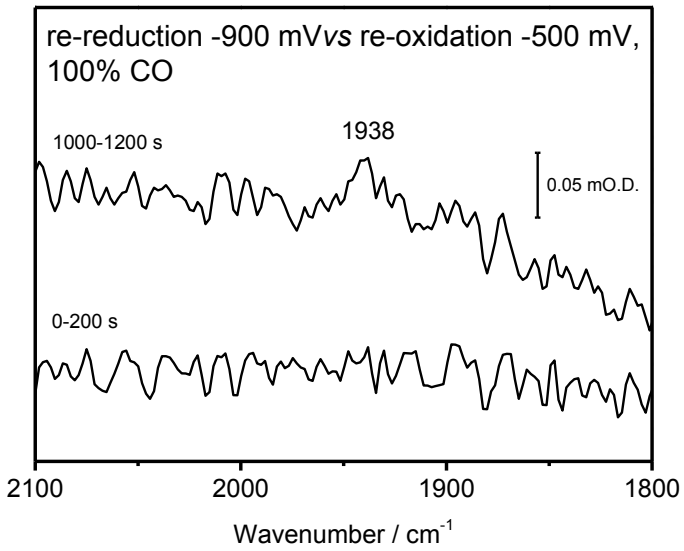

Figure 5-20: Diffrence spectra of the wild type MoFe protein under 100% CO condition recorded during re-reduction at –900 mV processed against a spectrum recorded at equilibrium after re-oxidation at –500 mV (500 scans co-added, resolution 4 cm^{-1}) .

5.4 Discussion

5.4.1 CO inhibition of wild type and β-98^{His} variant MoFe protein

The electrochemical results showed no significant catalytic current arising from proton reduction in both the wild type and β-98^{His} variant MoFe protein in the presence of saturated CO solution. This indicated that CO has the same inhibitory effect on the variant as the wild type MoFe protein that was previously discussed in section 4.4.3.

Under high CO concentration condition, the β-98^{His} variant MoFe protein exhibited a set of *ν*(CO) peaks following reduction at a potential of –800 mV. This potential is slightly more positive than the highest potential that catalytic current from proton reduction was observed (at –850 mV with the flow system, section 4.3.1). This shows that a more negative potential is required to drive the reaction of proton reduction than that to enable CO binding to the active site.

SEC results for the wild type MoFe protein in the presence of CO showed spectral changes in the *ν*(CO) region following application of a potential of –900 mV. This potential corresponds to the onset of proton reduction activity (catalytic current) by the wild type MoFe protein, as previously demonstrated in the electrochemical experiments in section 4.2. According to the electrochemical results in section 4.4, CO at both low and high concentration conditions could suppress the catalytic current from proton reduction in the wild type MoFe protein driven by mediated electron transfer from Eu^{II}-ligand mediators.

Together these results suggest that the observed changes in the IR spectra at low potentials in the presence of CO correspond to the interaction of CO at redox sites that provoke the inhibition of proton reduction of the MoFe protein. This is the first time that an activity

measurement for nitrogenase has been correlated directly with spectroscopic evidence for inhibitor binding.

5.4.2 CO bound peaks

In the case of β-98^{His} variant MoFe protein in the presence of saturated CO solution, the IR spectra showed *v*(CO) peaks at 1914, 1938, 1967, 2011 and 2048 cm^{-1}. Under the same CO concentration condition, the wild type MoFe protein exhibited at least three distinct *v*(CO) peaks at 1938, 2002 and 2048 cm^{-1} at the potential –900 mV. Another small band at 1900 cm^{-1}, overlapping with the stronger peaks at 1938 cm^{-1}, was found to be reversible upon re-oxidation and re-reduction. A SEC result for the apo-MoFe protein, containing only the P-cluster [8Fe-7S], in the presence of CO showed no significant spectral change in the *v*(CO) region, implying that all the changes observed in the case of the wild type MoFe protein arose from CO interacting with the FeMoco cluster.

In this study, the wavenumber of the principal peak at 1938 cm^{-1} observed in both the wild type and β-98^{His} variant MoFe protein cases is closely matched with the hi-CO peak at 1936 cm^{-1} reported by George and co-workers from the stopped-flow studies.[59, 68, 100] In previous studies, stopped-flow IR spectroscopy was used to study ATP-dependent CO binding to the wild type MoFe protein under the turnover conditions. Upon addition of the CO-saturated ATP solution to the mixture of the MoFe protein and the Fe protein, four *v*(CO) peaks at 1880, 1906, 1936 and 1960 cm^{-1} were observed as reproduced in Figure 5-21. All of these hi-CO peaks were assigned as terminally bound CO. It was found that appearance and wavenumber of these hi-CO peaks were indifferent between the MoFe protein from *K. pneumoniae* and *A. vinelandii*.[68, 100] Another study on different variants showed that substitution of amino acid at the α-70^{Val} position causes a wavenumber shift from 1936 cm^{-1}

to 1946 cm^{-1}, suggesting that the peak at 1936 cm^{-1} was involved with terminal CO binding to Fe-S core of the FeMoco at a site near the α-70^{Val} residue. [15]

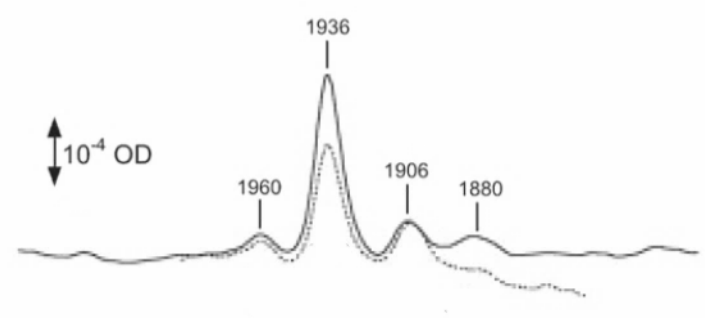

Figure 5-21: IR spectra of the *Azotobacter vinelandii* MoFe nitrogenase hi-CO complex formed under the turnover condition with the Fe protein and ATP. Spectra averaged 25–35 s (solid line) and 6–14 s (broken line) after mixing, were obtained by the stopped flow method (Reproduced with permission from ref. [100]) Copyright (c) 2011 Wiley-VCH Verlag GmbH & Co. KGaA, Weinheim.

Another small peak at 1900 cm^{-1} observed in this study both in the wild type and β-98^{His} variant MoFe protein cases could correspond to either 1906 or 1880 cm^{-1} of these previously reported hi-CO peaks. The small intensity of this peak relative to the 1938 cm^{-1} peak could reflect the difference in extinction coefficients. This is in agreement with the report of George *et al.*, in which the extinction coefficients of the hi-CO peaks were approximately 1930 M^{-1} cm^{-1} for the 1936 cm^{-1} peak, 400 M^{-1} cm^{-1} for the 1906 cm^{-1} peak and 350 M^{-1} cm^{-1} for the 1958 cm^{-1} peak. [68]

A partial loss of the peaks at 1936 and 1900 cm^{-1} after re-oxidation at –100 mV without appearance of any new positive peak nearby suggests dissociation of bound CO from the hi-CO complex at the more oxidized redox level, and indicates potential dependence of CO binding to the active site. This is similar to the redox dependence of CO binding to the isolated FeMoco.[92] CO could bind to the isolated FeMoco at the reduced state under the lo-CO condition, giving rise to *ν*(CO) peaks at 1808 and 1835 cm^{-1}. When the potential was increased to generate the oxidised level of FeMoco, CO was released from the CO-bound FeMoco complex, leading to a loss of both peaks.[92] The observation in the present study that

the peaks at 1936 and 1900 cm^{-1} were partially regained after the potential was decreased to –900 mV again, suggested that CO was able to re-bind to the MoFe protein again when the FeMoco was reduced to the CO-binding level.

These SEC results show that CO is able to bind to the activated active site of the wild type MoFe protein upon reduction *via* mediated electron transfer by low potential redox mediators. This is the first report of ATP-independent CO coordination to the MoFe protein. The advantage of electrochemical control allows the study of potential-dependence and reversibility of CO binding to the active site. However, the low intensity of *ν*(CO) peaks hinder a further characterisation of the CO-bound complex, including the new *ν*(CO) peaks observed at high wavenumber 2002 and 2048 cm^{-1}. A small population of CO-bound complexes generated in the SEC cell might be due to a poor ability of the wild type protein to accept electrons from redox mediators as previously reported in Chapter 4.

In the case of β-98^{His} variant MoFe protein, the similarity in wavenumber of *ν*(CO) peaks implied that the CO-binding sites on the FeMoco, and the protein environment surrounding it, were not altered much between the variant and the wild type MoFe protein. The stronger intensity of *ν*(CO) peaks for the variant indicated that a greater population of each CO-bound species was generated, as expected from the variant which accepts electrons more readily from Eu-ligand mediators.[55] Thus, both results from chronoamperometry and IR spectroscopy suggested that the substitution of the amino acid at the β-98 residue of the MoFe protein did not alter the interaction between CO and the active site.

The SEC study of the β-98^{His} variant showed that it could represent CO binding to the wild type MoFe protein and provide more information on nature of CO interaction by enhanced electron transfer to the active site of the MoFe protein.

5.4.3 Time course of CO binding

The wavenumbers of ν(CO) peaks observed in the β-98^{His} variant at 1914, 1938 and 1967 cm^{-1} closely correspond with the ν(CO) peaks at 1906, 1936 and 1960 cm^{-1} observed in the previous study on CO binding to the MoFe protein in the presence of Fe protein and ATP under the hi-CO condition by George and co-workers.[59, 68, 100] Also, the time-dependent growth of the peaks in the present study by IR spectroelectrochemical technique with mediated electron transfer approach corresponds well with that in the previous study by stopped flow IR spectroscopic technique as shown in Figure 5-22.

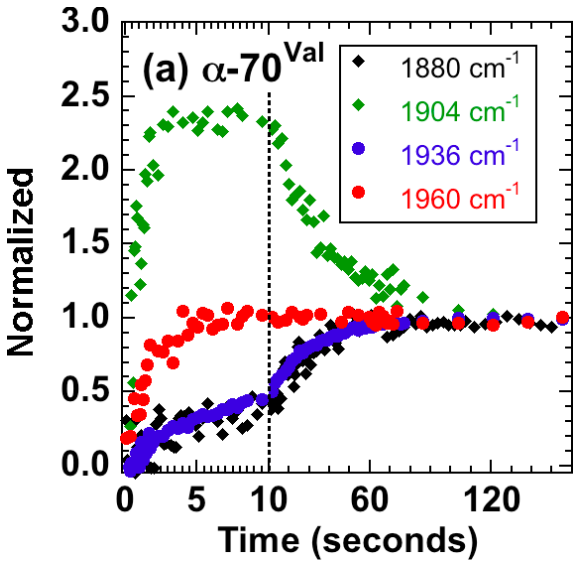

Figure 5-22: Time-dependent intensities from IR spectra of the wild type MoFe protein from *A. vinelandii* under turnover conditions in CO-saturated solution. (Reproduced with permission from ref. [100]. Copyright (c) 2011 Wiley-VCH Verlag GmbH & Co. KGaA, Weinheim.)

In this study the ν(CO) peak at 1914 cm^{-1} was formed first, at a potential of –800 mV, and the intensity of this peak was dominant for 200 s after applying the potential (Figure 5-10). This corresponds with the study by George and co-workers that observed rapid growth of a peak at 1906 cm^{-1} immediately after mixing ATP solution with the MoFe protein and Fe protein in the presence of saturated CO solution.[100] In an earlier study, it was shown that only the peak

at 1906 cm^{-1} was detected at short times under low CO concentration conditions, and so it was denoted as a lo-CO peak in both cases.[68]

In Figure 5-22, the result from the past study showed that the 1906 cm^{-1} peak reached a maximum value quickly and then started to decline slowly at longer times.[100] This might be a result of the depletion of ATP population in the system, suggesting that this species was sensitive to a change in redox state of the active site. One plausible explanation is that the 1906 cm^{-1} peak arises from an intermediate species and undergoes a conformational change or reacts further to form other CO-bound species at higher wavenumbers – the decrease in intensity of the 1906 cm^{-1} peak coincides with an apparent increase in the rate of formation of peaks at 1880 and 1936 cm^{-1}. This is paralleled by the observation in the present study that the ν(CO) peak at the 1914 cm^{-1} is formed within first 200 s after applying the potential, followed by the formation of a peak at 1938 cm^{-1} from 200 s onward (Figure 5-10).

Another small peak at 1967 cm^{-1} became more prominent in the study of the β-98^{His} variant compared with that of the wild type MoFe protein, due to better signal/noise as a result of a greater extent of interaction with CO. The time-dependent growth (Figure 5-10) of this peak is similar to the peak at 1914 cm^{-1}, consistent with the past study showing that the intensity of the peaks at 1906 and 1960 cm^{-1} reached maxima at almost the same time, although the peak at 1960 cm^{-1} did not subsequently decrease.[100] Meanwhile, the dominant peak at 1938 cm^{-1} in this study was found to grow more slowly following the potential step to –800 mV, paralleling slow evolution of a peak at 1936 cm^{-1} in the study by George *et al.*[100]

5.4.4 Potential-dependence of CO binding

The potential-dependence of ν(CO) peaks observed for the β-98^{His} variant showed that the intensity of peaks at 1914, 1938 and 1967 cm^{-1} were grew at more reducing potentials below

–800 mV. Since no other peaks were detected as the potential was lowered, this implies that all the CO binding sites became accessible at the same redox level. This could indicate that the increase in intensity of the peaks at more negative potentials was a result of an increase in population of the reduced active site available for CO binding. Interestingly, it showed that the intensity of peak at 1914 cm^{-1} deceased partially upon re-oxidation to –100 mV. This suggested that the formation of this particular CO-bound species was both potential-dependent and reversible.

From previous electrochemical data of CO coordination to the isolated FeMoco, it was suggested that the CO ligands could withdraw electron density from the isolated FeMoco, making the CO-bound FeMoco more difficult to be oxidized. [92] This might account for the partial reversibility observed in the present study; no loss of peaks apart from 1914 cm^{-1}, were observed upon re-oxidation at –100 mV. The results from the present study that show irreversibility of the peaks at 1938 and 1967 cm^{-1} upon re-oxidation, might indicate stronger binding to the active site for these species.

The high wavenumber peak at 2048 cm^{-1} remained unchanged as the applied potential became more negative. Apart from the difference in potential-dependent profile, it was noted that the 2048 cm^{-1} peak is sharper than other peaks when it appeared at the very first potential step. The high wavenumber peaks at 2011 and 2048 cm^{-1} are much higher wavenumber than most of the CO-bound species at Fe-S clusters previously reported.[95, 177] This suggests that these peaks arose from non-specific CO binding, probably from excess Mo atoms in the sample solution forming CO adducts like $Mo^{4+}CO$ (ν(CO) 2050 cm^{-1}) or $Mo(CO)_6$ (ν(CO) 2030 cm^{-1}).[178]

5.4.5 CO binding mechanism

The overall results point out that the substrate and inhibitor binding to the reduced state of FeMoco can be achieved electrochemically by mediated electron transfer, and corresponds to that achieved in the presence of the native redox partner Fe protein associated with hydrolysis of ATP. Electron transfer *via* redox mediators allows the application of precise potentials by a working electrode. This has allowed us, for the first time, to determine the potential required for substrate binding to FeMoco within the MoFe protein.

From the electrochemical and spectroelectrochemical results on CO inhibition of proton reduction for both wild type and variant MoFe protein, an outline mechanism of the protein-bound FeMoco (M) is proposed. At a potential of –900 mV, the cofactor at resting state (M^{rs}) is reduced by electron transfer from Eu^{II}-ligand mediators. The reduced cofactor (M^{red}) then can interact with a proton or CO present in the solution. In the case when a proton is bound, the extra electron can be stored in the form of a hydride (H^-) on the cofactor. This hydride-bound reduced FeMoco (M^{red}-H) can then be protonated by proton donation from a nearby amino acid or proton transfer from solution. Addition of another electron then results in evolution of hydrogen and returns the cofactor to its resting state.

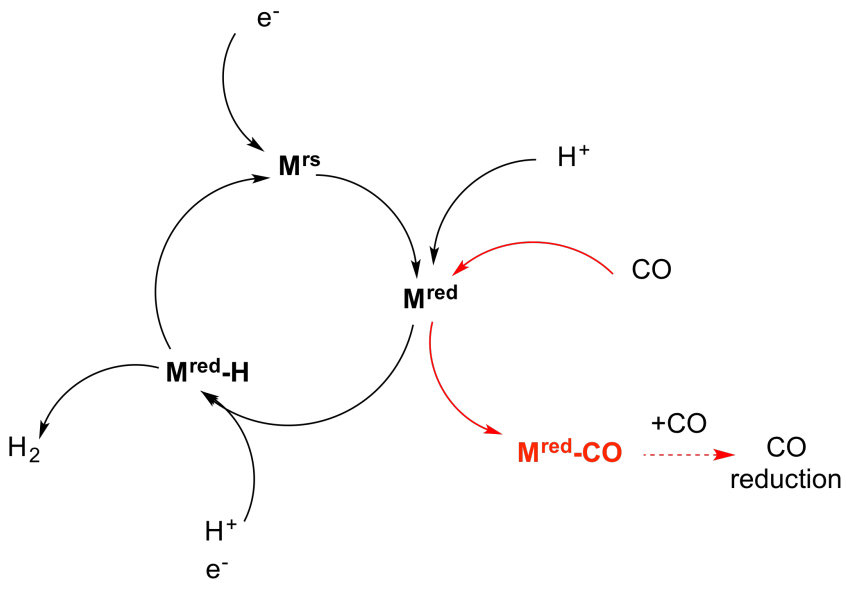

Figure 5-23: A proposed redox mechanism on the FeMoco inside the MoFe protein.

For the CO inhibition, it can be explained in terms of competitive binding of CO to FeMoco in the reduced state (M^{red}-CO). This, possibly coupled with further interaction with CO, could block the catalytic site for proton reduction, and therefore no proton reduction current is observed. In the case where the CO-bound cofactor proceeds to bind further CO, this could facilitate CO reduction providing that the necessary electron transfer steps can occur. However, in the present electrochemical setup application of potentials lower than –1000 mV is obstructed by proton reduction at the carbon paper working electrode.

In conclusion, this chapter has demonstrated the first direct IR evidence of ATP-independent CO binding to the active site of the MoFe protein, in both the wild type and β-98^{His} variant, and has correlated this ligand binding with a change in proton reduction activity. The peak wavenumber and time-dependent peak evolution found during this study are consistent with the results of CO coordination studies of nitrogenase obtained by electron transfer from the Fe protein driven by ATP. This strongly suggests that our mediated electron transfer approach can deliver low potential electrons into the MoFe protein and reduce the FeMoco to the

substrate binding level. Moreover, the electrocatalytic activity of the protein can be monitored and the change in redox activity can be related with the potential and ligand binding directly.

Looking forward, electrochemical control *via* a cocktail of redox mediators could be used as a powerful tool in conjunction with other characterization techniques to investigate *in situ* the potential-dependence and reversibility of substrate and inhibitor binding to the MoFe protein active site.

Chapter 6

Study of cyanide binding to the metal centres of nitrogenase

Cyanide is one of the exogenous ligands that are commonly used as probes in IR spectroscopic studies of proteins. Due to a difference in π-acid characteristics between CN^- and CO, cyano complexes can be formed with higher valent metal centres than carbonyl complexes. This could give us more information about a change between different redox states of enzyme active sites. This chapter will describe several IR spectroelectrochemical approaches for investigating cyanide binding to wild type and variant MoFe proteins of nitrogenase.

6.1 Introduction

A study of cyanide binding to metal clusters is another way to explore redox-dependent ligand binding in nitrogenase as cyanide is isoelectronic with both CO and N_2. However, cyanide has different electronic properties; the stronger σ-donor characteristics of cyanide enable it to coordinate with higher oxidation number metal central centres (see Chapter 1). As an IR spectroscopic probe, metal-cyano complexes generally give rise to vibrational bands in the mid-IR region at 2000 – 2200 cm^{-1}.[109]

6.1.1 Reduction of cyanide by nitrogenase

Studies of cyanide effects on nitrogenase have been of interest for a long time. Many early studies suggested that cyanide can bind to the active site of nitrogenase at a more oxidised level compared to dinitrogen or H^+, as outlined in Scheme 6-1.[85, 157, 179] J. Li *et al.* reported that the cyanide ion (CN^-) can inhibit total electron flow by uncoupling ATP hydrolysis and electron transfer. Cyanide inhibition was found to be reversible and was fully suppressed by CO and partially by azide (HN_3), suggesting a common binding site. On the other hand the protonated species, HCN, was found to be a substrate for six-electron reduction by nitrogenase, resulting in methane (CH_4) and ammonia (NH_3).[74]

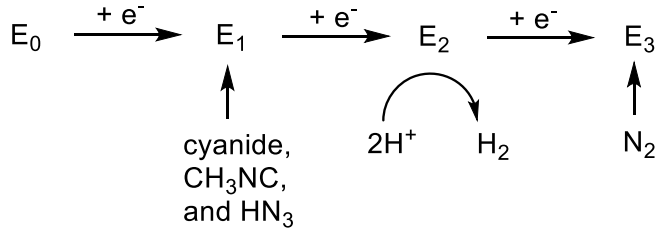

Scheme 6-1: Proposed redox states where different substrates bind to nitrogenase, adapted from ref. 4. (E_n represent n-electron reduced states of nitrogenase; E_0 is the resting state.)

According to a pre-steady-state kinetics study of cyanide reduction by Lowe *et al.*, it was proposed that the cyanide binding mechanism involves cyanide-induced ligand exchange as illustrated in Scheme 6-2. In the first step, CN^- binds reversibly to a single metal centre on the active site. Then, it undergoes a slow CN^- induced ligand replacement on the same metal cluster. The resulting CN^- bound active site would inhibit the further electron transfer as CN^- helps stabilise the oxidised state. When the bound CN^- is protonated, the stabilising effect is demoted and HCN could be successively reduced to either HCHO and NH_3, CH_3NH_2 or CH_4 and NH_3 *via* two-, four- or six-electron reduction, respectively.[75]

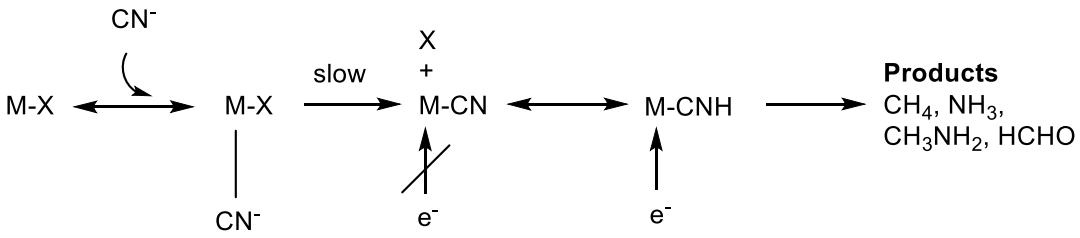

Scheme 6-2: A proposed mechanism of cyanide-induced ligand exchange at the active site.[75]

Interestingly, it was observed that the ratio of products from reduction of HCN largely depends on electron flux and concentration of substrates.[74, 85] A study by Fisher *et al.* showed that wild type nitrogenase produced more NH_3 than CH_4 at lower cyanide concentration. This could be explained by the fact that CH_2=NH, which is an intermediate in the 2-electron reduction of HCN, was likely to be displaced from the active site and released as HCHO and NH_3 so the amount of CH_4 produced, *via* 6-electron reduction, was decreased as shown in Scheme 6-3. It was suggested that high concentrations of cyanide could lower the affinity of nitrogenase for HCN and disfavoured the release of CH_2=NH. It was also reported that CH_4 production ability of wild type nitrogenase was enhanced in the presence of acetylene, implying different binding sites and a different effect on substrate affinity.[180] In the same report, the study of HCN reduction of different variants of nitrogenase with substituted amino acid residues revealed that α-191^{Gln} and α-195^{His} residues play key roles in the interaction with cyanide.[180]

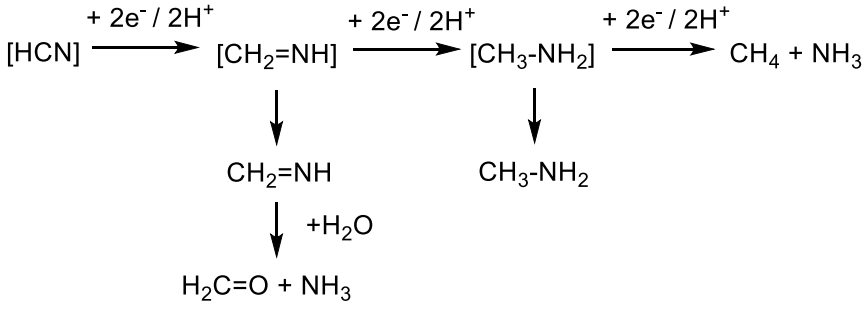

Scheme 6-3: A possible pathway of cyanide reduction by nitrogenase. Compounds in parenthesis represented enzyme-bound compounds.

Recent studies have shown that various modified nitrogenases are capable of the six-electron reduction of HCN to CH_4 even without the presence of Fe protein and ATP. Ribbe *et al.* reported that variant nitrogenase containing a pair of $[Fe_4S_4]$ clusters, a precursor of the P-cluster $[Fe_8S_7]$, is able to catalyse ATP-independent reduction of cyanide to CH_4 and other hydrocarbon products by using Eu^{II}-DTPA as a low potential reductant.[120] Roth *et al.* demonstrated a light-driven six-electron reduction of HCN by using modified MoFe protein with a covalently-attached Ru photosensitiser $[Ru(bipy)_2(phen)]^{2+}$.[153]

6.1.2 Cyanide binding to isolated FeMoco

Several cyanide binding studies have been carried out on the isolated active site of nitrogenase. An electrochemical study of isolated FeMoco, extracted into an organic solvent, by Pickett *et al.* showed that cyanide is able to bind to isolated FeMoco in the oxidised state (EPR silent) and significantly lowers the reduction potential of the $FeMoco^{semi\text{-}red/ox}$ couple. They proposed that the cyanide binding site was located on the central Fe-S core rather that the Mo atom. It was suggested that the shift in redox potential of the cyanide-bound FeMoco to more negative value is a result of the increasing electron density at the iron-sulphur core from the σ-donor ligand, making it more difficult to be reduced as indicated in Figure 6-1. This change in the electronic structure also led to the revelation of a new redox state, the super-oxidised state of cyanide-bound FeMoco (EPR signal S=1/2, low spin), which is electrochemically inaccessible for the unmodified cofactor.[94]

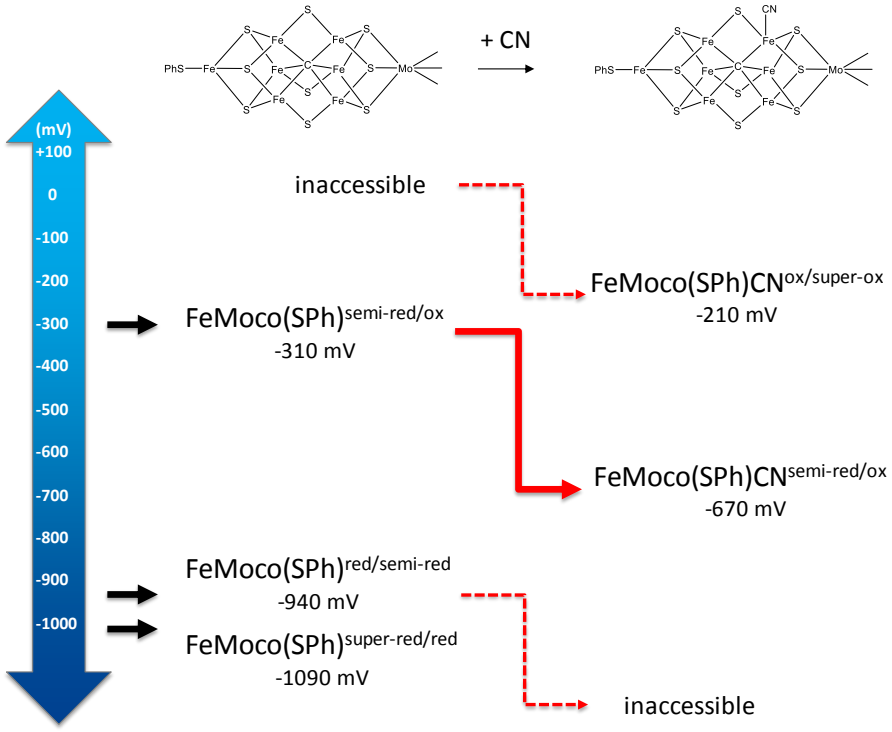

Figure 6-1: Redox states and reduction potentials of thiophenol-modified FeMoco, FeMoco(SPh), and cyanide-bound FeMoco, FeMoco(SPh)CN. The redox potentials are taken from the work of Pickett and co-workers.[92, 94]

More recently, Ribbe and co-workers reported that isolated clusters, FeMoco from the Mo-nitrogenase and FeVco from the V-nitrogenase, are capable of reduction of cyanide to various hydrocarbons including CH_4 by using Eu^{II}-DTPA as a reducing agent under ambient conditions.[119] Despite differences in the productivity compared to the protein-bound active site under the conventional Fe protein-ATP conditions, the similarity in their catalytic activity gives a useful insight into the enzyme mechanism and could be used to inspire the development of catalysts for hydrocarbon synthesis.

6.1.3 Previous spectroelectrochemical studies of FeMoco-CN

According to a SEC study by Pickett *et al.*, it was found that the redox-dependent interaction between isolated FeMoco and a cyanide ligand caused changes in the IR spectra. In Figure 6-2, a spectral shift in a ν(CN) peak from 2053 cm^{-1} to 2095 cm^{-1} was observed when the

FeMoco was oxidised from the oxidised to super-oxidised level in the presence of excess $[Et_4N]CN$. Therefore it was suggested that the *v*(CN) absorption bands at 2053 cm^{-1} and 2095 cm^{-1} were associated with cyanide ligand binding to the oxidised and super-oxidised states of the FeMoco, respectively. A loss *v*(CN) peak at 2053 cm^{-1} was also observed, without growth of a new *v*(CN) peak, when the FeMoco was reduced from oxidised to semi-reduced level, indicative of a dissociation of cyanide from the cofactor in the semi-reduced state. Moreover, they reported cooperative binding of cyanide and CO to the FeMoco. It was found that CO was able to coordinate with the isolated cofactor at the higher redox state in the presence of cyanide, leading to the proposal of that both cyanide and CO bind alongside on the iron core of the FeMoco.

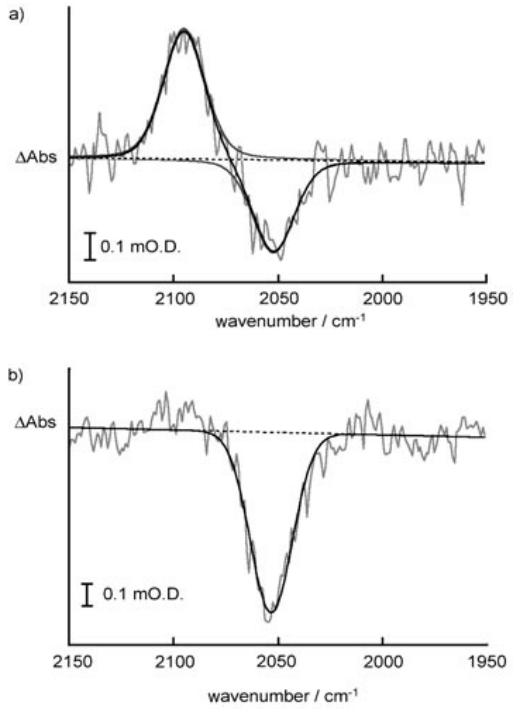

Figure 6-2: IR difference spectra showing cyanide-induced changes to isolated FeMoco in the 1800 – 2000 cm^{-1} region. (A) A positive peak at 2095 cm^{-1} and a peak loss at 2053 cm^{-1} upon oxidation following a potential step from *ca* –360 mV to *ca* –60 mV. (B) A loss of the peak at 2053 cm^{-1} upon reduction following a potential step from *ca* –360 mV to *ca* –870 mV. (Reproduced with permission from ref.[94]) Copyright (c) 2011 Wiley-VCH Verlag GmbH & Co. KGaA, Weinheim.

Although the redox levels of the isolated FeMoco in organic solvent are different from those of the protein-bound cofactor, the study by Picket and co-workers demonstrated the effect of cyanide ligation on the electronic characteristic of FeMoco. So far, no IR spectra of cyanide interaction with the cofactor inside the protein cavity have been reported. Thus the IR spectra of the isolated FeMoco-CN are useful as a spectral reference for the present study.

6.2 Cyanide binding to variant MoFe protein

Whereas the MoFe protein of wild type nitrogenase is unable to interact with any substrates or inhibitors unless it is in the reduced state, certain genetically-modified MoFe proteins can interact with cyanide in their resting state ($M^{semi\text{-}red}$, EPR signal S = 3/2). According to the previous report by Seefeldt *et al.*, the MoFe protein with substitution of one amino acid residue near the active site (from α-96^{Arg} to α-96^{Gln}, α-96^{Leu}, α-96^{His}, and α-96^{Ala}), exhibited changes in EPR signals of the FeMoco cluster upon addition of cyanide at their dithionite-reduced, resting state.[76] This α-96^{Arg} residue is located above the Fe-S sub-cluster where the ligand supposedly binds to FeMoco, as shown in Figure 6-3.

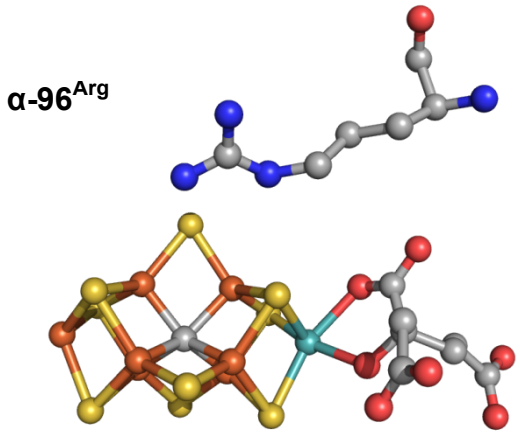

Figure 6-3: Location of α-96^{Arg} residue and the FeMoco cluster in wild type nitrogenase from *Azotobacter vinelandii* (3U7Q from RCSB PDB).

This ability of α-96^{Arg}-substituted variant nitrogenase to interact with cyanide ligands in the resting state will allow the use of the IR spectroelectrochemical technique described in Chapter 2 to investigate the mechanism of ligand binding to the more oxidised states of the nitrogenase active site. Moreover, together with the EPR data, IR spectra could provide more information about coordination chemistry and electronic structure of enzyme redox sites.

In this chapter an IR spectroelectrochemical study was performed aiming to explore cyanide binding to the redox states of the specific α-96^{Gln} variant MoFe protein. The SEC results from different MoFe proteins are presented and the interaction between the metal clusters and cyanide is discussed.

6.3 Experimental

6.3.1 Sample preparation

In the present work, α-96^{Gln} amino acid substituted MoFe proteins together with the wild type MoFe proteins and apo-MoFe proteins from *A. vinelandii* were provided by a collaborator, Lance Seefeldt, from Utah State University. Cell growth and protein isolation procedures are described elsewhere.[76] All proteins were carefully handled inside an anaerobic glove box (Glove Box Technology Ltd.) under a N_2 atmosphere (< 1 ppm O_2).

A reducing agent, sodium dithionite ($Na_2S_2O_4$) was added to protein samples to keep them in a reduced state during transportation. Before commencing a spectroscopic experiment, a methyl viologen paper was used to test for the presence of dithionite in the sample. For some SEC experiments $Na_2S_2O_4$ had to be washed out by buffer exchange using a centricon tube with a 100 kDa cut off membrane, in order to avoid competing redox chemistry from dithionite.

A solution of MoFe protein samples were prepared in 150 mM Tris-HCl buffer solution pH 7.4 with 100 mM NaCl unless stated otherwise. All redox mediators and cyanide solutions were prepared freshly on the day of the experiment. Cyanide solution was prepared from a stock solution of 1.0 M KCN and adjusted to neutral pH by adding 3 M HCl. An aliquot of cyanide solution was stored in a septum-sealed vial in order to prevent HCN evaporation (boiling point 25.6 °C) inside the glove box.

6.3.2 Preparation of the ATR-IR SEC cell

The ATR-IR SEC cell containing the protein sample in a Nafion layer was prepared as previously described in Chapter 2. In each experiment, the solution of protein sample was concentrated and then added to the Nafion mixture to give approximately 2.0 nmol of protein,

equivalent to 4.0 nmol of active sites, in the Nafion network layer. The cell was filled with a redox mediator cocktail in Tris-HCl buffer pH 7.4 as described in Chapter 3. A three-electrode system was used, consisting of a piece of carbon paper, a Pt wire and the custom-made SCE as working electrode, counter electrode and reference electrode, respectively. All potentials are quoted *versus* the standard hydrogen electrode (SHE, $E_{SHE} = E_{SCE} + 0.241$ V at 25 °C).

6.3.3 Cyanide in solution

A cyanide solution was prepared from potassium cyanide salt and has two cyanide species present; HCN and the CN^- anion. The ratio of these two species in solution depends on the pH value. HCN is a weak acid with a pK_a of 9.2, thus HCN is the major species in aqueous solution at neutral pH. A simple test of the cyanide solution was done using the ATR technique to verify this. An aliquot of KCN solution was added to the cell containing either buffer at a certain pH or water. An IR spectrum was recorded and processed against a background spectrum of the relevant solvent in the absence of cyanide. Figure 6-4 shows that a peak corresponding to ν(CN) of HCN at 2092 cm^{-1} was observed in a case of KCN in buffer solution at pH 7.4, confirming that the protonated species is dominant at this pH, while a peak of ν(CN) of CN^- at 2080 cm^{-1} was present in a solution of KCN in buffer-free water (final pH >10).[117]

A SEC test of cyanide solution was performed as a control experiment using the SEC setup and redox mediator system described in Chapter 3. In Figure 6-5, the peak at 2092 cm^{-1} immediately appeared following the addition of KCN solution to the cell and is assigned as ν(CN) of free HCN in solution. No reaction between cyanide and mediator was observed, and no significant spectral changes were observed upon stepping down to negative potentials.

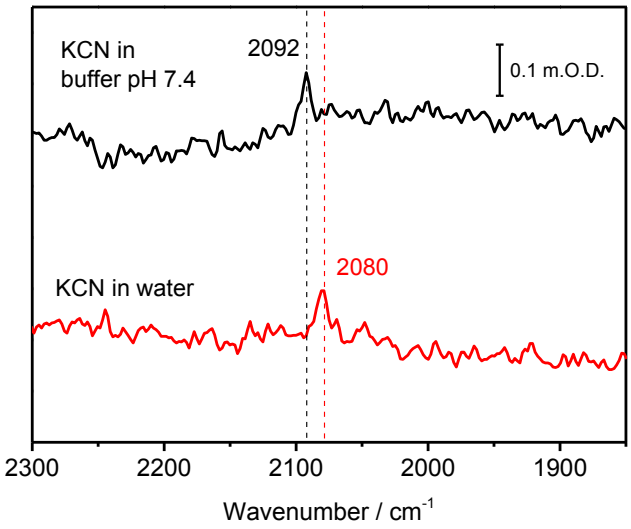

Figure 6-4: Difference IR spectra showing cyanide species in the solution of KCN 10 mM in Tris-HCl buffer pH 7.4 (black) compared with KCN 10 mM in water (red). Spectra were processed against a background spectrum of relevant solvents. (500 scans co-added, 4 cm^{-1} resolution.)

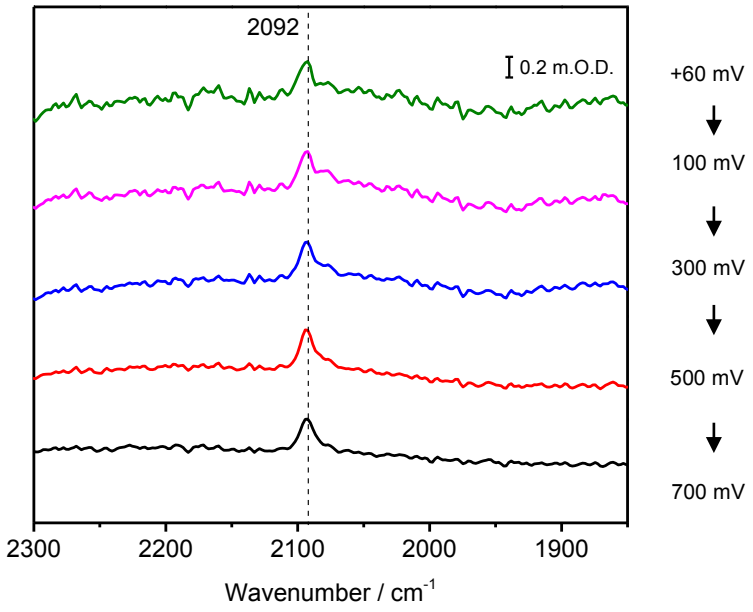

Figure 6-5: A set of spectra showing the *ν*(CN) peak of HCN following a sequence of potential steps. All spectra were processed against a background spectrum of the SEC cell containing Tris-HCl buffer pH 7.4 before addition of 20 mM KCN solution. (500 scans co-added, 4 cm^{-1} resolution.)

6.4 IR spectroelectrochemical studies on cyanide binding to the MoFe proteins

In this IR SEC study, the effect of cyanide on different variant of MoFe proteins has been investigated. An interaction between cyanide ligand and the metal clusters in different redox states was examined spectroscopically. The IR SEC results will be presented and discussed in this section. This should give some useful insights into the complex substrate-binding mechanism of nitrogenase.

6.4.1 Cyanide interactions at the resting state

In the primary set of experiments, the aim was to investigate the interaction between specific variant MoFe proteins with cyanide in the resting state as previously reported by Seefeldt *et al.*[76] In order to monitor *in situ* the cyanide-induced changes in the IR spectra, cyanide solution was sequentially injected into the system while the potential was held at a potential equal to the dithionite reducing level (*ca* –700 mV).

The ATR-IR SEC cell containing 1.8 nmol of dithionite-free α-96^{Gln} MoFe protein in a Nafion layer was prepared in combination with a cocktail of redox mediators in Tris-HCl buffer pH 7.4 as described in Chapter 3. A potential of –700 mV was applied to the protein-Nafion layer for 30 minutes (approximately equal to the midpoint potential of dithionite at pH 7.3 – 7.5).[181] A spectrum of cyanide-free MoFe protein was recorded to use as a background spectrum. Several aliquots of cyanide solution were then added to the cell and allowed to equilibrate before recording an IR spectrum after the addition of each aliquot.

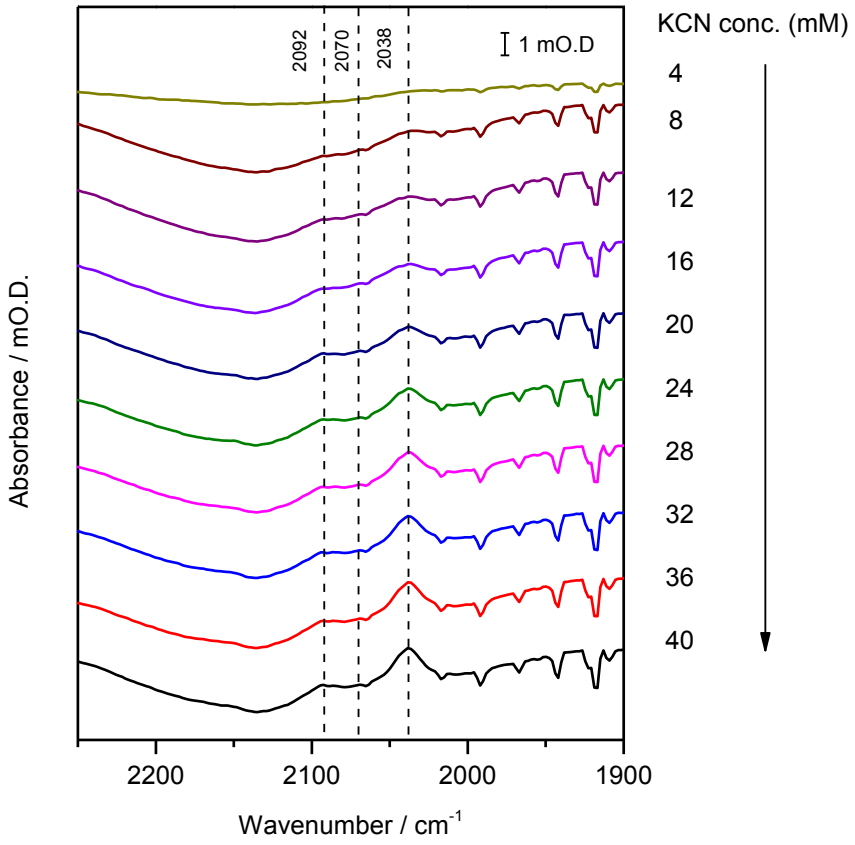

Figure 6-6: Difference spectra of α-96^{Gln} variant at –0.70 V *vs* SHE showing a growth of peaks at 2038 and 2092 cm^{-1} as the concentration of cyanide in solution increased from 4 to 40 mM. All spectra were processed against a background recorded in the absence of cyanide at –0.70 V (500 scans co-added, 4 cm^{-1} resolution). Changes in the 1900–2000 cm^{-1} region are due to changing background water vapour in the sample compartment.

Figure 6-6 shows the appearance of two broad peaks at 2038 and 2092 cm^{-1} upon addition of cyanide solution. A growth of those peaks continued as the concentration of cyanide increased. It was noted that both peaks became dramatically more intense upon addition of cyanide between 8 mM and 20 mM, with a possible shoulder peak at 2070 cm^{-1}. At total concentrations beyond 24 mM, only the peak at 2038 cm^{-1} increased in intensity.

Another set of experiments was performed on the dithionite-reduced MoFe protein. The chemically reduced protein sample was directly put into the ATR cell without electrochemical

control. Difference spectra showing changes upon addition of 10 mM cyanide to the protein are shown in Figure 6-7.

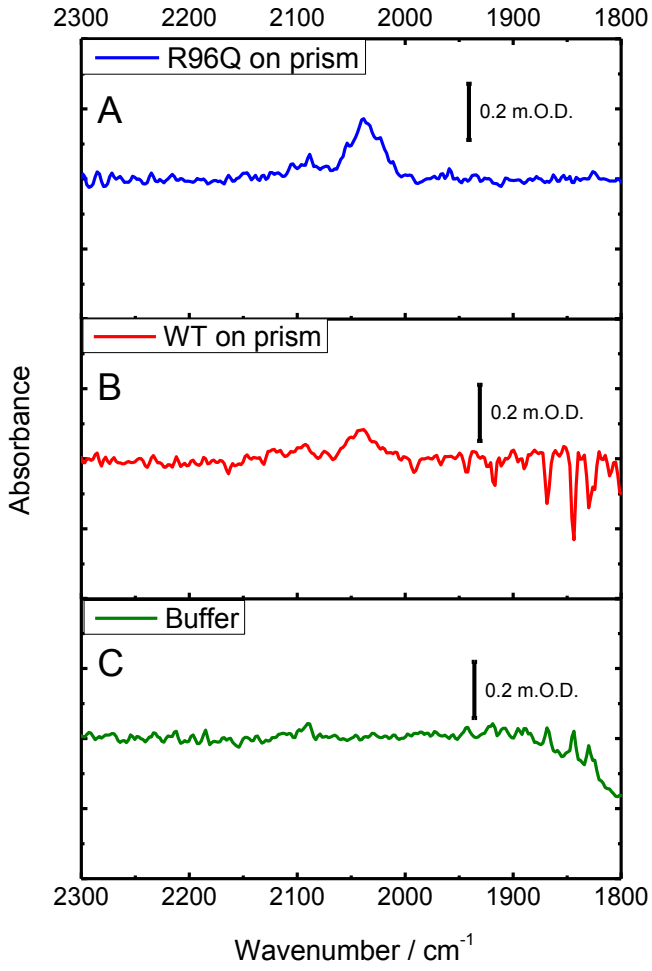

Figure 6-7: Difference spectra of dithionite-reduced α-96^{Gln} variant (A), wild type (B) MoFe protein sample and dithionite in buffer solution (C) in the ATR cell after addition of 10 mM KCN. Each spectrum was processed against a background of protein solution prior to addition of cyanide and baseline correction using a cubic spline function was applied. (250 scans co-added, 4 cm^{-1} resolution.)

In Figure 6-7, the difference spectra show a similar change in the *ν*(CN) region both in the case of α-96^{Gln} and wild type MoFe proteins, showing two peaks at 2038 and 2092 cm^{-1}. The peak at 2092 cm^{-1} could be assigned as *ν*(CN) of free HCN, as it is consistent with the peak position in the blank experiment (panel C) and the previous observation shown in section

6.3.3. No detectable change in the *ν*(CN) region was observed when adding cyanide to dithionite-free MoFe protein samples.

6.4.2 Potential-dependent cyanide binding to MoFe proteins

In order to assess the potential-dependence of cyanide binding to the α-96^{Gln} MoFe protein, IR SEC measurements were carried out. In this experiment, the potential was initially held at the supposedly oxidised state of FeMoco inside the MoFe protein, before introduction of cyanide. To monitor a redox-triggered change on the *ν*(CN) region, the potential was stepwise decreased to achieve the more reduced states of the active site.

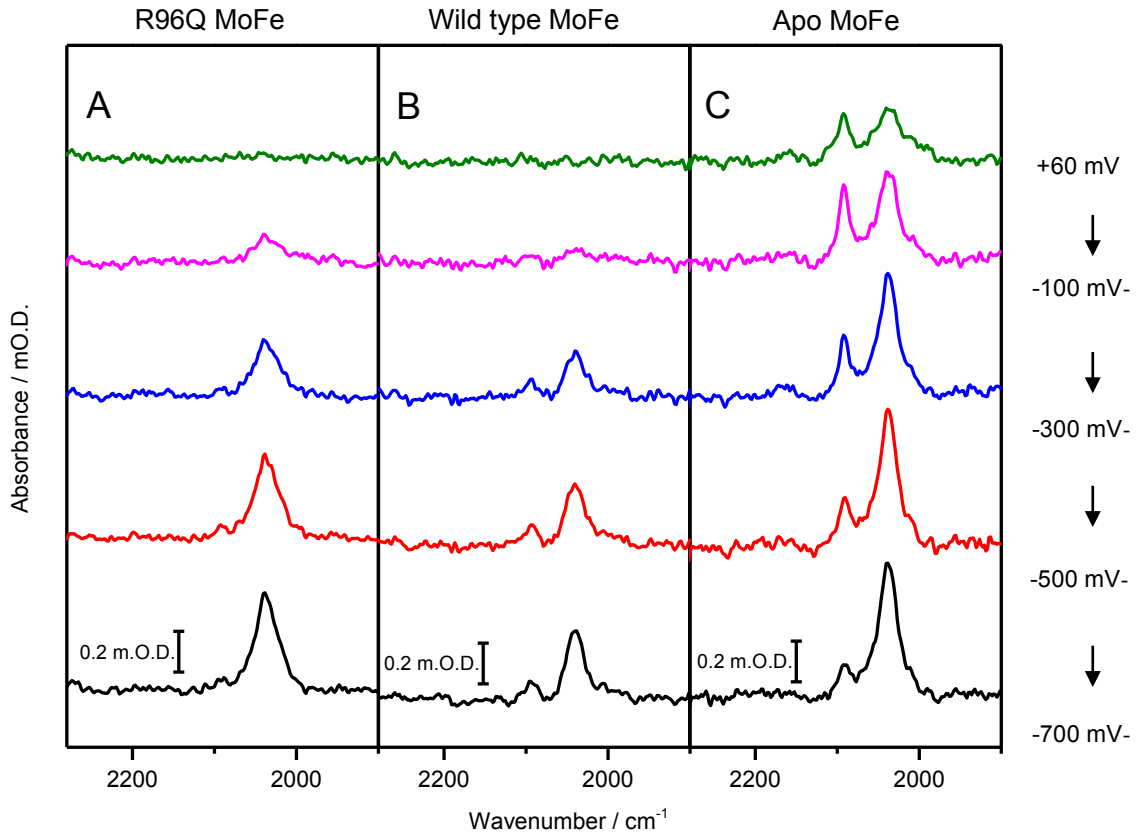

Figure 6-8: IR absorbance spectra of α-96^{Gln} variant (A), wild type (B) and apo- (C) MoFe protein after addition of 10 mM KCN followed by a series of negative potential steps. Each spectrum was recorded when the system was in equilibrium at each potential and processed against a background spectrum at + 60 mV prior to addition of KCN. (500 scans co-added, 4 cm^{-1} resolution.)

The ATR-IR SEC cell containing α-96^{Gln} MoFe protein was set up in the same way as the one in section 6.4.1. A potential of +60 mV was first applied on the SEC cell for 30 minutes (*ca* 100 mV above midpoint potential of enzyme-bound FeMoco$^{ox/semi\text{-}red}$ couple, –42 mV).[24] A spectrum of oxidised, cyanide-free MoFe protein was recorded to use as a background spectrum, before 10 mM KCN solution in Tris-HCl buffer pH 7.4 was injected into the cell.

In Figure 6-8A, no detectable spectral changes were observed upon addition of cyanide whilst holding the potential at +60 mV. A broad peak at 2038 cm^{-1} appeared when the potential was stepped to –100 mV, and continued to grow as the potential was decreased further to –300, –500 and –700 mV, with a small peak at 2092 cm^{-1} increasing slightly.

In Figure 6-8B, an equivalent experiment was done using the wild type MoFe protein. No peak was observed following the introduction of cyanide at a potential of +60 mV, similar to the α-96^{Gln} variant. As the potential was stepped to –100 mV, the spectrum shows small absorption peaks at 2038 and 2092 cm^{-1}, both increasing in intensity as the potential was stepped down to more negative values. It was noted that peaks observed in wild type sample are less intense and narrower compared to those of the α-96^{Gln} variant.

In Figure 6-8C, control experiments were conducted on MoFe protein, which contains only the [8Fe-7S] P-cluster and no FeMoco cluster. At the oxidised level at + 60 mV, two peaks were observed at 2038 and 2092 cm^{-1} shortly after adding cyanide to the cell. As the potential changed toward the negative range, the intensity of the peak at 2038 cm^{-1} increased, while that of the peak at 2092 cm^{-1} decreased.

Another set of experiments to assess the effect of different concentrations of cyanide was done on α-96^{Gln} MoFe protein. Figure 6-9A shows that, when the potential stepped down from +60 mV to –100 mV, the peak at 2038 cm^{-1} started to appear in the presence of 4 mM

cyanide. It was noted that the asymmetric peak shape could stem from overlapping between peaks at 2038 cm^{-1} and 2070 cm^{-1}. In the case of the wild type protein, Figure 6-9B shows that the band at 2038 cm^{-1} started to be recognisable in the presence of 6 mM cyanide and became a more peak shaped as the concentration increased further.

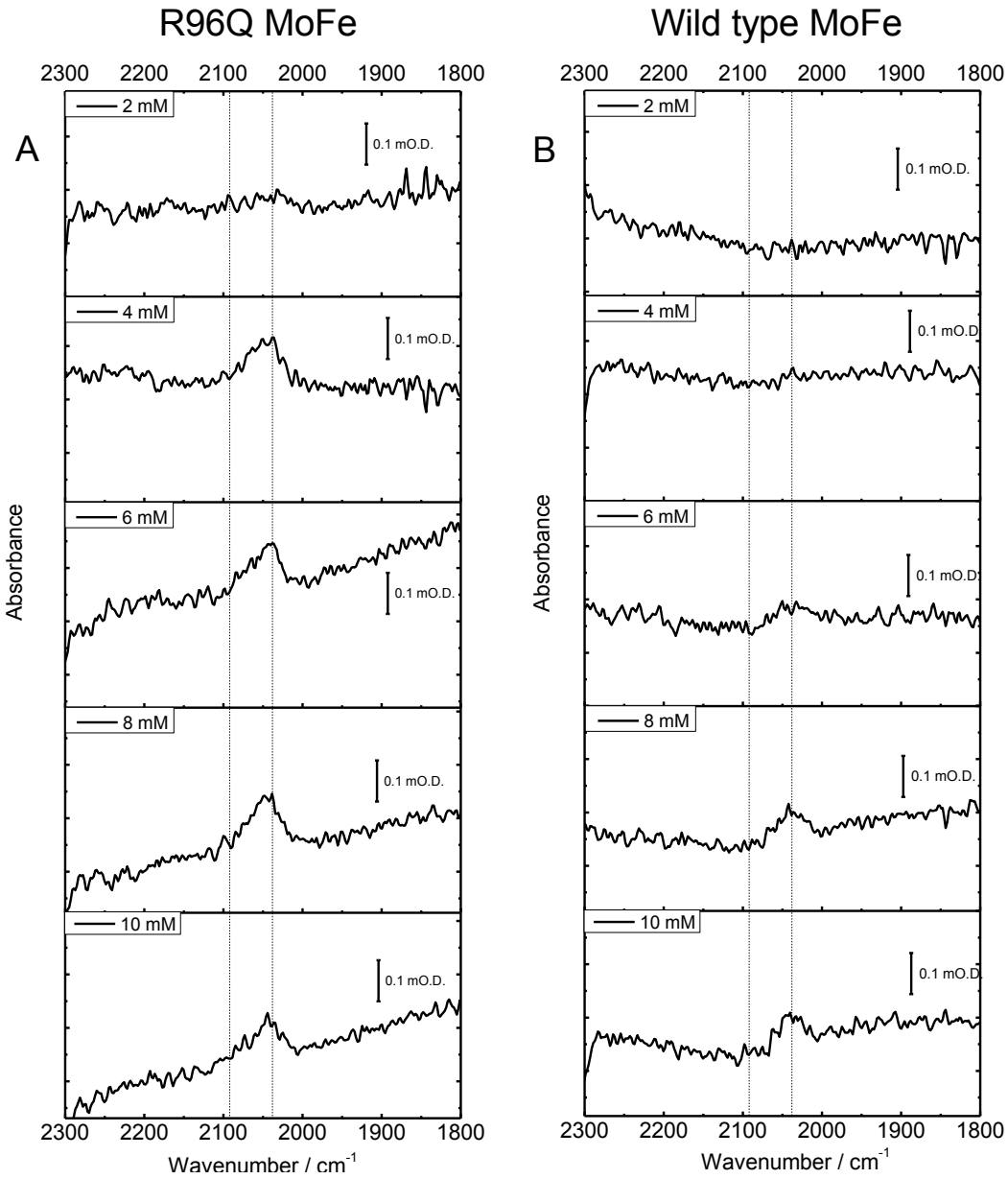

Figure 6-9: Difference spectra of α-96^{Gln} variant (A), and wild type (B) MoFe protein with varying cyanide concentration on reduction from +60 mV to –100 mV. Each spectrum was recorded when the potential was held at –100 mV and processed against a background spectrum recorded after addition of cyanide at a potential of +60 mV. (500 scans co-added, 4 cm^{-1} resolution.)

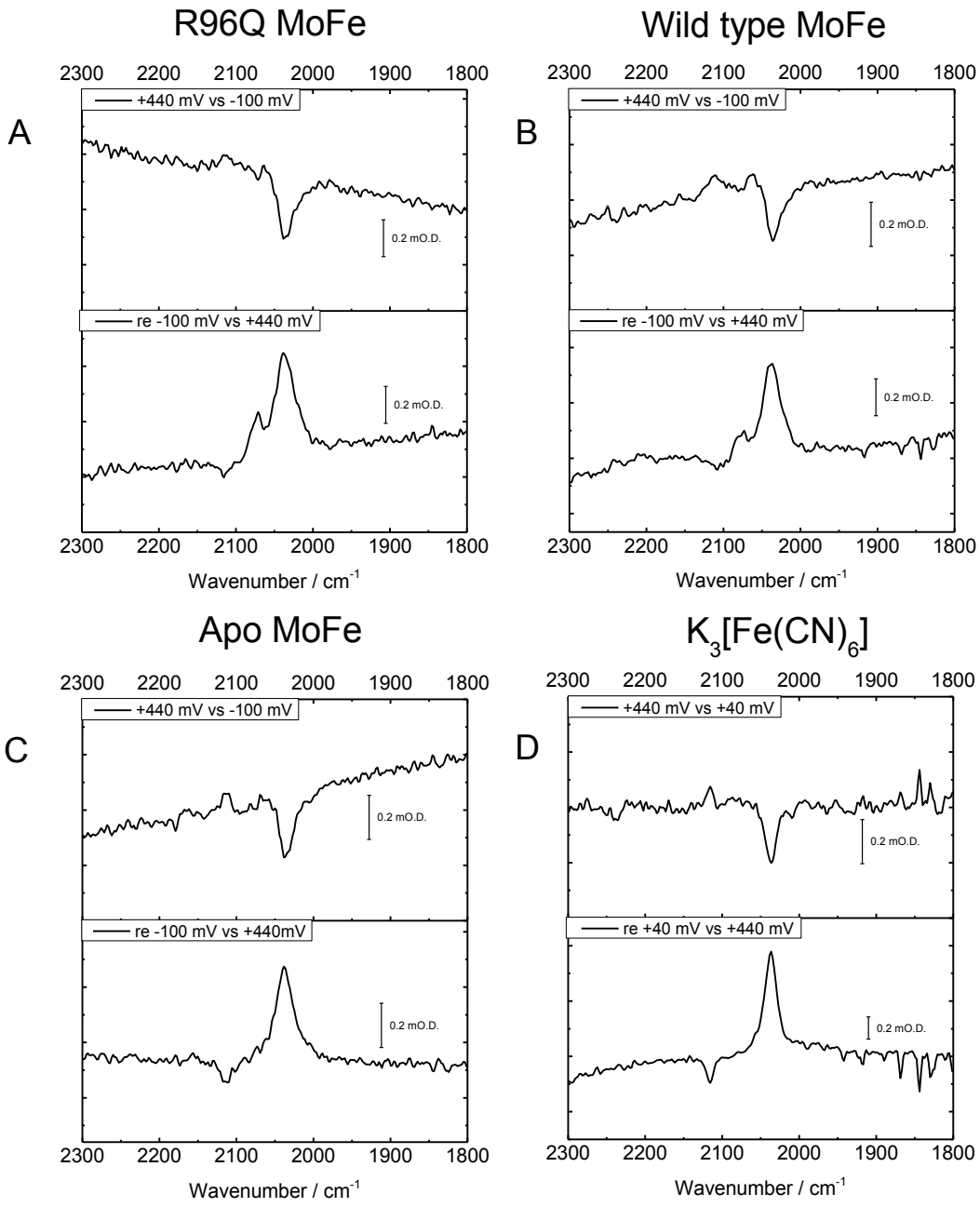

Figure 6-10: Difference spectra of α-96^{Gln} variant (A), wild type (B) and apo- (C) MoFe protein treated with 10 mM KCN on oxidation from –100 mV to +440 mV and re-reduction from +440 mV to –100 mV. Each spectrum was recorded when the potential was held for 20 minutes and processed against a background spectrum recorded during the previous potential step as stated on the spectra. Panel D shows difference spectra for oxidation and re-reduction of $[Fe(CN)_6]^{3-}$ (10 nmol) in Nafion between +40 mV and +440 mV. (500 scans co-added, 4 cm^{-1} resolution.)

The wavenumber position of the peak at 2038 cm^{-1} closely matches that of *ν*(CN) in $[Fe^{II}(CN)_6]^{4-}$ at 2036 cm^{-1} (see Section 3.3.1). To test this hypothesis, the potential was stepped up to +440 mV (Figure 6-10A to C); it was found that the peak at 2038 cm^{-1}

decreased while a peak around 2110 cm^{-1} increased in all samples. Upon re-reduction to –100 mV, the change was reversed which is consistent with the redox-dependent spectral change of the $[Fe(CN)_6]^{3-/4-}$ couple in solution as shown in Figure 6-10D. The smaller peak at 2070 cm^{-1} was observed upon re-reduction in both α-96^{Gln} and wild type MoFe protein. This could suggest that cyanide might interact specifically with the FeMoco cluster in the proteins.

6.4.3 Isotopically-labelled ^{13}CN

A supplementary set of experiments with isotopically-labelled cyanide (^{13}CN) was carried out to prove that the observed absorption peak at 2038 cm^{-1} did originate from the formation of metal-cyano complex. According to the simple harmonic oscillator model, the vibrational frequencies depend on the masses of oscillating atoms, i.e. smaller masses oscillate at a higher frequency than larger masses for a given bond stiffness. Thus, the wavenumber of $\nu(^{13}CN)$ peak was expected to shift to lower position compared to the $\nu(^{12}CN)$ peak.

A SEC experiment to probe the interaction of α-96^{Gln} MoFe protein with ^{13}CN was performed by adding an aliquot of 25 mM $K^{13}CN$ in buffer solution pH 7.4 to the SEC cell containing protein sample in a Nafion film. A sequence of potential steps was applied to the system and an IR spectrum was recorded when each step had reached equilibrium. The parallel experiment with 25 mM $K^{12}CN$ was done for the comparison.

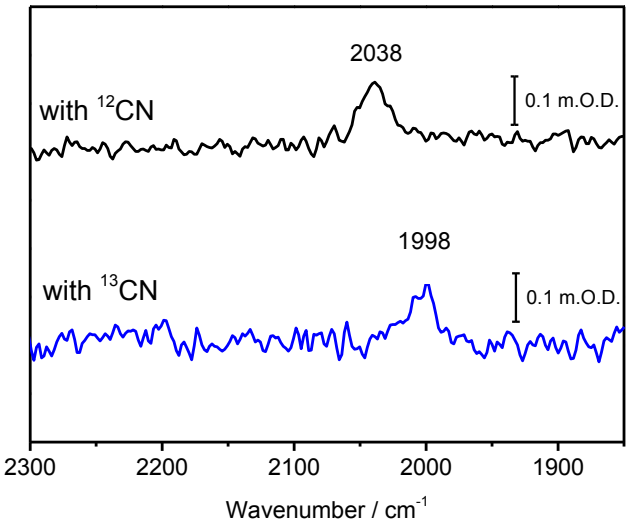

Figure 6-11: Difference spectra of α-96^{Gln} variant MoFe protein after addition of 25 mM K^{12}CN (black) and K^{13}CN (blue). Each spectrum was recorded at a potential of –700 mV after 600 s and processed against a background spectrum at 0 s. (500 scans co-added, 4 cm^{-1} resolution)

In Figure 6-11, it is showed that a ν(CN) peak of interest at 2038 cm^{-1} shifted to a lower wavenumber of 1998 cm^{-1} in the presence of ^{13}CN. This position is consistent with the predicted wavenumber for ν(^{13}CN) peak of 1995 cm^{-1}. The peak shift was calculated as derived below:

For vibrational wavenumber,

$$\tilde{\nu} = \frac{1}{2\pi c}\sqrt{\frac{k}{\mu}}$$

with reduced mass of CN,

$$\mu_{CN} = \frac{m_C . m_N}{m_C + m_N}$$

Hence, the coefficient for wavenumber shift from increasing masses of ^{12}CN to ^{13}CN is

$$\sqrt{\frac{\mu(^{12}C^{14}N)}{\mu(^{13}C^{14}N)}} = 0.979$$

(Given atomic masses for ^{12}C = 12.000, ^{13}C = 13.003 and ^{14}N = 14.007)

By multiplying the wavenumber of the observed $\nu(^{12}CN)$ peak position by 0.979, a predicted position for the $\nu(^{13}CN)$ peak is 1995 cm^{-1}.

6.4.4 Discussion

Formation of the $[Fe^{II}(CN)_6]^{4-}$ complex

In the experiments described in section 6.4.1 and 6.4.2, the wavenumber and redox-dependent profile of the ν(CN) absorption peak at 2038 cm^{-1} were shown to closely correspond with that of the $[Fe(CN)_6]^{4-/3-}$ couple. From a result of the ^{13}CN-labelled experiment in section 6.4.3, it confirms that the particular ν(CN) absorption peak at 2038 cm^{-1} arose from reaction with exogenous cyanide ligand. Thus, it is likely that addition of cyanide caused formation of $[Fe^{II}(CN)_6]^{4-}$ complex in the SEC cell.

The origin of a $[Fe^{II}(CN)_6]^{4-}$ could be the result of Fe-S cluster breakdown on interaction with CN^-, a strong σ-donor, although CN^- inhibition has not previously been shown to cause damage to the clusters of nitrogenase (5 – 120 mM).[75, 76, 119, 120] The source of the Fe atoms could be from the P-cluster, FeMoco, or both. Also, the sixteenth Fe atom located between two β-subunits of the MoFe protein could be the third possible Fe source.[47] The possible origin of the central Fe atom in $[Fe(CN)_6]^{4-}$ complex will be discussed further in this section.

Potential-dependent interaction

In the cases of α-96^{Gln} and wild type MoFe protein, they both showed no spectral change in the ν(CN) region at potential +60 mV in the presence of cyanide. This could suggest that cyanide ligand was unable to react with the metal clusters in high oxidation states. Although early studies have suggested that cyanide is capable of binding to less-reduced states of the enzyme compared to other substrates, including protons,[180] this redox level might be too oxidised relative to the dithionite-reduced level that cyanide has been shown to bind to. The

peak at 2038 cm^{-1} started to be distinguishable at a potential of –100 mV and became more well-defined at more negative potentials (the midpoint potential of the enzyme-bound $FeMoco^{ox/semi\text{-}red}$ and P-cluster, $P^{Ox/N}$, couples are –42 mV and –300 mV, respectively).[24, 91] It could imply that the reduced metal core became more reactive and could react with the ligand, resulting in collapse of some clusters and slow release of the free Fe atoms from the protein to spontaneously form the $[Fe(CN)_6]^{4-}$ complex in the solution.

Another plausible explanation is that the ligand access to the metal clusters inside the protein is more restricted at high redox levels. A few putative substrate and water channels in the MoFe protein have been previously studied.[182-184] According to a recent study by a molecular dynamics approach, it was revealed that the access into the active site *via* a substrate channel was restricted by a low energy barrier and involved some conformational change.[185] This could suggest that, after the potential decreased, the metal core might become more accessible and then the reduced metal could be extracted out of the protein by interaction with cyanide ligand.

The similarity in spectral changes of the variant and wild type protein at potentials down to the dithionite-reduced level implies that the change might stem from the P-cluster rather than the FeMoco, because the previous study has reported that only FeMoco inside the $\alpha\text{-}96^{Arg}$-substitued variant proteins were able to react with cyanide, while the one inside wild type protein was unable to at this resting state.[76] The P-cluster, $[Fe_8S_7]$ cluster as a double Fe-S cubane, is located near the Fe protein binding site and serves as the starting point of the electron relay in the MoFe protein, thus it is likely to be reduced and pulled out of the protein first. It has been reported that the reduction potential of the oxidised state and resting state P-cluster couple ($P^{Ox/N}$) is approximately –300 mV,[91] and the P-cluster undergoes conformational change during the oxidation, involving displacement of ligating amino acid

residues.[46] A study on synthetic Fe-S cluster has suggested that cyanide binding caused positive shift in reduction potential of synthetic $[Fe_4S_4]$ cubane and stabilised the all ferrous state of the isolated cluster as $[Fe_4S_4(CN)_4]^{4-}$.[186] This could encourage an extraction of the cluster in the presence of cyanide. A slight difference between two variants is that the α-96^{Gln} variant showed the sign of $[Fe^{II}(CN)_6]^{4-}$ complex formation at lower concentration of cyanide than the wild type one, indicating that the metal clusters inside the variant were more accessible.

However, there is the possibility that the FeMoco could fall out of the protein. The early studies on the isolated FeMoco by Pickett *et al.* suggested that coordination between cyanide and FeMoco caused a change in electron density on the metal clusters, resulting in a significant shift of the reduction potential of FeMoco to a more negative value. It also makes the super-oxidised state of FeMoco accessible.[94] As this highly oxidised state is not naturally attainable and the role is still unknown in the physiological path of the intact enzyme, such a cyanide-induced change might affect the stability of the cofactors inside the MoFe protein, especially without the presence of the Fe protein.

Free Fe atoms

In the case of the apo-protein, the *ν*(CN) peak at 2038 cm^{-1} appeared shortly after introduction of cyanide ligand at +60 mV. This indicated that the $[Fe(CN)_6]^{4-}$ complexes were generated spontaneously in the presence of cyanide. It implied that the free Fe atoms were released at this redox level, perhaps triggered by cyanide. It could suggest that a lack of FeMoco in the protein subunit destabilised the surrounding protein of the P-cluster, allowing ligand access to the P-cluster. However, this is opposite to the recent report that the P-cluster in the FeMoco-deficient MoFe protein was able to catalyse the reduction of cyanide by using reductant Eu^{II}-DTPA.[120] The catalytic activity of the P-cluster variant was reported to be 10 times less than

that of the variant containing a pair of P-cluster precursors. It has been suggested that the P-cluster was 'well-shielded' inside the protein making the substrate access to the P-cluster more difficult.

The alternative explanation for the free Fe atom in the apo-protein is that extra Fe atoms were already present in the protein sample. Partial FeMoco maturation within the apo-protein could account for excess Fe atoms. It also might be a result of cluster breakdown either during or after dithionite removal prior to experiment. A lack of FeMoco might be account for the vulnerability of this variant, i.e. prone to be over-concentrated, compared to the ones with the protein-bound FeMoco. This is supported by the observation of the 2038 cm^{-1} peak in the SEC study of some hydrogenase samples following over-concentration.[187] This suggests that it arises from CN^- interacting with Fe in a non-specific way.

Cyanide binding or adsorption of hexacyanoferrate species

The appearance of a peak at 2092 cm^{-1} was initially thought to be ν(CN) of HCN in solution, as it is consistent with the spectra from the SEC test of cyanide solution at pH 7.4, but its inconsistency across different protein samples pointed to another origin. Many cyanide bound to Fe-S cluster have exhibited ν(CN) adsorption around this wavenumber region. For instance, the IR SEC studies of [Fe-Fe] hydrogenase from various species, which contains two CN and three CO ligands in the di-iron active site as shown in Figure 6-12, have shown two ν(CN) absorption bands between 2070 – 2095 cm^{-1}.[95, 96, 177, 188] These ν(CN) were observed to shift to lower wavenumber upon reduction of the active site.[177] The presence of the CN ligand in the hydrogenase active site has been suggested to calibrate the electronic properties of the metal core and help intramolecular electron transfer.[189] Thus, an increase of a peak at 2092 cm^{-1} and small shoulder at 2072 cm^{-1} could indicate cyanide binding to multiple

sites on the metal clusters, but it is not clear whether this change is potential-dependent due to interference from the larger peak at 2038 cm^{-1} in the negative potential range.

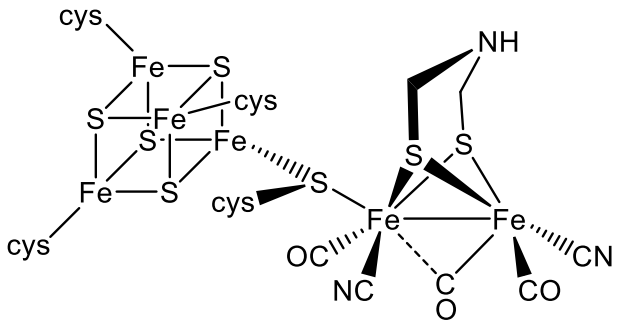

Figure 6-12: Structure of the active site of [FeFe] hydrogenase.

However, the possibility that the *ν*(CN) peak at 2092 cm^{-1} arises from an adsorbed species of $[Fe(CN)_6]^{4-}$ complexes cannot be ruled out. An early IR SEC study reported that soluble hexacyanoferrate species were found to adsorb on the Pt electrode in a thin-layer cell during potential cycling in a solution of $[Fe(CN)_6]^{3-/4-}$, giving rise to *ν*(CN) peaks at 2040, 2092 and 2115 cm^{-1}.[190] Another IR spectroscopic study of adsorption of hexacyanoferrate ions on different metal oxide films revealed that $[Fe(CN)_6]^{4-}$ and $[Fe(CN)_6]^{3-}$ ions can coordinate with different metal oxides and a ZnSe prism *via* ambidentate CN ligands (see Figure 6-13) and that these adsorbed species give rise to different *ν*(CN) bands.[191] The *ν*(CN) band at 2097 cm^{-1}, with a shoulder at 2070 cm^{-1} was assigned to adsorbed $[Fe(CN)_6]^{3-}$ on ZnSe. Nevertheless, this assumption is arguable that in the similar SEC study of $K_3[Fe(CN)_6]$ as a test system for the ATR SEC cell presented in Chapter 3, only *ν*(CN) peaks of solution-phase $[Fe(CN)_6]^{4-}$ and $[Fe(CN)_6]^{4-}$ were detected in IR spectra, implying no significant adsorption of $[Fe(CN)_6]^{3-/4-}$ complexes on the carbon working electrode and Si prism employed in the present setup. It is also possible that some metal hexacyanoferrate complexes, e.g. Prussian blue $[Fe_4[Fe(CN)_6]_3]$ *ν*(CN) 2080 cm^{-1}, were generated in the solution and then immobilised in the Nafion layer or adsorbed on prism surface.

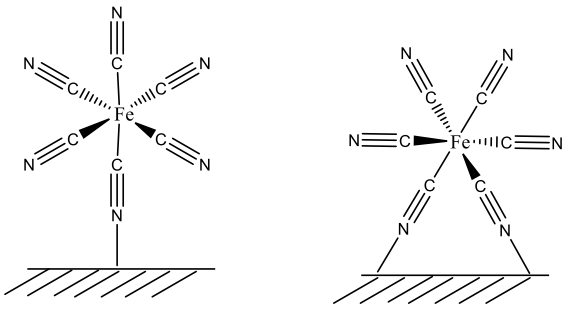

Figure 6-13: A model showing adsorption of hexacyanoferrate species with single (left) and double bridging (right) coordination *via* CN ligand. The change in the point group geometry from O_h to C_{4v} and C_{2v} gives rise to new *ν*(CN) bands in IR spectra.

6.5 Alternative approaches

Due to the undesirable formation of $[Fe^{II}(CN)_6]^{4-}$ complexes, the resulting strong *ν*(CN) absorption band at 2038 cm^{-1} could mask an underlying absorption band expected from cyanide interacting specifically with the protein-bound FeMoco cluster. In order to eliminate this interference, new approaches were tried and the results are presented in this section.

6.5.1 EDTA treatment

Ethylenediaminetetraacetic acid (EDTA) is a chelating agent that is commonly used to remove metal ions from a sample during protein purification. In order to get rid of excess Fe ions that might be released during the course of an SEC experiment, EDTA treatment was applied to the MoFe samples; an aliquot of EDTA solution was added to the protein sample and then carefully washed out in a centricon tube with a 100 kDa cut off membrane.

In the primary set of experiments with protein samples pre-treated with 1 mM EDTA, only a slight decrease of the peak at 2038 cm^{-1} was observed in the IR spectra of each sample. However, addition of 5 mM EDTA to apo-and variant MoFe proteins resulted in precipitation of proteins, while the wild type MoFe protein remained intact. This could imply that the

clusters inside these variants are more accessible than the wild type one, leading to easy damage, or perhaps these genetically-modified proteins are just less stable that the native one.

Figure 6-14 shows that wild type MoFe protein washed with 5 mM EDTA showed a less intense peak at 2038 cm^{-1} growing as the potential was decreased, compared to a non-treated sample. This suggests that the EDTA procedure helped to lower the concentration of non-specifically bound Fe in the protein sample. On the other hand, an increase of the $[Fe^{II}(CN)_6]^{4-}$ complexes at more negative potentials indicated that the some Fe atoms were partly released due to some redox-dependent changes within the protein.

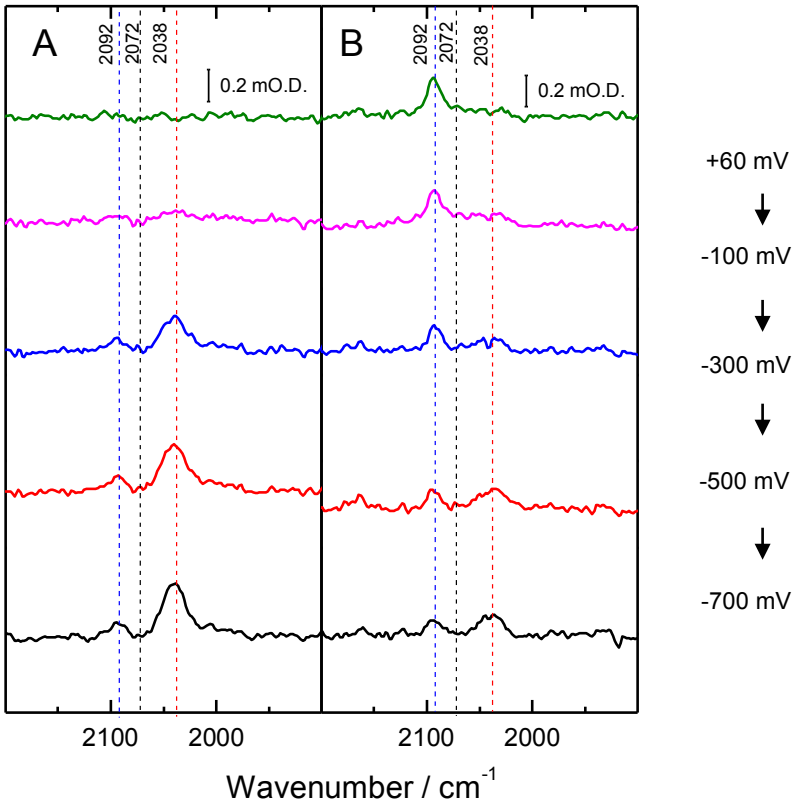

Figure 6-14: IR absorbance spectra of wild type MoFe protein after addition of 10 mM KCN, with no EDTA treatment (A) and after pre-treatment with EDTA (B) followed by a series of negative potential steps. Each spectrum was recorded when the system was in equilibrium at each holding potential and processed against a background spectrum at +60 mV prior to addition of KCN (500 scans co-added, 4 cm^{-1} resolution).

6.5.2 Solution displacement

In order to remove the interfering ν(CN) peak of $[Fe^{II}(CN)_6]^{4-}$ ions at 2038 cm^{-1}, a flow system was introduced to wash out low molecular weight species from the ATR cell after completing the reduction steps. This approach was applied to the α-96^{Gln} variant protein that was unstable to EDTA treatment. Fresh redox mediator cocktail was circulated by a peristaltic pump at a flow rate of 0.50 mL per minute for *ca* 10 minutes while the potential was held at –700 mV.

Figure 6-15 shows a result of the α-96^{Gln} MoFe protein case from introducing a flow solution to the cell after applied potential at –700 mV. In Figure 6-15A, after bulk solution was replaced by the flow system, the peak at 2038 cm^{-1} shift to 2070 cm^{-1}. In a difference IR spectrum Figure 6-15B, it shows the peak loss at 2038 cm^{-1} while the peak at 2070 cm^{-1} remained unchanged. This could suggest that the flow can only remove a part of free $[Fe(CN)_6]^{4-}$ in the solution but some species remained on the protein or prism surface.

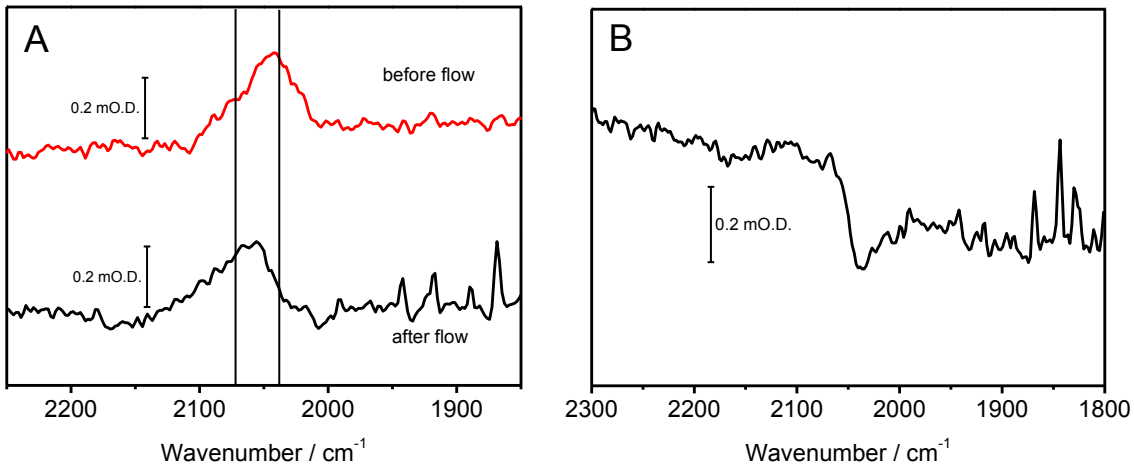

Figure 6-15: (A) IR spectra of α-96^{Gln} variant treated with 10 mM cyanide at a potential of -700 mV before (red) and after (black) the cell solution was replaced with fresh buffer solution by the flow system. Both spectra processed against a background spectrum recorded at –100 mV. (B) Difference spectrum between two spectra in panel A, showing a loss of the peak at 2038 cm^{-1}.

6.5.3 Dialysis membrane

An alternative approach has been designed to prevent hexacyanoferrate species becoming immobilised in the Nafion network. A dialysis membrane was utilised in place of Nafion polymer to trap the protein on the ATR prism and allow only small molecules to diffuse across the membrane.

A Nafion-free protein film of sample solution was prepared on the ATR prism surface and the SEC cell was setup as illustrated in Figure 6-16. First, a piece of carbon paper and carbon fibre connector was gently placed on top of the protein film. The protein layer and working electrode was then covered by a piece of dialysis membrane, soaked in oxygen-free buffer prior to use. Lastly, the SEC cell body was assembled and filled with the redox mediator cocktail in buffer solution.

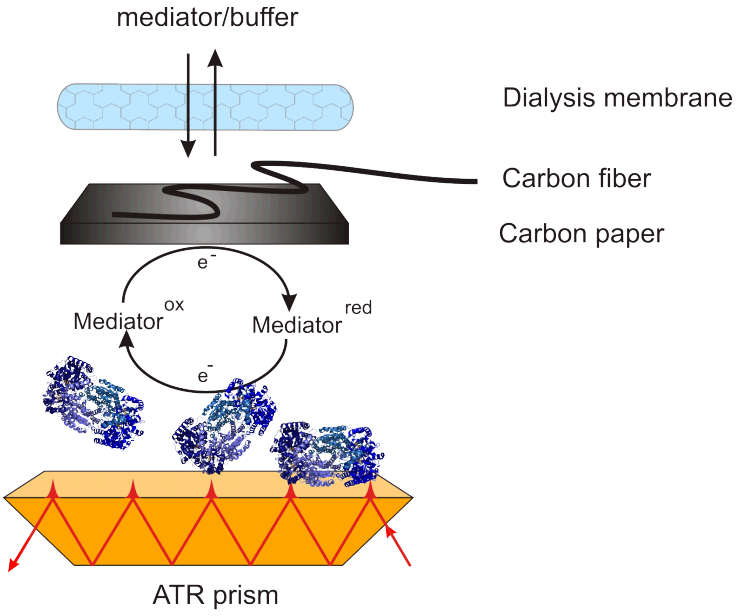

Figure 6-16: A representative layout of the protein film and working electrode covered with dialysis membrane in the SEC cell.

From the SEC study of the α-96^{Gln} MoFe protein, IR spectra show that only a trace of *ν*(CN) band appeared when 10 mM cyanide solution was added to the cell when using the dialysis membrane, as shown in Figure 6-17. It is implied that the amount of $[Fe(CN)_6]^{4-}$ ions

generated in the membrane method was smaller than that in the Nafion method or the $[Fe(CN)_6]^{4-}$ ions could diffuse away easier through the membrane. However, the electrochemical control was found to be significantly less efficient compared to the Nafion method. The small current could be a result of slow diffusion rates across the membrane that hinder charge transfer between the working electrode and counter electrode, *i.e*. introduce an extra resistive component to the cell, which would lead to a larger equilibration time.

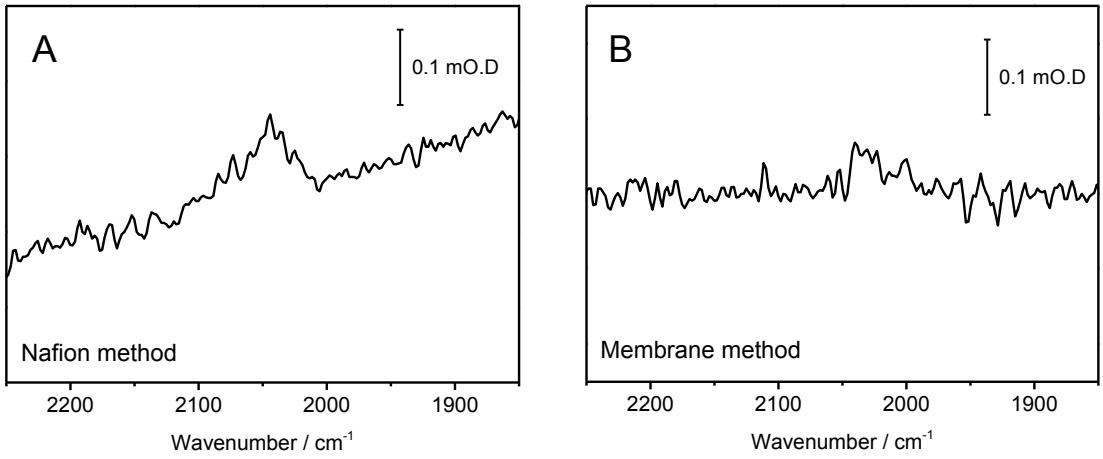

Figure 6-17: Difference spectra of α-96^{Gln} variant MoFe protein with 10 mM cyanide in the Nafion network (A) compared to the same measurement using dialysis membrane (B) on reduction from +60 mV to –100 mV. (500 scans co-added, 4 cm^{-1} resolution.)

6.6 Discussion

In this chapter, SEC results showing cyanide ligand interacting with different variant MoFe proteins was presented. Initially, the aim of the study was to investigate cyanide binding to the intact active site of the enzyme. However, the postulated formation of hexacyanoferrate complexes during the course of the experiments introduces major interference in the IR spectra as the strong absorption ν(CN) peak of $[Fe(CN)_6]^{4-}$ ions at 2038 cm^{-1} and of the adsorbed species at 2092 cm^{-1} masking most of the spectral region of interest. This makes it

difficult to differentiate the *ν*(CN) peaks with lower molar absorption coefficients that arise from cyanide bound to the intact active sites.

The effect of cyanide on different types of MoFe protein has been investigated. It was found that the MoFe proteins containing FeMoco clusters were more stable and showed no interaction with cyanide at positive potentials, unlike the apo-protein without FeMoco inside. Introduction of cyanide ligand to the apo-protein sample caused formation of $[Fe(CN)_6]^{4-}$ ions and the adsorbed species spontaneously. A lack of FeMoco cluster could account for greater exposure to exogenous ligand for this variant. At more negative potentials, both α-96^{Gln} MoFe protein and wild type MoFe protein were observed to become reactive with cyanide, leading to formation of $[Fe(CN)_6]^{4-}$. A further test revealed that the metal clusters inside the α-96^{Gln} variant were prone to be pulled out in the presence of cyanide at lower concentration than that of the wild type protein. This could suggest that a structural difference in α unit of the protein has a slight influence on the stability of the metal clusters.

Several approaches have been attempted to prevent and eliminate the interfering hexacyanoferrate complexes generated during the SEC experiment. An EDTA treatment was shown to minimise the formation of $[Fe(CN)_6]^{4-}$ ions at the beginning of the potential steps but it was found that more $[Fe(CN)_6]^{4-}$ ions were formed uncontrollably when the potential was stepped towards the negative range. This could imply that the source of extra Fe atoms became more accessible at low potential. Meanwhile, a flow system was used to flush this low molecular weight species out of the SEC cell. Free $[Fe(CN)_6]^{4-}$ ions could be removed from the solution, as the peak at 2038 cm^{-1} decreased after the flow but a band around 2070 cm^{-1} was still present. This band could arise from cyanide bound to the remaining metal cluster. The wavenumber of remaining peak is close to previously reported the peak of CN^- bound isolated cofactor at 2053 cm^{-1} forming at the oxidised state of the cofactor.[94]

Alternatively, it could arise from some hexacyanoferrate species that adsorbed on the prism surface or in the Nafion layer.

In order to determine this *ν*(CN) band of the interest, the Nafion network was replaced with a dialysis membrane on top of protein film and working electrode. This method showed that the smaller amount of $[Fe(CN)_6]^{4-}$ were generated and adsorbed in the IR sampling area, but no redox-dependent change was observed as the electrochemical control across the membrane proved less effective due to slow diffusion rate.

In summary, the interaction between cyanide ligand and different MoFe protein variants reflected the difference in stability and reactivity among these protein samples. This information is useful for handling a variety of genetic-modified proteins in the future experiments. Although the cyanide binding to the active site was unresolved in this SEC study, the first IR evidence for CN interacting with nitrogenase MoFe protein was demonstrated. Further studies need to be done with combination of different techniques to assign the cyanide binding.

Chapter 7

Electrochemical study of isolated cofactors

The redox study of small cofactor is generally fast and less complex than the intact one in the large protein. Although isolated cofactors have different environment and do not necessarily exhibit the same catalytic behaviour as the whole enzyme from the protein-bound ones, studying the electrochemical properties of isolated cofactors could give new insight of electron transfer outside the protein surrounding, which would reflect how the presence of protein helps to fine-tune this process.

In this chapter, two isolated cofactors from different metal-dependent nitrogenase were explored using electrochemical technique. The electrochemical characteristic of isolated FeVco was studied for the first time. A difference in chemical properties and inhibition of these two cofactors was reported and discussed here.

7.1 Experimental

7.1.1 Isolated cofactor samples

Cell growth, protein purification and cofactor isolation from nitrogenase were performed by collaborator Markus Ribbe's group of University of California, Irvine. FeMoco and FeVco were isolated from His-tagged MoFe and VFe protein, respectively, of nitrogenase from two

different strains of *Azotobacter vinelandii* as described elsewhere.[48] Both cofactors were extracted into *N*-methyl formamide (NMF). The approximate concentration of FeMoco and FeVco are *ca* 1.0 and 0.3 mM, respectively.

7.1.2 Electrochemical cell setup

The dynamic electrochemical technique, cyclic voltammetry, was used to investigate the electron transfer chemistry of isolated cofactors. Due to a small molecular size, the cofactors are able to diffuse to and exchange electrons with a working electrode directly. The electrochemistry measurement was performed in a custom-built cell designed for small volumes equipped with fittings for a three-electrode system, temperature control and gas flow (Figure 7-1). The voltage was controlled by a potentiostat. All cyclic voltammograms were recorded under anaerobic conditions in a glove box comprising a N_2 atmosphere[194] (O_2 < 1 ppm) at 25 °C unless otherwise stated.

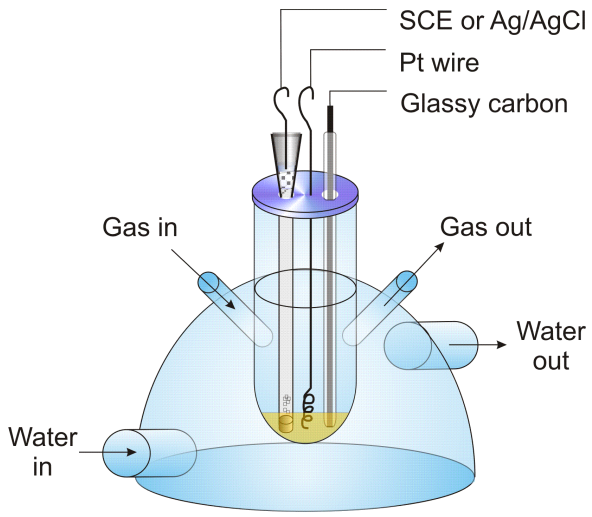

Figure 7-1: Small volume cell with water jacket and gas inlet. Glassy carbon and Pt wire were used as a working electrode and counter electrode, respectively, combined with either saturated calomel electrode (SCE) or Silver-Silver chloride (Ag/AgCl) electrode as reference electrode.

[1] Previous study showed no difference in both electrochemistry and spectroscopic properties of isolated cofactor under nitrogen and argon atmosphere (ref. 90 and 92).

7.2 Electrochemistry of FeMoco and FeVco

7.2.1 Isolated FeMoco

Isolated FeMoco has been studied previously, but FeMoco from a new isolation method developed by Ribbe and co-workers has never been electrochemically tested before. In this study, cyclic voltammograms of FeMoco in Figure 7-5A shows at least two reduction processes. The first process at E_p^{red} = –384 mV (process I) is a reversible reduction of oxidized state FeMoco ($FeMoco^{ox}$) to semi-reduced state ($FeMoco^{semi\text{-}red}$). A broad reduction peak of process I is from two unresolved peaks as a result of redox-related isomerism of two FeMoco rotamers as described in previous work by Pickett *et al.* and will be discussed in the following section.[92] The second catalytic reduction process at E_p^{red} = –1105 mV is from unresolved irreversible reductions labelled process II and III. According to previous work by Pickett *et al.*, process II is a reduction of the semi-reduced state ($FeMoco^{semi\text{-}red}$) to reduced state ($FeMoco^{red}$) and process II is a further reduction to a super-reduced state ($FeMoco^{super\text{-}red}$). The similarity of the voltammogram to the published FeMoco electrochemistry indicates that FeMoco isolated by the new method is structurally intact and behaves in the same way as previous samples in terms of its chemistry.

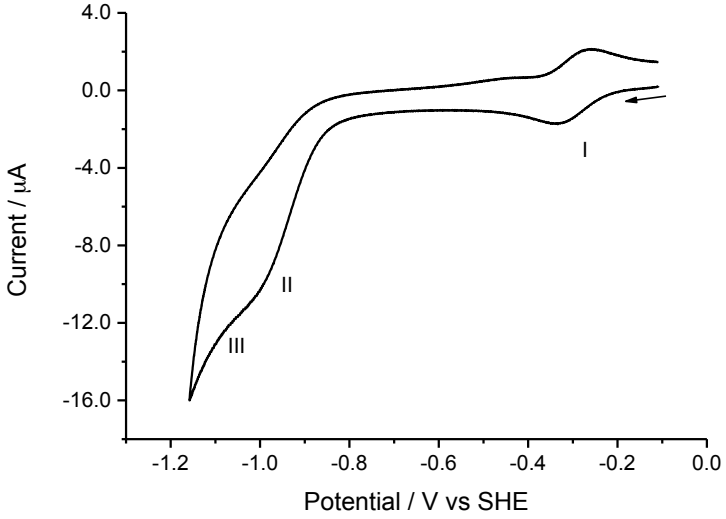

Figure 7-2: A cyclic voltammogram of isolated FeMoco *ca* 1.0 mM on glassy carbon electrode recorded at rate 10 mV.s^{-1}.

7.2.2 The effect of thiophenol

In order to confirm that the redox isomerism observed previously in the cyclic voltammogram of isolated FeMoco in Figure 7-2A, respond to thiophenolate in the same manner as previous batches, the effect of thiophenol was investigated as described in work by Pickett *et al.*[92] In the case of isolated FeMoco, a broad reduction peak of FeMoco$^{ox/semi\text{-}red}$ couple is proposed to arise from redox isomerism between two rotamer forms of deprotonated-NMF bound to terminal Fe atom, FeMoco$_A$ and FeMoco$_B$ (Figure 7-3).[92] A co-ordinate bond by oxygen to terminal Fe in FeMoco$_B$ makes it more difficult to reduce and causes an unresolved reduction peak at slightly more negative potential.

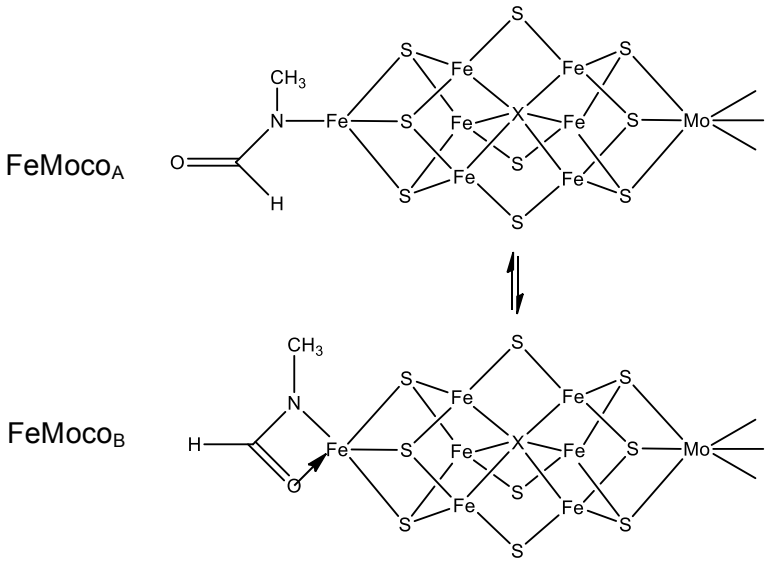

Figure 7-3: two rotamer forms of NMF bound to terminal Fe atom of isolated FeMoco as proposed in ref 20.

In Figure 7-4, addition of one molar equivalent of thiophenol (HSPh) shifted the reduction potential of process I slightly in a positive direction. The explanation of this observation is that the thiol group could replace solvent NMF binding to terminal Fe atom and results in collapse of the redox isomerism. A new single reversible reduction of FeMoco(SPh)$^{ox/semi\text{-}red}$ couple occurred at $E_p^{red} = -343$ mV, which is concordant with previous study. A thiol group is capable of mimicking the original amino acid ligand cysteine. Fay *et al.* suggested that it can induce a conformational change of isolated FeMoco to resemble the protein-bound FeMoco more closely.[49] This confirms that the new FeMoco sample is behaving the same as in previous study in terms of solvent ligation.

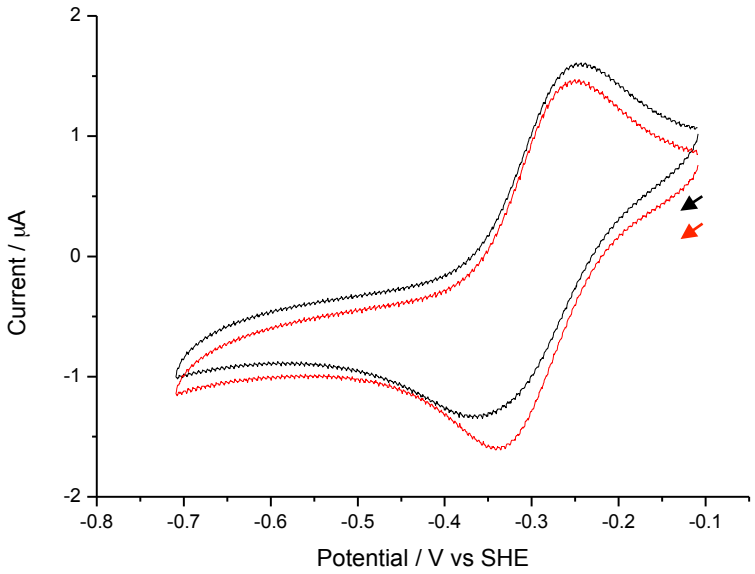

Figure 7-4: Cyclic voltammogram of FeMoco in NMF (black) and with 1 molar equivalent of thiophenol (red).

7.2.3 Isolated FeVco

In this study, the redox properties of isolated FeVco have been investigated for the first time. Figure 7-5 shows voltammograms of isolated FeVco in NMF comprising a quasi-reversible reduction process at E_p^{red} = –622 mV. It was found that the reduction current depleted as measurements were repeated several times, suggesting a catalytic process, presumably reduction of protons that becomes suppressed as the substrate is depleted close to the electrode.

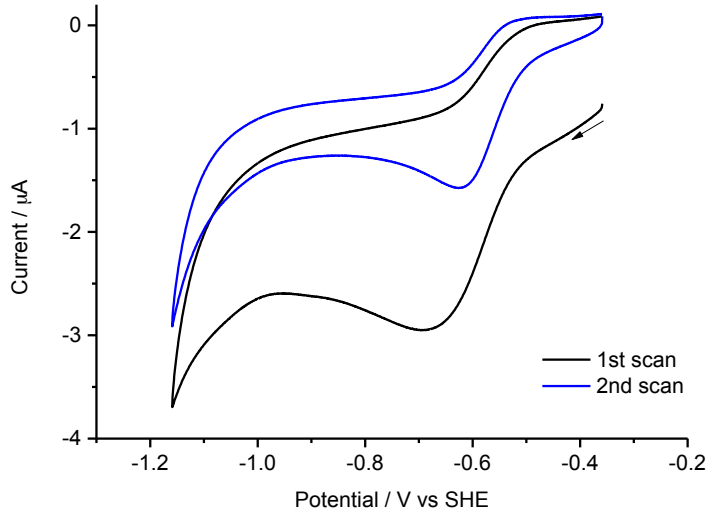

Figure 7-5: A cyclic voltammogram of isolated FeVco *ca* 0.3 mM at a glassy carbon electrode recorded at rate 10 mV.s^{-1}.

This is the first opportunity to electrochemically study the isolated cofactor from V-nitrogenase thanks to the new isolation method. Meanwhile, the redox states of these two processes still remain unclear. To assign redox state of isolated FeVco in relation to characterised states of the protein, it will necessary to correlate electrochemistry results with EPR spectroscopic data.

Unlike FeMoco, adding thiophenol had no effect on the cyclic voltammogram of FeVco. This could imply that there is no redox isomerism for isolated FeVco or thiophenol does not replace NMF and bind to terminal Fe like it does on FeMoco. These assumptions rise from the difference of structure between FeMoco and FeVco. The EXAFS study of isolated FeVco by Fay *et al.* has shown that isolated FeVco interacts with NMF more strongly than isolated FeMoco does.[49]

7.3 CO-binding to isolated cofactors

In this study, the CO binding to isolated FeVco has been probed. It was found that being exposed to CO for one minute caused a change in the reduction process (E_p^{red} = –622 mV). A sharp catalytic peak was decreased in intensity. In Figure 7-6, the longer exposure to CO (3 minutes) seems to suppress the catalytic process so that the redox process becomes more typical of a reversible reduction and re-oxidation.

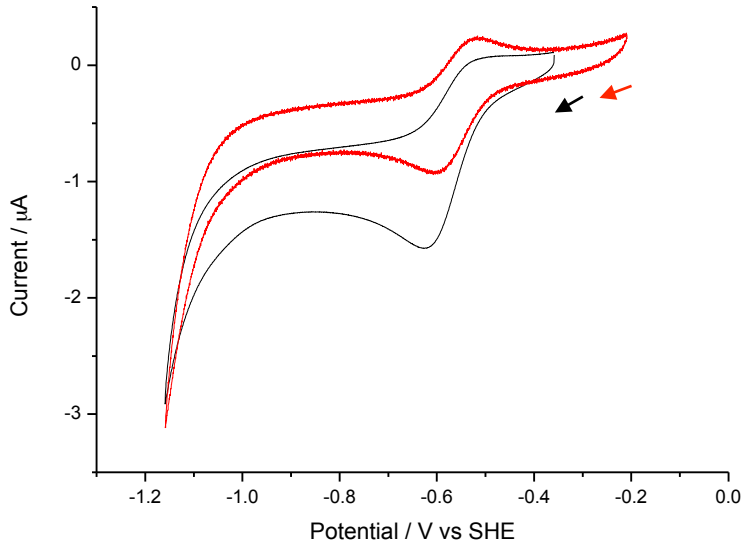

Figure 7-6: Cyclic voltammogram of isolate FeVco before (black) and after (red) exposure to CO for 3 minutes recorded at 10 mV.s^{-1}.

According to the electrochemical work by Pickett *et al.,* it was shown that CO binds to isolated FeMoco only at the reduced state as it caused a change to the reduction process II to be more resolved, while having no effect on process I. Reaction with CO led to two oxidation peaks of CO-bound intermediates.[92] Additionally, they suggested that up to 3 molecules of CO can bind to isolated FeMoco in at different binding sites under high CO concentration.

Presumably the reduction process observed in the FeVco is a proton reduction, these results could be concordant with previous study of V-nitrogenase from *Azotobacter vinelandii* by Chi *et al.*, revealing that activity of proton reduction by intact V-nitrogenase was decreased under

100% CO atmosphere.[48] Later, this observation has led to discovery of CO reduction by this alternative nitrogenase.[69] More recently, a study of isolated cofactors has shown that both isolated FeMoco and FeVco were able to catalyse reduction of CO using Eu-DPTA as a low potential reducing agent (–1140 mV at pH 8.0).[119] It was reported that the rate of CO reduction of isolated FeVco is smaller that of isolated FeMoco (*ca* 20 and 55 nmol CH_4 per μmol cofactor per hour, respectively). Regarding to that report, it could imply that the change in cyclic voltammogram observed in this present work was stemmed from CO bound to isolated FeVco, which may have been reduced at low potential corresponding to reduction potential of $Eu^{III/II}$-DTPA couple. This particular interaction might affect the redox properties of the metal centre, leading to inhibition of proton reduction as observed in this study.

7.4 Isocyanide binding to FeMoco

Isocyanide (RNC) is a strong π-acceptor and isolobal with CO and N_2. Methyl isocyanide (CH_3NC), which is the smallest species of isocyanide, can inhibit reduction of N_2 and act as substrate for nitrogenase resulting in formation of methane.[63] However, this methyl isocyanide is not commercially available. Methyl isocyanide was synthesised according to the method previously reported.[192]

7.4.1 Preparation of methyl isocyanide

Methyl isocyanide was prepared by a slight modification of the dehydration reaction of NMF as reported by Schuster *et al*.[193]

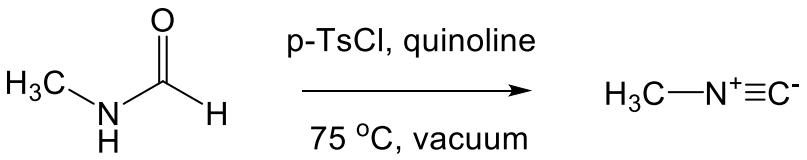

Quinoline (C_9H_7N, Sigma-Aldrich) was dried with Na_2SO_4 and purified by distillation over zinc dust under vacuum. In a three-necked flask connected to nitrogen inlet and vacuum pump, a solution of freshly purified quinoline (473 ml, 4.0 mol) and *p*-toluenesulfonyl chloride (286 g, 1.5 mol, Fisher Scientific) was vigorously stirred and heated to 75 °C at 15 mmHg under nitrogen. Maintaining those conditions, NMF (59 ml, 1.0 mol, Sigma-Aldrich) was added dropwise for 45 minutes and the distilled product was collected in a receiver cooled in a dry ice and acetone bath. The product was purified by fractional distillation under N_2 using a 15 cm Vigreux column. A strong-smelling colourless liquid CH_3NC (25 ml) was collected at 55–56 °C and then stored at low temperature to prevent isomerisation into acetonitrile (CH_3CN).

The product was characterised by NMR (^{1}H NMR (300MHz, D_2O) δ 4.646 (1H, s), 3.027 (3H, t)) and IR spectroscopy (ν_1 (CH stretching) 2953 cm^{-1}, ν_2 (NC stretching) 2163 cm^{-1}).

7.4.2 Titration of FeMoco with methyl isocyanide

The titration of FeMoco with methyl isocyanide was performed in order to study the effect of ligand molecular size on ligand binding to FeMoco. A change in redox properties of the FeMoco was observed and compared to previouse study on larger isocyanide, *t*-butyl isocyanide (Figure 7-7). This experiment was carrired out at low temperature as methyl isocyanide can undergo isomerisation to acetonitrile at room temperature.

In Figure 7-8A, adding 1 molar equivalent of methyl isocyanide has no effect on reduction process I of FeMoco, but adding 2 molar equivalents caused a slight drop in current at E_1 = –311 mV and a slight rise at E_2 = –413 mV ($E_{SHE} = E_{SCE} + 0.251$ V at 10 °C). Adding 3 molar equivalents resulted in a sharp single reduction peak at E_2, suggesting a single, clean product of isocyanide bound with FeMoco. The broad re-oxidation peak on the way back suggests

that methyl isocyanide binding is unstable in the semi-reduced state, restoring some unbound FeMoco.

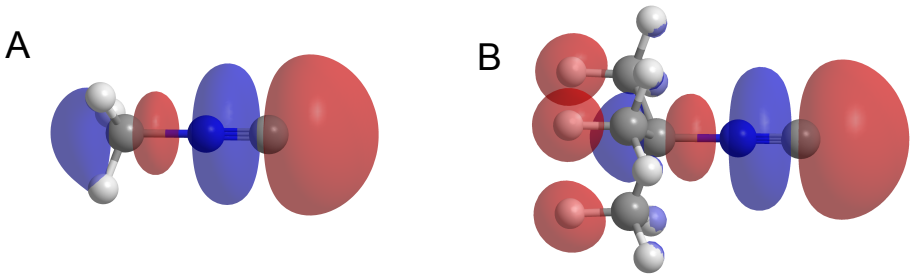

Figure 7-7: Structure of methyl isocyanide (A) and *t*-butyl isocyanide (B) showing molecular orbitals (extended Hückel HOMO).

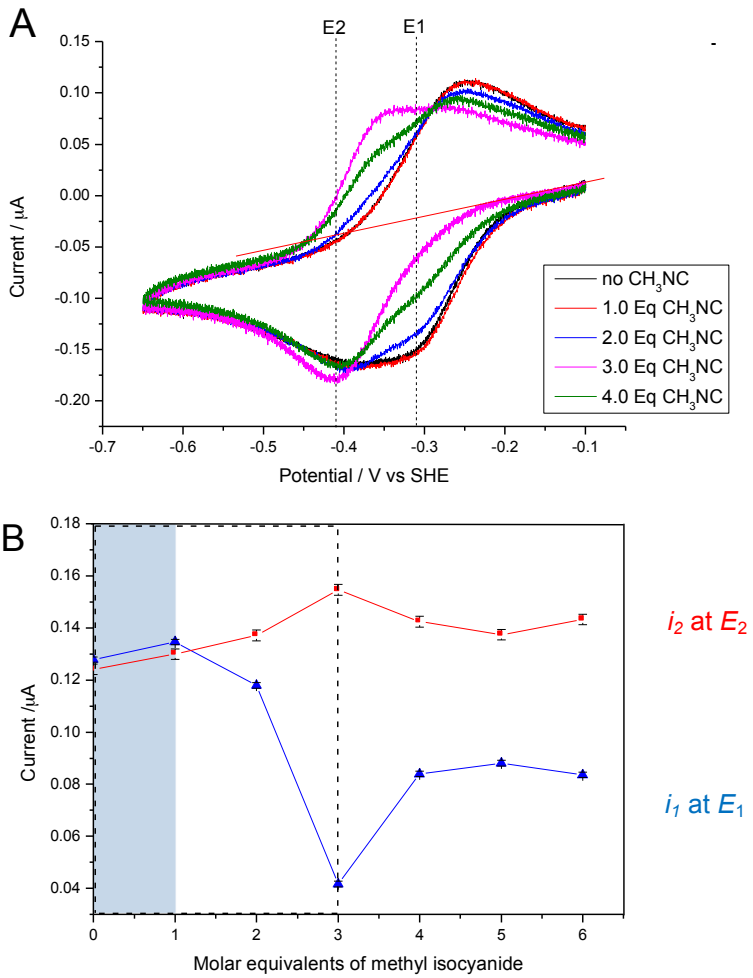

Figure 7-8: (A) Cyclic voltammograms of FeMoco titrated with methyl isocyanide in NMF at 10 °C recorded at 10 mV s^{-1}. (B) Titration curve showing current response at E_1= –311 mV and E_2= –413 mV as a function of methyl isocyanide concentration.

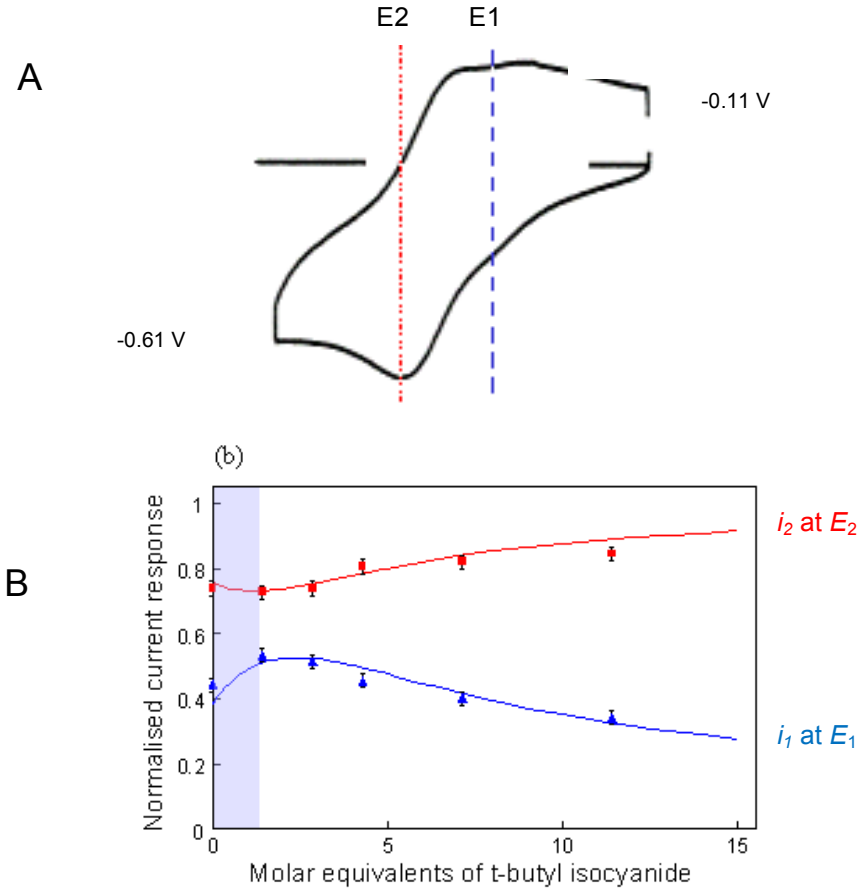

Figure 7-9: (A) Cyclic voltammograms of FeMoco in the presence of 12 molar equivalents of *t*-butyl isocyanide at 20 °C recorded at 50 mV s^{-1}. (B) Titration curves showing current response at E_1= –330 mV and E_2= –430 mV, respectively, as a function of *t*-butyl isocyanide concentration. (reproduced from ref [194])

Qualitatively, this is similar to a cyclic voltammogram of FeMoco with *t*-butyl isocyanide from previous work by Vincent in Figure 7-9A. This data was analysed using the approach employed by Vincent *et al.* for other isocyanide, a titration curve was plotted by monitoring current at two constant potentials (E_1 and E_2) on a series of cyclic voltammograms of FeMoco and methyl isocyanide as shown in Figure 7-8B. Up to 3 molar equivalents of methyl isocyanide, it showed a qualitative similarity to a titration curve on *t*-butyl isocyanide in previous work as shown in Figure 7-9B. According to analysis on *t*-butyl isocyanide binding to FeMoco, it was suggest that a first methyl isocyanide ligand could coordinate to the Mo atom and second isocyanide could coordinate to one of the central Fe atoms. As an electron-releasing group, methyl isocyanide makes the cluster more difficult to reduce leading to a

reduction peak at more negative potential. The effect of methyl isocyanide differs as the concentration increased. The difference in titration curves could imply that the smaller size of ligand allows another isocyanide binding site on FeMoco as shown in Figure 7-7.

7.4.3 Conclusion

In the present work, the first electrochemistry on extracted FeVco was recorded including studies of thiol effect and CO-binding. It was found that FeVco exhibited different electrochemistry characteristic from the related FeMoco. It showed a catalytic process at potential –622 mV, presumably proton reduction. The catalytic current of this process was suppressed by exposure to CO. It could imply that CO interacts with isolated FeVco, consistent with previous reports of CO reduction by isolated FeVco.

For isolated FeMoco, it was proved that new sample of FeMoco behaves consistently with earlier samples in electrochemistry. Also, the effect of methyl isocyanide was investigated and compared with other isocyanide from earlier work by Vincent *et al*. It showed that methyl isocyanide binding to the isolated FeMoco lowered the reduction potential of the first redox process of the FeMoco, indicative of an increase in electron density on the metal core. The difference in molar equivalents of different isocyanide added before a change in redox potential was observed. A greater amount of methyl isocyanide used reflected less steric effect due to smaller molecular size which allows another isocyanide binding site on the FeMoco.

Chapter 8

Conclusion

A method for studying the MoFe protein of nitrogenase without the requirement of the Fe protein and ATP has been developed in this Thesis. Electron transfer into the active site is achieved by using low potential redox mediators. This method has made it possible to electrochemically control electron transfer to the MoFe protein to support substrate reduction catalysed by the protein. By controlling the potential applied by the electrode, the catalytic activity and inhibition of the protein can be monitored simultaneously for the first time.

The ligand binding to the wild type and variant MoFe proteins has been investigated in this Thesis using an IR spectroelectrochemical approach combined with a mediated electron transfer system. The results from IR spectroelectrochemistry show CO binding to the reduced state of the MoFe protein, and are consistent with previous results from stopped flow experiments with electron transfer from the Fe protein and ATP.

Development of a mediated electron transfer system

The first challenge when it comes to the study of nitrogenase is the restriction of electron transfer in the enzyme. In order to overcome this obstacle, a mediated electron transfer system was developed for studying the MoFe protein without the presence of its native redox partner Fe protein and ATP. According to previous studies Eu^{II}-polyaminocarboxylate complexes,

Eu^{II}-DTPA and Eu^{II}-EGTA, were found to be able to deliver electrons into the β-98^{His} variant MoFe protein to support the reduction of hydrazine. Due to their low reduction potentials and reversible redox properties under conditions required for the MoFe protein and IR spectroelectrochemical experiments, $Eu^{III/II}$-ligand complexes have here been shown to be suitable as the low potential redox mediators for studying the nitrogenase MoFe protein.

Electrochemical control of the MoFe protein

In this study, the use of electron transfer *via* a series of redox mediators has allowed electrochemical control of the MoFe protein in a catalytically relevant potential range. The electrochemical study of the wild type and β-98^{His} variant MoFe protein showed that both MoFe proteins are able to catalyse proton reduction in the presence of $Eu^{III/II}$-ligand mediators at –900 mV and below. This potential is close to the reduction potential of $Eu^{III/II}$-EGTA and $Eu^{III/II}$-DTPA and no catalytic current was observed in the control experiment in the absence of Eu-ligand mediators, indicating that these mediators were required to transfer electrons into the MoFe protein. The MoFe protein-catalysed proton reduction was confirmed by the observation that introduction of inhibitor acetylene can suppress this process. This is the first evidence of electrochemically-driven proton reduction by the MoFe protein.

Moreover, the β-98^{His} variant MoFe protein showed a greater activity of proton reduction compared to that of wild type protein. This is in line with its ability to catalyse hydrazine reduction with Eu^{II}-ligand complexes as an electron donor which might be due to a conformational modification which lowers the reduction potential of the P-cluster, or decreases the electron transfer distance between the P-cluster and the FeMoco allowing faster electron transfer relative to the wild type MoFe protein.

CO binding to the MoFe protein

The electrochemical study of the wild type MoFe protein showed that the proton reduction by the MoFe protein was inhibited in the presence of saturated CO solution. This observed CO inhibition indicates that CO can react with the reduced MoFe protein under the experimental conditions. To investigate *in situ* the interaction of CO with the MoFe protein, an IR SEC approach was employed associated with a redox mediator cocktail.

From an IR SEC study, the wild type MoFe protein and the β-98^{His} variant exhibited a similar set of peaks in the ν(CO) region between $1800 - 2050$ cm^{-1} following reduction at low potential, consistent with the potential that proton reduction by the MoFe protein was observed. The wavenumbers of observed ν(CO) peaks are closely matched with those from the previous study of ATP-dependent CO binding to nitrogenase using stopped-flow IR spectroscopy. This indicates that the same CO-bound species of the wild type MoFe protein were observed in this study despite the difference in electron transfer methods. This is strong evidence that the redox mediators can deliver low potential electrons to the active site to achieve the reduced state that substrate and inhibitor binds to, although electrocatalytic dinitrogen reduction was not observed. The overall electron transfer process was proposed as shown in Figure 8-1. This technique also allows the characterisation of the interaction to be directly linked with the applied potential and activity of the enzyme for the first time.

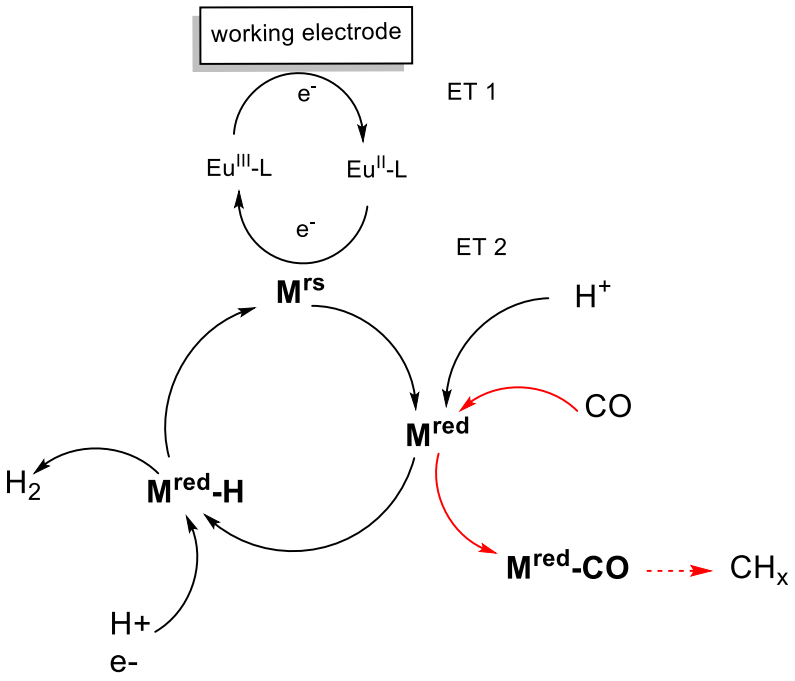

Figure 8-1: A proposed electron transfer and redox reaction of MoFe protein (M) *via* mediated electron transfer.

Cyanide binding to the MoFe protein

In this study, the same technique was applied to study cyanide binding to the α-96^{Glu} variant MoFe protein, which was reported to be able to bind cyanide at the resting state in contrast to the wild type. The results for the α-96^{Glu} variant MoFe protein showed some potential dependent changes in the *ν*(CN) region when changing potential to switch from the oxidised to semi-reduced level. The observed *ν*(CN) wavenumber of 2070 cm^{-1} is close to that of cyanide-bound isolated FeMoco at 2053 cm^{-1}. However, the interference from ferrocyanide and ferricyanide formed during the experiment masked some of the *ν*(CN) range and the peaks of interest could not be clearly resolved. The ferricyanide species was thought to be generated from some excess Fe atoms in the sample and/or degradation of the metal cluster during the experiment.

Study of the redox properties of the isolated cofactors

An electrochemical study on the isolated FeMoco and FeVco has been carried out as a parallel study to that of the intact protein. The redox chemistry of FeVco was studied for the first time. It showed some difference in redox processes to FeMoco including the interaction with CO. This might be relevant to the previous studies that reveal the CO reduction activity of V-nitrogenase and isolated FeVco.

Future work

For nitrogenase, the mediated spectroelectrochemical technique could be applied to study several catalytic reactions, such as the reduction of azide, hydrazine or CO_2. The catalytic products could be detected using suitable analytical techniques as shown in Figure 8-2. In addition, study of different ligands, binding as inhibitors at different redox levels of nitrogenase, is also possible *via* the mediated electron transfer method. Together with different physical approaches, this technique could thus provide new insight toward understanding biological nitrogen fixation.

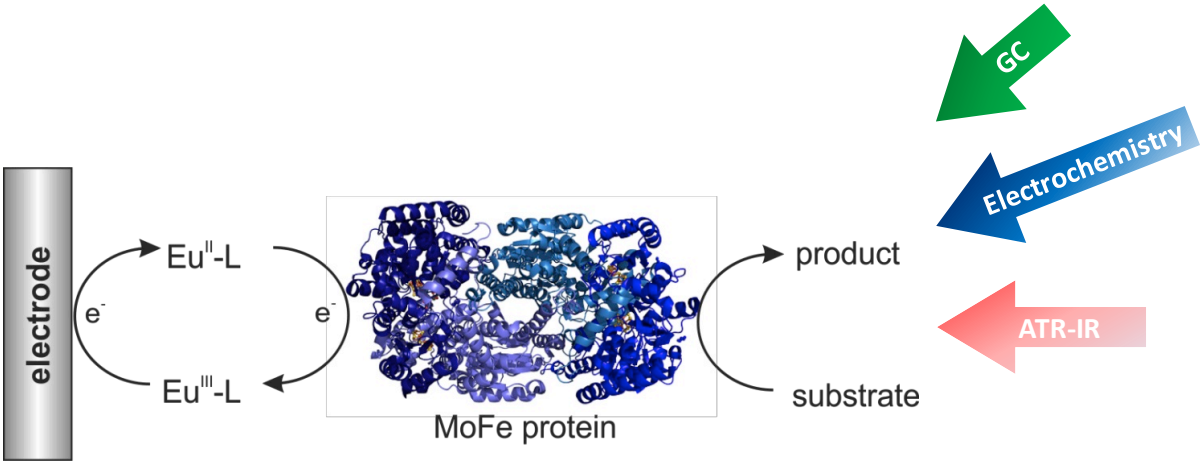

Figure 8-2: Scheme showing possible characteration of electrochemically-driven catalytic reactions of MoFe protein using various analytical techiniques.

This study has opened up a wide range of possibilities for studying redox enzymes, and is not limited to nitrogenase. The IR spectroelectrochemical technique also provides a useful way to characterise redox changes at the active site of enzymes while the activity of the enzyme can be monitored *via* the current at the same time. This approach can also be adapted for use with other analytical techniques that might help characterisation the different properties of the enzyme, for example gas chromatographic monitoring of products formed during electrocatalysis.

Bibliography

1. S. L. Tartowski and R. W. Howarth, in *Encyclopedia of Biodiversity*, ed. A. L. Simon, Elsevier, New York, 2001, pp. 377-388.

2. J. N. Galloway, in *Treatise on Geochemistry*, eds. D. H. Heinrich and K. T. Karl, Pergamon, Oxford, 2003, pp. 557-583.

3. M. Voss and J. P. Montoya, *Nature*, 2009, **461**, 49-50.

4. S. J. Ferguson, *Curr. Opin. Chem. Biol.*, 1998, **2**, 182-193.

5. D. E. Canfield, A. N. Glazer and P. G. Falkowski, *Science*, 2010, **330**, 192-196.

6. P. G. Falkowski, *Nature*, 1997, **387**, 272-275.

7. P. Atkins, T. Overton, J. Rourke, M. Weller and F. Armstron, *Shriver & Atkins' Inorganic Chemistry*, 5th edn., Oxford University Press, Oxford, 2010.

8. G. Ertl, *Catalysis Reviews*, 1980, **21**, 201-223.

9. J. N. Galloway, *Environ. Pollut.*, 1998, **102**, 15-24.

10. The International Fertilizer Industry Association; Production and trade statistics from 1999 to 2009, Available from: http://www.fertilizer.org. (Updated: 2 February 2010).

11. S. Ahlgren, S. Bernesson, A. Nordberg and P.-A. Hansson, *Bioresour. Technol.*, 2010, **101**, 7181-7184.

12. P. H. Beatty and A. G. Good, *Science*, 2011, **333**, 416-417.

13. D. V. Yandulov and R. R. Schrock, *J Am Chem Soc*, 2002, **124**, 6252-6253.

14. D. V. Yandulov and R. R. Schrock, *Science*, 2003, **301**, 76-78.

15. R. A. Kinney, R. L. McNaughton, J. M. Chin, R. R. Schrock and B. M. Hoffman, *Inorg. Chem.*, 2010, **50**, 418-420.

16. J. S. Anderson, J. Rittle and J. C. Peters, *Nature*, 2013, **501**, 84-87.

17. B. J. Hales, D. J. Langosch and E. E. Case, *The Journal of biological chemistry*, 1986, **261**, 15301-15306.

18. Y. Hu and M. W. Ribbe, *Coord. Chem. Rev.*, 2010.

19. L. C. Seefeldt, B. M. Hoffman and D. R. Dean, in *Annu. Rev. Biochem*, 2009, vol. 78, pp. 701-722.

20. B. J. Hales, E. E. Case, J. E. Morningstar, M. F. Dzeda and L. A. Mauterer, *Biochemistry*, 1986, **25**, 7251-7255.

21. D. H. Kim and M. S. Kim, *Bioresour. Technol.*, 2010.

22. M. Ribbe, D. Gadkari and O. Meyer, *J. Biol. Chem.*, 1997, **272**, 26627-26633.

23. J. C. Hwang and R. H. Burris, *Biochim. Biophys. Acta*, 1972, **283**, 339-350.

24. A. J. Pierik, H. Wassink, H. Haaker and W. R. Hagen, *Eur. J. Biochem.*, 1993, **212**, 51-61.

25. R. N. F. Thorneley, *Nature*, 1992, **360**, 532-533.

26. Y. Hu, A. W. Fay, C. C. Lee, J. A. Wiig and M. W. Ribbe, *Dalton Trans.*, 2010, **39**, 2964-2971.

27. M. W. Ribbe, Y. Hu, K. O. Hodgson and B. Hedman, *Chem. Rev.*, 2013.

28. A. C. Nyborg, J. A. Erickson, J. L. Johnson, A. Gunn, S. M. Truscott and G. D. Watt, *J. Inorg. Biochem.*, 2000, **78**, 371-381.

29. M. Guo, F. Sulc, M. W. Ribbe, P. J. Farmer and B. K. Burgess, *J. Am. Chem. Soc.*, 2002, **124**, 12100-12101.

30. K. A. Vincent, G. J. Tilley, N. C. Quammie, I. Streeter, B. K. Burgess, M. R. Cheesman and F. A. Armstrong, *Chem. Commun. (Cambridge)*, 2003, 2590-2591.

31. O. Einsle, F. A. Tezcan, S. L. A. Andrade, B. Schmid, M. Yoshida, J. B. Howard and D. C. Rees, *Science*, 2002, **297**, 1696-1700.

32. T. Spatzal, M. Aksoyoglu, L. Zhang, S. L. A. Andrade, E. Schleicher, S. Weber, D. C. Rees and O. Einsle, *Science*, 2011, **334**, 940.

33. K. M. Lancaster, M. Roemelt, P. Ettenhuber, Y. Hu, M. W. Ribbe, F. Neese, U. Bergmann and S. DeBeer, *Science*, 2011, **334**, 974-977.

34. J. A. Wiig, Y. Hu, C. C. Lee and M. W. Ribbe, *Science*, 2012, **337**, 1672-1675.

35. J. A. Wiig, C. C. Lee, Y. Hu and M. W. Ribbe, *J. Am. Chem. Soc.*, 2013, **135**, 4982-4983.

36. J. Imperial, T. R. Hoover, M. S. Madden, P. W. Ludden and V. K. Shah, *Biochemistry*, 1989, **28**, 7796-7799.

37. H. U. Yilin and M. W. Ribbe, *Acc. Chem. Res.*, 2010, **43**, 475-484.

38. A. W. Fay, M. A. Blank, J. M. Yoshizawa, C. C. Lee, J. A. Wiig, Y. Hu, K. O. Hodgson, B. Hedman and M. W. Ribbe, *Dalton Trans*, 2010, **39**, 3124-3130.

39. V. K. Shah and W. J. Brill, *Proc. Natl. Acad. Sci. U.S.A.*, 1977, **74**, 3249-3253.

40. F. A. Schultz, S. F. Gheller, B. K. Burgess, S. Lough and W. E. Newton, *J. Am. Chem. Soc.*, 1985, **107**, 5364-5368.

41. G. J. Leigh, *Science*, 2003, **301**, 55-56.

42. L. C. Seefeldt, I. G. Dance and D. R. Dean, *Biochemistry*, 2004, **43**, 1401-1409.

43. D. Lukoyanov, Z. Y. Yang, D. R. Dean, L. C. Seefeldt and B. M. Hoffman, *J. Am. Chem. Soc.*, 2010, **132**, 2526-2527.

44. C. C. Lee, M. A. Blank, A. W. Fay, J. M. Yoshizawa, Y. Hu, K. O. Hodgson, B. Hedman and M. W. Ribbe, *Proc. Natl. Acad. Sci. U.S.A.*, 2009, **106**, 18474-18478.

45. K. Rupnik, C. C. Lee, J. A. Wiig, Y. Hu, M. W. Ribbe and B. J. Hales, *Biochemistry*, 2014, **53**, 1108-1116.

46. J. W. Peters, M. H. Stowell, S. M. Soltis, M. G. Finnegan, M. K. Johnson and D. C. Rees, *Biochemistry*, 1997, **36**, 1181-1187.

47. L. Zhang, J. T. Kaiser, G. Meloni, K.-Y. Yang, T. Spatzal, S. L. A. Andrade, O. Einsle, J. B. Howard and D. C. Rees, *Angew. Chem. Int. Ed.*, 2013, **52**, 10529-10532.

48. C. L. Chi, Y. Hu and M. W. Ribbe, *Proc. Natl. Acad. Sci. U.S.A.*, 2009, **106**, 9209-9214.

49. A. W. Fay, M. A. Blank, C. C. Lee, Y. L. Hu, K. O. Hodgson, B. Hedman and M. W. Ribbe, *J. Am. Chem. Soc.*, 2010, **132**, 12612-12618.

50. K. Danyal, D. R. Dean, B. M. Hoffman and L. C. Seefeldt, *Biochemistry*, 2011.

51. S. Duval, K. Danyal, S. Shaw, A. K. Lytle, D. R. Dean, B. M. Hoffman, E. Antony and L. C. Seefeldt, *Proc. Natl. Acad. Sci. U.S.A.*, 2013, **110**, 16414-16419.

52. L. C. Seefeldt, B. M. Hoffman and D. R. Dean, *Curr. Opin. Chem. Biol.*, 2012, **16**, 19-25.

53. B. M. Hoffman, D. Lukoyanov, Z.-Y. Yang, D. R. Dean and L. C. Seefeldt, *Chem. Rev.*, 2014, **114**, 4041–4062.

54. R. N. Thorneley and D. J. Lowe, *Biochem. J*, 1984, **224**, 887-894.

55. K. Danyal, B. S. Inglet, K. A. Vincent, B. M. Barney, B. M. Hoffman, F. A. Armstrong, D. R. Dean and L. C. Seefeldt, *J. Am. Chem. Soc.*, 2010, **132**, 13197-13199.

56. L. E. Roth, J. C. Nguyen and F. A. Tezcan, *J. Am. Chem. Soc.*, 2010, **132**, 13672-13674.

57. W. W. Weare, X. Dai, M. J. Byrnes, J. M. Chin, R. R. Schrock and P. Müller, *Proc. Natl. Acad. Sci. U.S.A.*, 2006, **103**, 17099-17106.

58. R. R. Schrock, *Proc. Natl. Acad. Sci. U.S.A.*, 2006, **103**, 17087.

59. J. D. Tolland and R. N. F. Thorneley, *Biochemistry*, 2005, **44**, 9520-9527.

60. B. M. Barney, M. Laryukhin, R. Y. Igarashi, H.-I. Lee, P. C. Dos Santos, T.-C. Yang, B. M. Hoffman, D. R. Dean and L. C. Seefeldt, *Biochemistry*, 2005, **44**, 8030-8037.

61. B. M. Barney, R. Y. Igarashi, P. C. Dos Santos, D. R. Dean and L. C. Seefeldt, *J. Biol. Chem.*, 2004, **279**, 53621-53624.

62. L. C. Seefeldt, Z.-Y. Yang, S. Duval and D. R. Dean, *Biochim. Biophys. Acta*, 2013, **1827**, 1102-1111.

63. J. C. Hwang, C. H. Chen and R. H. Burris, *Biochim. Biophys. Acta*, 1973, **292**, 256-270.

64. M. R. Hyman, L. C. Seefeldt, T. V. Morgan, D. J. Arp and L. E. Mortenson, *Biochemistry*, 1992, **31**, 2947-2955.

65. D. Lukoyanov, Z.-Y. Yang, B. M. Barney, D. R. Dean, L. C. Seefeldt and B. M. Hoffman, *Proc. Natl. Acad. Sci. U.S.A.*, 2012, **109**, 5583-5587.

66. M. H. Matus, A. J. Arduengo and D. A. Dixon, *The Journal of Physical Chemistry A*, 2006, **110**, 10116-10121.

67. B. K. Burgess, *Biochemistry*, 1993, **32**, 13725-13731.

68. S. J. George, G. A. Ashby, C. W. Wharton and R. N. F. Thorneley, *J. Am. Chem. Soc.*, 1997, **119**, 6450-6451.

69. C. C. Lee, Y. Hu and M. W. Ribbe, *Science*, 2010, **329**, 642.

70. C. C. Lee, Y. Hu and M. W. Ribbe, *Angew. Chem. Int. Ed.*, 2011, **50**, 5545-5547.

71. Z. Y. Yang, D. R. Dean and L. C. Seefeldt, *J. Biol. Chem.*, 2011, **286**, 19417-19421.

72. Y. Hu, C. C. Lee and M. W. Ribbe, *Science*, 2011, **333**, 753-755.

73. C. C. Lee, Y. Hu and M. W. Ribbe, *Angew. Chem. Int. Ed.*, 2012, **51**, 1947-1949.

74. J. G. Li, B. K. Burgess and J. L. Corbin, *Biochemistry*, 1982, **21**, 4393-4402.

75. D. J. Lowe, K. Fisher, R. N. F. Thorneley, S. A. Vaughn and B. K. Burgess, *Biochemistry*, 1989, **28**, 8460-8466.

76. P. M. C. Benton, S. M. Mayer, J. Shao, B. M. Hoffman, D. R. Dean and L. C. Seefeldt, *Biochemistry*, 2001, **40**, 13816-13825.

77. L. E. Roth and F. A. Tezcan, *J. Am. Chem. Soc.*, 2012, **134**, 8416-8419.

78. M. M. Georgiadis, H. Komiya, P. Chakrabarti, D. Woo, J. J. Kornuc and D. C. Rees, *Science*, 1992, **257**, 1653-1659.

79. J. Kim and D. C. Rees, *Nature*, 1992, **360**, 553-560.

80. J. Kim and D. C. Rees, *Science*, 1992, **257**, 1677-1682.

81. R. Sarma, B. M. Barney, S. Keable, D. R. Dean, L. C. Seefeldt and J. W. Peters, *J. Inorg. Biochem.*, 2010, **104**, 385-389.

82. R. W. Strange, R. R. Eady, D. Lawson and S. S. Hasnain, *Journal of Synchrotron Radiation*, 2003, **10**, 71-75.

83. R. W. Strange, B. E. Smith, R. R. Eady, D. Lawson and S. S. Hasnain, *Journal of Synchrotron Radiation*, 2003, **10**, 197.

84. J. Chen, J. Christiansen, R. C. Tittsworth, B. J. Hales, S. J. George, D. Coucouvanis and S. P. Cramer, *J. Am. Chem. Soc.*, 1993, **115**, 5509-5515.

85. B. K. Burgess and D. J. Lowe, *Chem. Rev.*, 1996, **96**, 2983-3011.

86. L. C. Davis, M. T. Henzl, R. H. Burris and W. H. Orme-Johnson, *Biochemistry*, 1979, **18**, 4860-4869.

87. H. I. Lee, L. M. Cameron, B. J. Hales and B. M. Hoffman, *J. Am. Chem. Soc.*, 1997, **119**, 10121-10126.

88. L. M. Cameron and B. J. Hales, *Biochemistry*, 1998, **37**, 9449-9456.

89. G. D. Watt, Z. C. Wang and R. R. Knotts, *Biochemistry*, 1986, **25**, 8156-8162.

90. M. J. Ryle, W. N. Lanzilotta, L. E. Mortenson, G. D. Watt and L. C. Seefeldt, *J. Biol. Chem.*, 1995, **270**, 13112-13117.

91. W. N. Lanzilotta and L. C. Seefeldt, *Biochemistry*, 1997, **36**, 12976-12983.

92. C. Pickett, K. Vincent, S. Ibrahim, C. Gormal, B. Smith and S. Best, *Chem. Eur. J.*, 2003, 76-87.

93. S. K. Ibrahim, C. A. Gormal, B. E. Smith, C. J. Pickett, K. Vincent and S. P. Best, *Chem. Commun.*, 1999, 1019-1020.

94. C. Pickett, K. Vincent, S. Ibrahim, C. Gormal, B. Smith, S. Fairhurst and S. Best, *Chem. Eur. J.*, 2004, 4770-4776.

95. W. Roseboom, A. L. De Lacey, V. M. Fernandez, E. C. Hatchikian and S. P. Albracht, *J. Biol. Inorg. Chem.*, 2006, **11**, 102-118.

96. C. Tard and C. J. Pickett, *Chem. Rev.*, 2009, **109**, 2245-2274.

97. T. G. Spiro, A. V. Soldatova and G. Balakrishnan, *Coord. Chem. Rev.*, 2013, **257**, 511-527.

98. K. S. Reddy, T. Yonetani, A. Tsuneshige, B. Chance, B. Kushkuley, S. S. Stavrov and J. M. Vanderkooi, *Biochemistry*, 1996, **35**, 5562-5570.

99. Y.-W. Lin and J. Wang, *J. Inorg. Biochem.*, 2013, **129**, 162-171.

100. Z. Y. Yang, L. C. Seefeldt, D. R. Dean, S. P. Cramer and S. J. George, *Angew. Chem. Int. Ed.*, 2011, **50**, 272-275.

101. A. J. White, K. Drabble and C. W. Wharton, *Biochem. J*, 1995, **306**, 843-849.

102. A. J. Healy, P. A. Ash, O. Lenz and K. A. Vincent, *Phys. Chem. Chem. Phys.*, 2013, **15**, 7055-7059.

103. A. J. Healy, H. A. Reeve and K. A. Vincent, *Faraday Discuss.*, 2011, **148**, 345-357; discussion 421-441.

104. K. A. Vincent, *Philos. Trans. R. Soc. London, Ser. A*, 2010, **368**, 3713-3731.

105. B. Bleijlevens, F. Broekhuizen, A. Lacey, W. Roseboom, V. Fernandez and S. J. Albracht, *J. Biol. Inorg. Chem.*, 2004, **9**, 743-752.

106. A. L. De Lacey, V. M. Fernández, M. Rousset and R. Cammack, *Chem. Rev.*, 2007, **107**, 4304-4330.

107. P. N. Bartlett, *Bioelectrochemistry: Fundamentals, Experimental Techniques and Applications*, Wiley, 2008.

108. R. G. Compton and C. E. Banks, *Understanding Voltammetry*, 2nd edn., Imperial College Press, London, 2011.

109. K. Nakamoto, *Infrared and Raman Spectra of Inorganic and Coordination Compounds, Part B*, Wiley, New Jersey, USA, 2009.

110. K. Chu, J. Vojtchovsky, B. H. McMahon, R. M. Sweet, J. Berendzen and I. Schlichting, *Nature*, 2000, **403**, 921-923.

111. C. M. Moore, N. L. Akers, A. D. Hill, Z. C. Johnson and S. D. Minteer, *Biomacromolecules*, 2004, **5**, 1241-1247.

112. J. Huang, J. Zheng and Q. Sheng, *Microchim Acta*, 2011, **173**, 157-163.

113. A. J. Healy, H. A. Reeve, A. Parkin and K. A. Vincent, *Electrochim. Acta*, 2011, **56**, 10786-10790.

114. J. Christiansen, P. J. Goodwin, W. N. Lanzilotta, L. C. Seefeldt and D. R. Dean, *Biochemistry*, 1998, **37**, 12611-12623.

115. B. K. Burgess, D. B. Jacobs and E. I. Stiefel, *Biochim. Biophys. Acta*, 1980, **614**, 196-209.

116. J. Wiig, C.-C. Lee, A. Fay, Y. Hu and M. Ribbe, in *Nitrogen Fixation*, ed. M. W. Ribbe, Humana Press, 2011, vol. 766, pp. 93-103.

117. R. A. Penneman and L. H. Jones, *J. Chem. Phys.*, 1956, **24**, 293-296.

118. A. J. Bard and L. R. Faulkner, *Electrochemical Methods: Fundamentals and Applications*, 2nd edn., Wiley, New York, USA, 2000.

119. C. C. Lee, Y. Hu and M. W. Ribbe, *Angew. Chem. Int. Ed.*, 2012, **51**, 1947-1949.

120. C. C. Lee, Y. Hu and M. W. Ribbe, *Proc. Natl. Acad. Sci. U.S.A.*, 2012, **109**, 6922-6926.

121. J. E. Huheey, E. A. Keiter and R. L. Keiter, *Inorganic Chemistry: Principles of Structure and Reactivity*, 4th edn., Harper Collins, New York, 1993.

122. P. Caravan, É. Tóth, A. Rockenbauer and A. E. Merbach, *J. Am. Chem. Soc.*, 1999, **121**, 10403-10409.

123. L. Burai, É. Tóth, S. Seibig, R. Scopelliti and A. E. Merbach, *Chem. Eur. J.*, 2000, **6**, 3761-3770.

124. S. Seibig, É. Tóth and A. E. Merbach, *J. Am. Chem. Soc.*, 2000, **122**, 5822-5830.

125. É. Tóth, L. Burai and A. E. Merbach, *Coord. Chem. Rev.*, 2001, **216–217**, 363-382.

126. S. Siemann, K. Schneider, M. Drottboom and A. Muller, *Eur. J. Biochem.*, 2002, **269**, 1650-1661.

127. J. M. Chan, J. Christiansen, D. R. Dean and L. C. Seefeldt, *Biochemistry*, 1999, **38**, 5779-5785.

128. M. Sørlie, L. C. Seefeldt and V. D. Parker, *Anal. Biochem.*, 2000, **287**, 118-125.

129. H. C. Angove, S. J. Yoo, E. Münck and B. K. Burgess, *J. Biol. Chem.*, 1998, **273**, 26330-26337.

130. N. Ohno and M. A. Cusanovich, *Biophys. J.*, 1981, **36**, 589-605.

131. C. G. Eley, E. Ragg and G. R. Moore, *J. Inorg. Biochem.*, 1984, **21**, 295-310.

132. I. M. Kolthoff and W. J. Tomsicek, *J. Phys. Chem.*, 1934, **39**, 945-954.

133. L. H. Jones, *Inorg. Chem.*, 1963, **2**, 777-780.

134. D. M. Drew, *Anal. Chem.*, 1973, **45**, 2423-2424.

135. K. W. Hipps, S. D. Williams and U. Mazur, *Inorg. Chem.*, 1984, **23**, 3500-3505.

136. J. E. O'Reilly, *Biochim. Biophys. Acta*, 1973, **292**, 509-515.

137. M. P. Richards, *Antioxid. Redox Signaling*, 2013, **18**, 2342-2351.

138. J. S. Olson and G. N. Phillips Jr, *J. Biol. Inorg. Chem.*, 1997, **2**, 544-552.

139. T. G. Spiro, A. V. Soldatova and G. Balakrishnan, *Coord Chem Rev*, 2013, **257**, 511-527.

140. K. Nienhaus and G. U. Nienhaus, *Biochim. Biophys. Acta*, 2011, **1814**, 1030-1041.

141. G. N. Phillips, M. L. Teodoro, T. Li, B. Smith and J. S. Olson, *J. Phys. Chem. B*, 1999, **103**, 8817-8829.

142. C. Rovira, B. Schulze, M. Eichinger, J. D. Evanseck and M. Parrinello, *Biophys. J.*, 2001, **81**, 435-445.

143. M. W. Makinen, R. A. Houtchens and W. S. Caughey, *Proc. Natl. Acad. Sci. U.S.A.*, 1979, **76**, 6042-6046.

144. W. S. Caughey, H. Shimada, M. G. Choc and M. P. Tucker, *Proc. Natl. Acad. Sci. U.S.A.*, 1981, **78**, 2903-2907.

145. P. Ormos, D. Braunstein, H. Frauenfelder, M. K. Hong, S. L. Lin, T. B. Sauke and R. D. Young, *Proc. Natl. Acad. Sci. U.S.A.*, 1988, **85**, 8492-8496.

146. P. Jewsbury and T. Kitagawa, *Biophys. J.*, 1995, **68**, 1283-1294.

147. K. A. Merchant, W. G. Noid, D. E. Thompson, R. Akiyama, R. F. Loring and M. D. Fayer, *J. Phys. Chem. B*, 2002, **107**, 4-7.

148. J. M. Kriegl, K. Nienhaus, P. Deng, J. Fuchs and G. U. Nienhaus, *Proc. Natl. Acad. Sci. U.S.A.*, 2003, **100**, 7069-7074.

149. F. Yang and G. N. Phillips Jr, *J. Mol. Biol.*, 1996, **256**, 762-774.

150. A. Healy, DPhil Thesis, University of Oxford, 2013.

151. M. J. Dilworth, M. E. Eldridge and R. R. Eady, *Biochem. J*, 1993, **289**.

152. R. C. Tittsworth and B. J. Hales, *J. Am. Chem. Soc.*, 1993, **115**, 9763-9767.

153. L. E. Roth and F. A. Tezcan, *J. Am. Chem. Soc.*, 2012.

154. F. K. Yousafzai and R. R. Eady, *Biochem. J*, 1999, **339**, 511-515.

155. R. N. F. Thorneley and D. J. Lowe, *J. Biol. Inorg. Chem.*, 1996, **1**, 576-580.

156. R. R. Eady, *Chem. Rev.*, 1996, **96**, 3013-3030.

157. J. M. Rivera-Ortiz and R. H. Burris, *J Bacteriol*, 1975, **123**, 537-545.

158. I. Dance, *J. Am. Chem. Soc.*, 2005, **127**, 10925-10942.

159. R. Y. Igarashi, M. Laryukhin, P. C. Dos Santos, H.-I. Lee, D. R. Dean, L. C. Seefeldt and B. M. Hoffman, *J. Am. Chem. Soc.*, 2005, **127**, 6231-6241.

160. B. M. Hoffman, D. R. Dean and L. C. Seefeldt, *Acc. Chem. Res.*, 2009, **42**, 609-619.

161. M. C. Durrant, *Biochemistry*, 2002, **41**, 13946-13955.

162. P. C. Mitchell, *J. Inorg. Biochem.*, 1986, **28**, 107-123.

163. B. Seger, A. B. Laursen, P. C. K. Vesborg, T. Pedersen, O. Hansen, S. Dahl and I. Chorkendorff, *Angew. Chem. Int. Ed.*, 2012, **51**, 9128-9131.

164. M. Asadi, B. Kumar, A. Behranginia, B. A. Rosen, A. Baskin, N. Repnin, D. Pisasale, P. Phillips, W. Zhu, R. Haasch, R. F. Klie, P. Král, J. Abiade and A. Salehi-Khojin, *Nat Commun*, 2014, **5**.

165. P. D. Tran, S. S. Pramana, V. S. Kale, M. Nguyen, S. Y. Chiam, S. K. Batabyal, L. H. Wong, J. Barber and J. Loo, *Chem. Eur. J.*, 2012, **18**, 13994-13999.

166. Z. Maskos, K. Fisher, M. SÃ¸rlie, W. E. Newton and B. J. Hales, *J. Biol. Inorg. Chem.*, 2005, **10**, 394-406.

167. L. C. Davis and Y. L. Wang, *J Bacteriol*, 1980, **141**, 1230-1238.

168. R. C. Pollock, H.-I. Lee, L. M. Cameron, V. J. DeRose, B. J. Hales, W. H. Orme-Johnson and B. M. Hoffman, *J. Am. Chem. Soc.*, 1995, **117**, 8686-8687.

169. P. D. Christie, H.-I. Lee, L. M. Cameron, B. J. Hales, W. H. Orme-Johnson and B. M. Hoffman, *J. Am. Chem. Soc.*, 1996, **118**, 8707-8709.

170. H. I. Lee, B. J. Hales and B. M. Hoffman, *J. Am. Chem. Soc.*, 1997, **119**, 11395-11400.

171. Z. Maskos and B. J. Hales, *J. Inorg. Biochem.*, 2003, **93**, 11-17.

172. L. Yan, C. H. Dapper, S. J. George, H. Wang, D. Mitra, W. Dong, W. E. Newton and S. P. Cramer, *Eur. J. Inorg. Chem.*, 2011, **2011**, 2064-2074.

173. L. Yan, V. Pelmenschikov, C. H. Dapper, A. D. Scott, W. E. Newton and S. P. Cramer, *Chem. Eur. J.*, 2012, **18**, 16349-16357.

174. T. Spatzal, K. A. Perez, O. Einsle, J. B. Howard and D. C. Rees, *Science*, 2014, **345**, 1620-1623.

175. M. Högbom, *Science*, 2014, **345**, 1568.

176. A. Barth and C. Zscherp, *Quarterly Reviews of Biophysics*, 2002, **35**, 369-430.

177. A. Silakov, C. Kamp, E. Reijerse, T. Happe and W. Lubitz, *Biochemistry*, 2009, **48**, 7780-7786.

178. C. C. Williams and J. G. Ekerdt, *J. Phys. Chem.*, 1993, **97**, 6843-6852.

179. D. R. Biggins and M. Kelly, *Biochim Biophys Acta*, 1970, **205**, 288-299.

180. K. Fisher, M. J. Dilworth, C.-H. Kim and W. E. Newton, *Biochemistry*, 2000, **39**, 10855-10865.

181. S. G. Mayhew, *Eur. J. Biochem.*, 1978, **85**, 535-547.

182. M. C. Durrant, *Biochem. J.*, 2001, **355**, 569-576.

183. B. M. Barney, M. G. Yurth, P. C. Dos Santos, D. R. Dean and L. C. Seefeldt, *J. Biol. Inorg. Chem.*, 2009, **14**, 1015-1022.

184. I. Dance, *Dalton Trans*, 2012, **41**, 7647-7659.

185. D. Smith, K. Danyal, S. Raugei and L. C. Seefeldt, *Biochemistry*, 2014, **53**, 2278-2285.

186. T. A. Scott, C. P. Berlinguette, R. H. Holm and H.-C. Zhou, *Proc. Natl. Acad. Sci. U.S.A.*, 2005, **102**, 9741-9744.

187. M. Chung and K. A. Vincent, unpublished work.

188. P. Knörzer, A. Silakov, C. E. Foster, F. A. Armstrong, W. Lubitz and T. Happe, *J. Biol. Chem.*, 2012, **287**, 1489-1499.

189. M. Bruschi, C. Greco, L. Bertini, P. Fantucci, U. Ryde and L. D. Gioia, *J. Am. Chem. Soc.*, 2010, **132**, 4992-4993.

190. C. M. Pharr and P. R. Griffiths, *Anal. Chem.*, 1997, **69**, 4673-4679.

191. K. D. Dobson and A. James McQuillan, *Phys. Chem. Chem. Phys.*, 2000, **2**, 5180-5188.

192. R. E. Schuster, J. E. Scott and J. J. Casanova, *Org. Synth.*, 1973, **5**, 772.

193. R. E. Schuster, J. E. Scott and J. J. Casanova, *Org. Synth.*, 1966, **46**, 75.

194. K. A. Vincent, PhD Thesis, University of Melbourne, 2002.